NOAA Technical Report NOS OES 012

NATIONAL OCEAN SERVICE PARTNERSHIP: DGPS-SUPPORTED HYDROSURVEY, WATER LEVEL MEASUREMENT, AND MODELING OF GALVESTON BAY

DEVELOPMENT AND APPLICATION OF THE NUMERICAL CIRCULATION MODEL

Silver Spring, Maryland
March 1996

noaa National Oceanic And Atmospheric Administration

U.S. DEPARTMENT OF COMMERCE
National Ocean Service
Office of Ocean and Earth Sciences
Marine Analysis and Interpretation Division
Coastal and Estuarine Oceanography Branch

Office of Ocean and Earth Science
National Ocean Service
National Oceanic and Atmospheric Administration
U.S. Department of Commerce

The Office of Ocean and Earth Sciences provides for the understanding of the coastal and ocean environment through the conduct of applied research and development in geophysics; the measurement, analyses, and product development of ocean and lake water levels; the collection, analyses, product development, and dissemination of coastal and global marine data; and the synthesis and interpretation with numerical and mechanistic modeling of global marine data sets. The Office cooperates with the U.S. Navy in conducting oceanographic activities for defense and mixed defense-civil sector purposes and applications.

It plans, develops and coordinates NOAA participation in Federally conducted oceanographic programs and activities, and facilitates cooperative programs, projects, and activities with the oceanographic research community. It monitors and analyzes oceanographic activities between NOAA and other organizations and agencies; identifies potential conflicts, overlaps, and opportunities for joint or cooperative efforts; and develops and maintains cooperative agreements, Memoranda of Understanding and other arrangements as appropriate to resolve issues and to ensure maximum benefits from programs of mutual interest. It develops and maintains inventories of oceanographic programs, projects, systems, and activities of other organizations and agencies to provide a basis for integrating current and future programs, systems and activities to ensure maximum efficiency, and effectiveness in meeting national goals and requirements. The Office conducts research and development; carries out theoretical studies, data analyses, and engineering development; and formulates and executes programs encompassing technological development and application to oceanography, geophysics, geodesy, and related fields.

For the Great Lakes, coastal estuaries, sea coast, and oceans, the Office plans, develops, and applies numerical and mechanistic models and produces predictions, forecasts, and analysis guidance materials of oceanographic and related marine meteorological phenomena; collects, analyzes, and disseminates tide and water-level observations and associated information; and computes water-level datums for hydrographic, marine boundary, and other special surveys. It evaluates and improves methods of data analysis; compares and integrates existing and new classes of data and products; provides and quality controls data sets and an array of output products; and assures science and technology transfer to and from the Office's programs and projects. The Office produces and disseminates operational marine environmental forecast and analysis guidance materials; manages and supports ocean climate studies; installs and operates real-time marine data collection systems; and formulates requirements for marine data sets and for data processing and communications systems; and designs and manages computer-based systems in support of these requirements.

NOAA Technical Report NOS OES 012

NATIONAL OCEAN SERVICE PARTNERSHIP: DGPS-SUPPORTED HYDROSURVEY, WATER LEVEL MEASUREMENT, AND MODELING OF GALVESTON BAY

DEVELOPMENT AND APPLICATION OF THE NUMERICAL CIRCULATION MODEL

Richard A. Schmalz, Jr.

March 1996

noaa National Oceanic And Atmospheric Administration

U.S. DEPARTMENT OF COMMERCE
Michael Kantor, Secretary

National Oceanic and Atmospheric Administration
D. James Baker, Under Secretary

National Ocean Service
W. Stanley Wilson
Assistant Administrator

Office of Ocean and Earth Sciences
David Evans, Acting Director

Marine Analysis and Interpretation Division
Frank W. Maloney, Acting Chief

Coastal and Estuarine Oceanography Branch
Bruce Parker, Chief

NOTICE

Mention of a commercial company or product does not constitute an endorsement by NOAA. Use for publicity or advertising purposes of information from this publication concerning proprietary products or the tests of such products is not authorized.

TABLE OF CONTENTS

LIST OF FIGURES

LIST OF FIGURES (CONT.)

LIST OF FIGURES (CONT.)

LIST OF FIGURES (CONT.)

LIST OF TABLES

GALVESTON BAY BASE MAP

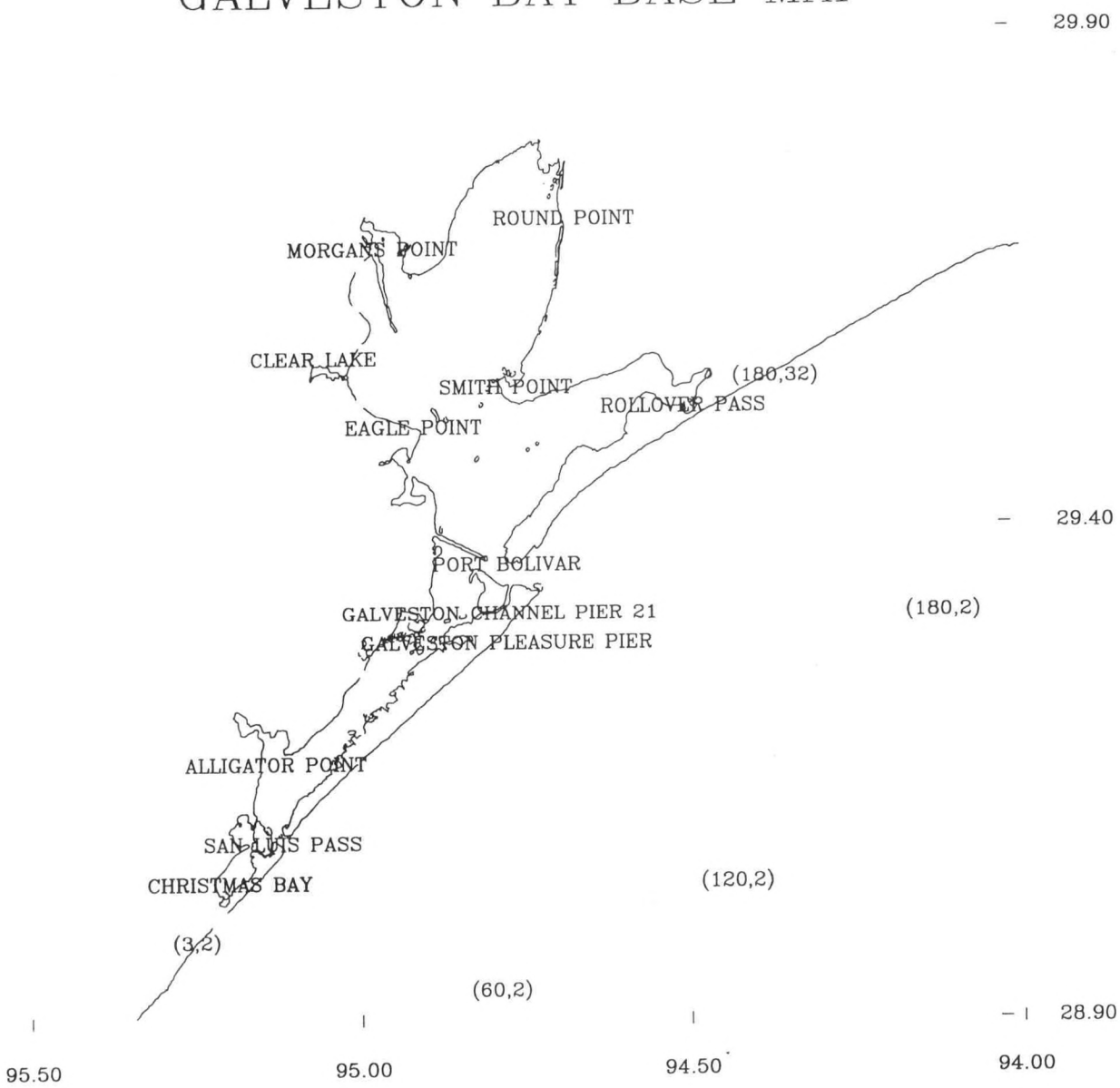

Galveston Bay area base map showing locations mentioned in this report. Note key open boundary grid cell centers are located at the center of their grid cell notations.

ABSTRACT

The National Ocean Service (NOS), as part of its Partnership Project Program, has performed a Differential Global Positioning System (DGPS) supported hydrographic survey of Galveston Bay during June - July 1995. Tidal benchmark elevations with respect to the DGPS ellipsoid reference frame were determined using static DGPS at each of 10 shore-based tide gauges. The US Army Corps of Engineers obtained six-minute water level data using DGPS on a buoy outside the Entrance to Galveston Bay. These data were analyzed to determine harmonic constants and tidal datums. This report focuses on the development and application of a three-dimensional circulation model for the Bay and near shelf using a limited observational data set (including water level, salinity, and temperature) for model calibration and validation. The model is based on the Princeton University ocean model code and has a sigma coordinate with five levels in the vertical and orthogonal curvilinear coordinates in the horizontal. The model equations are listed and the grid development is described. The model code has been modified to include spatially varying atmospheric pressure anomaly and wind field forcings as developed from Coastal-Marine Automated Network (C-MAN), National Data Buoy Center (NDBC) buoys, and National Weather Service (NWS) surface weather stations.

Modeled and observed water levels have been compared for a thirty day astronomical tide calibration over May 1995 and for a meteorologically forced simulation over June 1995. Salinity and temperature comparisons are also performed for the June 1995 simulation. Mean Lower Low Water (MLLW) fields within the DGPS ellipsoid reference frame based on these two thirty day simulations are developed and adjusted to tidal epoch. These fields will be used to transform hydrosurvey soundings taken in ellipsoid space to depths with respect to nautical chart MLLW datum. Spatial variations in the tidal epoch fields are investigated, conclusions drawn, and recommendations for additional work advanced.

1. INTRODUCTION

1.1. THE GALVESTON BAY PARTNERSHIP PROJECT

The National Oceanic and Atmospheric Administration's (NOAA's) National Ocean Service (NOS) has completed the Galveston Bay Partnership Project. The Project consisted of four major components:

- an intensive, one-month hydrographic survey using kinematic Differential Global Positioning Systems (DGPS) along with CTD profiling;
- determination of epoch tidal datums with respect to the DGPS ellipsoid at 10 shore based tide gauge stations using static DGPS;
- measurement of six-minute water levels using DGPS on a buoy outside the Galveston Bay entrance; and
- development and application of a three-dimensional circulation model to provide tidal epoch MLLW.

DGPS have the potential of determining vertical position to 1-3 centimeter accuracy. Within NOS, this potential capability has several important implications, which can lead to significant cost savings and improved product quality. First, the use of DGPS during a hydrographic survey could reduce the number of simultaneous survey control tide gauge installations. Since the depth soundings are made with respect to DGPS ellipsoid space, if the geographic distribution of the MLLW chart datum is known, the soundings can be transformed directly to chart datum, eliminating the need for tide correction. The numerical model documented here is used to provide the geographic distribution of Mean Lower Low Water (MLLW) chart datum with respect to the DGPS ellipsoid. Second, offshore water level measurements can be made using a DGPS receiver installed on a buoy, with those measurements referenced directly to MLLW, allowing offshore datum determination (not possible with bottom pressure sensors). Third, DGPS-produced water levels from a buoy can provide better offshore boundary conditions for hydrodynamic models, while DGPS-produced water levels from hydrosurvey tracks can provide unique spatial water level data for model calibration (calibration is thus no longer limited to the usual coastal tide gauge locations).

This projects seeks to demonstrate the feasibility of using DGPS for these purposes. It has taken advantage of NOS hydrosurveying and Physical Oceanographic Real Time System (PORTS), (NOS, 1995), activities previously underway in Galveston Bay. It included as NOS partners the Nautical Charting Division (NCD) of the Coast and Geodetic Survey (CGS) and three different groups (Coastal and Estuarine Oceanography Branch (CEOB), Geosciences Laboratory (GL), and Ocean and Lake Levels Division (OLLD)) within Office of Ocean and Earth Sciences (OES), and, as outside partners the U.S. Army Topographic Engineering Center (TEC) and Lamar University.

Each group provided a unique and critical contribution to the project. NCD performed a DGPS-based hydrosurvey in Galveston Bay. NCD, TEC, and GL processed and analyzed the DGPS

signals. CEOB implemented and validated a numerical hydrodynamic model of Galveston Bay and approaches, and with this model provided NCD with the geographic distribution of chart datum, MLLW. TEC installed and operated a DGPS receiver on a buoy off the entrance to Galveston Bay to obtain a monthly time series of six-minute water level measurements. OLLD in cooperation with Lamar University provided water level data from a tide gauge network around Galveston Bay, on the open coast, and offshore. OLLD also provided water level from its two gauges. DGPS-produced water level data from the offshore buoy were provided to CEOB for analysis and model boundary conditions. DGPS-produced water level data from the NCD hydrosurvey tracks and Lamar University tide gauge data were provided to CEOB for model validation.

1.2. THE NUMERICAL CIRCULATION MODEL

A version of the Princeton three-dimensional numerical circulation model (Blumberg and Mellor, 1987; Mellor, 1993) has been applied to the Bay to develop the tidal epoch MLLW distribution for use in DGPS hydrosurveying. The model uses a terrain-following vertical sigma coordinate and orthogonal curvilinear coordinates in the horizontal to depict currents, salinities, and temperatures over depth.

This model of the Bay can also improve navigational safety in several ways. It can interpolate tidal water level response characteristics between shoreline gages and throughout the Bay, including the navigation channels, to enhance the spatial coverage of predictions. The model can also be used to construct tidal atlas products (Parker and Patchen, 1987) as well as provide current and water level forecasts to help correlate modeled currents to those disseminated by the PORTS. The model could also be used to produce residual circulation fields to supplemennt salinity intrusion studies (Berger et al., 1994a) and water quality studies sponsored by the Galveston Bay National Estuary Program (Ward and Armstrong, 1992).

1.3. OCEANOGRAPHIC CHARACTERIZATION OF GALVESTON BAY

Galveston Bay is comprised of an Upper and Lower Bay as shown in Figure 1.1. Trinity Bay is attached to the eastern portion of the Upper Bay. The Trinity River inflow enters at the head of Trinity Bay and represents the largest freshwater inflow (83% of inflow). The lower Bay is attached to the East Bay System, which weakly communicates (1% of tidal prism) with the Gulf through a weir inflow/outflow structure at Rollover Pass. The lower Bay is also attached to the West Bay System, which communicates with the Gulf through San Luis Pass (19% of tidal prism), whose features are continually evolving. The Houston Ship Channel (HSC) extends from the northern portion of the Upper Bay to the City of Houston with important inflows from the San Jacinto (8% of mean annual inflow) and from the Buffalo Bayou (6% of mean annual inflow) at Houston. The total mean annual inflow to the Bay is 275 m^3/s. The main exchange (80% of the tidal prism) between the Gulf and the Galveston Bay System is through the jettied entrance at Galveston. The tidal prism has been estimated at 350 x 10^6 m^3 (Ward, 1980). The volume and surface area of the Bay are about 4,300 x 10^6 m^3 and 1,420 km^2, respectively, (Ward, 1980). The mean depth is thus 2-3 meters, although the Galveston Harbor Channel

(GHC), HSC, Galveston Channel (GC), Texas City Channel (TCC), and Gulf Intercoastal Waterway (GIWW) as shown in Figure 1.1 are dredged to nominal depths of 13, 13, 12, 12, and 4 meters, respectively.

Galveston Bay is a shallow sub-tropical bay similar in many respects to Tampa Bay. As a result, the approach of Hess (1994) for discussing the properties of Tampa Bay is followed here. Galveston Bay is subject to the tides of the adjacent Gulf of Mexico, which are mixed diurnal. Mean ranges are on the order of 0.5 and 0.3 meters in the lower and upper Bay, respectively. The phase lag is approximately 6.3 hours from outside the entrance at Pleasure Pier to Morgans Point in upper Galveston Bay, due to the shallowness of the estuary. Because the tides are mixed, the diurnal inequality, or difference between successive highs or lows, is likely to be large. Following Defant (1958), the ratio

$$r = \frac{K_1 + O_1}{M_2 + S_2} = 1.6 \qquad (1.1)$$

at Galveston Pier 21 indicates that the tide is mixed but strongly diurnal. Monthly variations in the tide are coupled to both the moon's declinational cycle (tropic tides) and the perigee-apogee cycle (spring-neap tides). A standard least-squares harmonic analysis (Zetler, 1982) of year-long tidal records that yields amplitudes of 37 constituents at Galveston Pier 21 indicates that the shallow water tides and the overtides are relatively small.

Strong meteorological forcing can significantly affect daily currents and water level variations in Galveston Bay due to the Bay's shallowness and the small astronomical tidal range. Extreme wind and storm surge conditions have occurred during the passage of hurricanes. Strong winds are likely to be associated with summertime localized thunderstorms and with wintertime frontal passages, and moderate winds will occur during daily landbreeze-seabreeze situations.

The Bay's climate is subtropical, with rainfall nearly evenly distributed throughout the year with slightly higher rainfall in the late summer months of frequent convective thunderstorm activity (Shipley and Kiesling, 1994). During the late winter, cold fronts moving down across the Texas coast bring less frequent but longer duration rain showers. Peak flow in the annual cycle occurs in April-May, with a secondary peak in February-March. Since freshwater inflow is large relative to Trinity and Upper Bay volumes, salinity stratification is strong resulting in large horizontal density gradients in the upper and lower Bay. Therefore, buoyancy-driven currents are significant. The timescales of the effects of freshets, frontal passages, and Gulf salinity on the Bay salinity have been estimated by Orlando et al., (1990).

Oceanographic studies of Galveston Bay have been conducted by NOAA, U.S. Army Corps of Engineers, and local state agencies. The major studies are briefly described here. Pullen et al. (1971) reported on a physical and chemical oceanographic survey of Galveston Bay. Water temperature and salinity data, taken during 1963-1966, and dissolved organic nitrogen, total phosphorus, and dissolved oxygen data, taken during 1964-1966, were analyzed by area and habitat. In 1988, NOS measured current profiles using a self-contained 1200 kHz ADCP at the

reference station in Galveston Bay Entrance and at the secondary station at the intersection of the HSC with the GIWW (Williams et al., 1990). Current data were analyzed for times and velocities of maximum flood current and maximum ebb current, and times of slack before flood and slack before ebb. Water level data measured at Galveston Pier 21 were analyzed for times of mean high and low tides. The differences between new observations and NOAA predictions, based on data from a circulation survey in 1937, with some additional measurements in 1963 were tested against NOS working standards. At Galveston Bay Entrance, only the predictions for the speed of maximum flood current are within working standards. At the second location in the HSC at Bolivar Roads, predictions for all table values are outside working standards. For water levels, only the low water heights approach working standards. To improve knowledge of currents, a PORTS (Bethem and Frey, 1991) has recently been installed in the Bay. General hydrographic features of the Bay and salinity characteristics have been compiled by NOS for resource management purposes. In order to update the nautical charts for the Bay, NOS is in the process of completing hydrographic surveys in the Approaches and within Galveston Bay. The DGPS survey of this project was conducted in conjunction with these surveys.

The Corps of Engineers conducted a detailed study of the tides in 1936-1937. Although much valuable raw data were lost, Ward (1993) analyzed remaining information and estimated several tidal prisms for specific areas of the Bay. Additional measurements of tides, currents, and salinity have been made by the Corps of Engineers to support physical modeling studies (Bobb et al., 1973) and the more recent numerical model investigations (Berger et al., 1994b).

The Texas Water Development Board (TWDB) maintains a set of five mid-depth salinity and temperature stations in conjunction with the Texas Coastal Ocean Observation Network (TCOON) of tide gauges, which is operated according to NOS standards. The Texas Natural Resource Conservation Commission measures temperature, conductivity, salinity, and pH in addition to conventional water quality parameters. Texas Department of Health, Texas Parks and Wildlife Department, and the City of Houston also conduct various bacteriological, species variability, and supplemental water quality studies, respectively (Lane, 1994).

1.4. OCEANOGRAPHIC CHARACTERIZATION OF TEXAS SHELF

Chuang and Wiseman (1983) investigated coastal sea level response to frontal passages on the Louisiana-Texas shelf at Galveston, Texas and Eugene Island, Louisiana over the five month period from October 24, 1962 to March 23, 1963. The surface wind fields associated with cold-front passages on time scales from 4-7 days are well organized in the north-south or cross-shelf direction. Regional sea level response shows considerable variability. It is mainly a response to alongshore wind (east-west) at Galveston and to cross-shelf (north-south) wind at Eugene Island. Cochran and Kelly (1986) further examined low-frequency circulation on the Texas-Louisiana Shelf. They inferred from coastal winds, scattered current measurements, and distributions of surface salinity and geopotential that a cyclonic gyre elongated along the shelf is a dominant feature. The shoreward component of the gyre is the coastal jet driven by wind with a downcoast component except in July-August. The shoreward prevailing wind results in a seaward flow which forms the lower component of the gyre. A prevailing countercurrent (north or eastward) flow closes the gyre offcoast. Monthly mean wind stress at Galveston exhibits northerly

components during the months of April through August based on airport records from October 1978 through August 1984. To support a northerly directed alongshore current via geostrophy, the monthly sea level offcoast should be elevated relative to shore stations.

Temple et al. (1977) report on monthly temperature and salinity measurments over the shelf water in 10 sections from off Mobile Bay (section 1) to off Brownsville, Texas (section 10) made from 1963 to 1965. Section 7 is immediately off Galveston, Texas. These data are used subsequently to develop offshore salinity and temperature boundary conditions for the circulation model. Dinnel and Wiseman (1986) have reported on the role of freshwater on the Louisiana and Texas shelf. Hydrographic data collected on monthly cruises over the West Louisiana and Texas shelf from 1963 to 1965 were analyzed and the volume of fresh water on the shelf was estimated. The freshwater volume exhibts an annual cycle that is dominated by the spring flood of the Mississippi and Atchafalaya rivers. During the winter, shelf freshwater content is low, with the higher content appearing as a discontinuous band along the inner shelf. In summer, an isolated high-content region is present in the center of the shelf. This high-content region dissipates and the pattern migrates toward the southeast in the late summer.

1.5. PREVIOUS MODELING STUDIES OF GALVESTON BAY

All of the early simulations of Galveston Bay used two-dimensional, vertically-integrated numerical models. Reid and Bodine (1968) used a two-dimensional, vertically integrated model to investigate storm surge in Galveston Bay. Shankar and Masch (1970) used a two-dimensional, vertically integrated hydrodynamic and transport model to study the relationship between freshwater inflows and salinity intrusion. Sparr et al. (1973) developed a runoff routing model, which used USGS measured inflows to compute the flushing times of various Bay sections. To study levee protection requirements, Butler (1980) used an exponentially stretched grid within an implicit two-dimensional, vertically integrated modeling approach similar to Leendertse (1967), which incorporated weir and draining within the wetting and drying procedure. Recently, Solis (1994) at the TWDB has used a two-dimensional finite element model to study freshwater effects on salinity intrusion.

Shaffer et al. (1986) described the National Weather Service's SLOSH storm surge modeling program for the U.S. East and Gulf coasts. Model basins included one developed for Galveston Bay. The vertically-integrated surge model (Jelesnianski et al., 1984) operates on a polar grid that covers the northern portion of the Texas coast with a grid cell size of 4 kilometers, and has higher resolution (cell size approximately 1 kilometer) inside the Bay. This model did not, however, simulate astronomical tidal variations.

With the advent of faster computers has come the feasibility of running fully three-dimensional numerical models. Wang (1994) at the University of Houston has used a non-orthogonal boundary fitted grid in the horizontal with vertical sigma stretching in five vertical layers to study circulation in Galveston Bay. A twenty nine day simulation from December 9, 1970 to January 7, 1971 was performed with the same freshwater inflows as used by Shankar and Masch (1970) to study the three-dimensional salinity distributions in and around the HSC. In order to assess the impact of deepening this channel from 42 to 52 feet and widening from 400 to 600

feet, Berger et al. (1994a) have applied a three-dimensional finite element model to Galveston Bay using a mixture of both 2D and 3D elements. Simulated salinity distributions under alternate channel designs will be input to ecologic models to study the effect on the oyster population.

1.6. PREVIOUS MODELING STUDIES OF TEXAS SHELF

Reid and Whitaker (1981) developed a two-dimensional vertically integrated finite difference approximation to the depth integrated linearized equations in spherical coordinates to study tides over the Gulf of Mexico. They employed a 15 second horizontal spacing resulting in 2228 grid cells. A staggered grid ADI approach similar to Leendertse (1967) was employed in the numerics. Harmonic constituents were developed for the five major tidal constituents K_1, O_1, P_1, M_2, and S_2. These constants were used by Schmalz (1985) in a numerical modeling investigation of tidal properties in Mississippi Sound. Recently, Westerink et al. (1993) has developed and applied a two-dimensional finite element model to study tides within the Gulf of Mexico and Carribean sea using several grid resolutions.

Oey (1995) has used a numerical model to investigate wind, eddy, and buoyancy influences on the mean cyclonic gyre. The Princeton Ocean Model is employed using a 20 km rectilinear grid with 20 equally spaced sigma levels. The modeled loop current sheds eddies at irregular periods of 6-20 months with an average of 8-13 months based on several ten year experiments. The modeled loop current eddies have somewhat weaker peak surface currents than observations, having otherwise approximately the right sizes ($\sim$300 km), westward propagation speeds ($\sim$ 4 km/day), and tracks. The Loop Current eddies may serve in addition to wind to cause flow convergence in the southwestern portion of the shelf. The eddy forcing produces eastward current along the shelfbreak, and accounts for shoreward intrusion along the Mississippi Canyon, which is crutial in closing the eastern limb of the cyclonic gyre noted by Cochran and Kelly (1986). Dietrich and Lin (1994) have also studied eddy shedding in the Gulf of Mexico using a rigid lid 16 level Eulerian model to investigate the depth structure of both the anticyclonic and cyclonic rings produced during an eddy shedding sequence. Surface forcings were not considered.

Sturges and Welsh (1991) employed a fully nonlinear primitive equation model developed by Bryan and Cox (1968) to the western north Atlantic from the mid-Atlantic ridge into the Caribbean Sea, the Gulf of Mexico, and the east coast of the United States to Cape Hatteras. The initial density fields as well as the vertical shears at the eastern boundary are set by climatological mean density (Levitus, 1982), and the total transport by the curl of the wind stress, which are derived form the Hellerman and Rosenstein (1983) mean winds. The model was spun up using a 1° resolution and run for an additional seven years at 1/4° resolution. Loop Current rings form with a mean time between separations of roughly 30 weeks. At depths greater than 1300m, weak vortex-like features, having horizontal scales smaller than the upper-layer warm core rings and speeds typical of topographic Rossby waves develop. These features move to the west in company with the upper warm core rings, but move relative to the rings and travel slightly faster.

1.7. ORGANIZATION OF THIS REPORT

This report describes the development and application of the NOS Galveston Bay model. Section 2 lists the circulation model equations in the curvilinear, sigma coordinates and defines the turbulence closure scheme and the generic boundary conditions. The model grid development and the bathymetry discretization are also discussed.

Section 3 describes the astronomical tide calibration during May 1995. Texas shelf boundary conditions are presented along with the development of climatological river inflows. Bay surface temperature specification as well as initial salinity and temperature field synthesis are also discussed. Finally, detailed water level comparisons between model and reconstructed astronomical tides are presented.

Section 4 describes the validation of the model for water levels under complete meteorological forcings over the month of June 1995. The development of Texas shelf boundary conditions, river discharges, and surface boundary conditions for this period are discussed. Model initialization procedures are outlined followed by water level as well as salinity and temperature model versus data comparisons.

In Section 5, the determination of the tidal epoch MLLW field is discussed. The nature of the issue is introduced followed by the evaluation of this field for both the astronomical tide calibration and complete meteorologically forced simulations. Differences between the two fields are discussed.

Section 6 lists the major findings and summarizes the entire effort and is followed by the references and acknowledgements.

Numerical model versus DGPS derived water levels along launch tracks during the June 1995 hydrosurvey are compared in graphical and tabular formats in Appendix A and B, respectively.

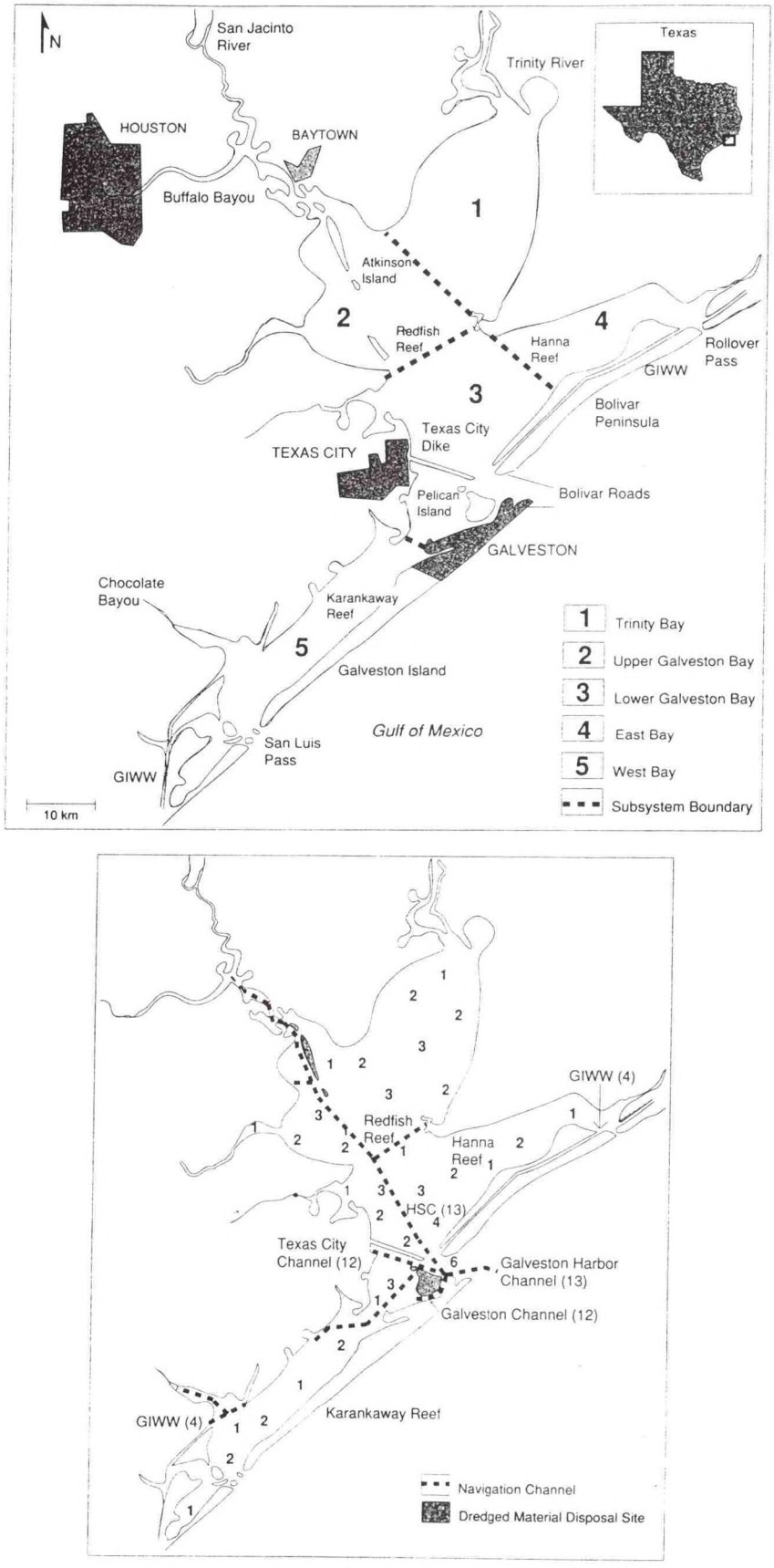

Figure 1.1. Galveston Bay System (From Orlando et al., 1993). Top panel shows how the bay is divided into subsystems. Bottom panel shows channels and mean depths (m)

2. MODEL FORMULATION

To meet the NOS Partnership Project's modeling goals, the numerical model must be capable of simulating water surface elevation fluctuations in Galveston Bay at small time scales (minutes) for long time periods (up to 3 months). To represent accurately the significant horizontal and vertical salinity and temperature gradients that were observed by NOS in Galveston Bay during the CTD component of the hydrosurvey and their effects on water levels within and outside the navigation channels, the model must include:

1. velocities, salinities, and temperatures that are three-dimensional and time-dependent;
2. a free-surface;
3. non-linear horizontal advection;
4. horizontal and vertical density gradients; and
5. variable grid spacing to resolve major navigation channels.

The Princeton three-dimensional numerical circulation model (Blumberg and Mellor, 1987) was chosen as the formulation best suited to meet the above requirements. This model includes a dimensionless sigma vertical coordinate, a level 2-1/2 turbulence closure representation, and an orthogonal curvilinear horizontal coordinate system. The code is also highly vectorized for use on high-speed vector oriented supercomputers. The major focus of the model application in Galveston Bay in this study is on the accurate representation of the water surface elevation fluctuations due to astronomical and meteorological forcings. Since meteorological forcings are also considered, it is hoped that the modeling effort might also be used to provide nowcast and forecast of currents within the HSC and GBC. A further potential use of the model would be to provide nowcast and forecast of salinity and temperature fields throughout the Bay to monitor the effects of freshwater inflows in conjunction with oyster population management. Thus the model developed here represents both water level fluctuations and circulation of shelf, Bay, and navigation channel waters.

Hess (1994) has recently, successfully adapted the Princeton model to Tampa Bay, which has many characteristics similar to those of the shallow Galveston Bay system. The following discussion, form of model equations, and boundary conditions are based on the work of Hess (1994) in Tampa Bay.

Occasional problems arising from the use of sigma coordinates have been noted in the literature. Haney (1991) reported that potential errors in the horizontal pressure gradient are alleviated by using uniform sigma intervals, reducing cell spacing in regions of large bottom slopes, subtracting the mean water density from the local density, and using a carefully-selected finite difference expression. Another potential problem is improperly large vertical diffusion when bottom slopes are large: this was corrected by altering the diffusion terms (Mellor and Blumberg, 1985). A final problem of the exchange through advection of lighter, lower layers in shallow water with adjacent denser, lower layers in deep water can be alleviated by using more horizontal grid cells (Sheng, Lee, and Wang, 1990). No problems with the use of sigma coordinates have been noted in the simulations performed in this study, which used slightly non-uniform sigma intervals with no removal of the mean water density.

2.1. MODEL EQUATIONS

The model solves the equations of fluid motion (momentum balance, mass conservation, equation of state, salinity and temperature conservation, and hydrostatic balance) at all cells in the three-dimensional grid. The equations in three-dimensional Cartesian space are recast in generalized horizontal orthogonal curvilinear coordinates, and further transformed using a vertical dimensionless sigma coordinate. Details of the derivation are given in Blumberg and Mellor (1987) and Blumberg and Herring (1987) and will not be repeated here. Additional important information appears in Mellor (1993) and Schmalz (1994). The full set of equations is as follows. Here u, v, and w are the x, y, and z components of velocity, t is time, S is salinity, θ is potential temperature, ρ is water density (Mellor, 1991), ρ_o is a reference water density (1000 kg/m^3), f is the Coriolis parameter, g is gravitational acceleration, P is pressure, P_a is atmospheric pressure, η is the departure of water elevation from mean sea level at z = 0, H is water depth at mean sea level, K_m and K_h are the vertical eddy mixing coefficients for momentum and heat/salt, respectively, A_m and A_h are the horizontal eddy mixing coefficients for momentum and heat/salt, respectively, and h_1 and h_2 are metrics (corresponding to grid dimensions ΔX and ΔY). In the temperature conservation equation (Eq. 2.5), R_θ is the heating due to short wave radiation.

Sigma coordinate:

$$\sigma = \frac{z - \eta}{H + \eta} = \frac{z - \eta}{D} \tag{2.1}$$

Continuity:

$$h_1 h_2 \frac{\partial \eta}{\partial t} + \frac{\partial}{\partial x}(h_2 u D) + \frac{\partial}{\partial y}(h_1 v D) + h_1 h_2 \frac{\partial \omega}{\partial \sigma} = 0 \tag{2.2a}$$

Vertically-integrated continuity:

$$h_1 h_2 \frac{\partial \eta}{\partial t} + \frac{\partial}{\partial x}\left(h_2 D \int_{-1}^{o} u\, d\sigma\right) + \frac{\partial}{\partial y}\left(h_1 D \int_{-1}^{o} v\, d\sigma\right) = 0 \tag{2.2b}$$

X-direction momentum:

$$\frac{\partial (h_1 h_2 D u)}{\partial t} + \frac{\partial}{\partial x}(h_2 D u^2) + \frac{\partial}{\partial y}(h_1 D u v) + h_1 h_2 \frac{\partial (\omega u)}{\partial \sigma} - D v\left(f - \frac{u}{h_1}\frac{\partial h_1}{\partial y} + \frac{v}{h_2}\frac{\partial h_2}{\partial x}\right)$$

$$= -h_2\left(gD\frac{\partial \eta}{\partial x} + \frac{1}{\rho_o}\frac{\partial P_a}{\partial x}\right) - \frac{gD^2 h_2}{\rho_o}\int_{\sigma}^{o}\left[\frac{\partial \rho}{\partial x} - \frac{\sigma}{D}\frac{\partial D}{\partial x}\frac{\partial \rho}{\partial \sigma}\right]d\sigma + \frac{\partial}{\partial x}\left[A_m D\left(\frac{h_2}{h_1}\frac{\partial u}{\partial x}\right)\right]$$

$$+ \frac{\partial}{\partial y}\left[A_m D\left(\frac{h_1}{h_2}\frac{\partial u}{\partial y} + \frac{\partial v}{\partial x}\right)\right] + \frac{h_1 h_2}{D}\frac{\partial}{\partial \sigma}\left(K_m \frac{\partial u}{\partial \sigma}\right) \tag{2.3}$$

Y-direction momentum:

$$\frac{\partial(h_1h_2Dv)}{\partial t} + \frac{\partial}{\partial x}(h_2Duv) + \frac{\partial}{\partial y}(h_1Du^2) + h_1h_2\frac{\partial(\omega v)}{\partial\sigma} + Du(f - \frac{u}{h_1}\frac{\partial h_1}{\partial y} + \frac{v}{h_2}\frac{\partial h_2}{\partial x})$$

$$= -h_2(gD\frac{\partial\eta}{\partial y} + \frac{1}{\rho_o}\frac{\partial P_a}{\partial y}) - \frac{gD^2h_1}{\rho_o}\int_\sigma^o [\frac{\partial\rho}{\partial y} - \frac{\sigma}{D}\frac{\partial D}{\partial y}\frac{\partial\rho}{\partial\sigma}]d\sigma + \frac{\partial}{\partial y}[A_mD(\frac{h_1}{h_2}\frac{\partial v}{\partial y})]$$

$$+ \frac{\partial}{\partial x}[A_mD(\frac{h_2}{h_1}\frac{\partial v}{\partial x} + \frac{\partial u}{\partial y})] + \frac{h_1h_2}{D}\frac{\partial}{\partial\sigma}(K_m\frac{\partial v}{\partial\sigma}) \qquad (2.4)$$

Conservation of heat:

$$\frac{\partial(h_1h_2D\theta)}{\partial t} + \frac{\partial}{\partial x}(h_2Du\theta) + \frac{\partial}{\partial y}(h_1Dv\theta) + h_1h_2\frac{\partial(\omega\theta)}{\partial\sigma} \qquad (2.5)$$

$$= \frac{\partial}{\partial x}(A_hD\frac{h_2}{h_1}\frac{\partial\theta}{\partial x}) + \frac{\partial}{\partial y}(A_hD\frac{h_1}{h_2}\frac{\partial\theta}{\partial y}) + \frac{h_1h_2}{D}\frac{\partial}{\partial\sigma}(K_h\frac{\partial\theta}{\partial\sigma}) + h_1h_2DR_\theta$$

Conservation of salt:

$$\frac{\partial(h_1h_2DS)}{\partial t} + \frac{\partial}{\partial x}(h_2DuS) + \frac{\partial}{\partial y}(h_1DvS) + h_1h_2\frac{\partial(\omega S)}{\partial\sigma} \qquad (2.6)$$

$$= \frac{\partial}{\partial x}(A_hD\frac{h_2}{h_1}\frac{\partial S}{\partial x}) + \frac{\partial}{\partial y}(A_hD\frac{h_1}{h_2}\frac{\partial S}{\partial y}) + \frac{h_1h_2}{D}\frac{\partial}{\partial\sigma}(K_h\frac{\partial S}{\partial\sigma})$$

Conservation of turbulent kinetic energy:

$$h_1h_2\frac{\partial(Dq^2)}{\partial t} + \frac{\partial}{\partial x}(h_2Duq^2) + \frac{\partial}{\partial y}(h_1Dvq^2) + h_1h_2\frac{\partial(\omega q^2)}{\partial\sigma} \qquad (2.7)$$

$$= \frac{\partial}{\partial x}(A_hD\frac{h_2}{h_1}\frac{\partial q^2}{\partial x}) + \frac{\partial}{\partial y}(A_hD\frac{h_1}{h_2}\frac{\partial q^2}{\partial y}) + \frac{h_1h_2}{D}\frac{\partial}{\partial\sigma}(K_q\frac{\partial q^2}{\partial\sigma})$$

$$+ h_1h_2\{\frac{2K_m}{D}[(\frac{\partial u}{\partial\sigma})^2 + (\frac{\partial v}{\partial\sigma})^2] + \frac{2g}{\rho_o}K_h\frac{\partial\rho}{\partial\sigma} - \frac{2Dq^3}{B_1\lambda}\}$$

Conservation of turbulent macroscale:

$$h_1h_2\frac{\partial(Dq^2\lambda)}{\partial t} + \frac{\partial}{\partial x}(h_2Duq^2\lambda) + \frac{\partial}{\partial y}(h_1Dvq^2\lambda) + h_1h_2\frac{\partial(\omega q^2\lambda)}{\partial\sigma} \tag{2.8}$$

$$= \frac{\partial}{\partial x}(A_hD\frac{h_2}{h_1}\frac{\partial q^2\lambda}{\partial x}) + \frac{\partial}{\partial y}(A_hD\frac{h_1}{h_2}\frac{\partial q^2\lambda}{\partial y}) + \frac{h_1h_2}{D}\frac{\partial}{\partial\sigma}(K_q\frac{\partial q^2\lambda}{\partial\sigma})$$

$$+ h_1h_2\{\frac{\lambda E_1K_m}{D}[(\frac{\partial u}{\partial\sigma})^2 + (\frac{\partial v}{\partial\sigma})^2] + \frac{\lambda E_1g}{\rho_o}K_h\frac{\partial\rho}{\partial\sigma} - \frac{q^3D}{B_1}[1 + E_2(\frac{\lambda}{\kappa L})^2]\}$$

where L is a scale length

$$L^{-1} = (\eta - z)^{-1} + (H + z)^{-1} \tag{2.9}$$

Equation of State:

Density is expressed in terms of σ_t as follows

$$\sigma_t = (\rho/\rho_m - 1)10^3 \tag{2.10}$$

where σ_t ≡ sigma t and ρ_m ≡ density of distilled water at 4 °C (999.975 kg/m^3).

Then σ_t is expressed as a function of salinity, S, and temperature, T as given by

$$\sigma_t = \Sigma_t + (\sigma_o - \Sigma_o)\left[1 - A_t + B_t(\sigma_o + \Sigma_o)\right] \tag{2.11}$$

where

$$\Sigma_t = -(T - 3.98)^2\frac{(T + 283)}{503.570\,(T + 67.26)} ,$$

$$\Sigma_o = -0.1324 ,$$

$$\sigma_o = -.093445862 + .814876576S - .00048249614S^2 + .676786135 \times 10^{-6}S^3 ,$$

$$A_t = 4.7867 \times 10^{-3}T - 9.8185 \times 10^{-5}T^2 + 1.0843 \times 10^{-6}T^3 , \text{ and}$$

$$B_t = 1.8030 \times 10^{-5}T - 8.164 \times 10^{-7}T^2 + 1.667 \times 10^{-8}T^3 .$$

The Coriolis parameter is

$$f = 2\Omega\sin(\phi) \tag{2.12}$$

where ϕ is latitude.

The vertical and horizontal mixing coefficients are expressed as follows.

Horizontal mixing coefficients:

$$A_m = C_H h_1 h_2 [(\frac{\partial u}{\partial x})^2 + \frac{1}{2}(\frac{\partial v}{\partial x} + \frac{\partial u}{\partial y})^2 + (\frac{\partial v}{\partial y})^2]^{1/2} \tag{2.13}$$

$$A_h = \frac{A_m}{N_p} \tag{2.14}$$

where the Smagorinsky horizontal eddy coefficient C_H = (0.005,0.05) and the Prandtl number N_p = 1.0.

Vertical mixing coefficients:

$$K_m = S_m q \lambda \tag{2.15}$$

$$K_h = S_h q \lambda \tag{2.16}$$

$$K_q = 0.41 S_m q \lambda \tag{2.17}$$

where

$$S_h[1 - (3A_2B_2 + 18A_1A_2)G_h] = A_2[1 - 6\frac{A_1}{B_1}] \tag{2.18}$$

$$S_m[1 - 9A_1A_2G_h] - S_h[(18A_1^2 + 9A_1A_2)G_h] = A_1(1 - 3C_1 - 6\frac{A_1}{B_1}) \tag{2.19}$$

$$G_h = \frac{\lambda^2}{q^2}\frac{g}{\rho_o}(\frac{1}{D}\frac{\partial \rho}{\partial \sigma}) \tag{2.20}$$

and

$$(A_1,A_2,B_1,B_2,C_1,E_1,E_2) = (0.92,\ 0.74,\ 16.6,\ 10.1,\ 0.08,\ 1.8,\ 1.33) \tag{2.21}$$

2.2. BOUNDARY CONDITIONS

Lateral Boundary Conditions

At land boundaries, momentum, mass, and heat flux normal to the land are zero. At open ocean boundaries, either the water level or the external-mode velocity is explicitly specified. The

internal-mode velocity is determined by an Orlanski (1976) radiation boundary condition

$$\frac{\partial u_n}{\partial t} + (\frac{\Delta\rho}{\rho_o} g D)^{1/2} \frac{\partial u_n}{\partial x} = 0 \tag{2.22}$$

where u_n is the normal velocity component and $\Delta\rho$ is the difference between the top and bottom densities. Further discussion of the open (ocean and river) boundary conditions appears in Sections 3 and 4.

Surface Boundary Conditions

Momentum is added at the water surface by winds and the atmosphere adds (or removes) heat and water. Surface stresses are transferred to the internal mode velocities by

$$(K_m \frac{\partial u}{\partial z})|_s = \frac{\tau_{sx}}{\rho_s} \tag{2.23}$$

$$(K_m \frac{\partial v}{\partial z})|_s = \frac{\tau_{sy}}{\rho_s} \tag{2.24}$$

where the subscript "s" means the surface. The formulation of Large and Pond (1981) is used to determine the wind stress from 10m over water winds. Net evaporation (or negative precipitation) is Π (m/s) and there is no salt flux across the interface. Downward heat flux across the upper surface, Q_s, can be specified as the long-wave downward radiation but is set to zero in this study.

$$(K_h \frac{\partial S}{\partial z})|_s = S_s \Pi = 0 \tag{2.25}$$

$$(K_h \frac{\partial \theta}{\partial z})|_s = Q_s = 0 \tag{2.26}$$

The Bay and shelf surface temperature field is specified using techniques described in Schmalz (1994). The surface conditions on turbulent kinetic energy, q^2, and the product $q^2\lambda$ are

$$q^2|_s = B_1^{2/3} u_{*s}^2 \tag{2.27}$$

$$q^2\lambda|_s = 0 \tag{2.28}$$

where B_1 is defined in Eq. 2.24 and the surface friction velocity, u_{*s}, is

$$u_{*s}^2 = (\frac{\tau_{sx}}{\rho_s})^2 + (\frac{\tau_{sy}}{\rho_s})^2 \tag{2.29}$$

Bottom Boundary Conditions

Bottom stresses are related to the internal mode velocities by

$$(K_m \frac{\partial u}{\partial z})|_b = \frac{\tau_{bx}}{\rho_b}$$
$$(K_m \frac{\partial v}{\partial z})|_b = \frac{\tau_{by}}{\rho_b} \qquad (2.30)$$

where the subscript "b" denotes the bottom. The velocity matching condition (incorporating a bottom logarithmic velocity profile) is also required to compute the bottom drag coefficient

$$C_b = [\frac{1}{\kappa} \ln(\frac{H + z_b}{z_o})]^{-2} \qquad (2.31)$$

where z_b is the depth of the modeled velocity at the level closest to the bottom, κ is von Karman's constant (0.40), and z_o is the roughness height. The salt and heat flux across the bottom are

$$(K_h \frac{\partial S}{\partial z})|_b = 0 \qquad (2.32)$$

$$(K_h \frac{\partial \theta}{\partial z})|_b = Q_b \qquad (2.33)$$

where Q_b is the downward heat flux across the bottom (assumed here to be zero). The bottom conditions on turbulent kinetic energy, q^2, and the product $q^2\lambda$ are

$$q^2|_b = B_1^{2/3} u_{*b}^2 \qquad (2.34)$$

$$q^2\lambda|_b = 0 \qquad (2.35)$$

where

$$u_{*b}^2 = (\frac{\tau_{bx}}{\rho_o})^2 + (\frac{\tau_{by}}{\rho_o})^2 \qquad (2.36)$$

2.3. MODEL GRID DEVELOPMENT

The Galveston Bay model runs on an orthogonal curvilinear grid closely fitted to the Bay's lateral boundaries (Figure 2.1). A 181 x 101 = 18,281-cell, orthogonal curvilinear mesh was formed using an elliptic equation grid generation technique developed by Wilken (1988) based

on the conformal mapping algorithm of Ives and Zacharias (1987). The actual grid generation code was obtained from Professor George L. Mellor, Princeton University. Grid cells are closely spaced in regions where higher resolution is needed, such as near the major navigation channels, and through the Galveston Bay entrance. The grid configuration includes the two Entrance jetties to Galveston and the Texas City dike. Cell spacing varies from 254 meters to 2428 meters and from 580 meters to 3502 meters in the x and y directions, respectively. Each cell has a depth value obtained from bathymetric data for Galveston Bay available from NOAA's National Geophysical Data Center in gridded (15-second interval) format. Bathymetry generated from these data is shown in Figure 2.2.

A substantial number of cells cover the Texas shelf region east of the Bay entrance. This placement of the boundaries allows for internal dynamics to dominate the simulation of currents and the density field in the bathymetrically complex Galveston Entrance region, rather than increase uncertainty by specifying the boundary condition in an oversimplified manner and risk imposing a dynamic inconsistency. The grid has additional connections to the shelf through San Luis Pass at the entrance to West Bay and through Rollover Pass in East Bay.

The grid covers most of the water area of Galveston Bay, but cannot resolve all the small features along the shore such as the GIWW. The grid is detailed enough to represent the following features explicitly: Trinity River, San Jacinto River, and Buffalo Bayou as well as the GHC, HSC, GC, and TCC.

In the vertical, there are six sigma levels of varying thickness: σ = (0.0, -.1667, -.4167, -.5833, -.7643, -.9167, -1.00). This is considered sufficient to resolve the density stratification observed. Considering cell lengths and depths, the model is run with an external-mode time step of 10 s and an internal mode time step of 60 s. A 30-day simulation requires approximately 15 hours on an SGI Challenge L computer using 4 TFP chip cpus at full utilization with level two (O2) optimization.

The numerical model simulation requires driving forces (water levels, river discharges, winds) that are applied at the open boundaries on the grid. Each open boundary cell along the Texas shelf (Figure 2.1) requires a water level value and salinity and temperature values at all vertical levels at each model time step. The river boundaries require discharge, salinity, and temperature values. The wind is applied at the surface of all cells. At the closed boundaries there is zero momentum, salt transfer, and heat transfer. These requirements are discussed in detail for the astronomical tide simulation in Section 3 and for the complete meteorologically forced simulation in Section 4.

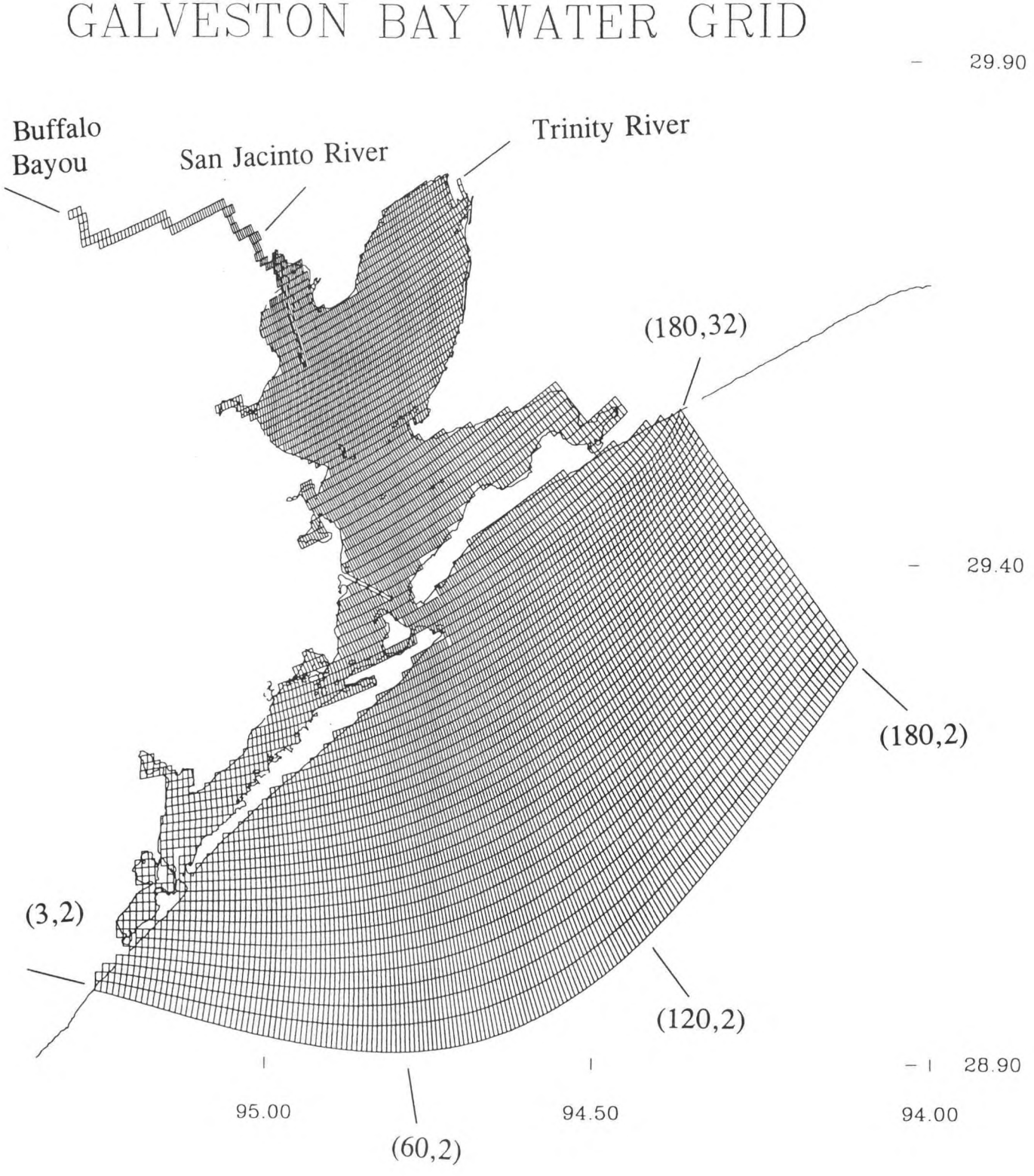

Figure 2.1. Galveston Bay curvilinear orthogonal grid, Texas shelf boundaries, and three rivers.

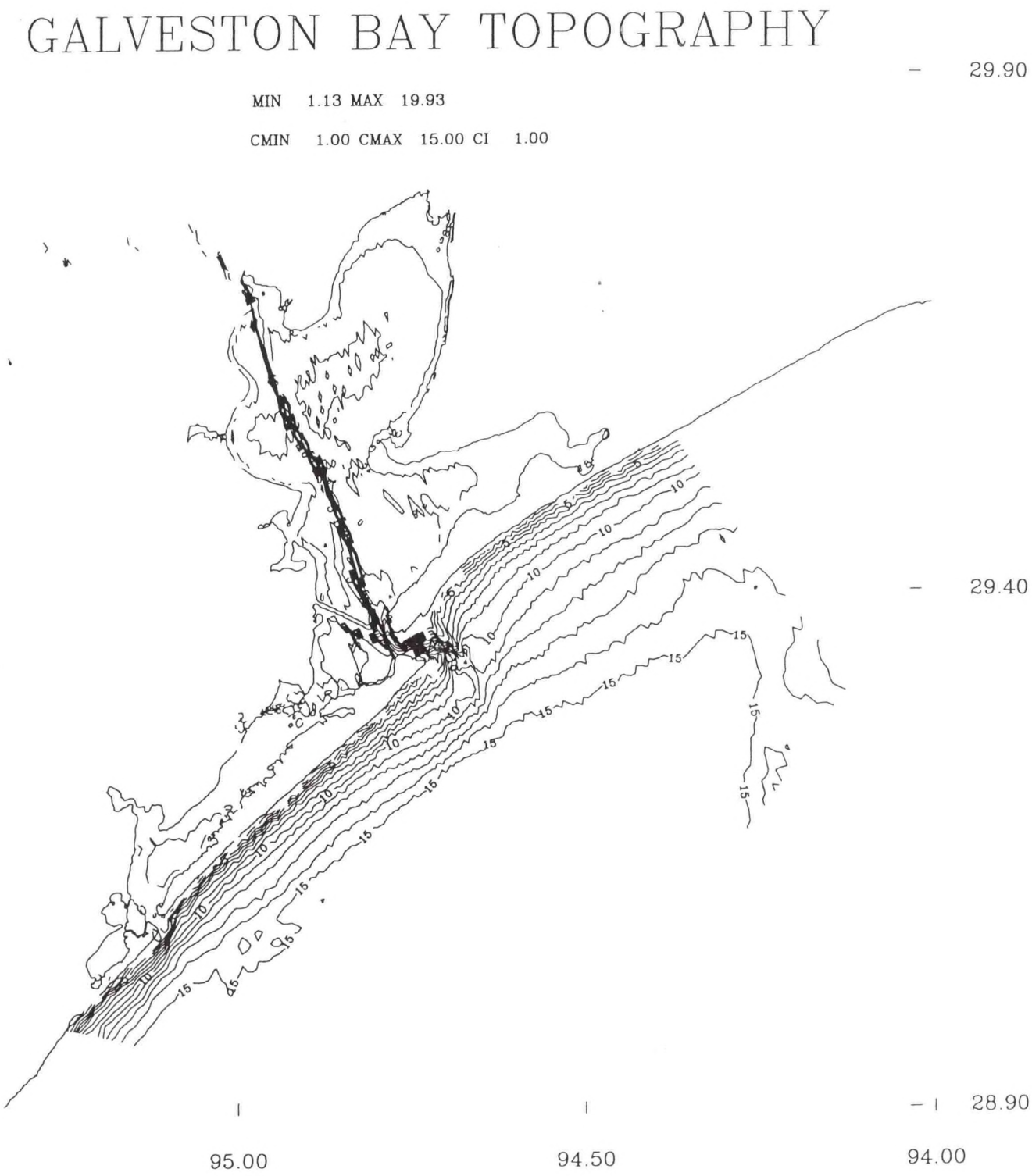

Figure 2.2. Isobaths contoured at 1-meter intervals.

3. ASTRONOMICAL TIDE CALIBRATION: MAY 1995

The computational grid was developed to accomodate a northwesterly propagating tide wave as well as a southwest to northeast coastal current system, which is developed during May in response to climatological northerly directed winds. The grid extended out onto the shelf in order to include the Galveston Approaches and Fairways, which were also to be surveyed. By extending the grid onto the shelf, it was hoped that the Gulf of Mexico order 9 km horizontal resolution numerical model being developed within the NOS Coastal Forecasting System Project could be used to provide offshore tidal and subtidal water level forcings and boundary density structures.

3.1. TEXAS SHELF BOUNDARIES

To define the tidal boundary condition, five points along the Gulf open boundary of the grid were used to specify tidal signals as indicated in the base map; namely, (3,2), (60,2), (120,2), (180,2), and (180,32). Between neighboring points a linear interpolation in the appropriate coordinate index was used to determine the tidal signal at each grid point. In addition, an attempt was made to use the results from the Oregon State University (OSU) global ocean inverse model solution using techniques developed by Bennett (1990) at each of these five points for M_2, S_2, N_2, K_2, K_1, O_1, P_1, and Q_1. The Bennett solution technique employs a 0.5° horizontal resolution and seeks to improve the 1° horizontally resolved results produced by Schwiderski (1980). Twelve additional constituents (J_1, M_1, OO_1, 2Q, ρ, 2N, R_2, T_2, λ_2, μ_2, ν_2, and L_2) were determined from the OSU solution based on formulas given by Schureman (1958). The long period constituents (Mf, Mm, Ssa) were also estimated using techniques developed by Foreman (1995). A second approach was also followed in which the near shore stations at Freeport, Galveston Pleasure Pier, Port Bolivar, and High Island were extended to the appropriate neighboring boundary points.

Vertical Datum Definitions

The following three vertical datums were considered in this study.

1) Mean Sea Level: (MSL) -- Tidal epoch (1960-1978) local mean sea levels at long term tide stations were considered to form a equipotential surface or constitute a vertical datum over the Galveston Bay System and adjacent continental shelf.

2) National Geodetic Vertical Datum 1929: NGVD (1929) -- Local mean sea levels at 24 locations throughout Canada and the United States were connected (held fixed) and assumed to form a equipotential surface. Approximately 100,000 km of leveling was used to define the 1929 vertical control network.

3) North American Vertical Datum 1988: NAVD (1988) -- 625,000 km of leveling has been added to the 1929 vertical control network. First order releveling of major portions of 1929 vertical control network was performed. Only the height of the primary tidal benchmark at Father Point, Rimouski, Quebec Canada was held fixed.

In developing 2) and 3), Helmert blocking was used to perform a simultaneous least-squares adjustment of the entire set of leveling observations (Zilkoski et al., 1992).

In this study, we adopted approach 1) and used tidal epoch mean sea level as model datum but did not consider it as an equipotential surface. Water depths with respect to tidal epoch mean sea level were established. It was recognized that freshwater inflows would establish a mean simulation period water level surface over the Bay system. As a result, to affect a smooth transition of the mean water level fields through the Passes and account for shelf circulation, water level offsets at cell locations shown in Figure 2.1 along the open boundary were applied as given in Table 3.1 below.

Table 3.1. Open boundary signal water level offsets

Signal No.	Boundary Grid Cell	Water Level Station	May 1995 Offset (cm)	Calibration Mean (cm)	June 1995 Simulation Offset (cm)	Mean (cm)
1	(3,2)	877-2440	3.0	6.7	3.0	24.4
2	(60,2)	877-1510	3.5	6.4	3.5	23.9
3	(120,2)	877-1510	4.0	7.0	4.0	24.0
4	(180,2)	877-1328	-13.5	7.0	29.0	21.1
5	(180,32)	877-0923	3.0	15.1	3.0	26.4

Approach 3) is to be preferred over approaches 1) and 2) and was used in the Long Island Sound Study (Schmalz et al., 1994) along with water level offsets along the open boundary calibrated based on ADCP derived East River subtidal transports. Due to subsidence issues, NGVD (1929) and NAVD (1988) are not considered reliable within the study area. Additional efforts are in progress to update the NAVD (1988) datum and when this work is complete, approach 3) should be considered.

Specification of Water Level Forcings

$$h_I(t) = H_0^I + \sum_{j=1}^{37} f_j H_{jI} \cos\left(a_j t + (V_0 + u)_j^G - \kappa'_{jI}\right) \tag{3.1}$$

where

$h_I(t)$ ≡ predicted elevation at time t for boundary signal I (m),
f_j ≡ node factor for constituent j for the prediction period,
$(V_0 + u)_j^G$ ≡ Greenwich equilibrium argument for constituent j for the prediction period (°),
a_j ≡ constituent j speed (°/hr),
H_{jI} ≡ amplitude of constituent j (ft) for boundary signal I,
κ'_{jI} ≡ phase of constituent j (°) for boundary signal I,

t	$\equiv$	local Standard Time (hrs) from January 1, 1995, and
H^I_o	$\equiv$	mean water level relative to the model vertical datum (m)

The above equation is used to reconstruct the predicted water level based upon the set of harmonic constants $(H_{jI}\ ,\ \kappa'_{jI})$. As indicated in the second column of Table 3.1, the tidal boundary signals at (3,2), (60,2), (120,2), (180,2), and (180,32) were modified from the Freeport (877-2440), Galveston Pleasure Pier (877-1510), Galveston Pleasure Pier (877-1510), Port Bolivar (877-1328), and High Island (877-0923), Texas tidal signals, by applying the following dimensionless amplitude adjustment and phase lag in hours to each constituent at each station, (1.0, -0.5 hr), (1.02, -0.3 hr), (1.04, -1.0 hr), (1.024, -0.6 hr), and (1.2, 0.0 hr), respectively. The final sets of tidal constituents used at each of the five boundary points are given in Table 3.2.

Note H^I_o corresponds to the water level offsets to be applied along the open Texas Shelf boundary and were varied as described below as shown in columns three and five in Table 3.1.

The total water level for each boundary signal is given by the following relationship.

$$ht_I\ (t) \ = \ h_I\ (t) \ + \ \alpha r_I\ (t) \qquad (3.2)$$

where

$ht_I\ (t)$	$\equiv$	Total elevation at time t for boundary signal I.
$h_I\ (t)$	$\equiv$	Predicted elevation at time t for boundary signal I.
α	$\equiv$	Switch equal to either zero or one for boundary signal I.
$r_I\ (t)$	$\equiv$	Residual elevation at time t for boundary signal I.

For the May 1995 simulation $\alpha = 0$, and the subtidal water level residuals are set to zero. In this case H^I_o is determined in the following manner. In Equation (3.1) compute the average of $h_I\ (t)$ over the one month simulation period with H^I_o assumed zero, $<h_I\ (t)>$. Then based on the resulting means adjusted to give the desired tilt, $<h_{dI}\ (t)>$, finally we compute $H^I_o = <h_{dI}\ (t)> - <h_I\ (t)>$. Note from Table 3.1 the onshore decrease in mean water surface elevation of 8.1 cm from (180,32) to (180,2) to support the expected northerly directed shelf current.

For the June 1995 simulation $\alpha = 1$, and the subtidal water level residuals are considered. In this case H^I_o is determined by a slightly more involved procedure. Again in Equation (3.1) compute the average of $h_I\ (t)$ over the one month simulation period with H^I_o assumed zero, $<h_I\ (t)>$. Next compute the average of $r_I\ (t)$ over the simulation period, $<r_I\ (t)>$. As a first guess use the May 1995 H^I_o, H^{iI}_o. Then compute the initial means in column 6 of Table 3.1, $<h_{dI}\ (t)> = H^{iI}_o + <r_I\ (t)> + <h_I\ (t)>$. Adjust H^{iI}_o to H^I_o such that the desired boundary tilts are obtained to support the expected current systems. Note from Table 3.1 the onshore decrease in mean water surface elevation of 5.3 cm from (180,32) to (180,2) to support the northerly directed shelf current.

As noted in Table 3.1, Port Bolivar was used to form the open boundary signal 4 at cell (180,2). The Sa and Ssa at Port Bolivar provided by OLLD are substantially different than those at the other stations provided by OLLD used to form open boundary signals 1-3 and 5. This necessitated the use of water level offset factors at boundary cell (180,2), which were larger in magnitude than those used at the other open boundary cells shown in Table 3.1. To obtain a more uniform range in offsets, the Sa and SSa must be spatially consistent at all stations. Ideally they should be determined based on several years or even over a tidal epoch. From Table 3.3, the harmonic constants at Port Bolivar were based on only six months of data, while those used at the other open boundary stations were based on one year of data.

A linear spatial interpolation was performed in the first grid index between signals 1 and 2, 2 and 3, and 3 and 4, to determine the water surface elevation signals between (3,2) - (60,2), (60,2) - (120,2), (120,2) - (180,2), respectively, and in the second grid index between signals 4 and 5, to determine water surface elevation signals between (180,2) - (180,32).

Specification of Density Forcings

In specifying the salinity and temperature boundary condition, three points along the open Gulf boundary of the grid were used as shown in Figure 2.1; namely, (3,2), (180,2), and (180,32). Between neighboring points a linear interpolation in the appropriate coordinate index was used to determine the signal at each grid point. Linear temporal interpolation of climatological profiles were used based on techniques described in 3.4 below.

3.2. RIVER BOUNDARIES

The Trinity River, San Jacinto River, and Buffalo Bayou were specified as outlined in Schmalz (1994) as inflows to cells (164,74), (73,83), and (15,94), respectively. The mean monthly average flow of the Trinity River at Romayor, Texas over the period 1924 - 1990 was used to develop mean monthly streamflows. The Trinity River at Romayor, Texas gage readings were divided by 0.87 to obtain the total freshwater inflows into the Bay. The Trinity River was assumed to represent 87% of the total freshwater inflow. To determine the San Jacinto River inflow, we assumed that for Trinity River inflows greater than 250 m^3/s, the San Jacinto River inflow was 8% of the total inflow. If Trinity River inflows were not greater than 250 m^3/s, the San Jacinto River inflow was assumed to be zero. The Buffalo Bayou inflow was assumed equal to 6% of the total freshwater inflow. Average daily inflows were determined by linear interpolation of the mean monthly Trinity River at Romayor, Texas gaged flows and the application of the above rules and are shown in Figures 3.1 - 3.3. River inflow salinity was assumed zero, while river temperatures were set equal to those of the cell in which they entered.

3.3. THE AIR-SEA BOUNDARY

In the astronomical tide simulation, wind and atmospheric pressure anomaly forcings were set to zero. Tidal potential generation was not considered. The sea surface temperature was specified by linear interpolation of climatological sigma level one fields determined on 1 January, 1 April, and 1 July using grid patch interpolation as discussed below.

3.4. INITIALIZATION

Following the grid patch interpolation procedures developed in the Long Island Sound Study (Schmalz, 1994), representative salinity profiles were determined at the four corners of the each grid patch. A separate set of grid patches was used to cover the entire grid to represent salinity conditions on 1 January, 1 April, and 1 July based on characteristic salinity fields developed by Orlando, et al. (1993). An inverse distance squared interpolation procedure (Schmalz, 1994) was used to develop the salinity at patch internal cell at the appropriate z level water depth. In addition, it was necessary to use uni-directional interpolation through the Passes, and user controlled Laplacian smoothing to obtain the final salinity fields. A temporal linear interpolation was used to produce the near surface and near bottom salinity fields corresponding to 1 May 1995, which are shown in Figures 3.4 and 3.5, respectively.

For temperature, the same grid patch interpolation procedures were used. Offshore temperatures were available from Templeton et al. (1963) and it was assumed that on 1 January Bay temperatures were 0.5 °C colder, while on 1 July they were 0.5 °C warmer. This allowed the Bay interior grid cell patch corner temperature profiles to be determined required by the interpolation procedure. Bay-wide temperatures ranged form 8.9 - 9.2 °C, 19.7 - 19.2 °C, and 27.5 - 27.8 °C on 1 January, 1 April, and 1 July, respectively. A temporal linear interpolation was used to produce the near surface and near bottom temperature fields corresponding to 1 May 1995, which are shown in Figures 3.6 and 3.7, respectively. Note initial model velocities were set to zero.

3.5. SUMMARY OF EXPERIMENTS AND FINAL WATER LEVEL COMPARISONS

The following five day experiments were initially performed over the period 1-5 May 1995 prior to complete month experiments. The purpose of these experiments was to initially assess the model water level response using reconstructed signals from the harmonic constants sets in Table 3.3 at Eagle Point, Clear Lake, Morgans Point, Galveston Pier 21, and Galveston Pleasure Pier. Changes in geometry and open boundary forcings were assessed. In all simulations, the bottom roughness in Equation (3.31), z_o=1.0 cm, and the Smagorinsky horizontal eddy coefficient in Equation (2.13) , C_H = 0.05.

I. Experiment D0: OSU tide solution with no water level offsets on the open boundary. No river No water level offsets along the open boundary. Rms difference between the simulated and reconstructed signals at the above 5 stations was order 11 cm.

II. Experiment D1: OSU tide solution with no water level offsets along the open boundary. Climatological river inflows included. Rms differences were order 10 cm.

III. Experiment D2: OSU tide solution except for M2 (used Galveston Pleasure Pier values) with climatological river inflows. Water level offsets, 3-4 cm, along the open boundary were applied. Rms differences were order 10 cm.

IV. Experiment D3: Galveston Pleasure Pier tidal constituents applied with no amplitude and

phase adjustments to open boundary. Water level offsets, 3-4 cm, along the open boundary were applied. Climatological river inflows also included. Rms differences were order 6 cm with improved agreement in shape.

V. Experiment D4: Same characteristics as D3 but with a revised geometry through Galveston Entrance and San Luis Pass. Depths were modified to include HSC, GC, and TCC navigation channels which were not accurately represented in the NOS 15 second bathymetry. Jetties were added to the Galveston Entrance. Amplitude adjustment factors 1.1-1.2 and phase leads of 0.3-1.0 hour relative to Galveston Pleasure Pier signal were applied along the boundary. Rms differences were order 5.5 cm.

VI. Experiment D5: Same characteristic as D4 but with new amplitude adjustments along the boundary. Amplitude adjustment factors reduced to 1.02-1.04 relative to Galveston Pleasure Pier were applied along the open boundary. Rms differences were order 5.0 cm.

A preliminary astronomical tide calibration over 1-31 May 1995 with the characteristics of D5 simulation was then performed using the above five stations. Rms differences were order 5 cm.

Upon completion of the analysis of tide gauge data in West Bay, additional experiments were performed to improve simulated tidal characteristics in this region as well as within Galveston Bay. Along the open boundary signals at cells (3,2), 180,2), and (180,32), were specified via modification of the Freeport, Port Bolivar, and High Island reconstructed signals as given in Table 3.1. The configuration of the San Luis Pass was altered and the grid bathymetry modified to more closely align with the HSC. In addition, the bottom roughness z_o was reduced by a factor of five to 0.2 cm and the Smagorinsky horizontal eddy coefficient C_H was reduced by a factor of 10 to 0.005. The effect on simulated water levels due to the reduction of the bottom roughness was under 1 cm. Simulated water level ranges were increased by approximately 2 cm by reduction of the Smagorinsky horizontal eddy coefficient. The interpolation procedure along the open boundary from cells (3,2) to (60,2) was modified such that from (3,2) to (54,2) signal 1 was directly applied with the interpolation between signals 1 and 2 concentrated between cells (54,2) and (60,2). This revised interpolation resulted in slight improvements in water level comparsions at Alligator Point and in Christmas Bay, while results in Galveston Bay were unchanged. All in all a total of 13 five day and 4 thirty day simulations were performed.

Final simulated and predicted water levels are compared at the tide gauge locations shown in Figure 3.8 over the period 2-31 May, 1995. The first day was considered as the spin-up period. In the reconstruction of water levels, the harmonic analysis process is as summarized in Table 3.3. For the NOS and TCOON stations a 365 day least squares harmonic analysis was used except at Port Bolivar, where only a 185 day least squares analysis was performed due to data gaps. Demeaned water level time series are compared for each station in Figures 3.9 - 3.22. Root mean square (rms, RMS) differences and a dimensionless relative error (RE), which ranges from zero (perfect agreement) to one (no agreement), developed by Wilmott et al. (1985) are given in Table 3.4. Simulated and observed water level means are shown in Table 3.5. In general, simulated water levels are in agreement with reconstructed levels to within 5 cm rms and relative errors are less than 0.05. From Figures 3.9 - 3.11, additional improvements in the tidal boundary signals could be made, which would further improve near shelf simulation

characteristics and thereby translate into improvements within the Bay proper. Note in these figures, the indicator of agreement (IND AGRMT) equals one minus the relative error (RE). Discrepancies between simulated and reconstructed water levels appear to be more pronounced during the third Spring tide cycle. Mean water levels offshore were adjusted to the values shown in Table 3.1 in order to provide for a smooth transition in mean water level fields through the Passes in response to freshwater inflow set-up within the Bay. While no direct measurements of tide cycle averaged transports through the Passes were available to calibrate the adjustment of these offshore boundary water level offsets, the 7-8 cm downward tilt from (180,32) to (180,2) would geostrophically support an order 30 cm/s northerly directed coastal current.

3.6 ADDITIONAL ISSUES

To improve the astronomical calibration the following additional experiments appear to be warranted:

1) spatial variation of the bottom roughness, z_0, based on bottom characteristics determined from sediment mappings.

2) spatial or system-wide adjustment of water depths with respect to model datum to account for subsidence effects or other changes in water depth.

3) further adjustment of mean water level offsets along the open boundary to account for shelf circulation.

4) investigation of the inclusion of the tide generation potential.

In addition, 29-day harmonic analysis (Dennis and Long, 1971) of simulated water levels should be performed in order to partition rms differences into amplitude and phase errors. Gain and phase lag statistics as outlined by Hess and Bosley (1992) could then be used to more formally assess the water level calibration.

Table 3.2. Open boundary cell water surface elevation harmonic constants

	Boundary Cell (3,2)		Boundary Cell (60,2)		Boundary Cell (120,2)	
Cons.	Amp (m)	Kp (o)	Amp (m)	Kp (o)	Amp (m)	Kp (o)
M2	0.097	90.300	0.137	92.200	0.139	71.900
S2	0.025	83.600	0.031	84.000	0.031	63.000
N2	0.024	72.300	0.033	77.900	0.034	58.000
K1	0.155	290.500	0.171	293.900	0.175	283.400
M4	0.005	154.400	0.006	195.600	0.006	155.000
O1	0.145	290.700	0.158	292.800	0.161	283.000
M6	0.001	163.300	0.001	45.900	0.001	345.000
MK3	0.001	140.500	0.001	90.000	0.001	59.200
S4	0.001	289.000	0.001	352.400	0.001	310.400
MN4	0.003	101.800	0.002	154.500	0.002	114.300
V2	0.005	78.600	0.006	71.600	0.006	51.700
S6	0.001	66.700	0.001	50.200	0.001	347.300
U2	0.003	20.600	0.005	5.000	0.005	345.400
2N2	0.004	52.700	0.008	48.200	0.008	28.700
OO1	0.005	308.500	0.007	328.800	0.007	317.500
LB2	0.001	50.600	0.001	152.900	0.001	132.300
S1	0.009	213.400	0.013	235.000	0.013	224.500
M1	0.011	313.500	0.013	310.300	0.013	300.200
J1	0.009	279.900	0.010	270.900	0.011	260.000
MM	0.017	303.800	0.032	261.700	0.033	261.300
SSA	0.095	51.200	0.113	56.500	0.116	56.500
SA	0.057	154.400	0.080	171.500	0.082	171.500
MSF	0.015	231.500	0.027	295.200	0.028	294.500
MF	0.016	305.500	0.003	194.100	0.003	193.400
RHO1	0.007	296.400	0.008	293.100	0.008	283.600
Q1	0.033	274.800	0.035	280.300	0.035	271.000
T2	0.004	117.200	0.004	109.600	0.004	88.600
R2	0.002	56.400	0.002	11.900	0.002	350.900
2Q1	0.004	219.900	0.002	322.500	0.002	313.500
P1	0.050	290.400	0.050	290.800	0.051	280.300
2SM2	0.001	136.400	0.001	192.700	0.001	171.000
M3	0.002	131.000	0.002	129.500	0.002	99.000
L2	0.003	132.600	0.005	132.500	0.005	111.900
2MK3	0.001	83.700	0.001	71.800	0.001	41.800
K2	0.005	97.100	0.005	83.800	0.005	62.800
M8	0.001	236.100	0.001	58.900	0.001	337.700
MS4	0.002	171.100	0.004	226.700	0.004	185.400

Table 3.2. (Cont.) Open boundary water surface elevation harmonic constants

	Boundary Cell (180,2)		Boundary Cell (180,32)	
Cons.	Amp (m)	Kp (o)	Amp (m)	Kp (o)
M2	0.068	102.100	0.191	98.500
S2	0.010	134.000	0.053	89.100
N2	0.020	76.300	0.046	78.400
K1	0.113	324.700	0.205	296.800
M4	0.002	54.700	0.008	231.600
O1	0.120	326.800	0.189	295.600
M6	0.002	83.700	0.002	70.200
MK3	0.012	202.100	0.002	75.200
S4	0.001	66.700	0.003	357.100
MN4	0.002	50.400	0.003	187.400
V2	0.005	49.800	0.005	75.600
S6	0.000	66.200	0.001	309.300
U2	0.002	35.100	0.005	17.900
2N2	0.005	6.000	0.009	67.400
OO1	0.016	359.800	0.008	311.300
LB2	0.005	252.800	0.002	295.900
S1	0.010	160.100	0.016	197.900
M1	0.011	333.100	0.017	328.600
J1	0.005	339.700	0.008	309.100
MM	0.007	247.500	0.024	287.500
SSA	0.375	78.100	0.183	60.000
SA	0.449	312.100	0.096	140.100
MSF	0.042	313.600	0.041	287.300
MF	0.032	273.000	0.003	312.000
RHO1	0.011	304.200	0.008	327.800
Q1	0.026	309.500	0.039	285.600
T2	0.006	75.500	0.005	153.600
R2	0.014	270.900	0.004	11.000
2Q1	0.004	108.000	0.001	128.000
P1	0.038	347.000	0.061	289.500
2SM2	0.002	137.200	0.001	153.500
M3	0.002	65.300	0.001	359.000
L2	0.004	203.000	0.009	127.000
2MK3	0.010	212.600	0.002	19.000
K2	0.023	158.100	0.010	107.100
M8	0.000	144.000	0.000	286.500
MS4	0.002	57.900	0.004	235.900

Table 3.3. Water level station harmonic analysis summary

Note * designates a station which is used directly or extrapolated to form an open boundary signal.

Location	Station No.	Analysis Type	Analysis Period
*Freeport, TX	877-2440	365 Day LS	Oct 1, 1993 - Sep 30, 1994
Smith Point, TX	877-0931	29 Day	Jun 1, 1995 - Jun 29, 1995
Round Point, TX	877-0559	29 Day	Apr 1, 1994 - Apr 29, 1994
Galveston GPS Buoy, TX	877-1624	29 Day	Jul 13, 1995 - Aug 10, 1995
Trinity River Channel Platform	877-1021	29 Day	May 21, 1995 - Jun 18, 1995
*Port Bolivar, TX	877-1328	185 Day LS	Oct 29, 1994 - May 1, 1995
Christmas Bay, TX	877-2132	365 Day LS	Jan 1, 1994 - Dec 31, 1994
Morgans Point, TX	877-0613	365 Day LS	Jan 1, 1994 - Dec 31, 1994
Clear Lake, TX	877-0933	365 Day LS	Jan 1, 1994 - Dec 31, 1994
Eagle Point, TX	877-1013	365 Day LS	Jan 1, 1994 - Dec 31, 1994
Galveston Pier 21, TX	877-1450	365 Day LS	Jan 1, 1994 - Dec 31, 1994
*Galveston Pleasure Pier, TX	877-1510	365 Day LS	Jan 1, 1994 - Dec 31, 1994
Rollover Pass, TX	877-0971	365 Day LS	Jun 1, 1994 - May 31, 1995
*High Island, TX	877-0923	365 Day LS	Jun 1, 1994 - May 31, 1995

Table 3.4 Astronomical tide calibration RMS and RE summary

NOS-DGPS 30-DAY CALIBRATION:
ELEVATION (M) JULIAN DAYS (1995) 122.00 - 152.00

STATION	RMS ERROR	RELATIVE ERROR
GALVESTON PLEASURE PIER	0.05	0.02
GALVESTON CHANNEL PIER 21	0.06	0.05
MORGANS POINT	0.05	0.04
CLEAR LAKE	0.07	0.09
EAGLE POINT	0.05	0.04
PORT BOLIVAR	0.07	0.05
GALVESTON PIER 21 (677)	0.04	0.02
GALVESTON PLEASURE PIER (677)	0.04	0.01
OFFSHORE BOUNDARY (3,2)	0.00	0.00
OFFSHORE BOUNDARY (60,2)	0.01	0.00
OFFSHORE BOUNDARY (120,2)	0.01	0.00
OFFSHORE BOUNDARY (180,2)	0.00	0.00
OFFSHORE BOUNDARY (180,32)	0.01	0.00
SMITH POINT	0.07	0.09
ROUND POINT	0.07	0.07
TRINITY RIVER CH. PLT.	0.07	0.09
GALVESTON, GPS BUOY	0.07	0.03
ROLLOVER PASS	0.08	0.11
HIGH ISLAND	0.04	0.01
CHRISTMAS BAY	0.06	0.10
ALLIGATOR POINT	0.03	0.02

Table 3.5 Astronomical tide calibration mean water level summary

NOS-DGPS 30-DAY CALIBRATION:
ELEVATION (M) JULIAN DAYS (1995) 122.00 - 152.00

STATION	MODEL MEAN	OBSERV. MEAN
GALVESTON PLEASURE PIER	0.12	0.02
GALVESTON CHANNEL PIER 21	0.14	0.03
MORGANS POINT	0.15	0.07
CLEAR LAKE	0.15	0.06
EAGLE POINT	0.15	0.05
PORT BOLIVAR	0.13	0.21
GALVESTON PIER 21 (677)	0.14	0.03
GALVESTON PLEASURE PIER (677)	0.12	0.03
OFFSHORE BOUNDARY (3,2)	0.07	0.04
OFFSHORE BOUNDARY (60,2)	0.07	0.03
OFFSHORE BOUNDARY (120,2)	0.07	0.03
OFFSHORE BOUNDARY (180,2)	0.08	0.22
OFFSHORE BOUNDARY (180,32)	0.15	0.10
SMITH POINT	0.14	0.00
ROUND POINT	0.16	0.00
TRINITY RIVER CH. PLT.	0.14	0.00
GALVESTON, GPS BUOY	0.11	0.00
ROLLOVER PASS	0.14	0.09
HIGH ISLAND	0.14	0.10
CHRISTMAS BAY	0.14	0.01
ALLIGATOR POINT	0.14	0.01

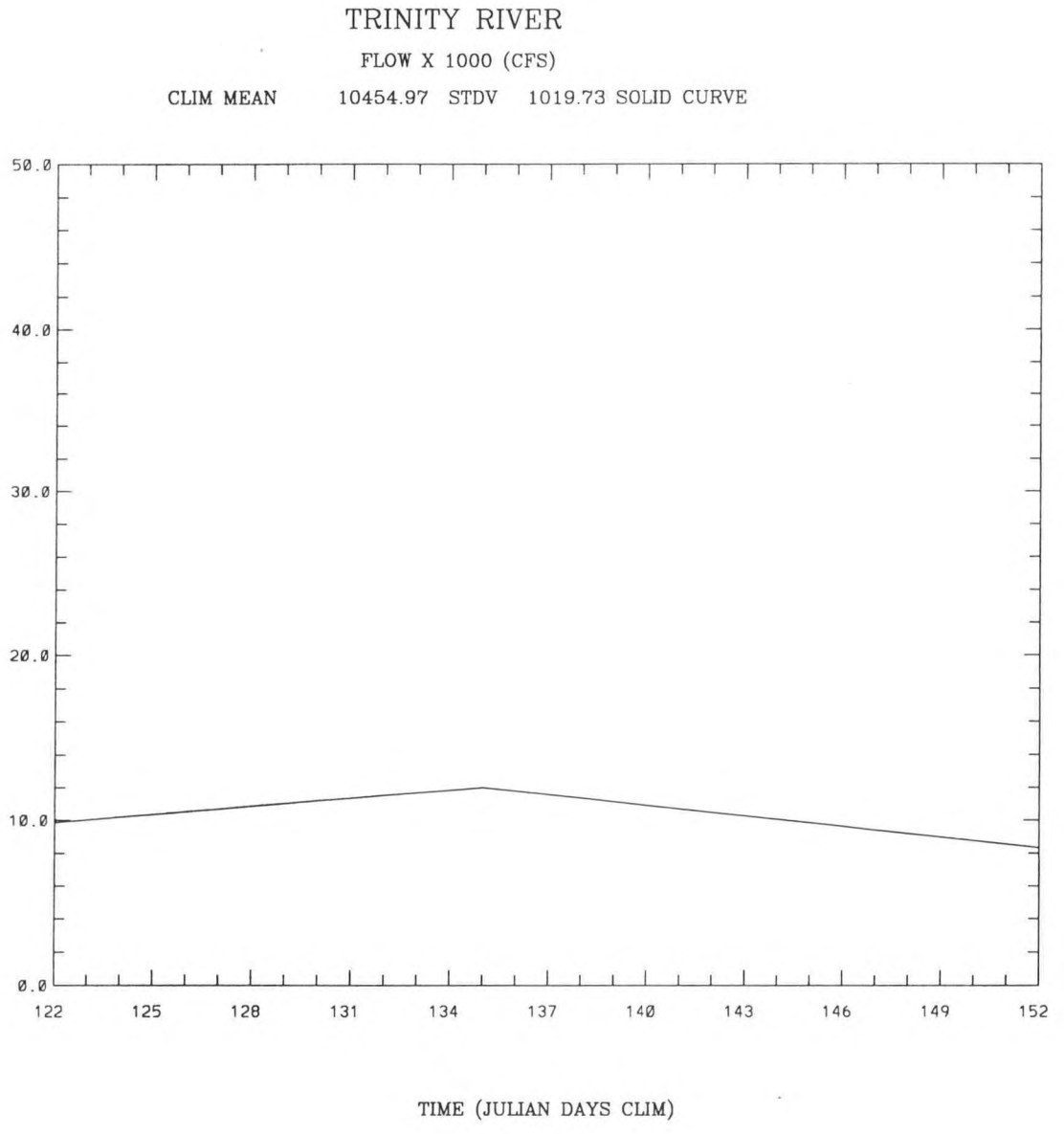

Figure 3.1. Trinity River May 1995 climatological flow rate (cfs)

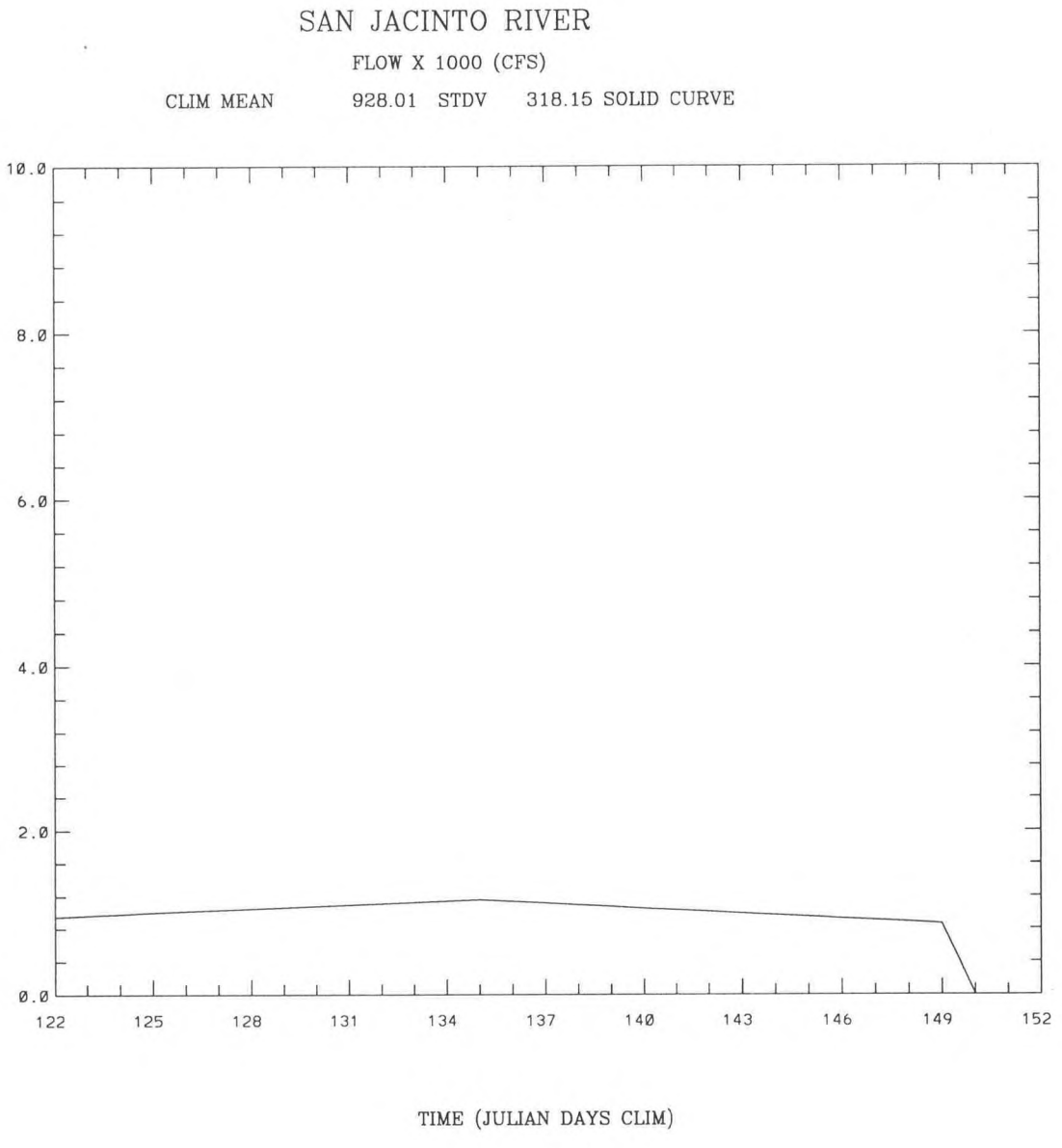

Figure 3.2. San Jacinto River May 1995 climatological flow rate (cfs)

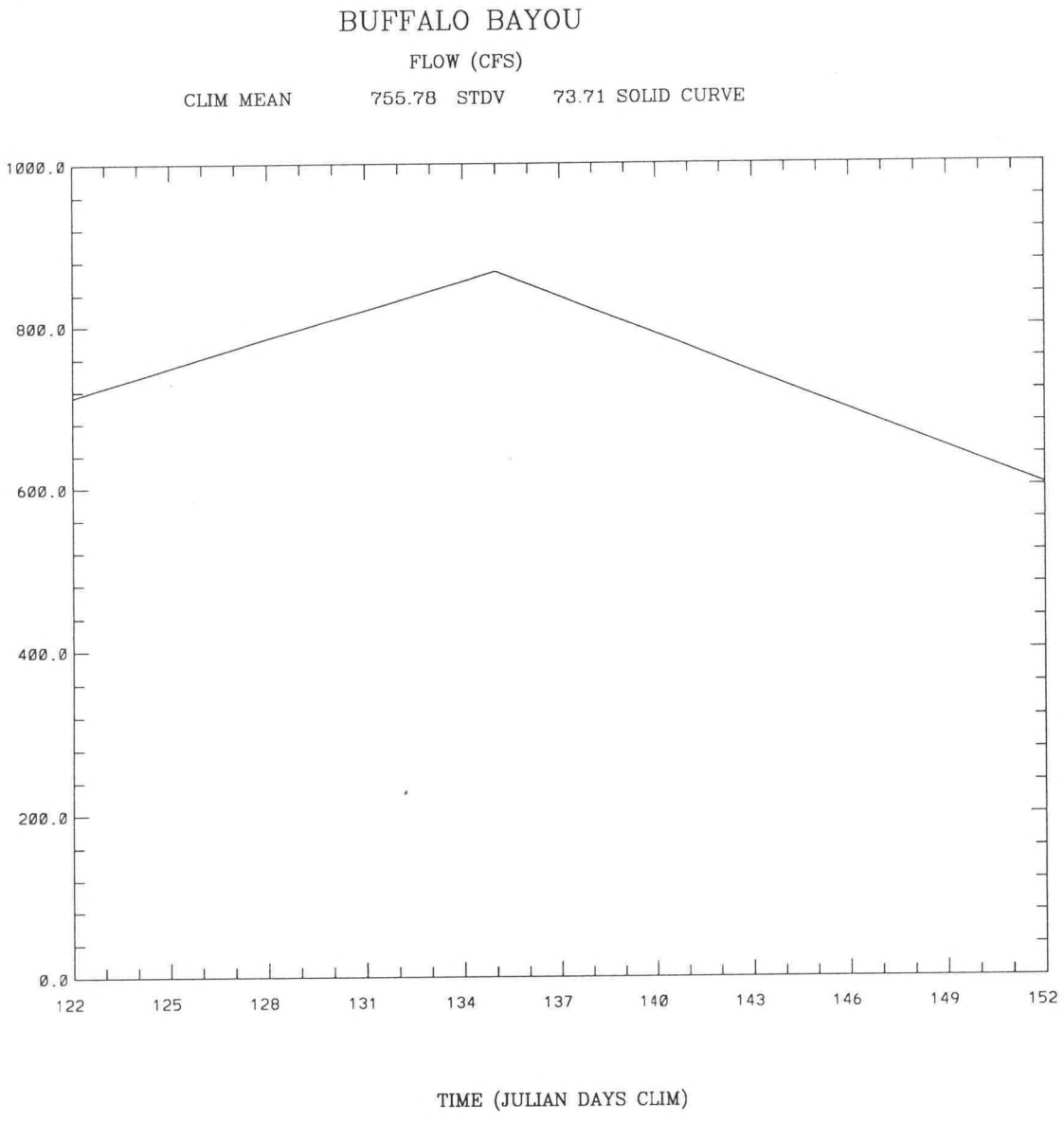

Figure 3.3. Buffalo Bayou May 1995 climatological flow rate (cfs)

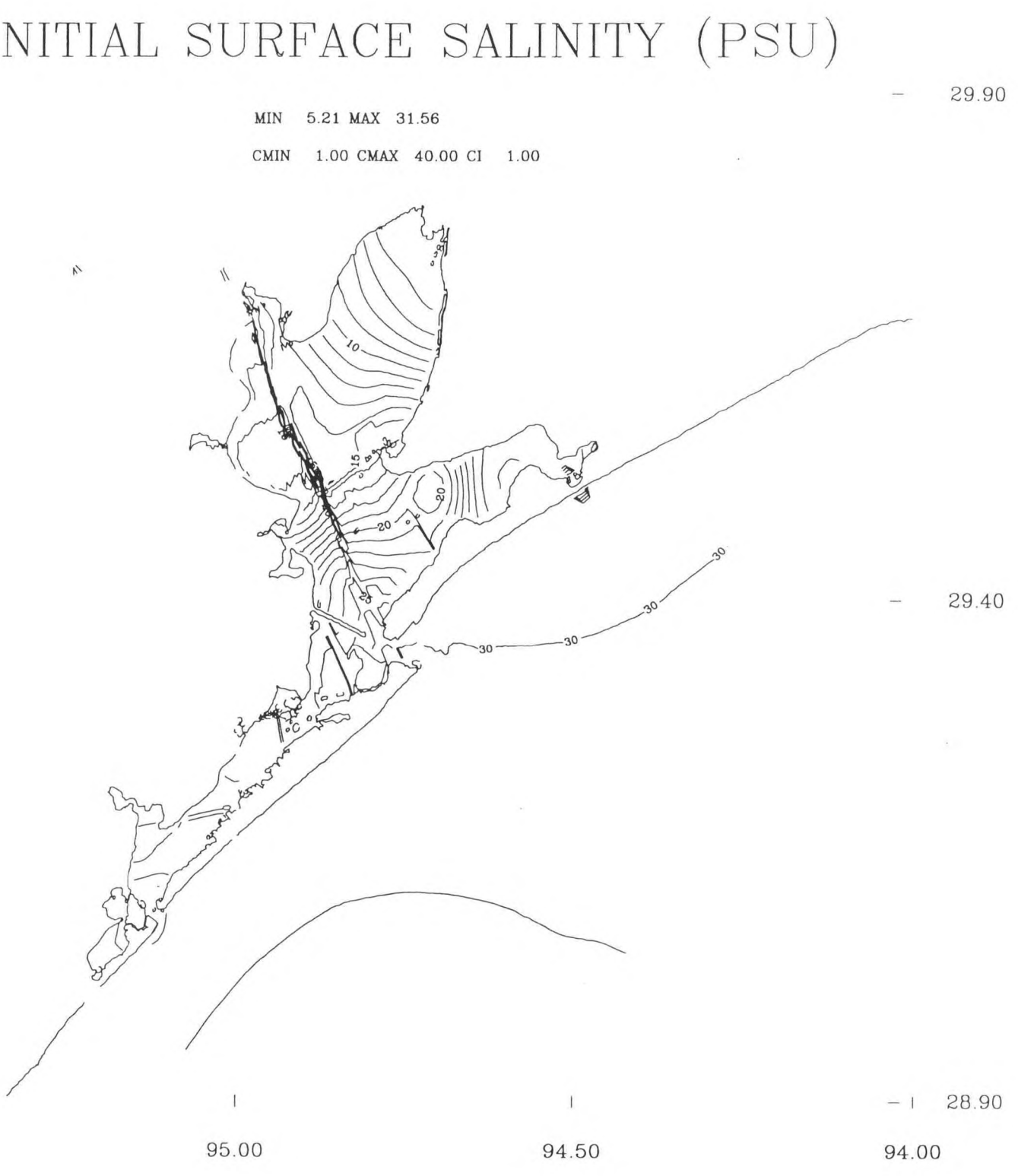

Figure 3.4. 1 May 1995: initial near-surface salinity field

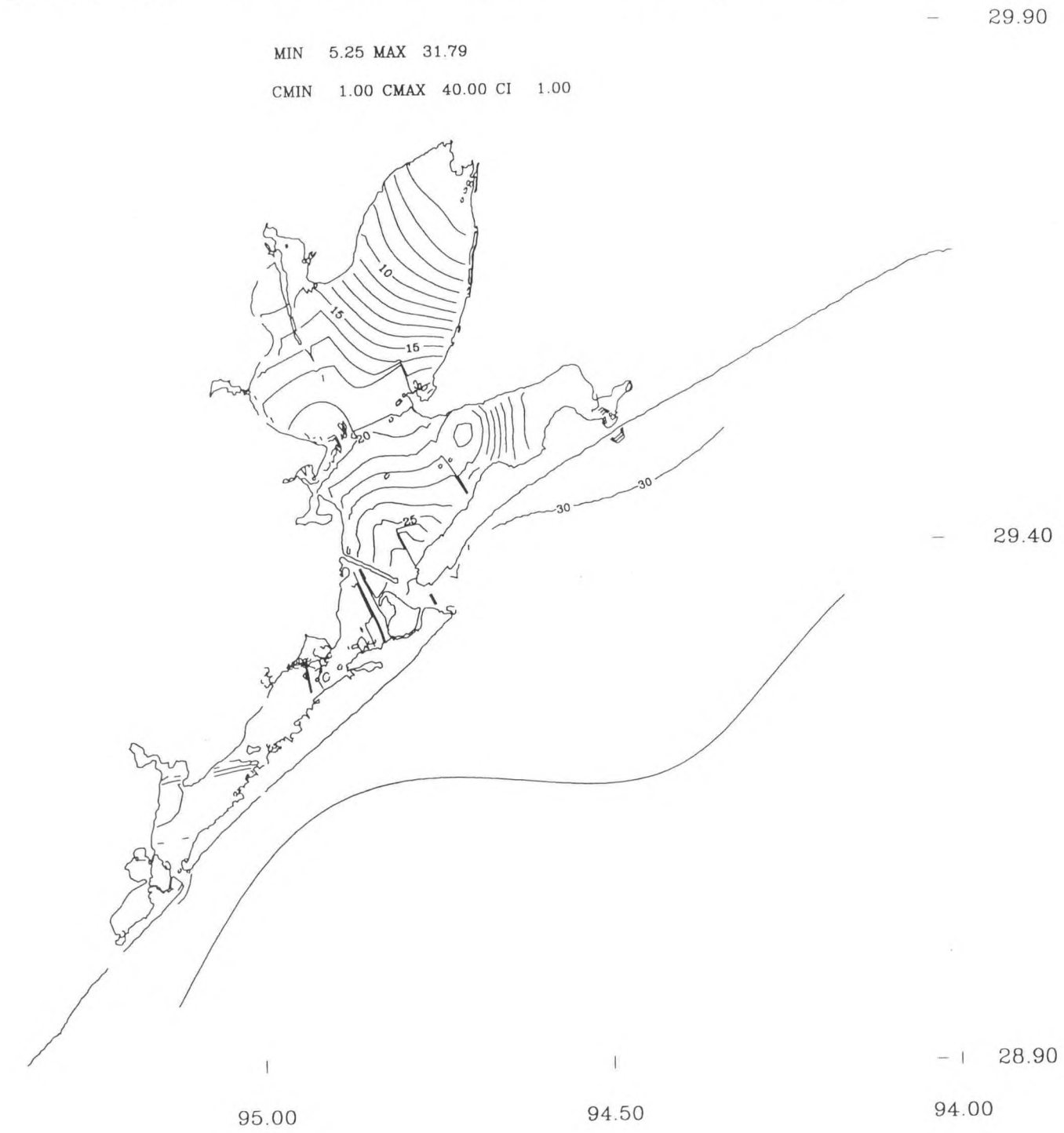

Figure 3.5. 1 May 1995: initial near-bottom salinity field

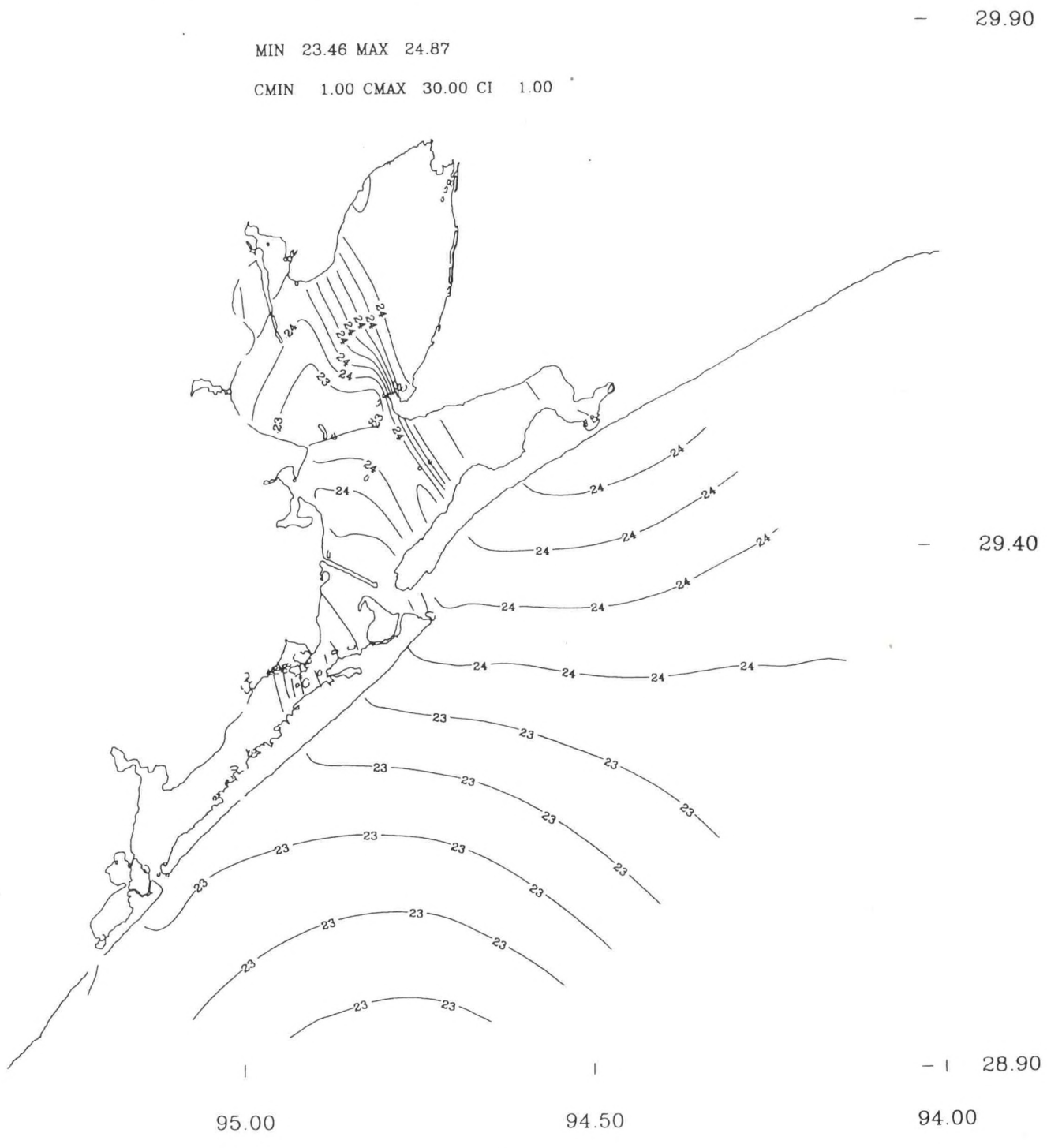

Figure 3.6. 1 May 1995: initial near-surface temperature field

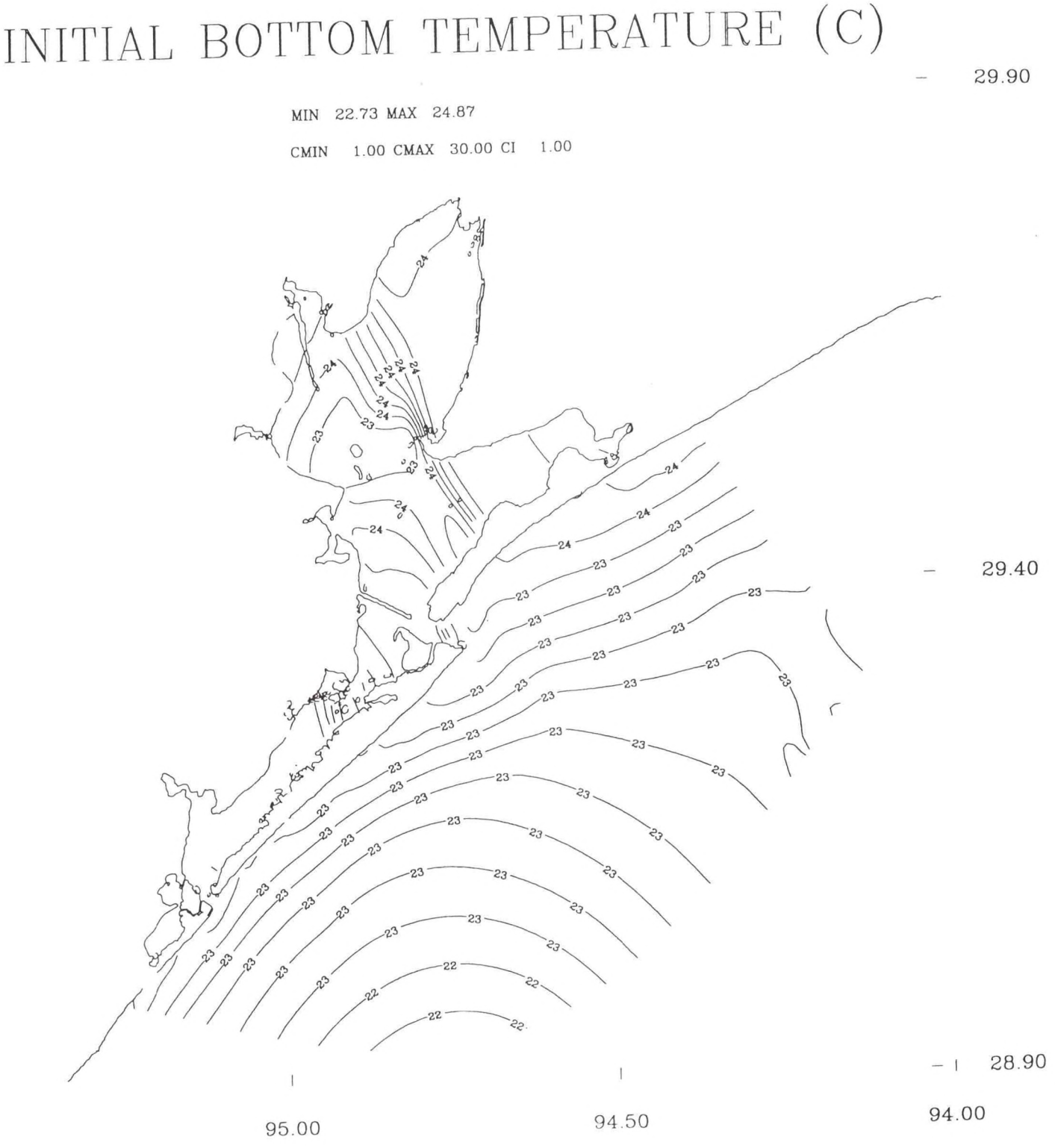

Figure 3.7. 1 May 1995: initial near-bottom temperature field

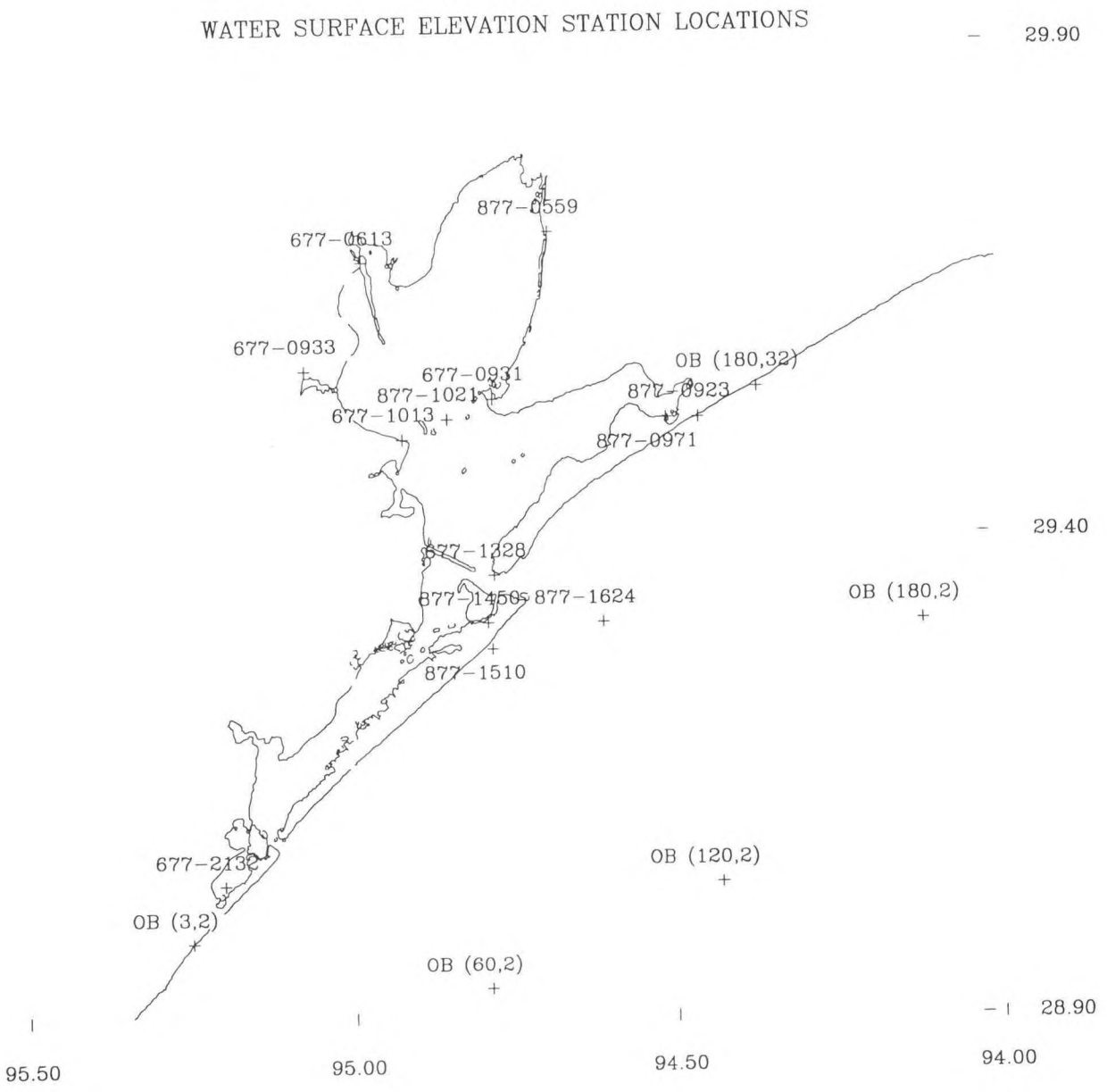

Figure 3.8. May 1995 Astronomical tide simulation water level gauge locations

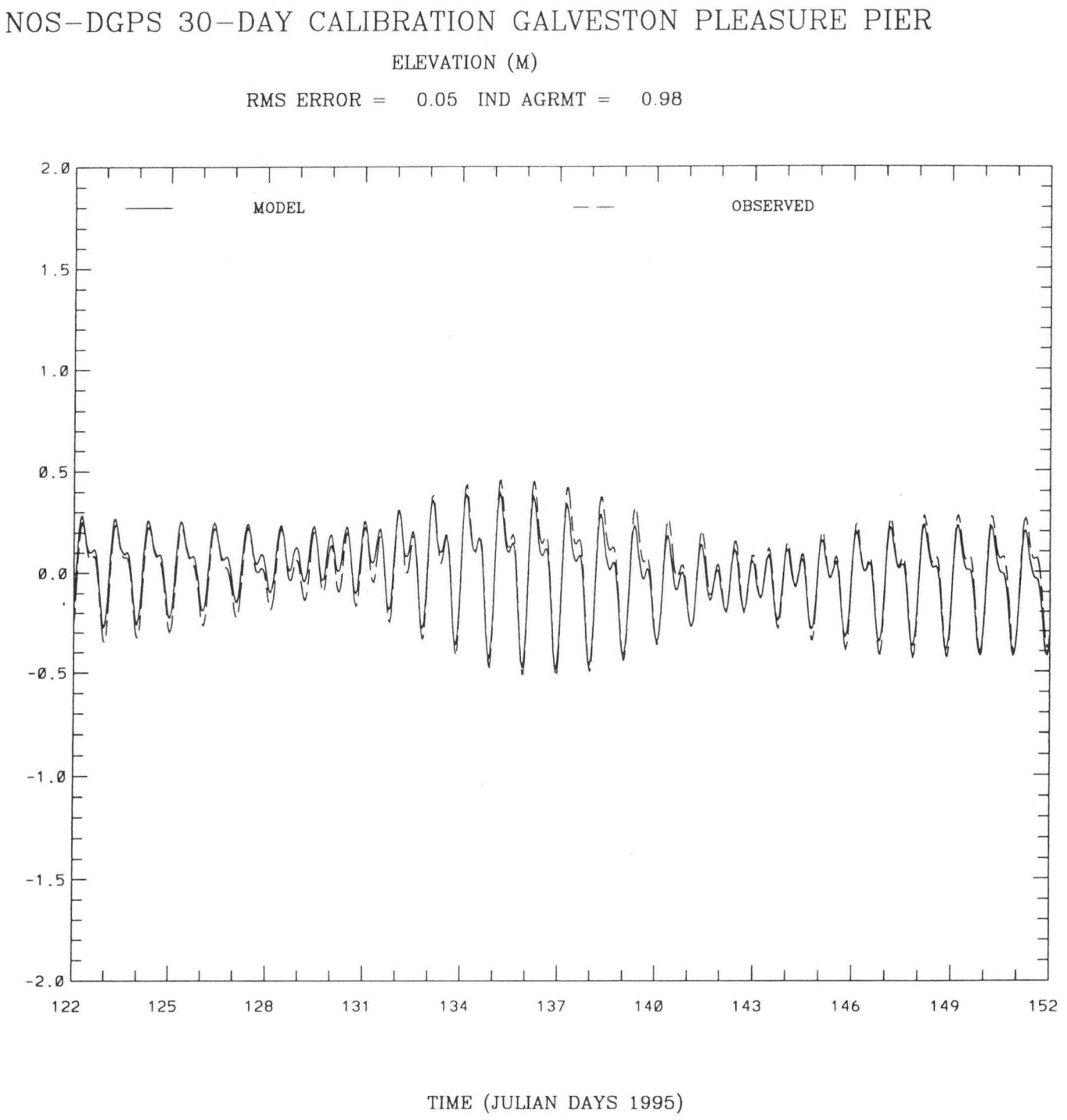

Figure 3.9. May 1995 Astronomical tide simulation: model vs predicted demeaned water level at Galveston Pleasure Pier

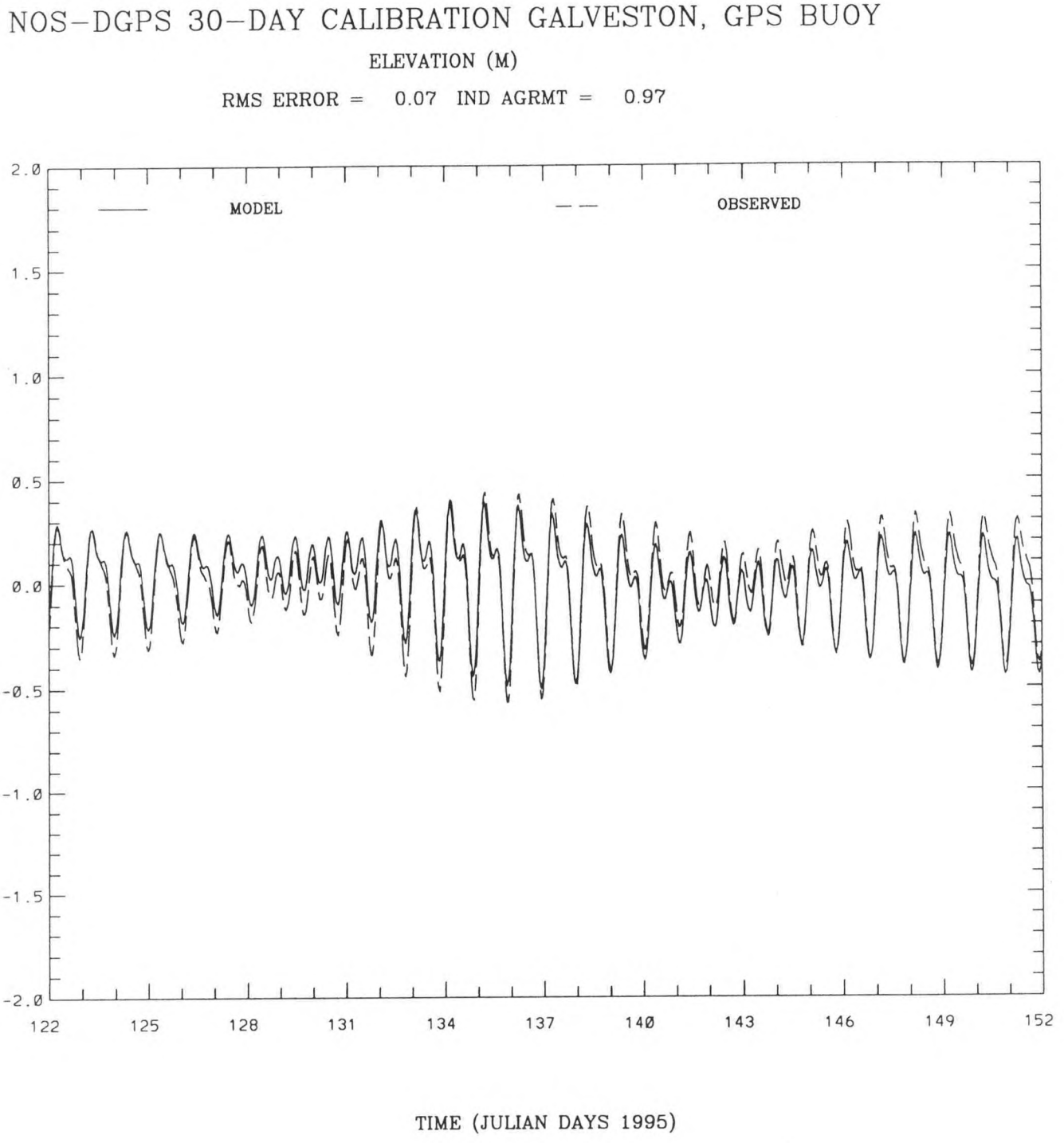

Figure 3.10. May 1995 Astronomical tide simulation: model vs predicted demeaned water level at Galveston GPS Buoy

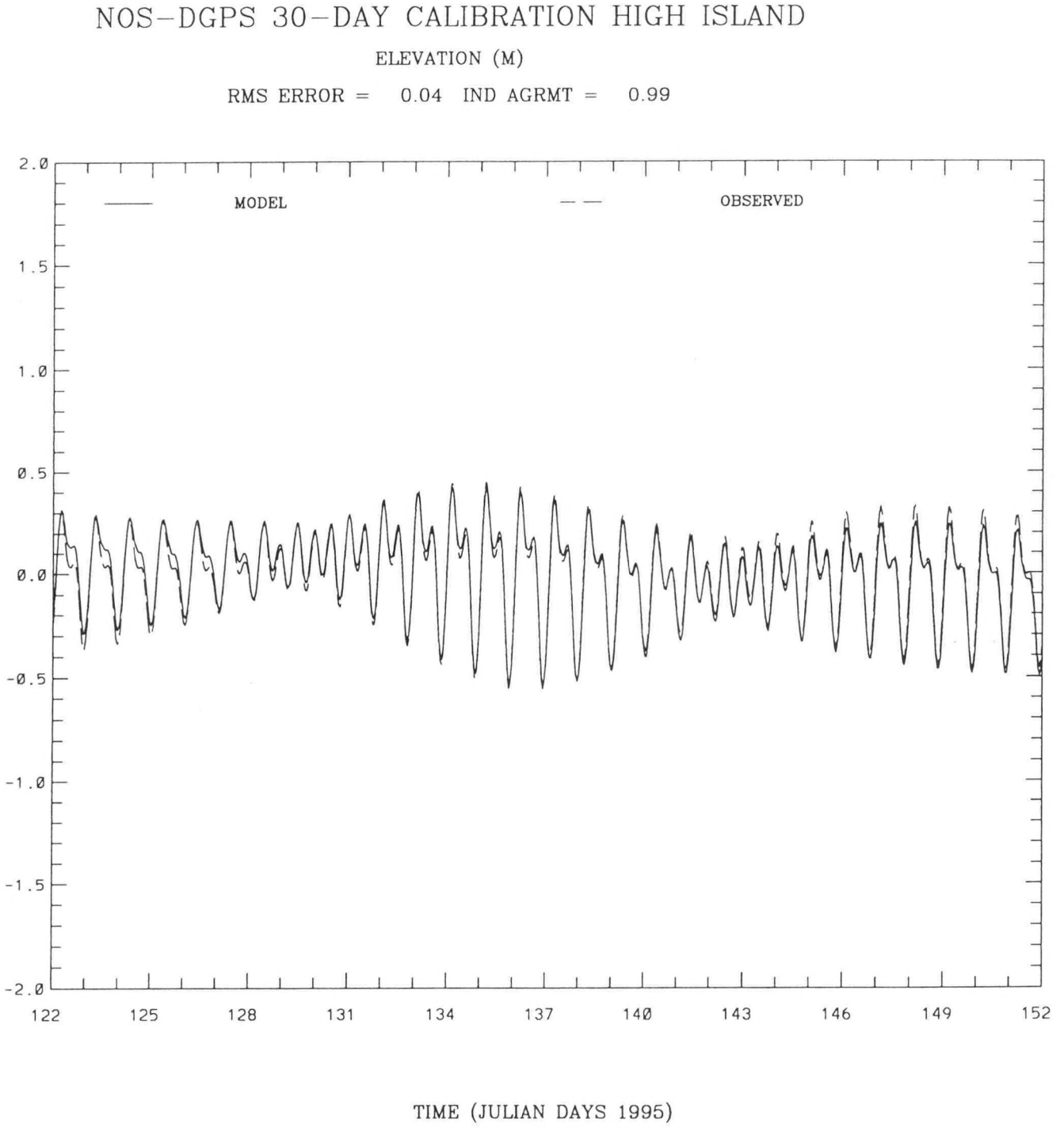

Figure 3.11. May 1995 Astronomical tide simulation: model vs predicted demeaned water level at High Island

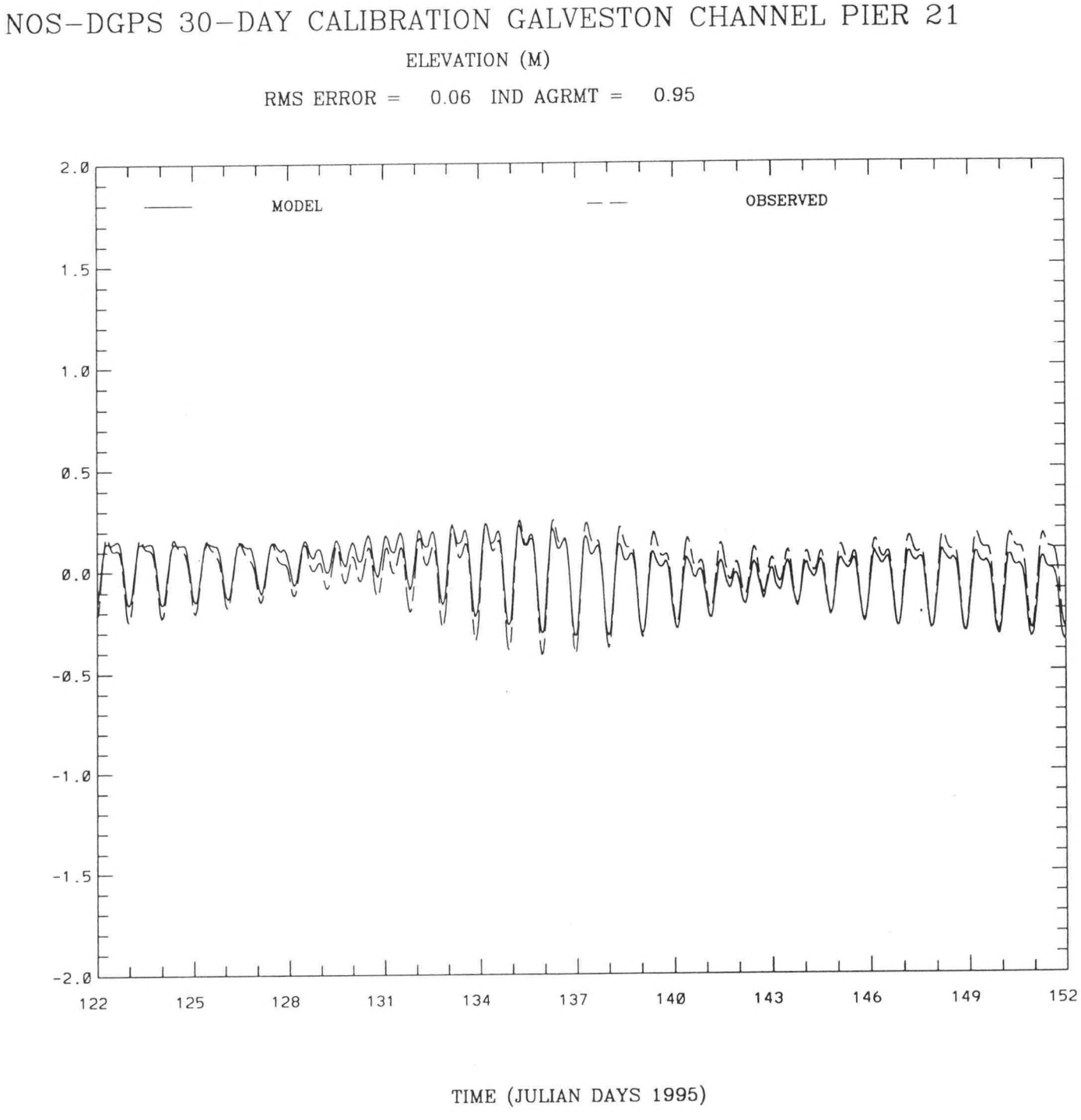

Figure 3.12. May 1995 Astronomical tide simulation: model vs predicted demeaned water level at Galveston Pier 21

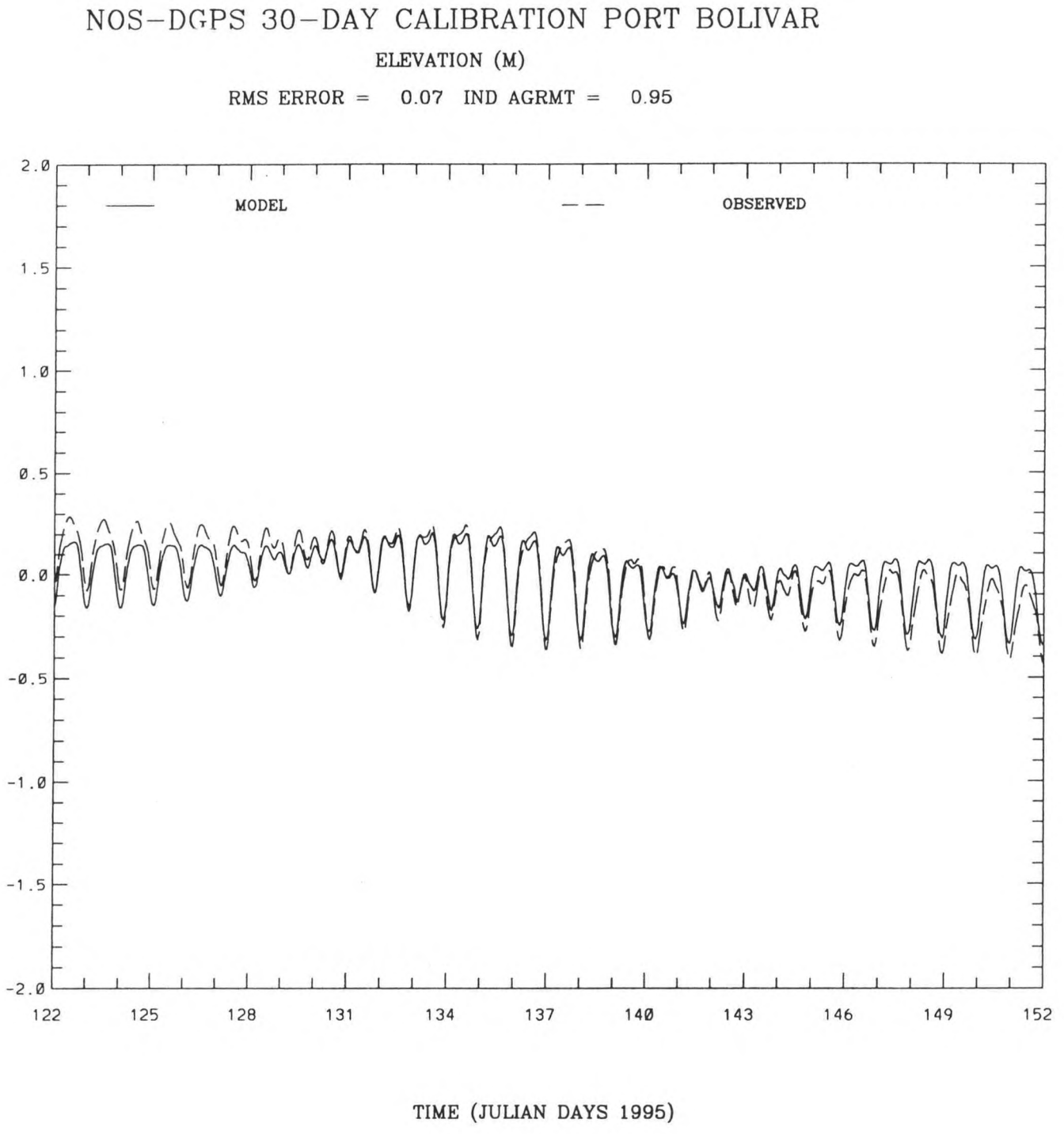

Figure 3.13. May 1995 Astronomical tide simulation: model vs predicted demeaned water level at Port Bolivar

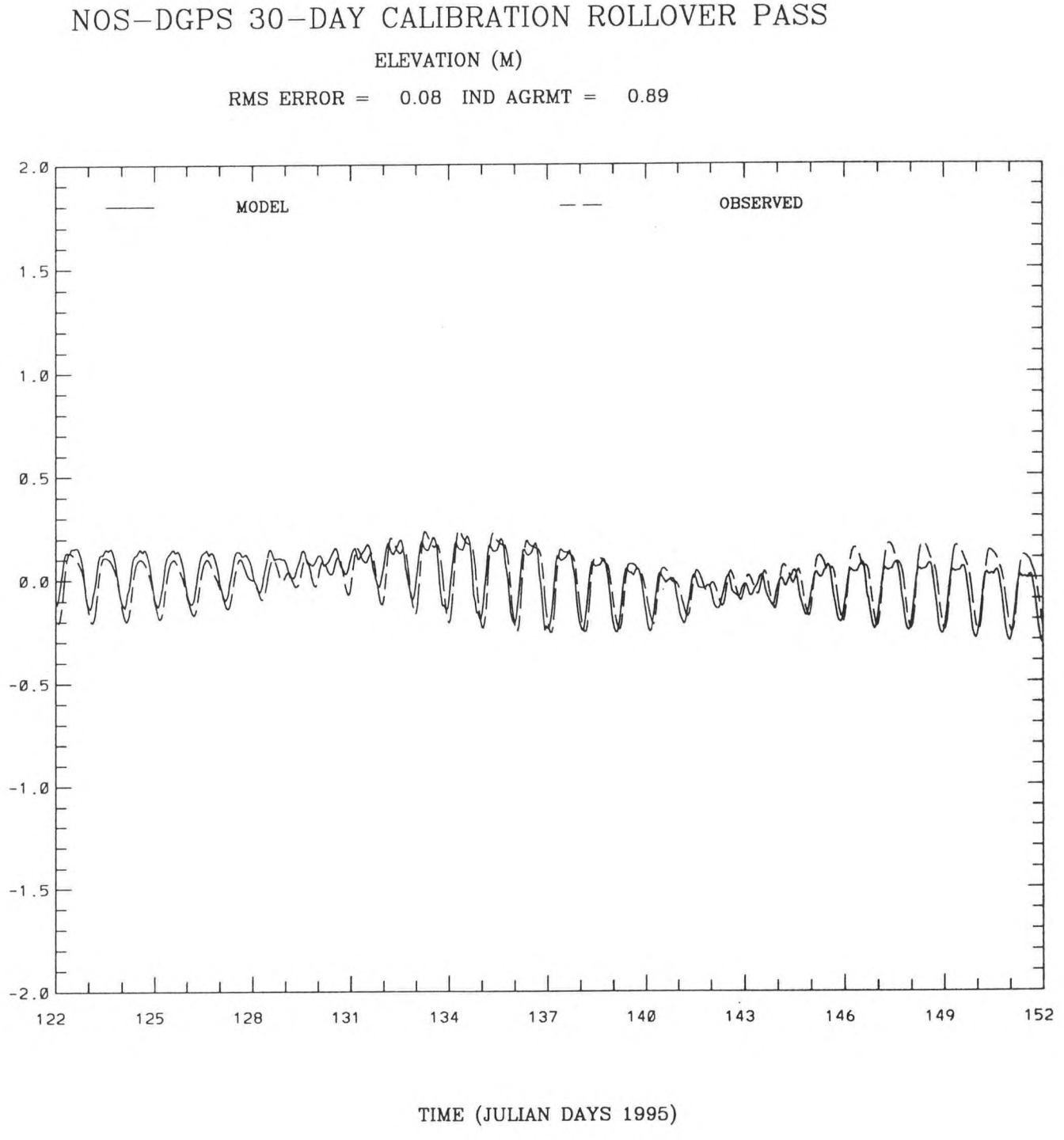

Figure 3.14. May 1995 Astronomical tide simulation: model vs predicted demeaned water level at Rollover Pass

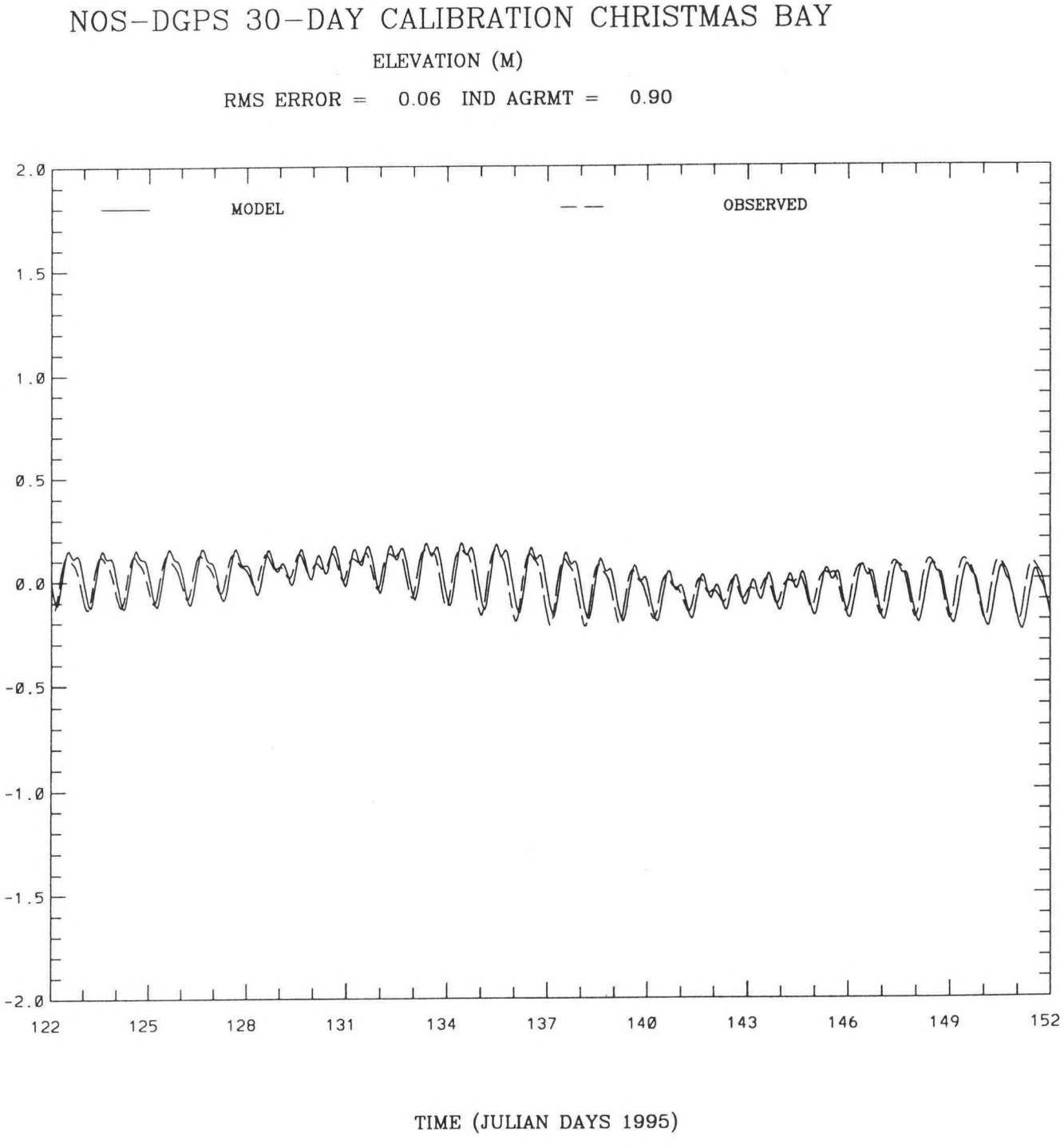

Figure 3.15. May 1995 Astronomical tide simulation: model vs predicted demeaned water level at Christmas Bay

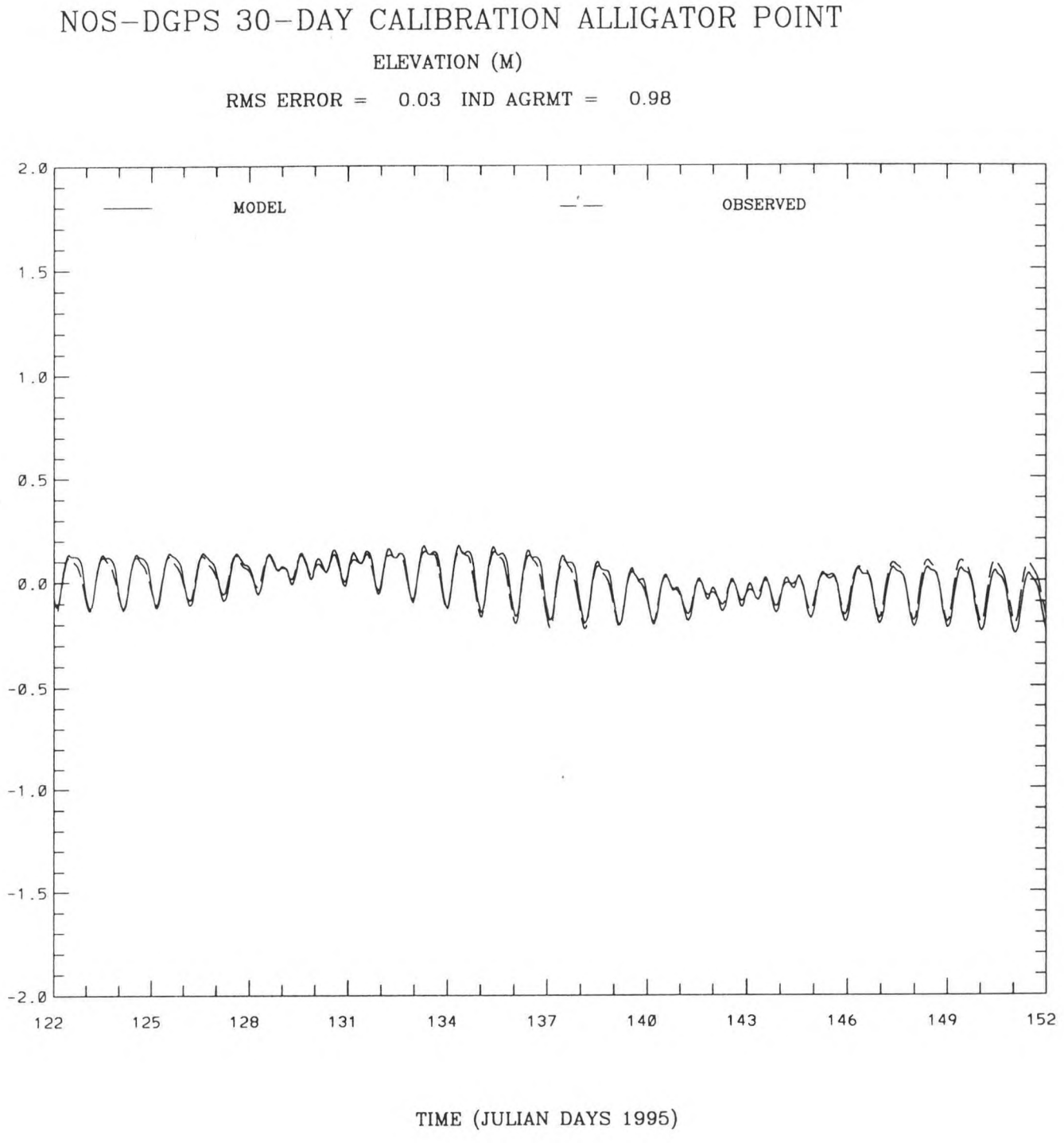

Figure 3.16. May 1995 Astronomical tide simulation: model vs predicted demeaned water level at Alligator Point

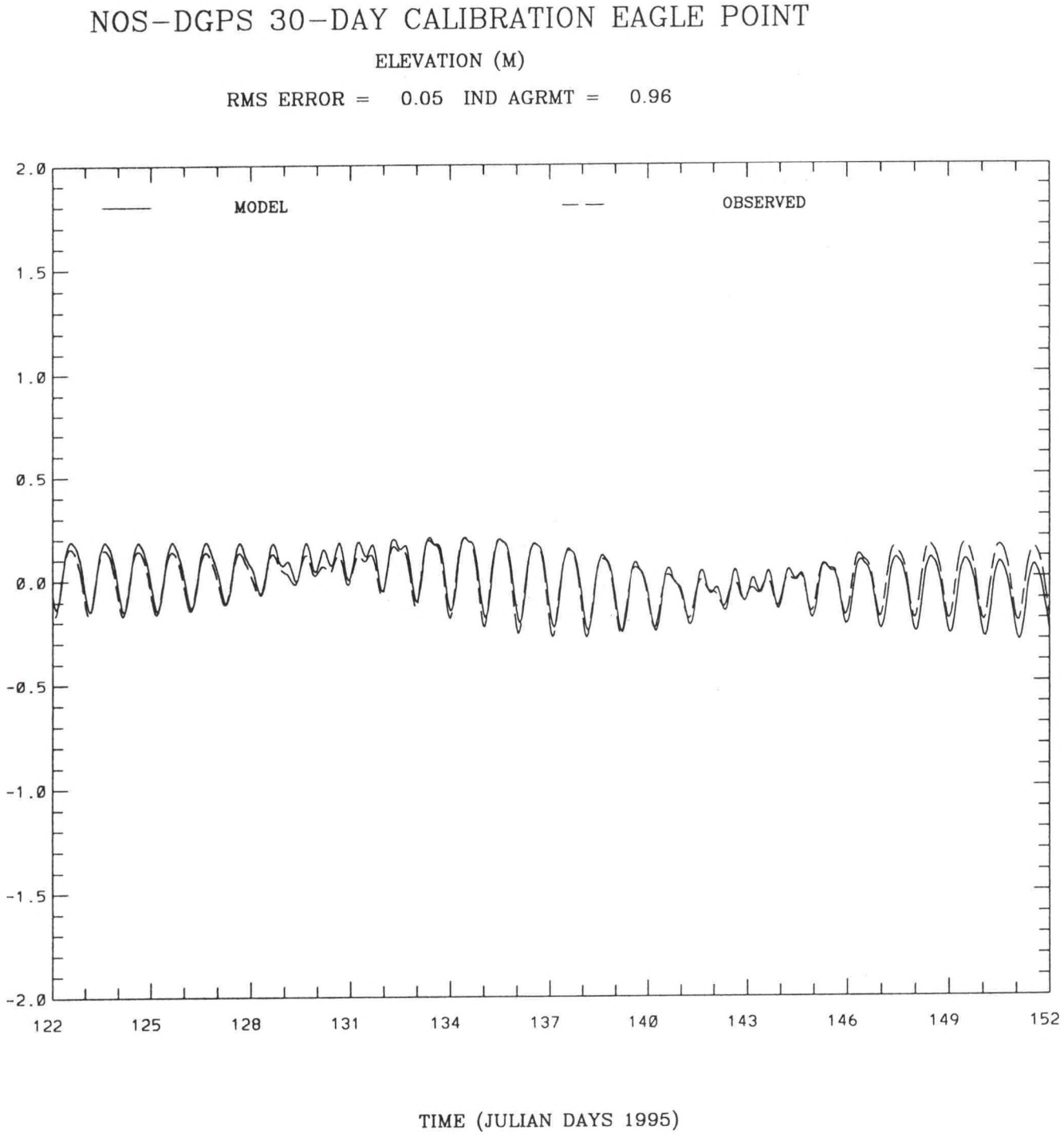

Figure 3.17. May 1995 Astronomical tide simulation: model vs predicted demeaned water level at Eagle Point

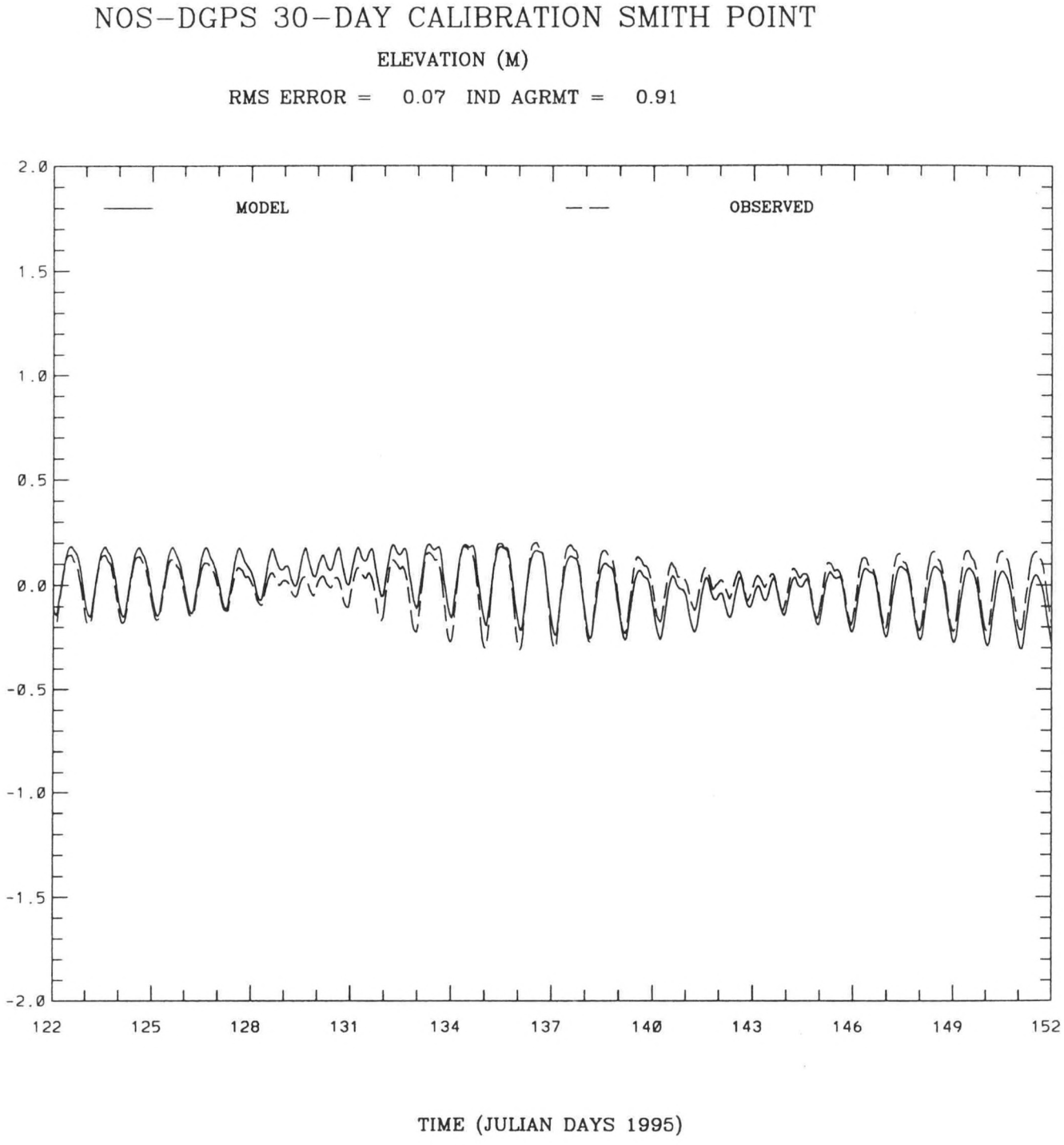

Figure 3.18. May 1995 Astronomical tide simulation: model vs predicted demeaned water level at Smith Point

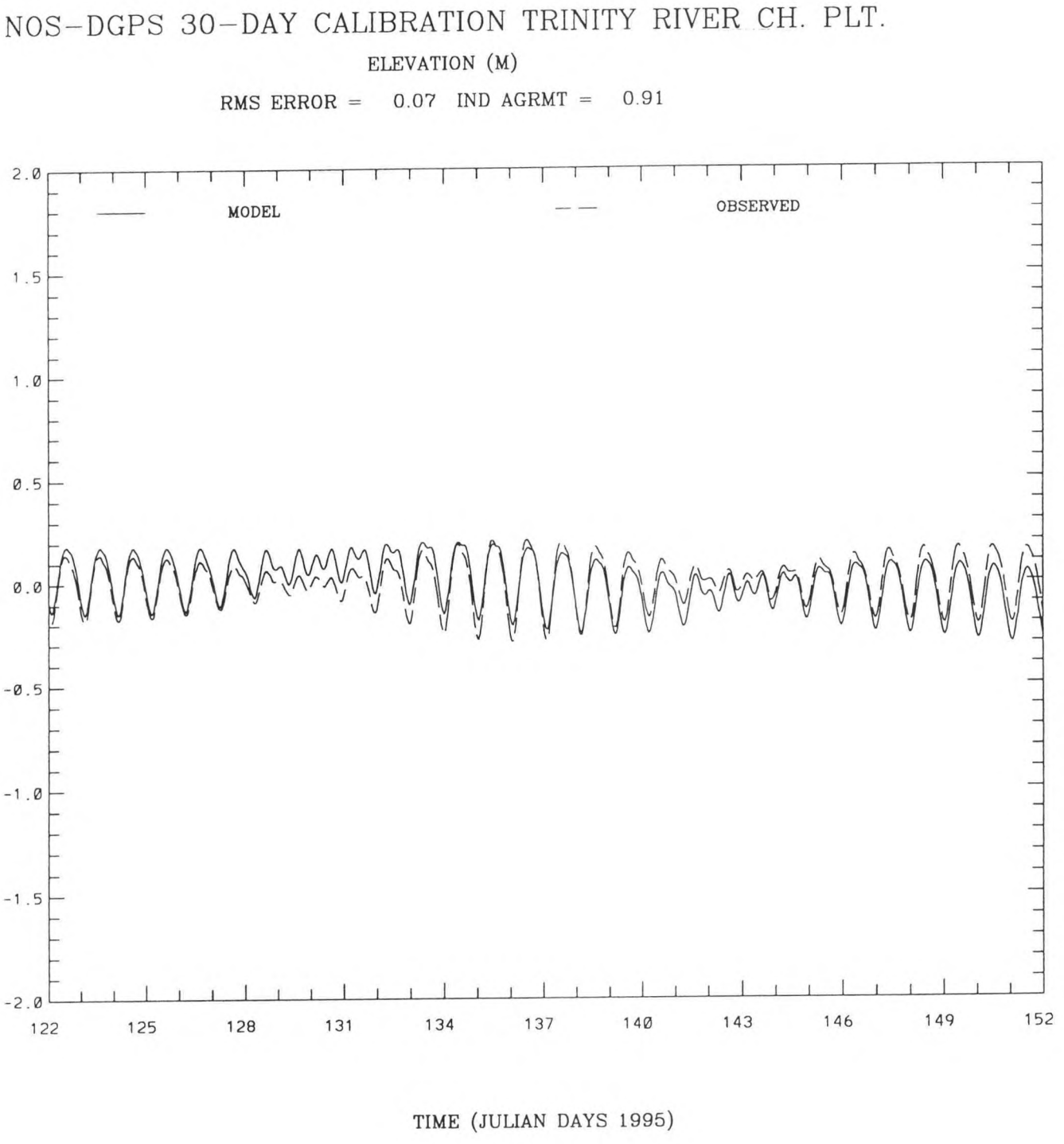

Figure 3.19. May 1995 Astronomical tide simulation: model vs predicted demeaned water level at Trinity River Channel Platform

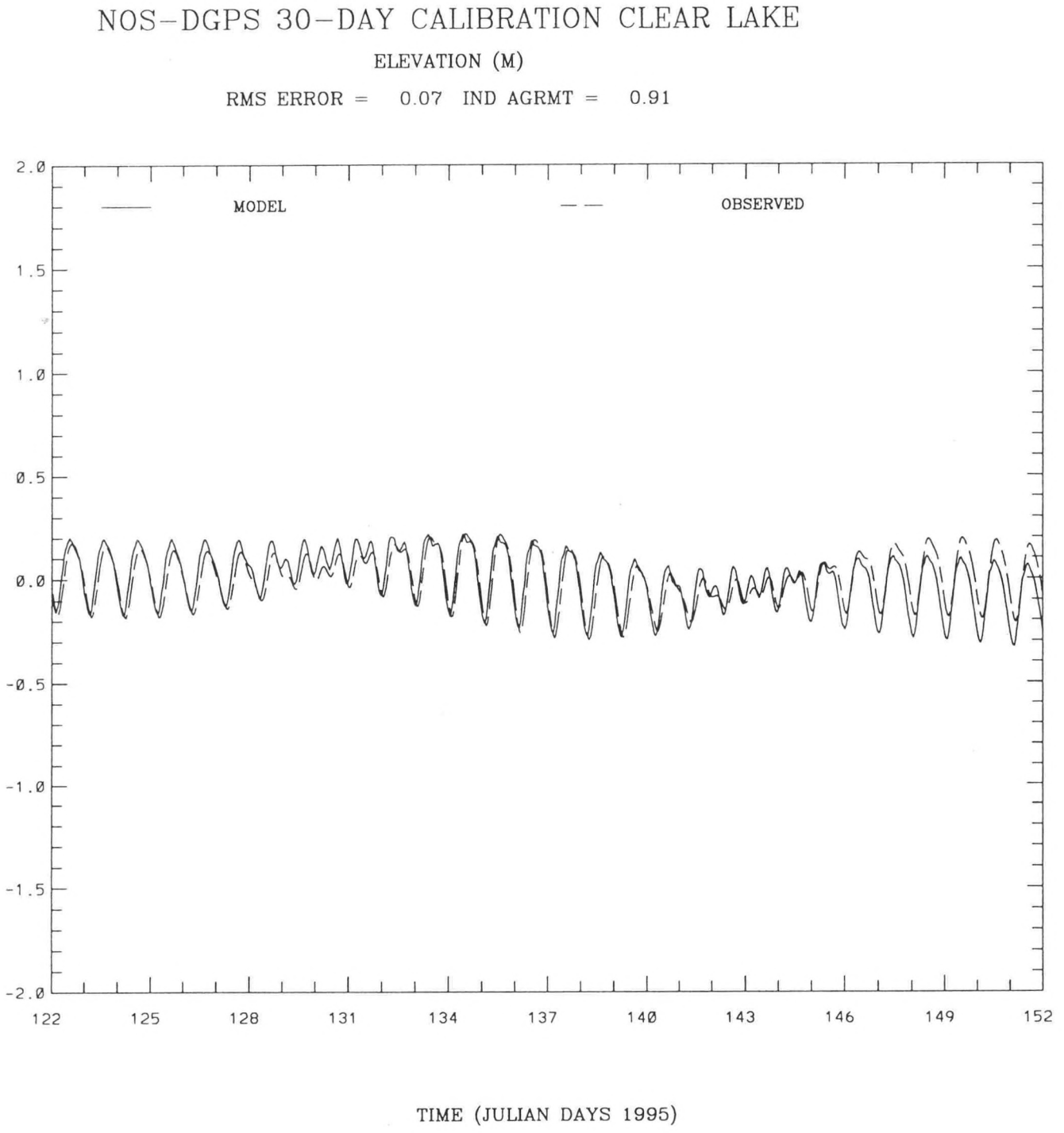

Figure 3.20. May 1995 Astronomical tide simulation: model vs predicted demeaned water level at Clear Lake

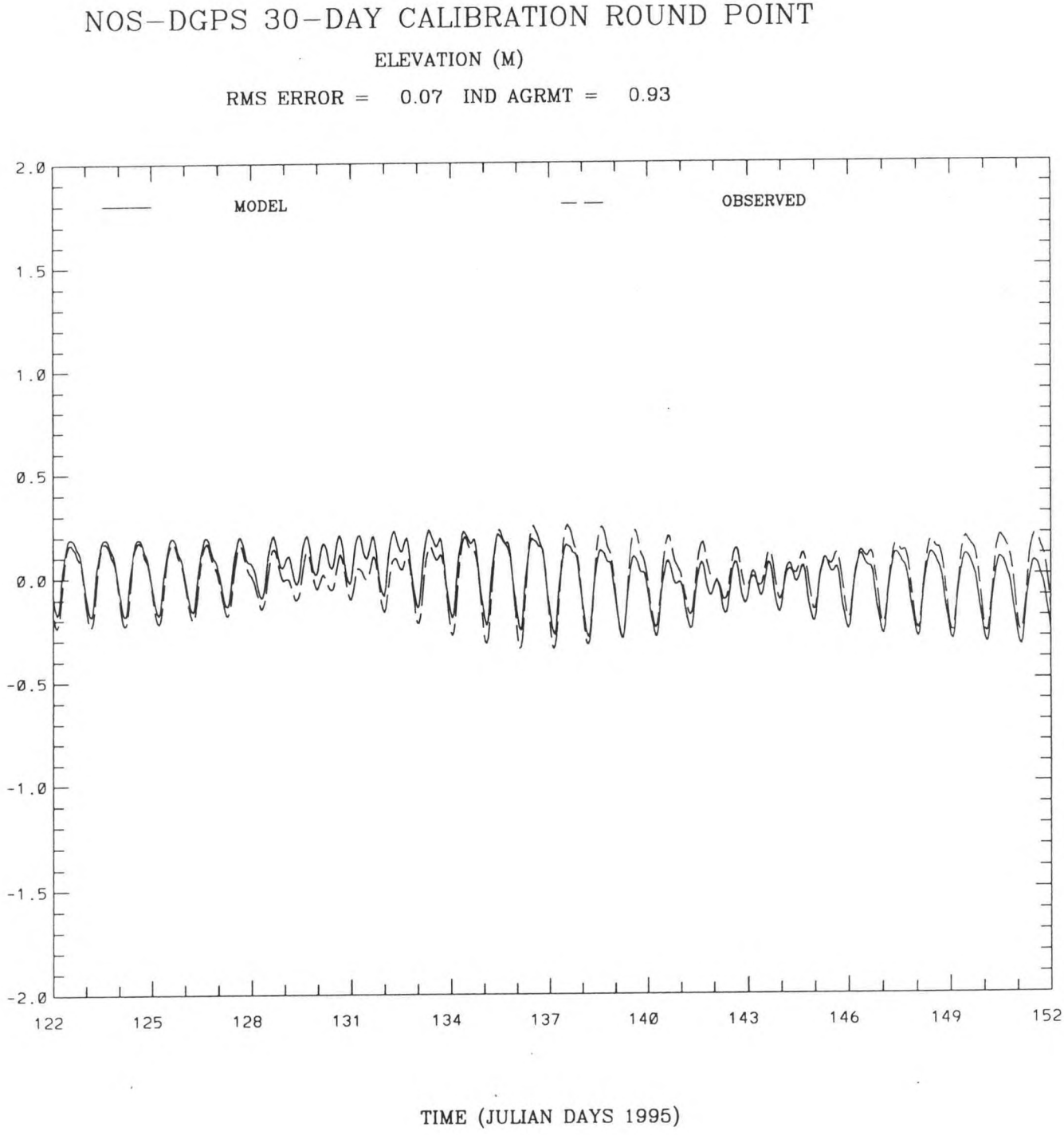

Figure 3.21. May 1995 Astronomical tide simulation: model vs predicted demeaned water level at Round Point

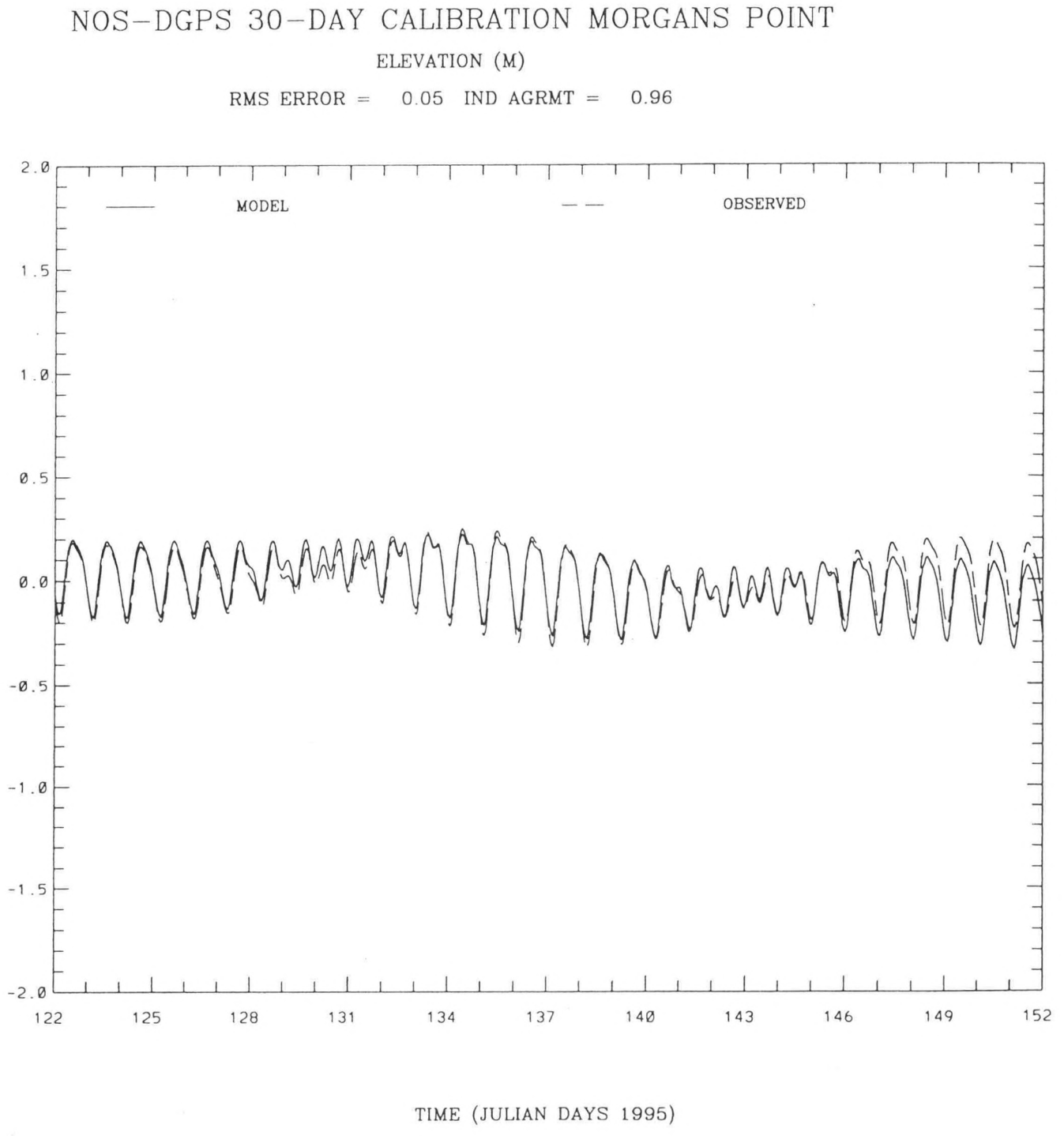

Figure 3.22. May 1995 Astronomical tide simulation: model vs predicted demeaned water level at Morgans Point

4. METEOROLOGICAL SIMULATION: JUNE 1995

A thirty day simulation over June 1995 was performed, in which the total water levels were imposed along the offshore boundaries. Wind and atmospheric pressure fields were developed and applied as surface forcings. Sea surface temperature and density initial and boundary conditions were specified based on climatology, as previously. Freshwater inflows during June 1995 for the Trinity and San Jacinto Rivers and Buffalo Bayou were obtained from USGS records and input on an average daily basis. The bottom roughness, z_o, and Smagorinsky horizontal eddy coefficient, C_H, were set to 1 cm and 0.005, respectively. Total water level comparisons were made at seven shore based tide gauge stations and along the launch DGPS hydrosurvey tracks. Simulated salinity and temperature profiles were compared with hydrosurvey launch CTD casts. Simulated salinity and temperature time series were compared with TWDB time series mid-depth data. Details of the forcings, water level, salinity, and temperature comparisons are presented in turn below followed by a discussion of additional issues.

4.1. TEXAS SHELF BOUNDARIES

In specifying the tidal boundary condition, five points along the grid were used to specify tidal signals as shown in Figure 2.1; namely, (3,2), (60,2), (120,2), (180,2), and (180,32). Between neighboring points a linear interpolation in the appropriate coordinate index was used to determine the tidal signal at each grid point. The previous tidal constituents were used to reconstruct the astronomical tide signals. However, it was necessary to increase the mean offset at (180,2) from -13.5 cm to 29.0 cm, as noted in Table 3.1, to alleviate the Sa and Ssa consistency problem discussed in section 3.1. The water level residual at Galveston Pleasure Pier was computed by subtraction of the reconstructed water levels based on the harmonic constant set given in Table 3.3 from the observed water levels over June 1995. The resulting residual signal is shown in Figure 4.1 and was added to each of the five tidal signals to produce the five total water surface elevation signals; e.g., in Equation 3.2, $\alpha = 1$. In specifying the salinity and temperature boundary condition, three points along the open Gulf boundary of the grid were used as indicated in Figure 2.1; namely, (3,2), (180,2), and (180,32). Between neighboring points a linear interpolation in the appropriate coordinate index was used to determine the signal at each grid point. Linear temporal interpolation of climatological profiles was used as previously discussed.

4.2. RIVER BOUNDARIES

The Trinity River, San Jacinto River, and Buffalo Bayou average daily inflows as shown in Figures 4.2 - 4.4 were obtained at USGS gages 0807 6300, 0807 2000, and 0807 3770, respectively. The San Jacinto inflows are based on a stage discharge curve recently developed by Dr. Fred Liscum, USGS Houston Field Office, for the Lake Houston Dam near Sheldon, Texas. The Trinity River inflow decreased from over 32,000 to 10,000 cfs (906 - 283 m^3/s) over the period 1 - 12 June and then increased to 18,000 cfs (509 m^3/s) on 19 June. It subsequently subsided to a climatological value based on 1924 - 1990 monthly records of order 6,000 cfs (170 m^3/s) by the end of June. These average daily inflows were interpolated to each internal mode time step and specified, as outlined in Schmalz (1994), as inflows to cells (164,74), (73,83), and (15,94), respectively. River inflow salinity was assumed zero, while river temperatures were set equal to those of the cell in which they entered.

4.3. THE AIR-SEA BOUNDARY

The sea surface temperature was specified by linear interpolation of the first sigma level fields determined on 1 January, 1 April, and 1 July using grid patch interpolation as previously discussed. Standard meteorological data were obtained at C-MAN stations S-2 at Sabine, Texas and S-4 at Port Aransas, Texas and for 3m discus buoys 42020 and 42035 from the National Data Bouy Center (NDBC). Surface weather observations at Houston IAH, Port Arthur, and WSO Galveston, Texas were obtained from the National Climatic Data Center (NCDC).

Wind speeds (m/s) were adjusted to 10m. Prior to interpolation wind speeds at the buoys were adjusted to overland values based on Hsu (1988). At the C-MAN stations and WSO Galveston, if the wind direction was in the range of 45 - 135 °M, winds were considered overwater and were adjusted to overland values. For wind directions outside this band, the winds were considered to be overland and thus need no adjustment. The following interpolation was used to determine the overland wind field components, $T_{i,j}$ at the center of each (i,j) cell with latitude, $alat_{i,j}$, and longitude, $alon_{i,j}$, over the computational grid. For each n and quantity T_n to be interpolated, where $n = 1,nint$ and $nint=7$, of the seven meteorological stations , let (λ_n, L_n) denote their corresponding latitude and longitude. The following equations are next used in which $hav(x)=sin^2(x/2)$.

$$x_n = hav(\lambda_n - alat_{i,j}) + \cos(\lambda_n)\cos(alat_{i,j})hav(L_n - alon_{i,j}) \tag{4.1}$$

$$y_n = 2\sin^{-1}(\sqrt{x_n}) \tag{4.2}$$

$$d_n = y_n^{-2} \tag{4.3}$$

$$d_T = \sum_{n=1}^{nint} d_n \quad , \quad \omega_n = \frac{d_n}{d_T} \tag{4.4}$$

$$T_{i,j} = \sum_{n=1}^{nint} \omega_n T_n \tag{4.5}$$

Upon completion of the interpolation of both overland wind components, the overland wind magnitude was computed and adjusted to overwater values based on Hsu (1988) for all water grid cells. Sea level atmospheric pressure fields (mb) were determined using the same inverse squared distance interpolation procedure. Both fields were generated at three hour intervals over the entire 30-day period with adjustments made to account for missing station values. Wind and atmospheric pressure fields are summarized on a daily basis in Table 4.1 and shown at five day intervals, in Figures 4.5 - Figures 4.11 and in Figures 4.12 - 4.18, respectively. Air temperature (°C), wet bulb temperature (°C), and cloud cover (-) fields were developed using the same interpolation procedures at three hour intervals for use in future heat flux studies.

Table 4.1. Meteorological simulation average daily wind and atmospheric pressure extremes

	Wind Speed (m/s)		Air Pressure (mb)	
Day	Min	Max	Min	Max
1	2.155	8.652	1011.156	1013.424
2	3.722	7.547	1012.752	1014.270
3	5.119	8.849	1012.494	1013.742
4	3.250	7.284	1012.000	1013.767
5	2.319	5.752	1009.398	1010.949
6	5.356	8.321	1006.242	1007.768
7	6.496	9.284	1007.111	1008.375
8	6.719	9.460	1010.513	1011.589
9	7.990	9.775	1013.133	1014.855
10	7.067	8.772	1014.087	1015.045
11	4.554	10.141	1014.150	1015.684
12	5.358	10.358	1015.565	1019.957
13	3.168	6.727	1016.042	1018.228
14	2.363	5.441	1016.856	1018.456
15	3.495	7.153	1017.471	1018.858
16	3.906	8.106	1018.137	1019.724
17	5.841	9.588	1018.090	1019.885
18	5.412	10.007	1017.457	1019.201
19	2.992	7.204	1016.573	1018.373
20	2.243	6.087	1013.835	1015.233
21	3.293	6.328	1011.789	1012.776
22	3.832	6.813	1011.939	1013.270
23	3.443	6.301	1012.145	1013.042
24	3.626	6.514	1010.437	1011.731
25	4.548	6.478	1009.491	1010.965
26	3.130	6.610	1011.827	1013.585
27	2.589	6.382	1013.338	1014.650
28	3.095	7.537	1013.005	1014.159
29	4.396	9.432	1011.669	1013.767
30	3.147	10.823	1011.309	1014.079

4.4 INITIALIZATION

Following the grid patch interpolation procedures used previously, initial near surface and near bottom salinity fields shown in Figures 4.19 and 4.20, respectively, and near surface and near bottom temperature fields shown in Figures 4.21 and 4.22, respectively, were developed. These fields are based on climatology and were the best that could be generated in the absence of field measurements. Model velocities were initially set to zero.

4.5. WATER LEVEL COMPARISONS

Simulated total water levels are compared at the seven tide gauge locations shown in Figure 4.23 after a one day spin-up period. Demeaned water level time series are compared for each station in Figures 4.24 - 4.30. Root mean square differences and the previous dimensionless relative error are given in Table 4.2. In general, simulated water levels are in agreement with measured levels to within 10 cm rms and relative errors are less than 0.10. Simulated and observed water level means are shown in Table 4.3. Note a 7 cm tilt over Galveston Bay is indicated between

Table 4.2. Meteorological simulation: simulated vs observed RMS and RE water level summary

ELEVATION (M) JULIAN DAYS (1995) 153.00 - 182.00

STATION	RMS ERROR	RELATIVE ERROR
GALVESTON PLEASURE PIER	0.10	0.05
GALVESTON CHANNEL PIER 21	0.08	0.05
MORGANS POINT	0.08	0.04
CLEAR LAKE	0.09	0.05
SMITH POINT	0.07	0.04
EAGLE POINT	0.08	0.05
PORT BOLIVAR	0.13	0.11

Table 4.3. Meteorological simulation: simulated vs observed mean water level summary

ELEVATION (M) JULIAN DAYS (1995) 153.00 - 182.00

STATION	MODEL MEAN	OBSERV. MEAN
GALVESTON PLEASURE PIER	0.28	0.20
GALVESTON CHANNEL PIER 21	0.29	0.19
MORGANS POINT	0.36	0.23
CLEAR LAKE	0.36	0.20
SMITH POINT	0.33	0.22
EAGLE POINT	0.34	0.22
PORT BOLIVAR	0.29	0.17

the simulated mean levels at Galveston Pier 21 and Morgans Point. In the Upper Bay, significant subtidal events observed in the water level time series are captured in the simulated levels. Simulated water levels at 470 points along the DGPS hydrosurvey tracks were compared with six-minute averaged 1 second water levels estimated using DGPS adjusted for settlement (static) and squat (dynamic) launch characteristics. The DGPS phase data were forward and reverse processed by NCD on a second by second basis using ASHTECH's PNAV software. Simulated water levels versus corresponding hydrosurvey track elevations are summarized in Table 4.4. Individual survey tracks and water level comparisons are given in the plot set in Appendix A. Comparisons are categorized by distance from the nearest tide gauge and launch speed and tabulated in Appendix B. There appears to be no major correlation of the discrepancies between model and DGPS water levels with launch speed or distance from the nearest tide gauge. While daily comparisons range from 7 - 27 cm rms, the global, over all 470 points, comparison is order 15 cm. Relative error statistics are substantially larger than those obtained at the shore-based tide gauges.

4.6 SALINITY AND TEMPERATURE COMPARISONS

TWDB mid-depth salinity and temperature data available at the stations shown in Figure 4.31 are compared with model sigma level 3 at corresponding grid locations in Figures 4.32 - 4.36

Table 4.4. Meteorological simulation: simulated vs DGPS track statistics

JULIAN DAY	RMS ERROR	RELATIVE ERROR
164.59 - 164.84	0.19	0.68
165.55 - 165.77	0.18	0.68
166.61 - 166.66	0.25	0.75
167.57 - 167.83	0.20	0.64
170.57 - 170.78	0.11	0.61
171.59 - 171.73	0.21	0.73
172.56 - 172.77	0.07	0.63
173.56 - 173.77	0.09	0.66
174.55 - 174.75	0.09	0.63
177.55 - 177.74	0.09	0.63
178.50 - 178.73	0.12	0.40
179.54 - 179.67	0.27	0.75
180.56 - 180.73	0.14	0.43
181.57 - 181.63	0.18	0.75

and in Figures 4.37 - 4.41, respectively. Rms and dimensionless relative error are given for salinity and temperature in Tables 4.5 and 4.6, respectively. Simulated salinity and temperature mean comparisons with observations are given in Tables 4.7 and 4.8, respectively. There appears to be a biological fouling problem associated with the conductivity sensor at Dollar Point as indicated by the discontinuity in the observations on June 15 as shown in Figure 4.34. Salinity rms errors are order 2-4 psu at stations where biological fouling is not a problem. Temperature rms errors are order 1 °C.

Hydrosurvey launch CTD were obtained using a SeaBird 911 in a side-mounted configuration with a pump in order to resolve density structures over the shallow regions of the Bay outside the HSC. The location of the launch hydrosurvey CTD stations are shown in Figure 4.42, while supplemental CTD locations are shown in Figure 4.43. Instrument data were processed by the NCL. CEOB plotted all downcasts and reviewed the profiles for spiking. Problematic casts order 10 out of a total of 143 were then edited by CEOB. Salinity and temperature comparisons are summarized in Tables 4.9 and 4.10, respectively, in terms of rms (RMS) and observed (STR. D) and simulated (STR. M) stratification. Simulated near surface (sigma level 1) and near bottom (sigma level 5) salinity and temperature time series are compared with CTD casts at the vertices of the triangular hydrosurvey track in Figures 4.44 - 4.46 and Figures 4.47 - 4.49, respectively. The overall rms salinity and temperature errors are 1-4 psu and 1-2 °C, respectively. Based on the TWDB and hydrosurvey launch CTD temperature comparisons, the climatological SST specification used in the present study appears to be quite adequate.

4.7 ADDITIONAL ISSUES

Once the additional issues outlined in Section 3.6 to improve the astronomical calibration have been addressed, it would appear useful to investigate the Barnes (1973) interpolation scheme as

Table 4.5. Meteorological simulation: simulated vs TWDB RMS and RE salinity summary

SALINITY (PSU) JULIAN DAYS (1995) 153.00 - 182.00

STATION	RMS ERROR	RELATIVE ERROR
PORT BOLIVAR	10.16	0.49
TRINITY BAY-DBC	0.54	0.96
DOLLAR POINT	8.63	0.44
HANNAH REEF	1.94	0.67
RED BLUFF	4.27	0.38

Table 4.6. Meteorological simulation: simulated vs TWDB RMS and RE temperature summary

TEMPERATURE (C) JULIAN DAYS (1995) 153.00 - 182.00

STATION	RMS ERROR	RELATIVE ERROR
PORT BOLIVAR	1.20	0.52
TRINITY BAY-DBC	1.38	0.54
DOLLAR POINT	1.19	0.54
HANNAH REEF	1.10	0.57
RED BLUFF	1.21	0.54

Table 4.7. Meteorological simulation: simulated vs TWDB mean salinity summary

SALINITY (PSU) JULIAN DAYS (1995) 153.00 - 182.00

STATION	MODEL MEAN	OBSERV. MEAN
PORT BOLIVAR	21.24	11.95
TRINITY BAY-DBC	0.39	0.03
DOLLAR POINT	17.12	9.43
HANNAH REEF	7.54	6.42
RED BLUFF	9.25	5.49

Table 4.8. Meteorological simulation: simulated vs TWDB mean temperature summary

TEMPERATURE (C) JULIAN DAYS (1995) 153.00 - 182.00

STATION	MODEL MEAN	OBSERV. MEAN
PORT BOLIVAR	27.68	28.54
TRINITY BAY-DBC	28.50	27.70
DOLLAR POINT	27.61	28.32
HANNAH REEF	28.02	27.80
RED BLUFF	27.59	28.28

Table 4.9. Meteorological simulation: simulated vs DGPS launch salinity statistics

SALINITY (PSU) JULIAN DAYS (1995) 153.00 - 182.00

STATION	NOBS	RMS	STR. D	STR. M
LGB1	7	4.29	3.73	3.73
LGB2A	5	3.63	0.54	2.05
LGB2B	3	4.14	5.12	6.53
LGB3	5	2.83	0.36	2.24
LGB4	14	1.09	0.33	0.55
LGB5B	9	2.70	10.60	6.39
LGB6	7	2.05	1.15	2.49
LGB7	5	1.48	0.17	0.01
LGB8	7	3.90	2.22	1.16
LGB9	7	3.88	6.56	5.75
LGB10	7	3.17	2.39	3.49
LGB11	6	3.91	8.35	13.56
TB1	3	2.49	0.07	1.89
TB3	4	1.45	0.01	1.33
TB5	3	0.12	0.00	0.01
HSC1	4	1.38	0.81	0.90
HSC3	6	2.18	5.11	3.18
GBE	14	1.32	2.67	3.00
GMHA	3	2.90	7.80	3.10

Table 4.10. Meteorological simulation: simulated vs DGPS launch temperature statistics

TEMPERATURE (C) JULIAN DAYS (1995) 153.00 - 182.00

STATION	NOBS	RMS	STR. D	STR. M
LGB1	7	0.62	0.41	0.34
LGB2A	5	0.72	0.12	0.21
LGB2B	3	0.40	0.17	0.36
LGB3	5	0.61	0.09	0.43
LGB4	14	0.86	0.23	0.19
LGB5B	9	0.63	0.52	0.37
LGB6	7	0.68	0.23	0.33
LGB7	5	0.87	0.15	0.01
LGB8	7	0.63	0.63	0.30
LGB9	7	0.64	0.96	0.32
LGB10	7	0.82	0.77	0.24
LGB11	6	0.22	0.65	0.15
TB1	3	1.27	0.05	0.57
TB3	4	1.80	0.30	0.63
TB5	3	1.88	0.24	0.34
HSC1	4	0.52	0.49	0.49
HSC3	6	0.53	0.45	0.66
GBE	14	0.81	1.03	0.39
GMHA	3	0.45	0.64	0.35

an alternative to the inverse squared distance interpolation procedure for developing the wind and atmospheric pressure fields. In addition, the effectiveness of using NOAA's National Center for Environmental Prediction meso-ETA and AVIATION atmospheric models for predicted wind and atmospheric pressure fields over Galveston Bay and the near Texas Shelf could also be evaluated. Harmonic analysis of simulated water levels for both the astronomic tide calibration and the meteorological simulation should be performed and compared to assess the variability of model derived harmonic constant sets. The investigation of northers and extreme freshwater inflow conditions, such as reported by Liscum and East (1995), would also be of interest in extending the model's capability to simulate extreme conditions.

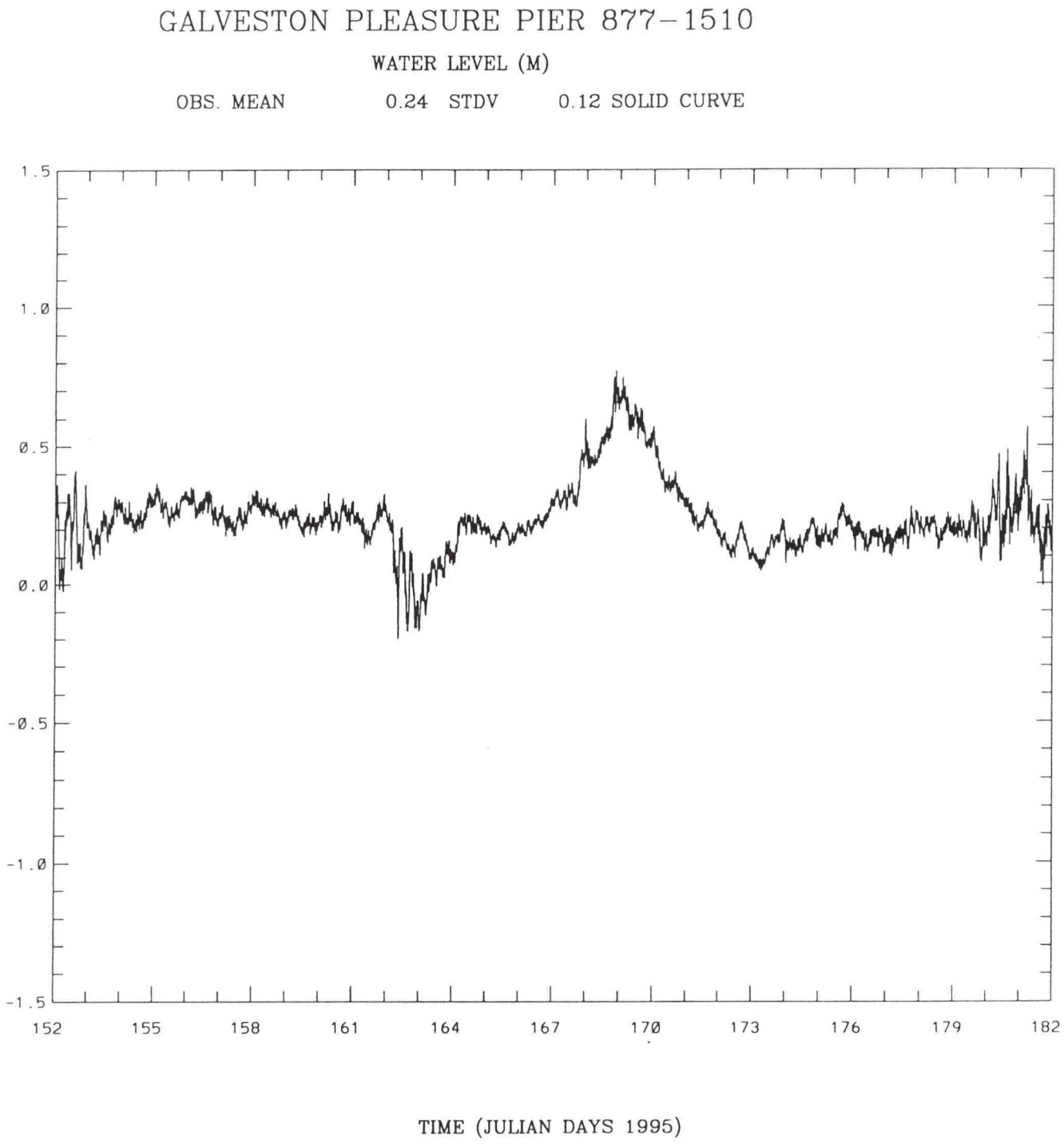

Figure 4.1. Galveston Pleasure Pier water level residual (June 1995)

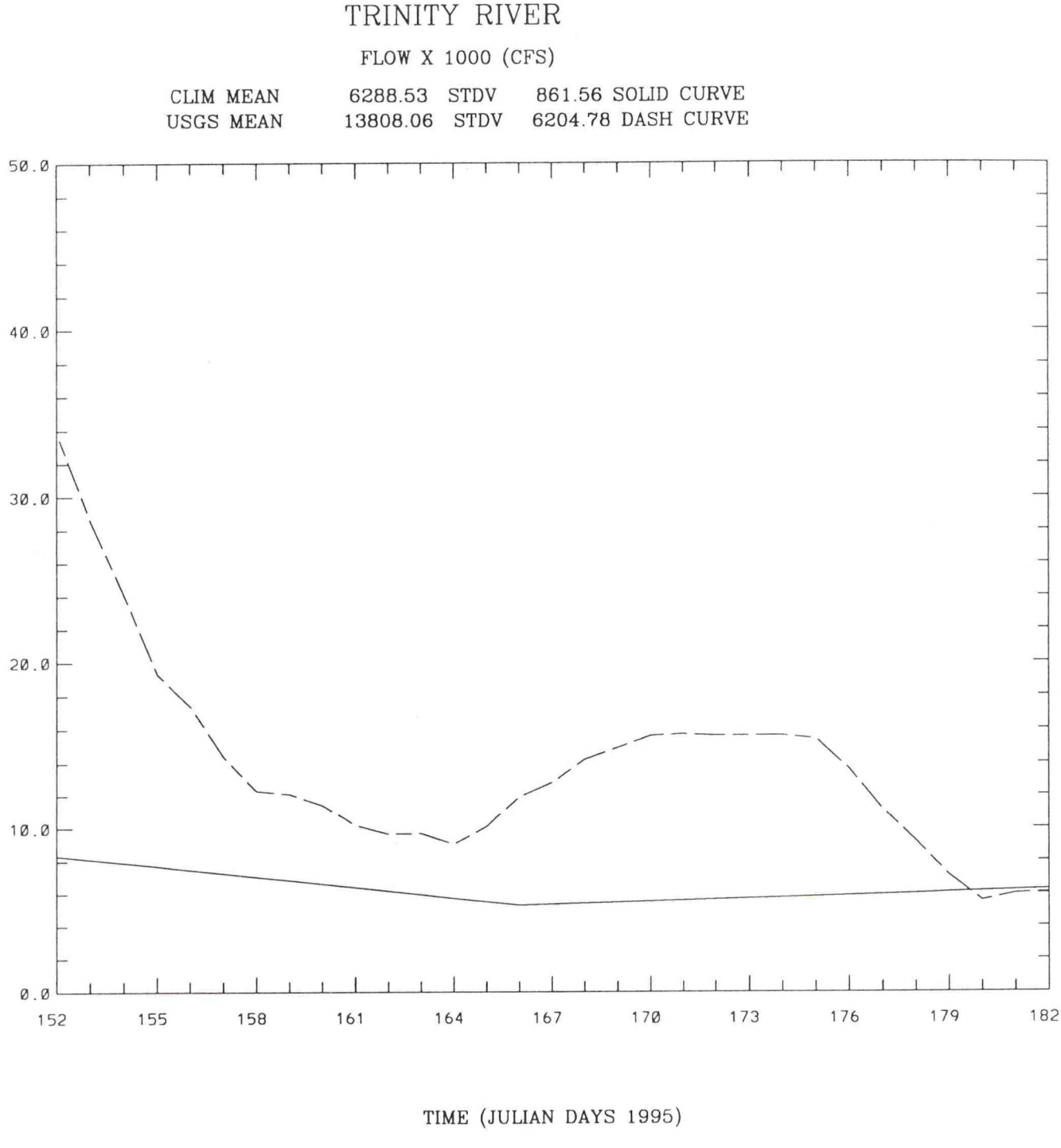

Figure 4.2. Trinity River flow (June 1995)

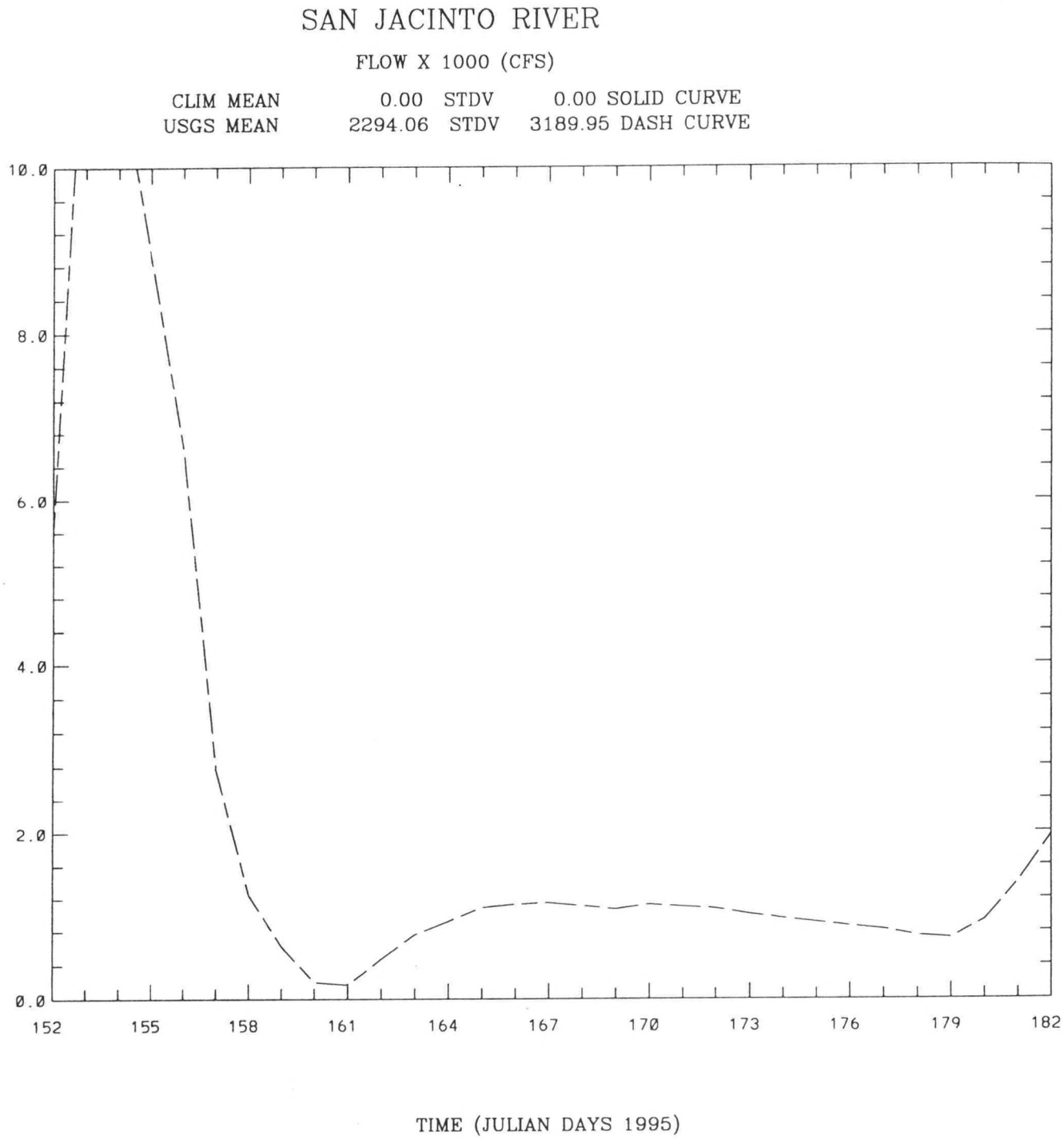

Figure 4.3. San Jacinto River flow (June 1995)

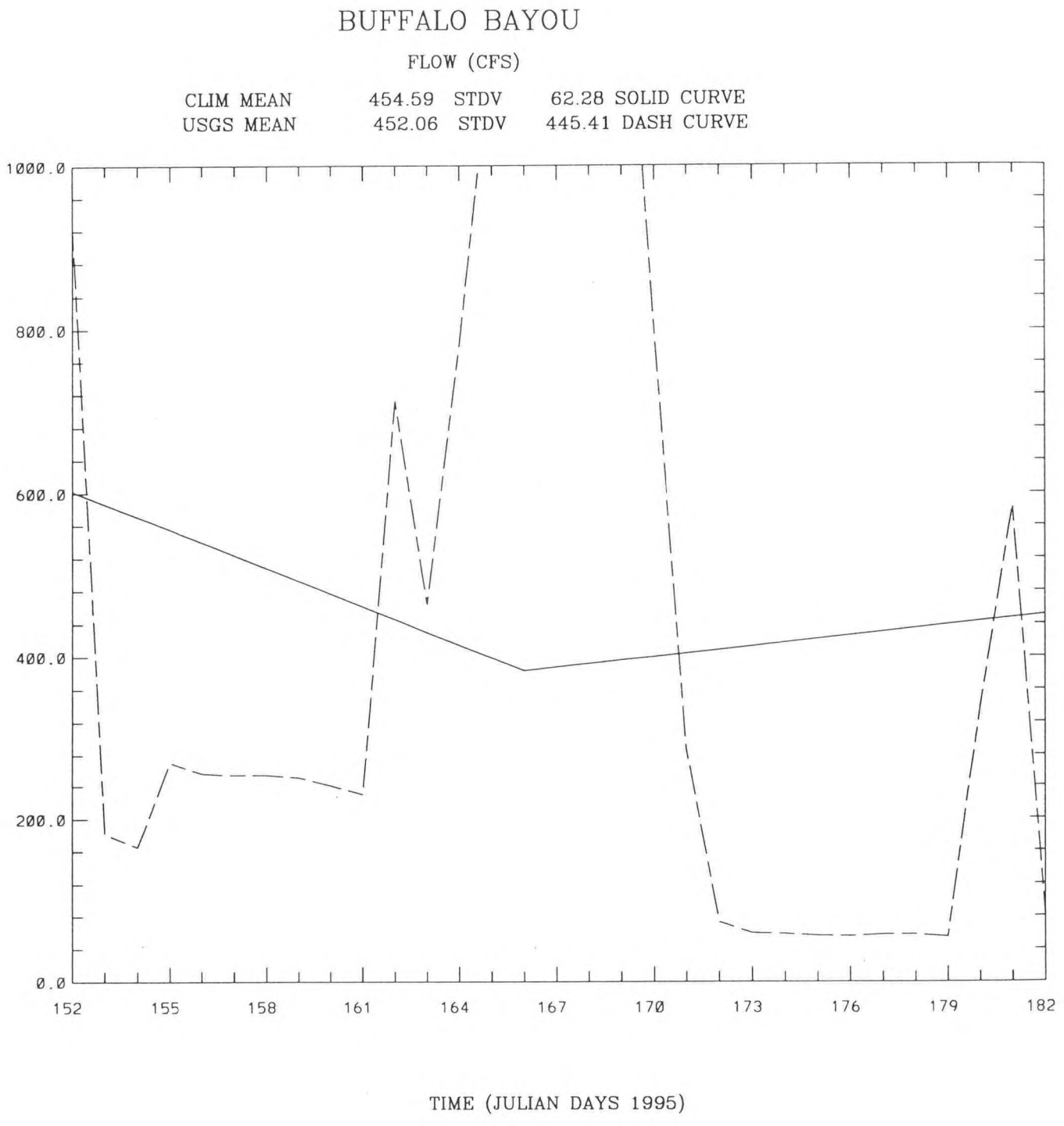

Figure 4.4. Buffalo Bayou flow (June 1995)

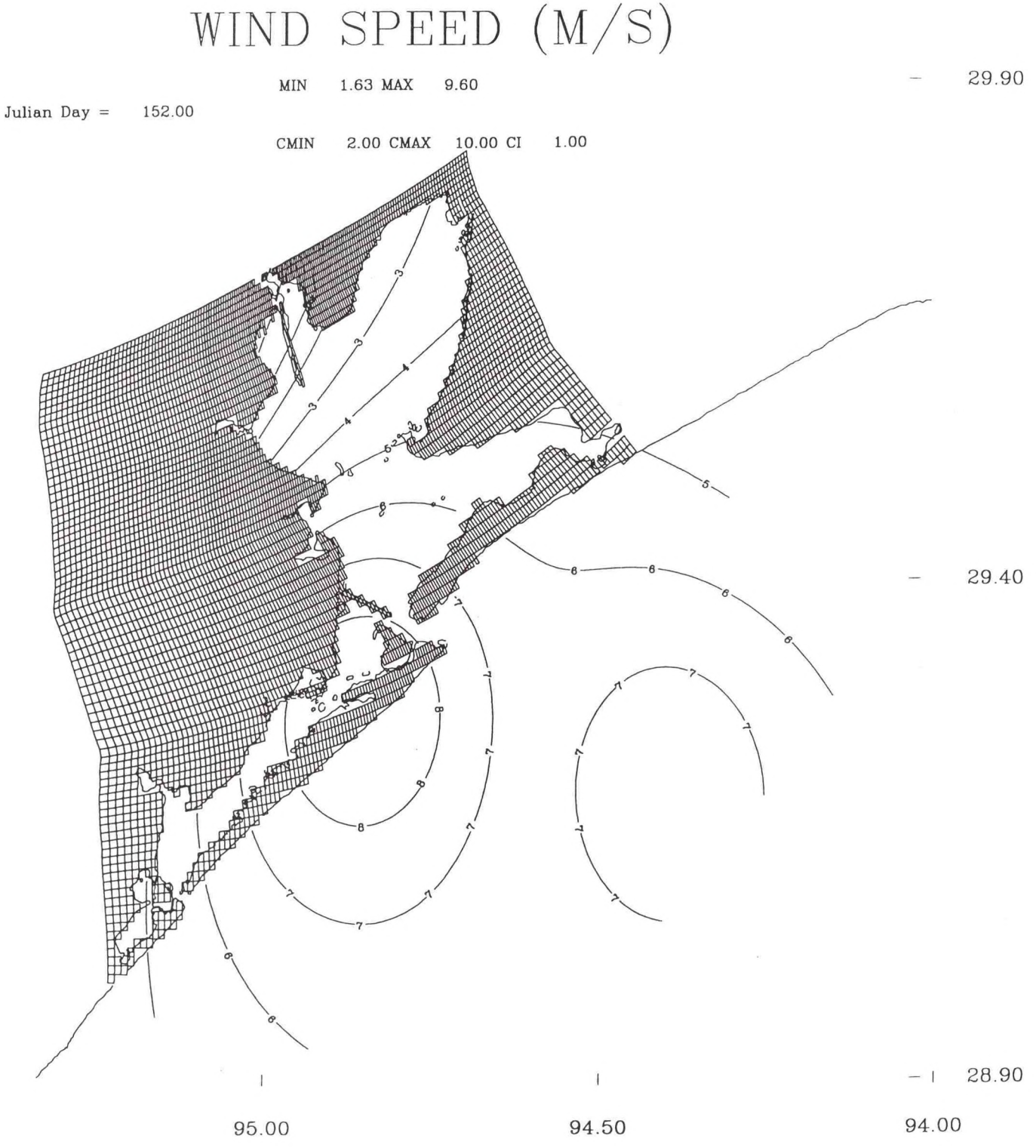

Figure 4.5. Wind field at 10m 1 June LST 0

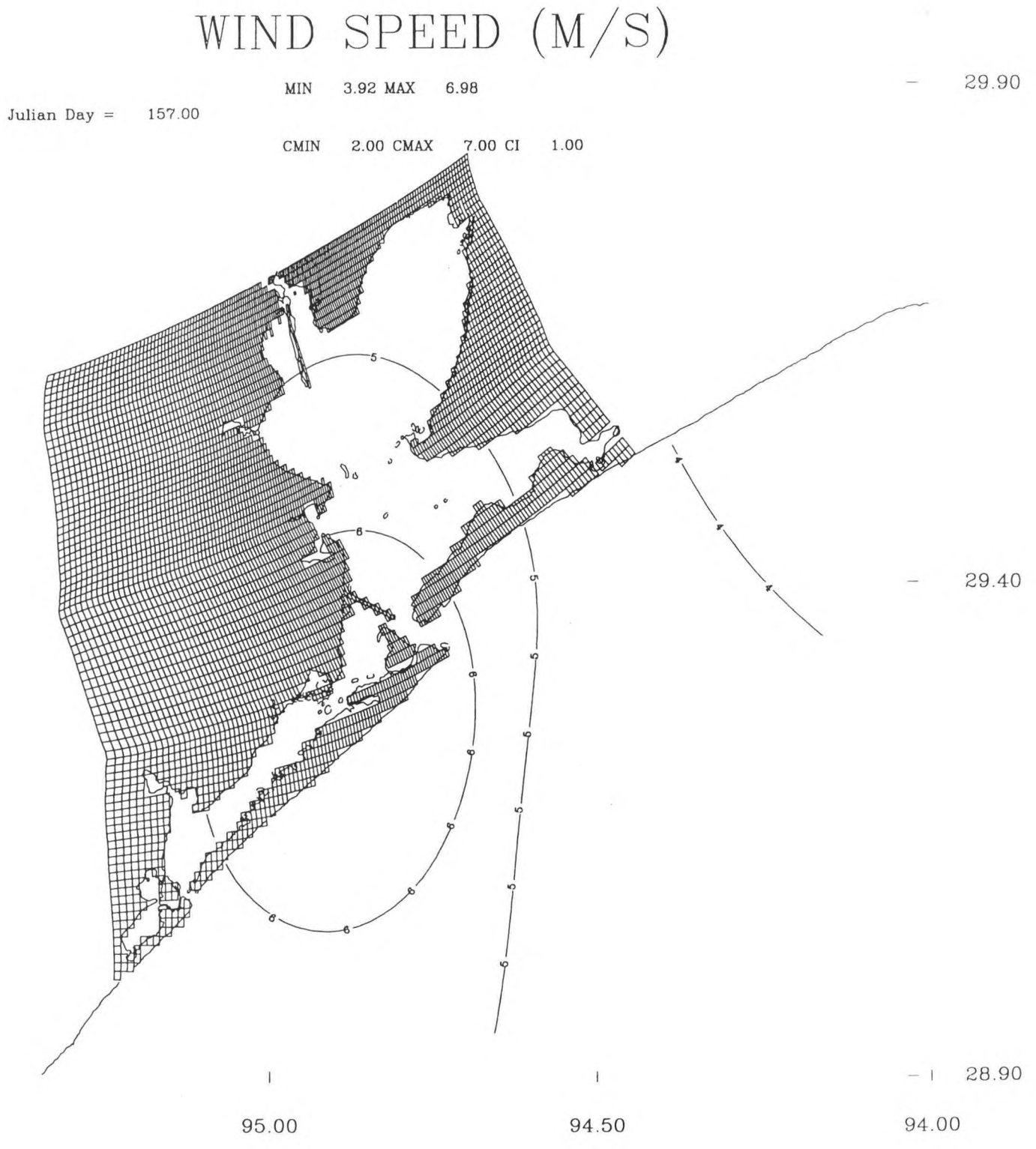

Figure 4.6. Wind field at 10m 6 June LST 0

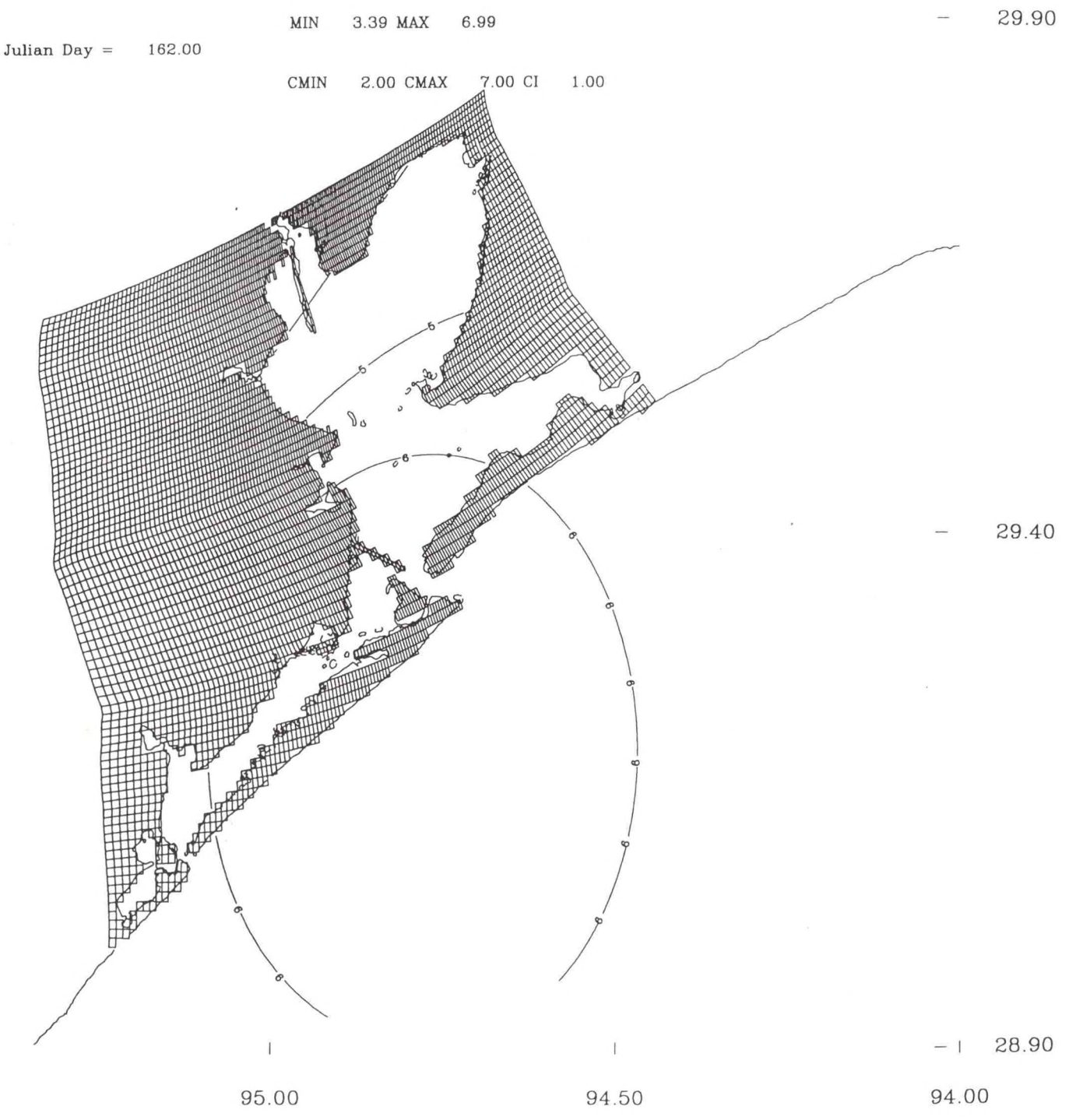

Figure 4.7. Wind field at 10m 11 June LST 0

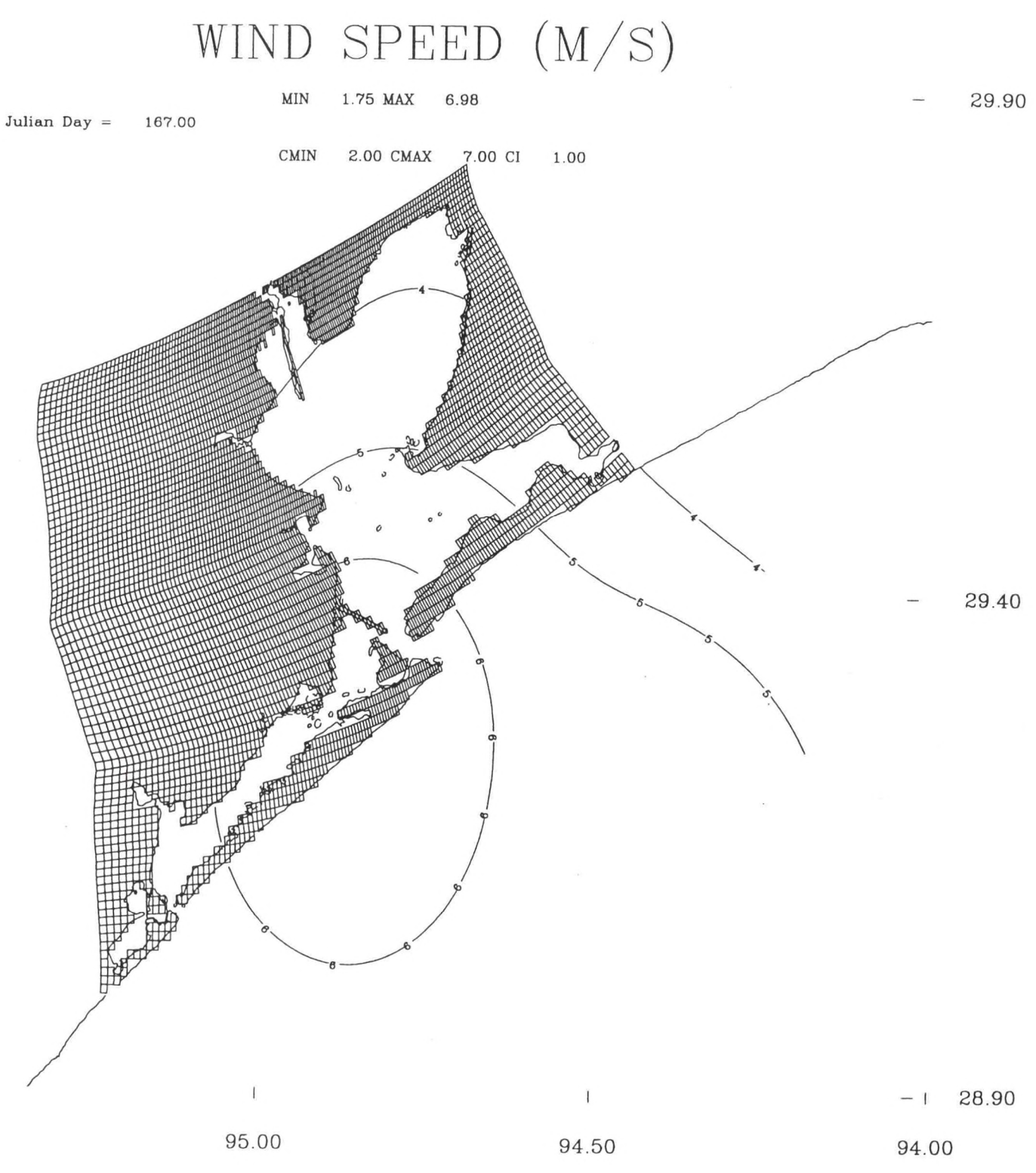

Figure 4.8. Wind field at 10m 16 June LST 0

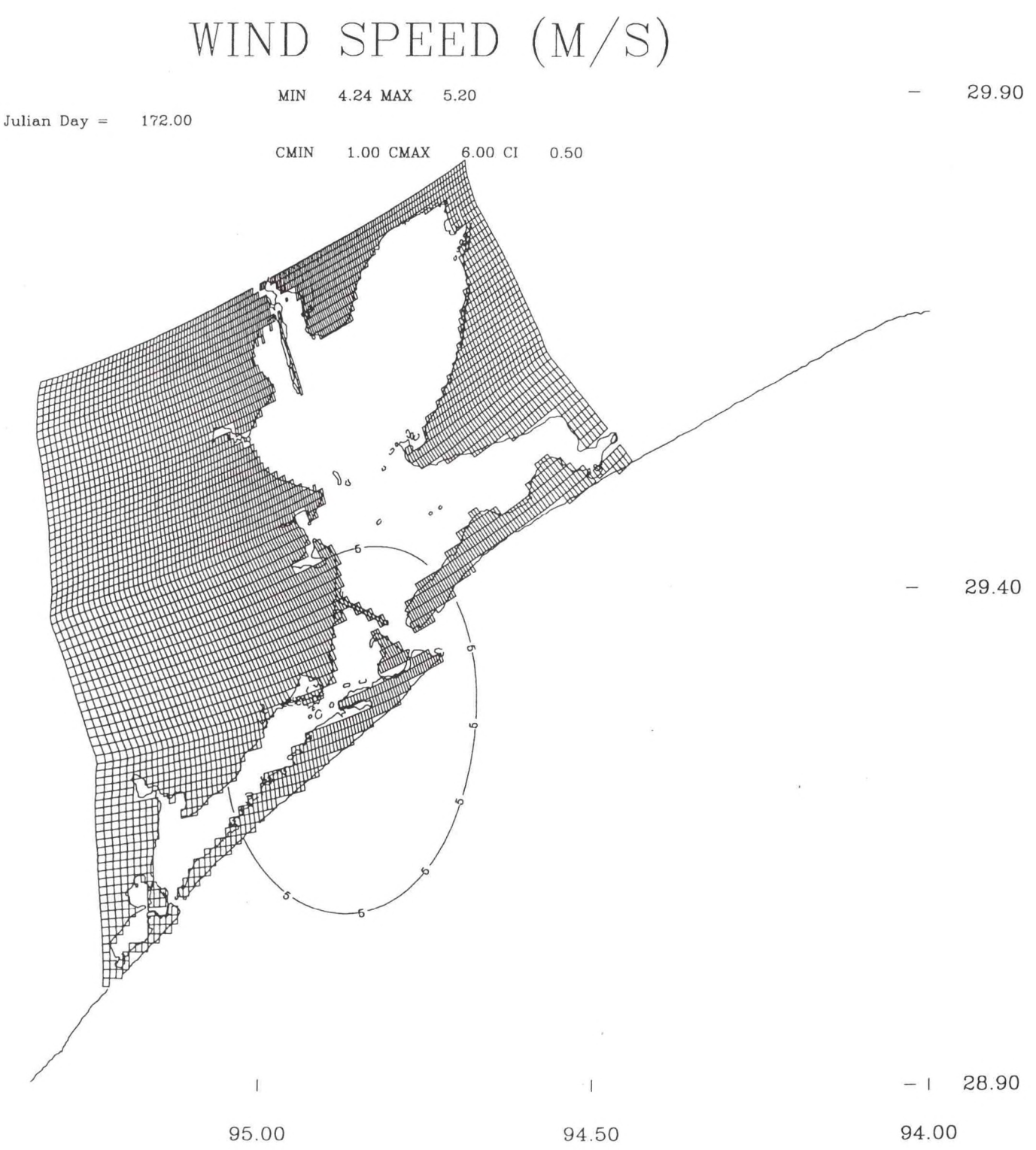

Figure 4.9. Wind field at 10m 21 June LST 0

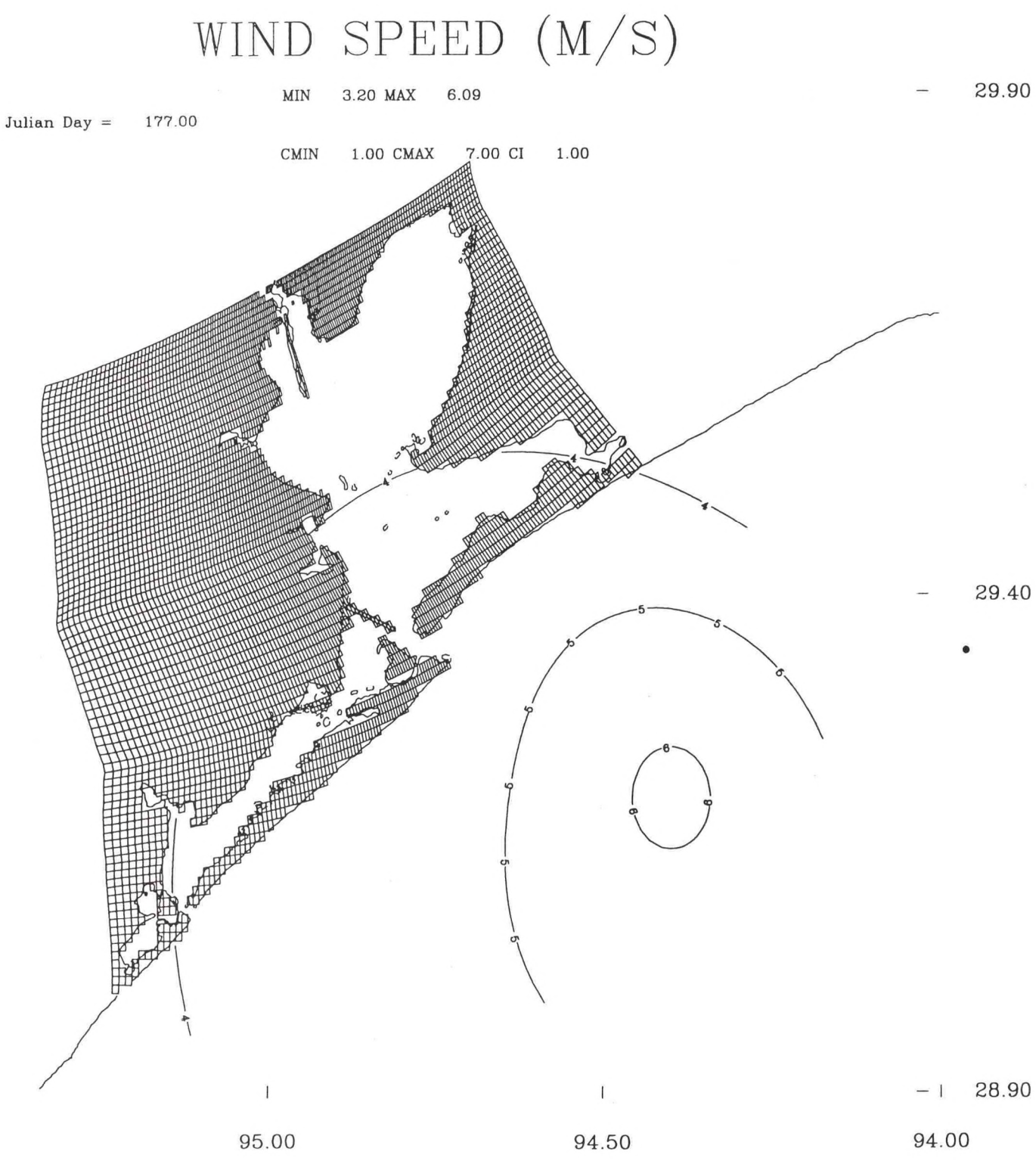

Figure 4.10. Wind field at 10m 26 June LST 0

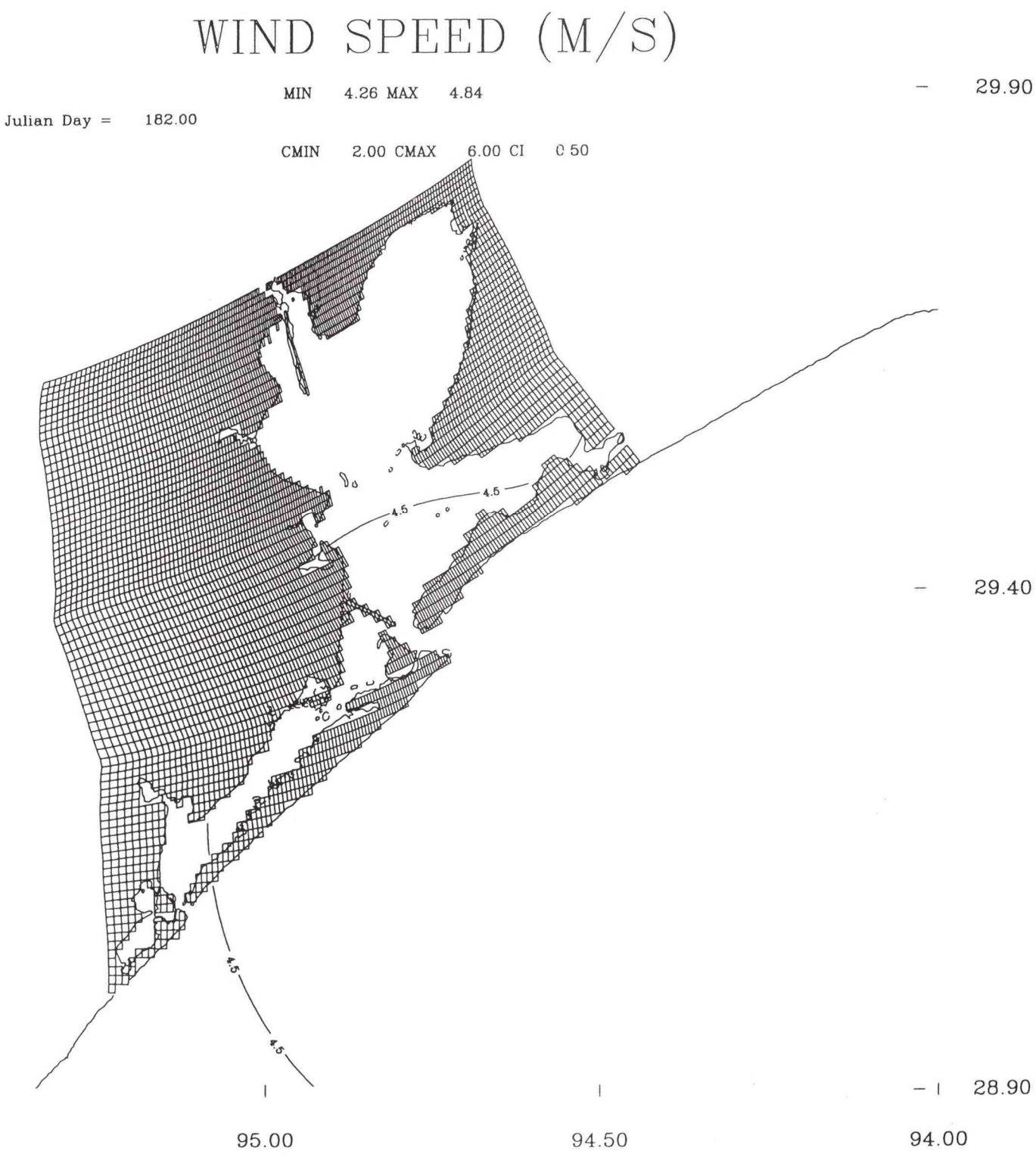

Figure 4.11. Wind field at 10m 1 July LST 0

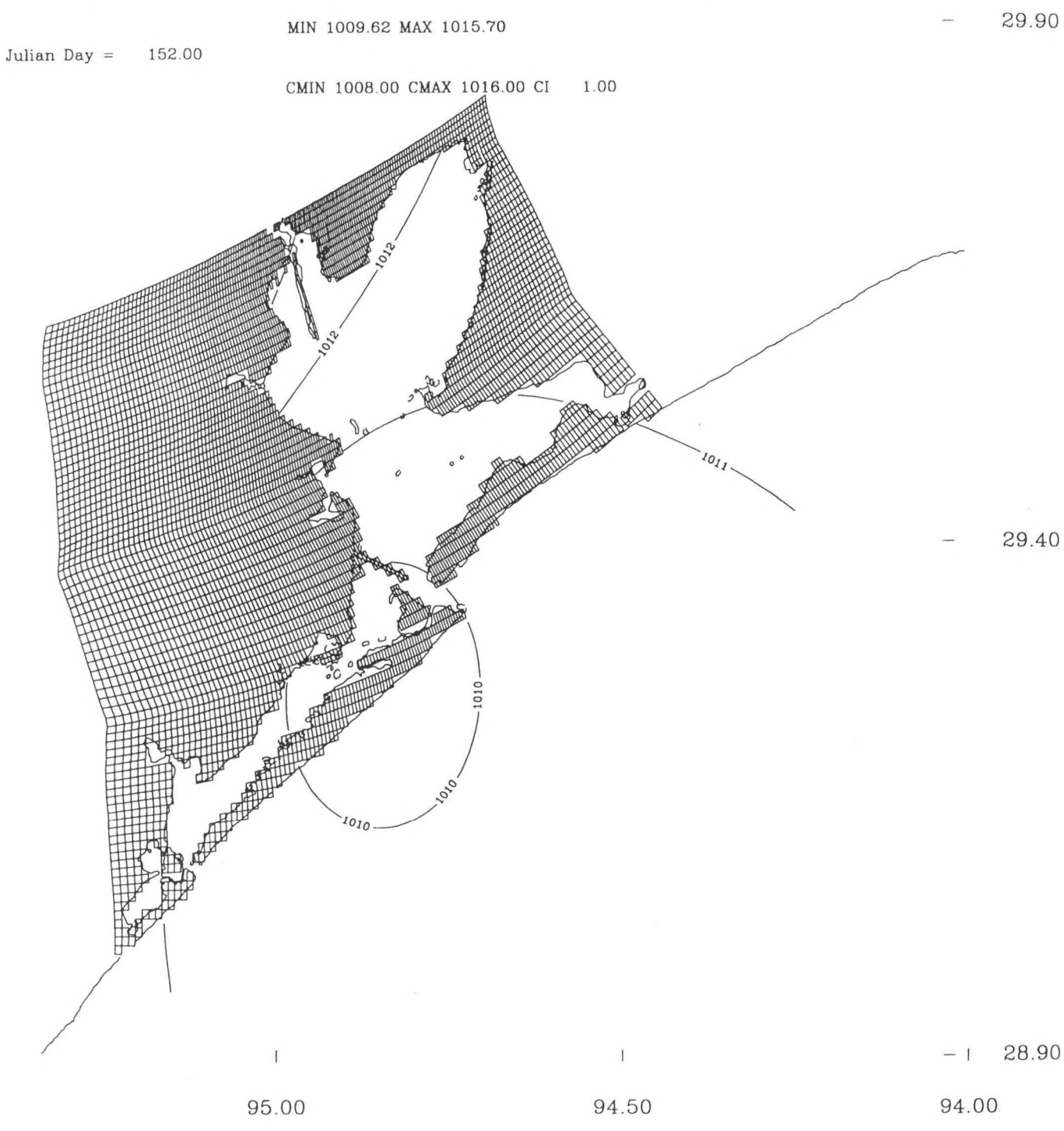

Figure 4.12. Surface atmospheric pressure field 1 June LST 0

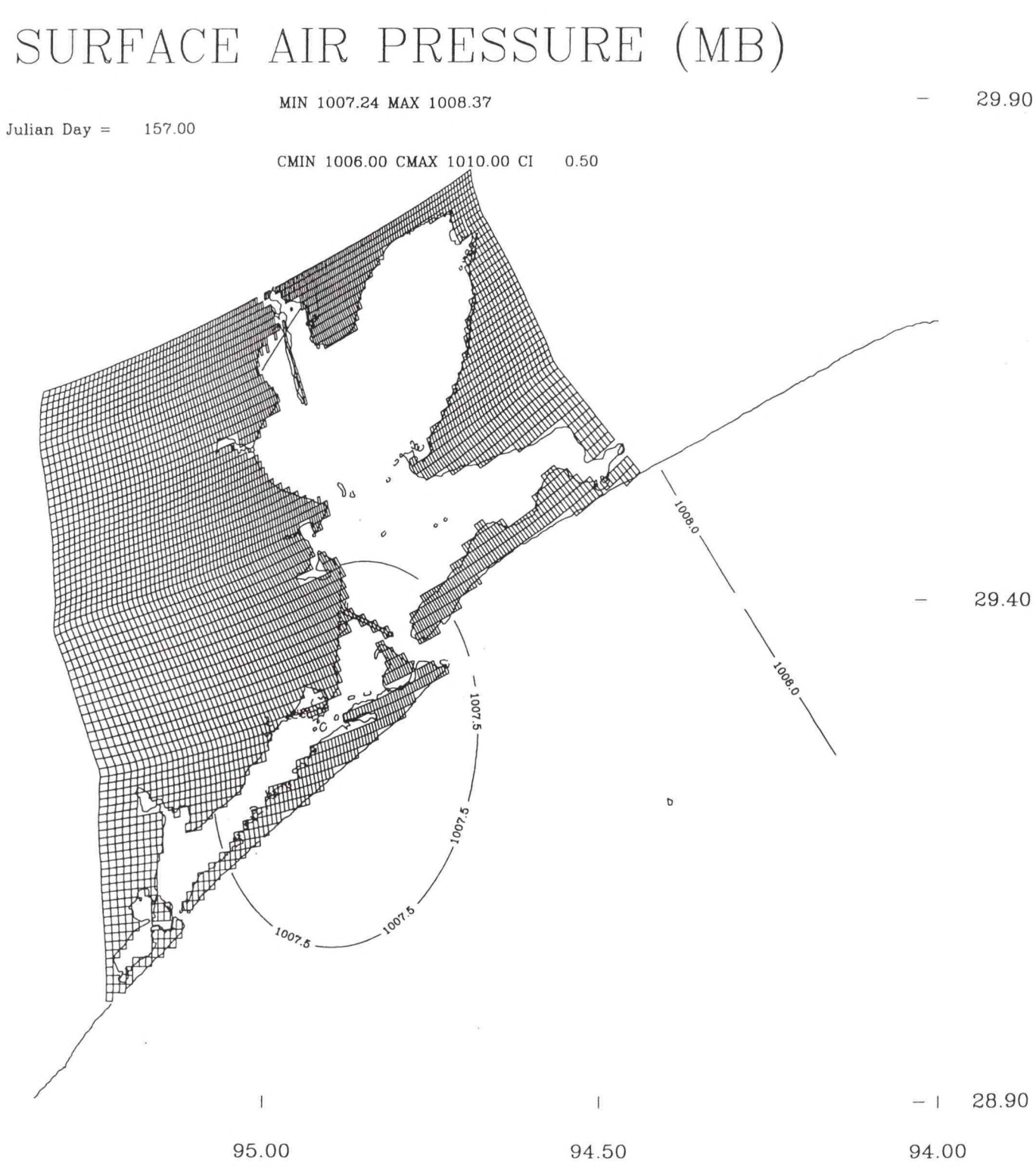

Figure 4.13. Surface atmospheric pressure field 6 June LST 0

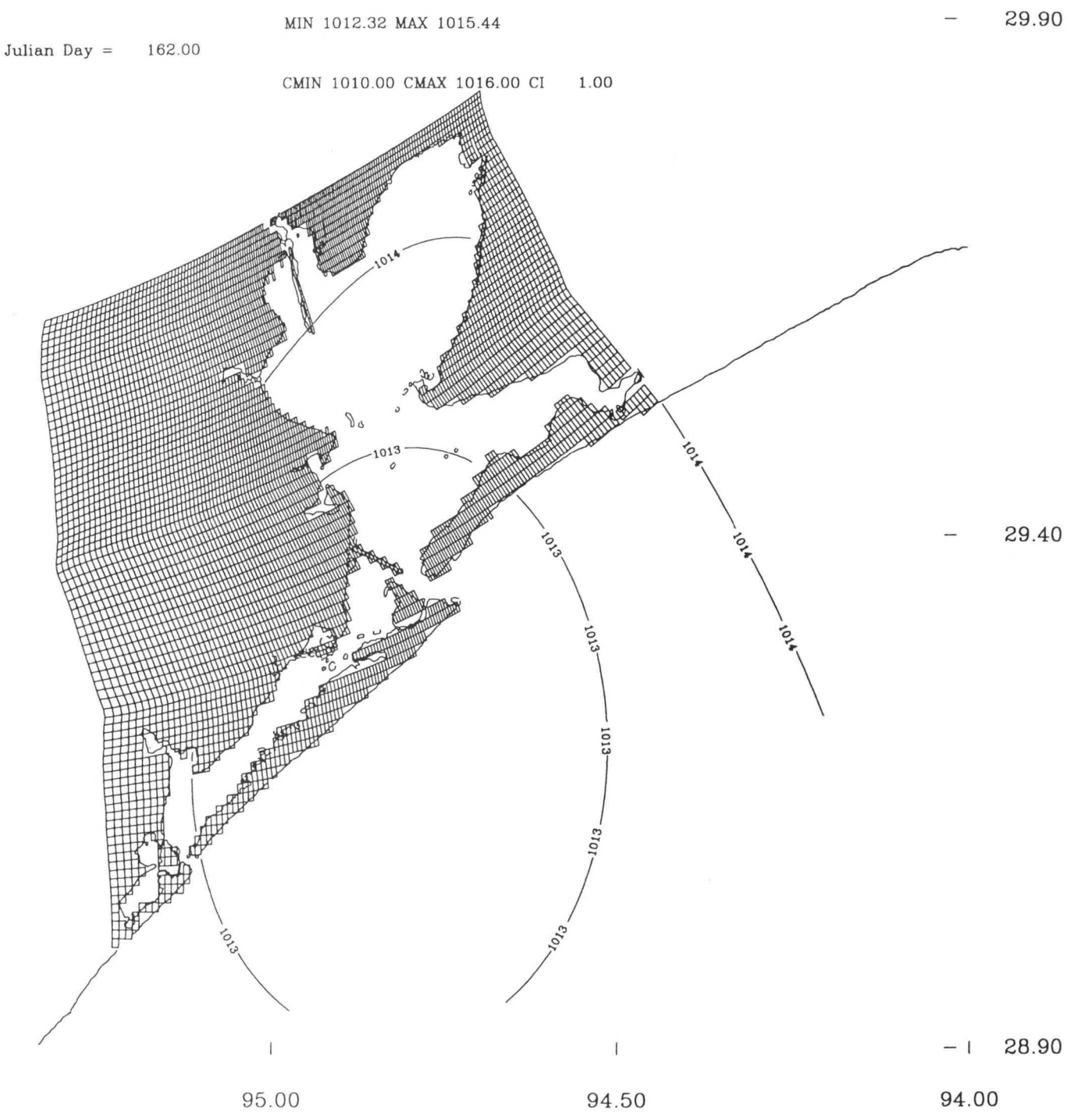

Figure 4.14. Surface atmospheric pressure field 11 June LST 0

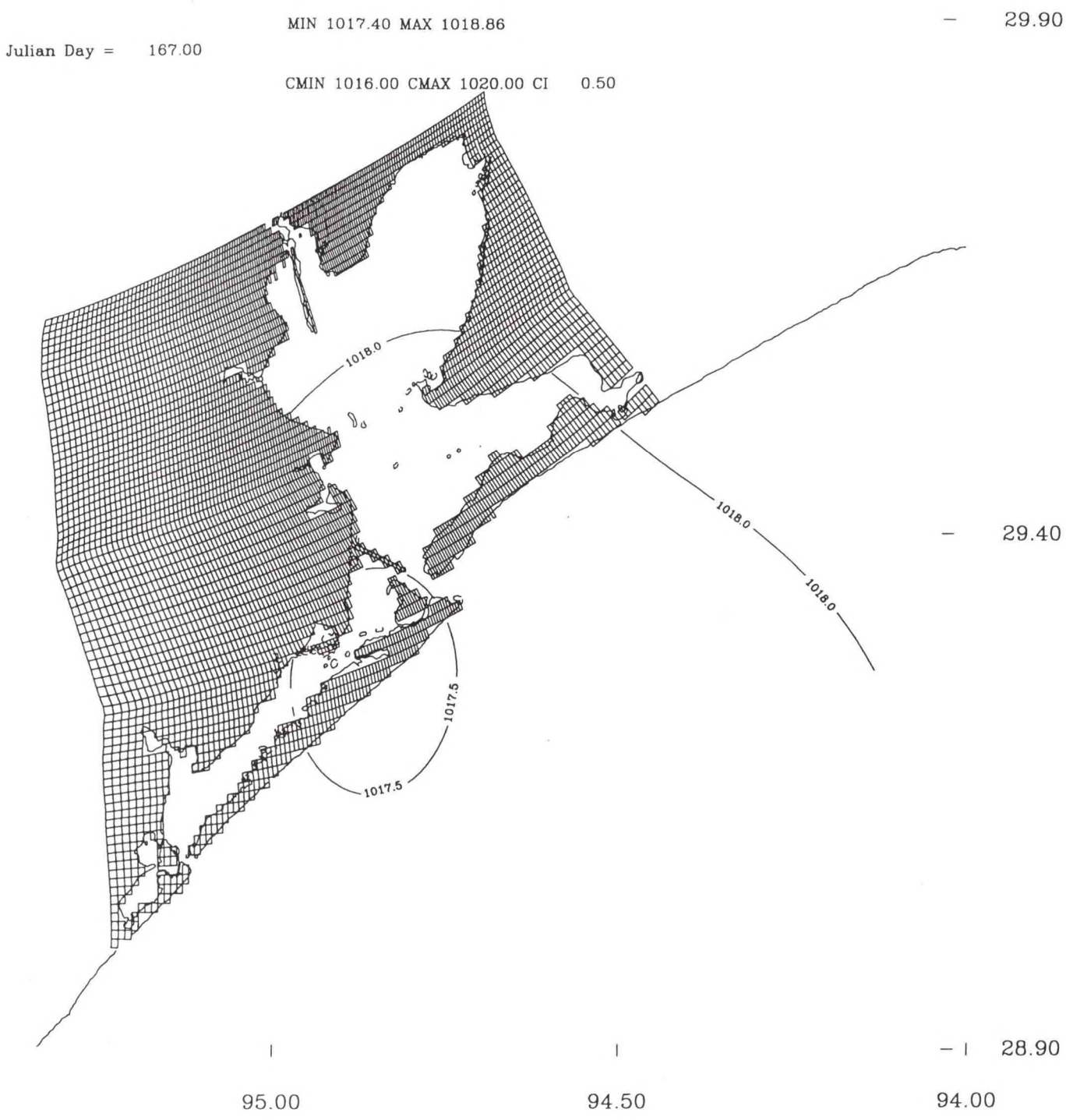

Figure 4.15. Surface atmospheric pressure field 16 June LST 0

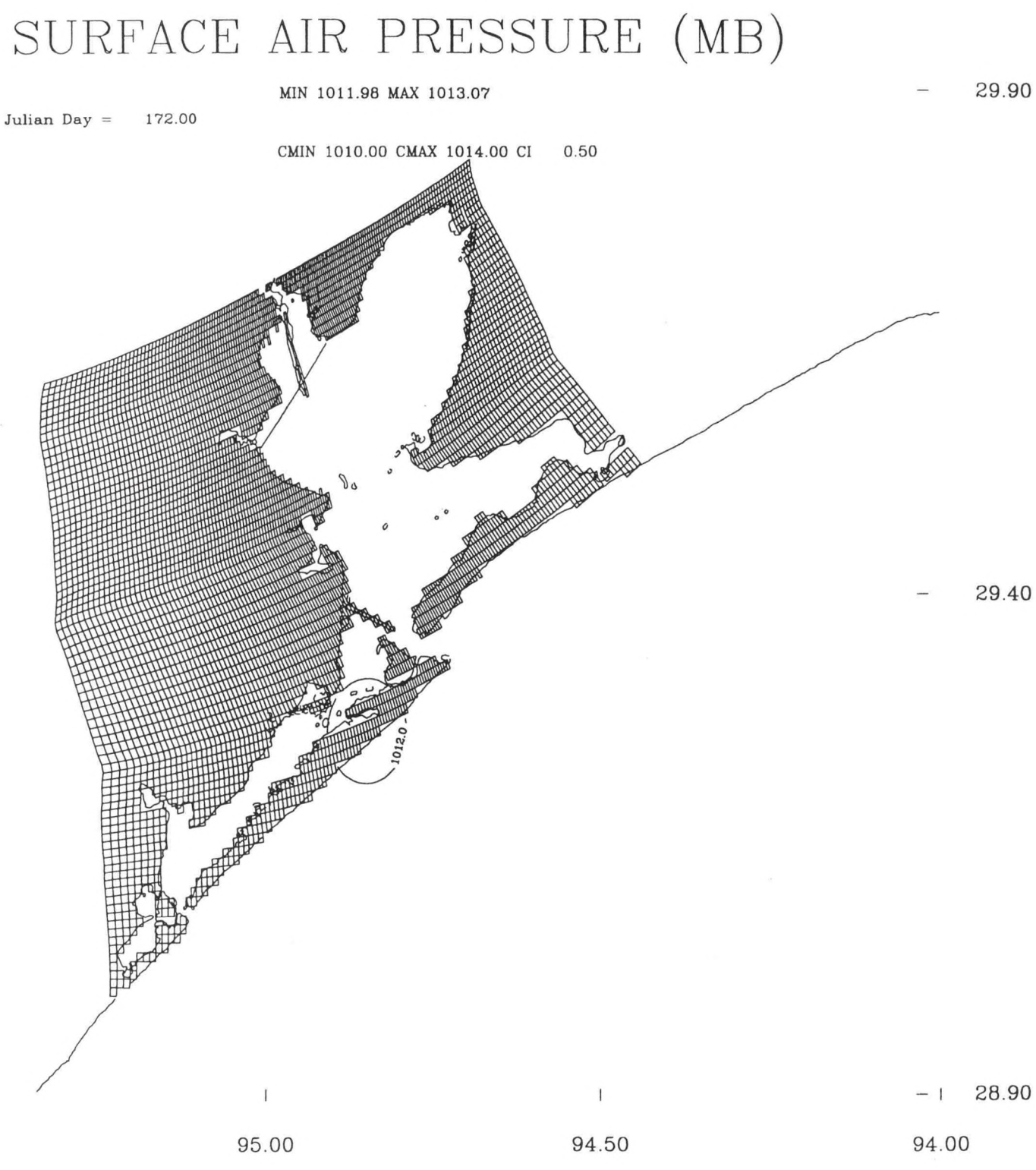

Figure 4.16. Surface atmospheric pressure field 21 June LST 0

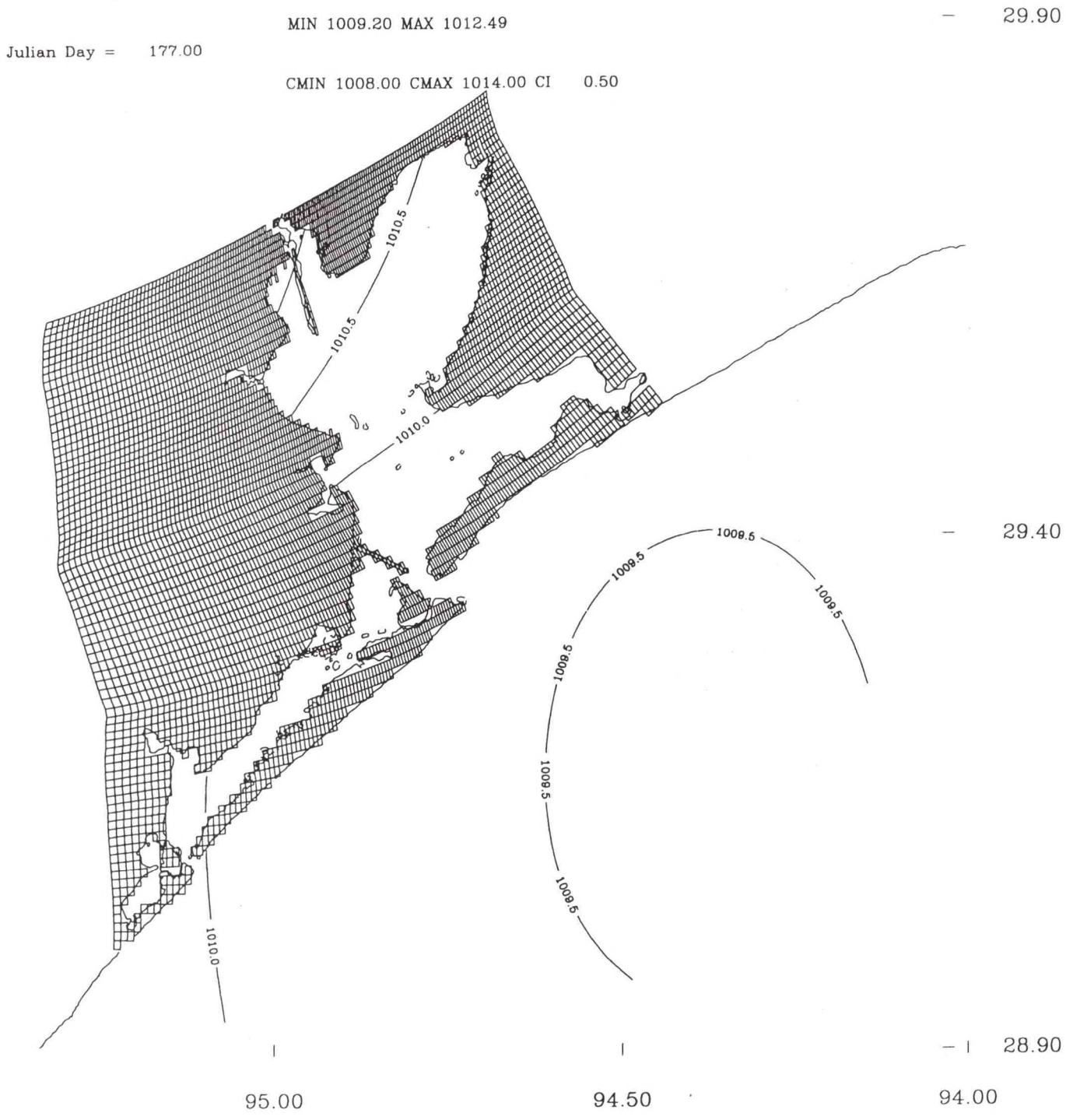

Figure 4.17. Surface atmospheric pressure field 26 June LST 0

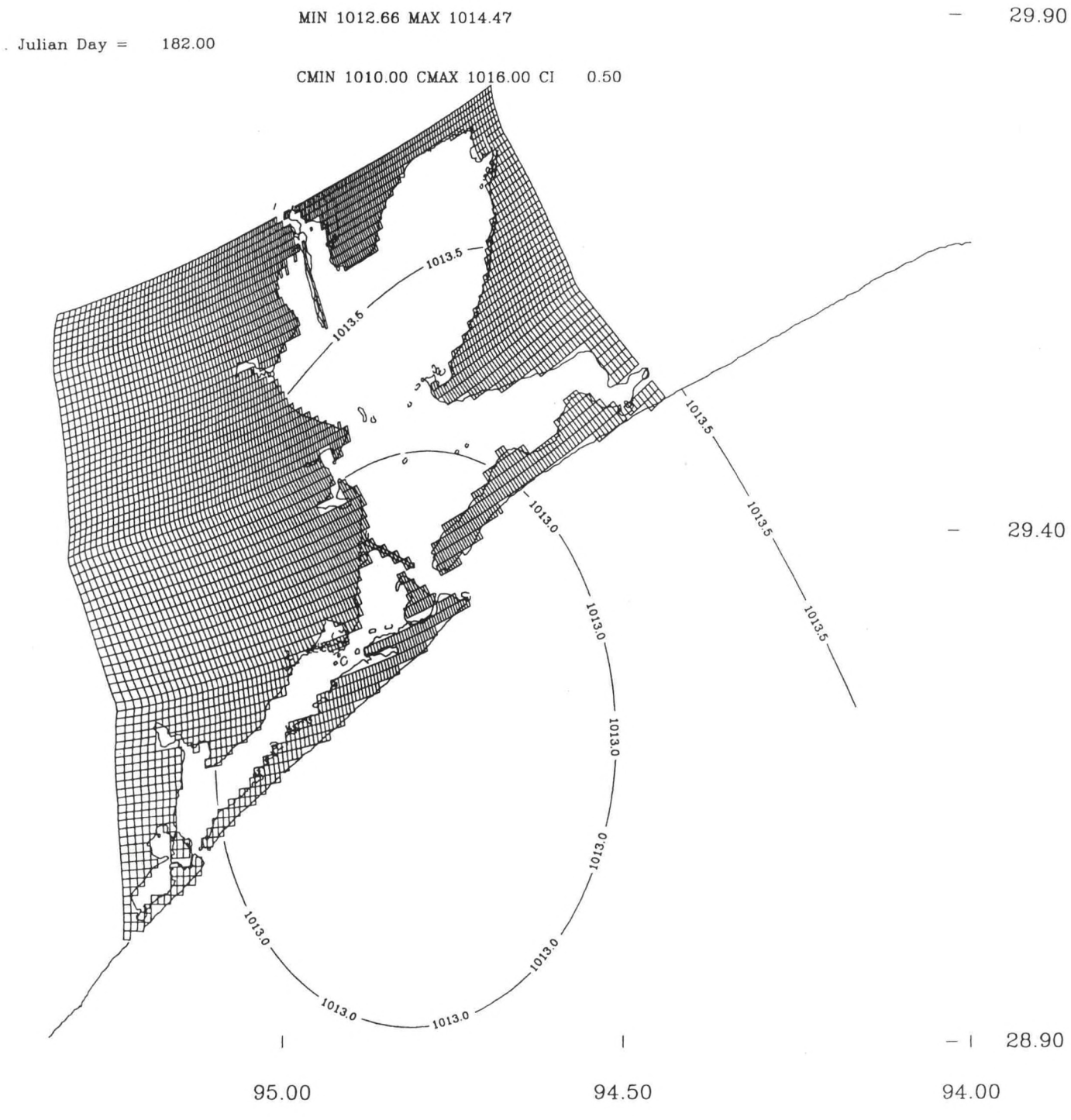

Figure 4.18. Surface atmospheric pressure field 1 July LST 0

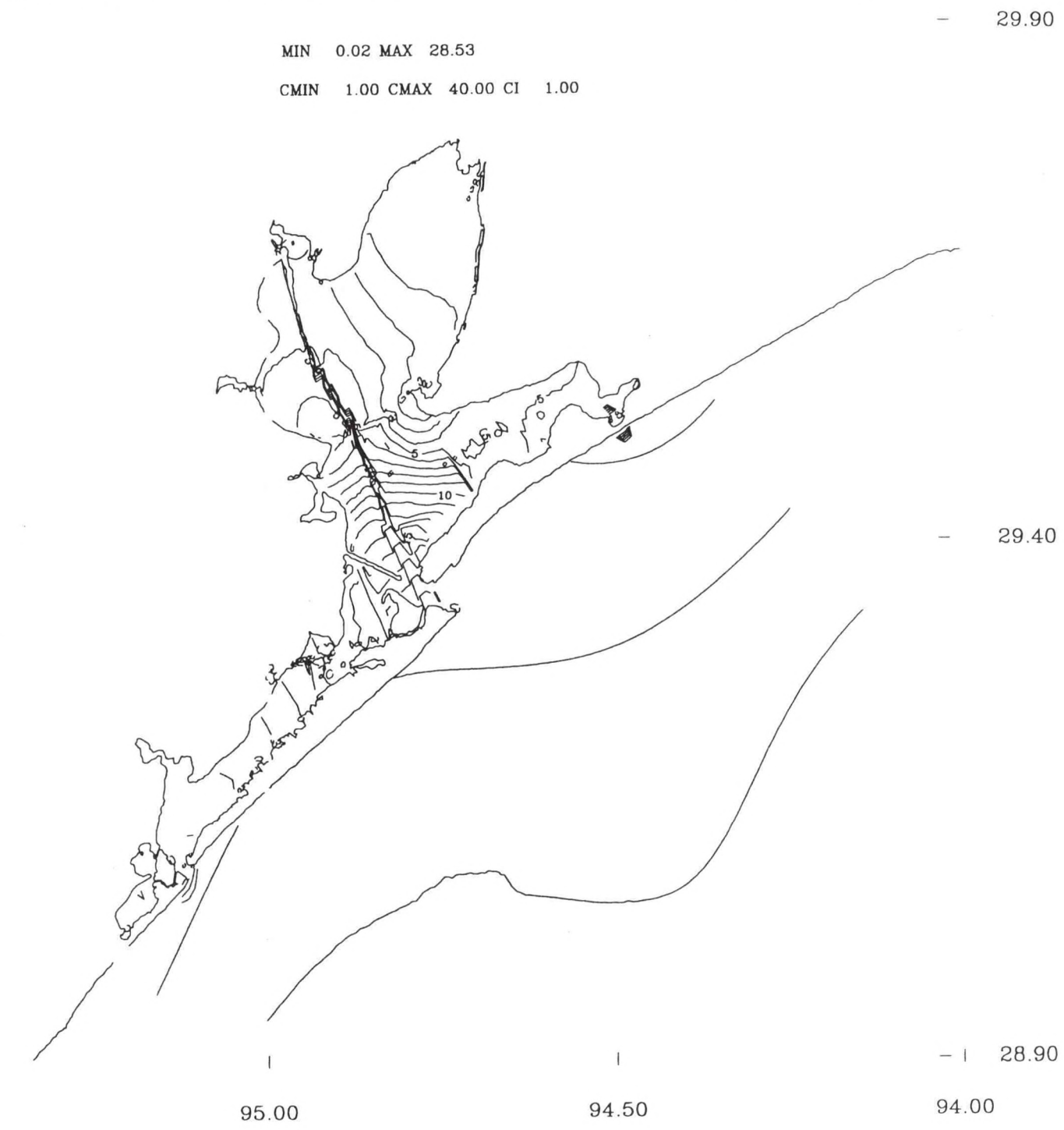

Figure 4.19. 1 June 1995 initial near-surface salinity field

Figure 4.20. 1 June 1995 initial near-bottom salinity field

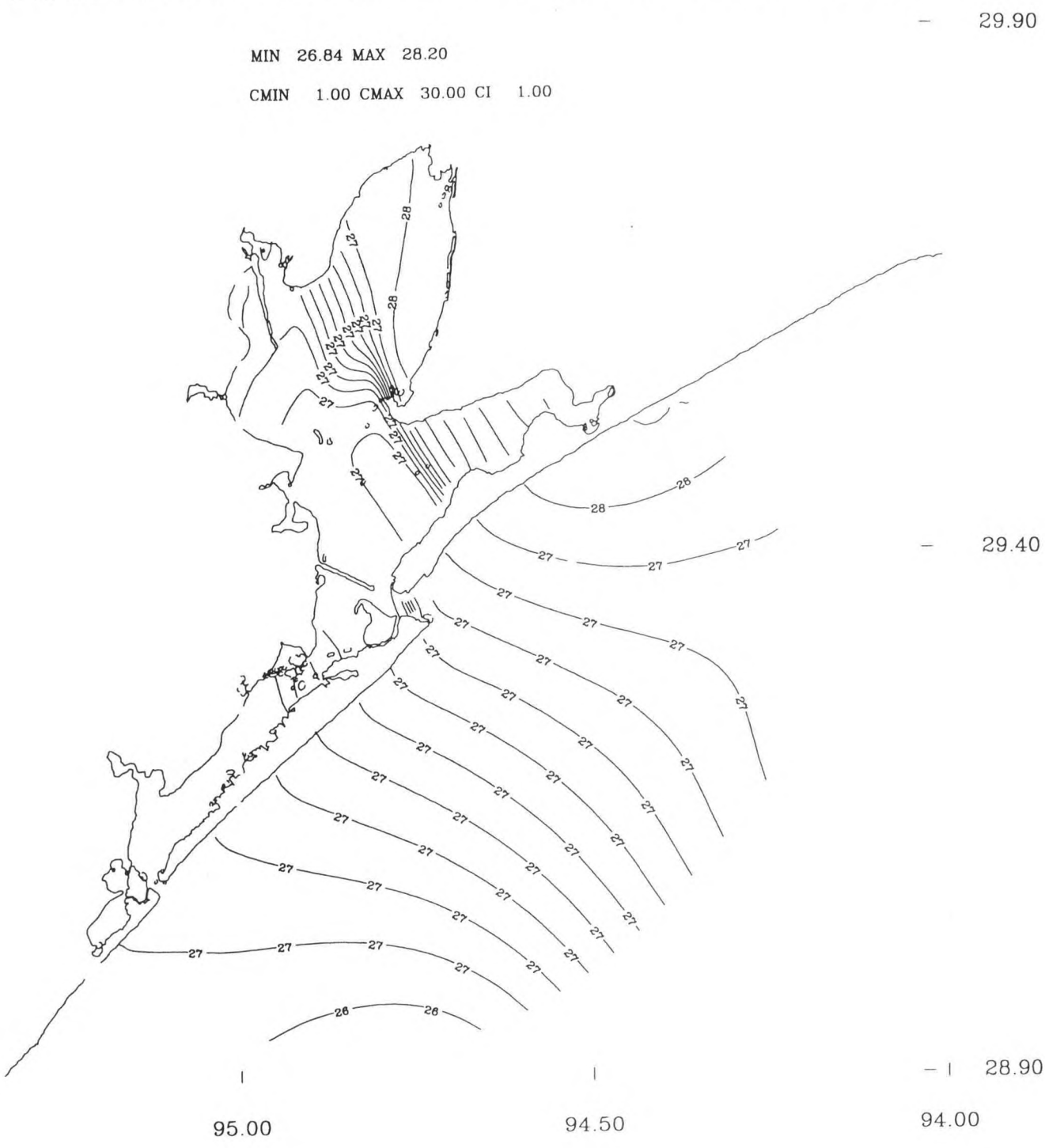

Figure 4.21. 1 June 1995 initial near-surface temperature field

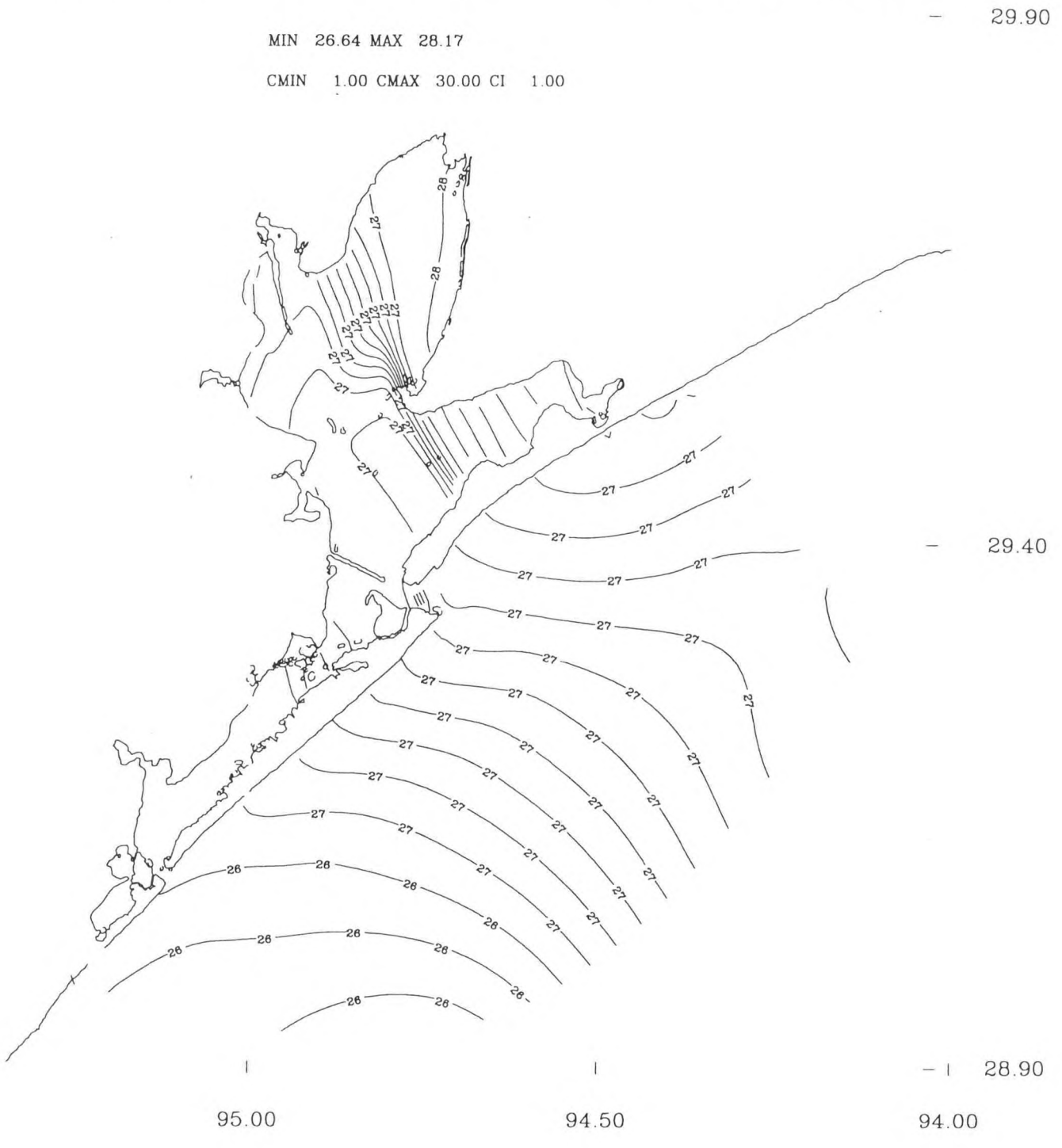

Figure 4.22. 1 June 1995 initial near-bottom temperature field

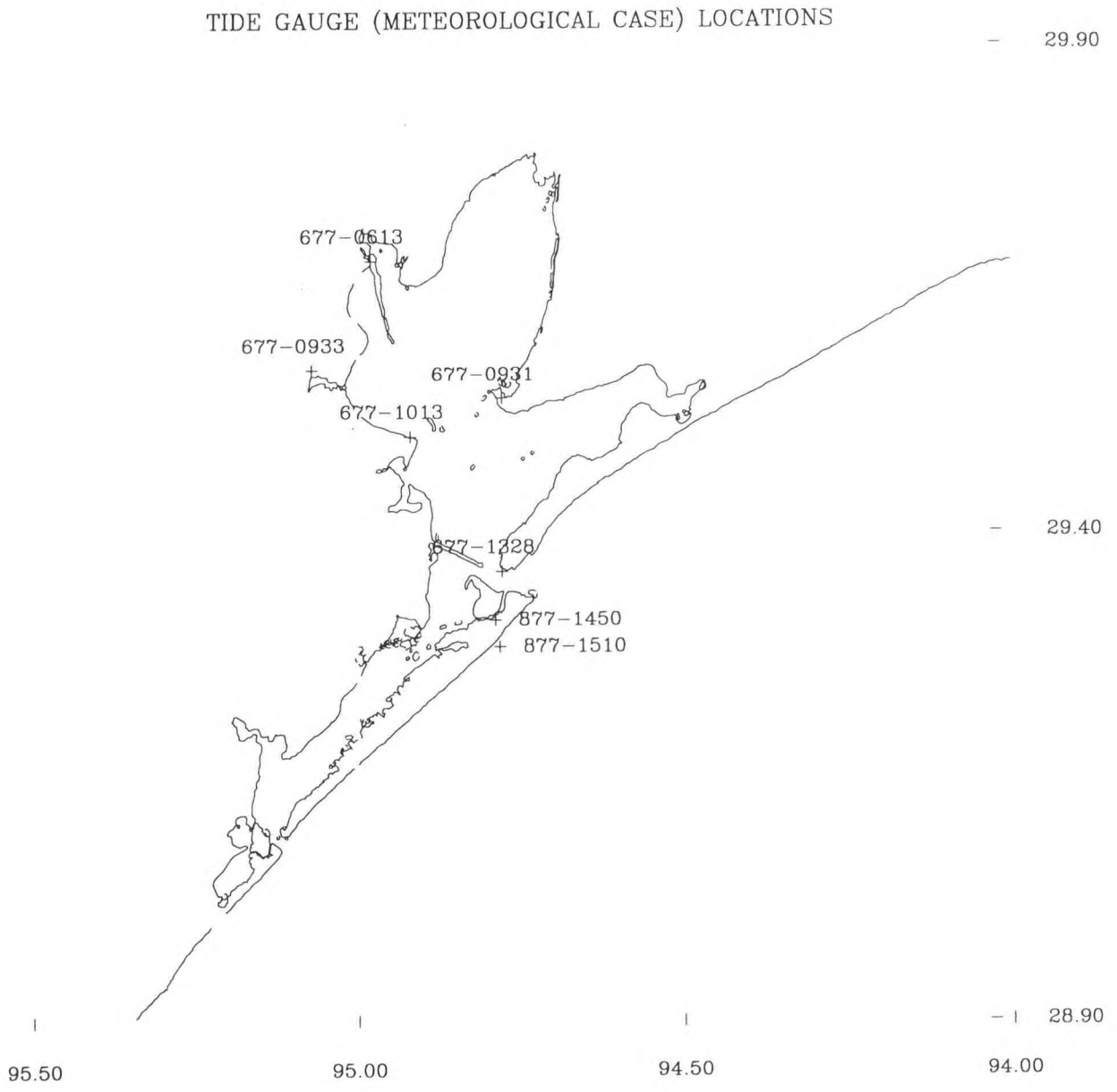

Figure 4.23. June 1995 meteorological simulation water level gauge locations

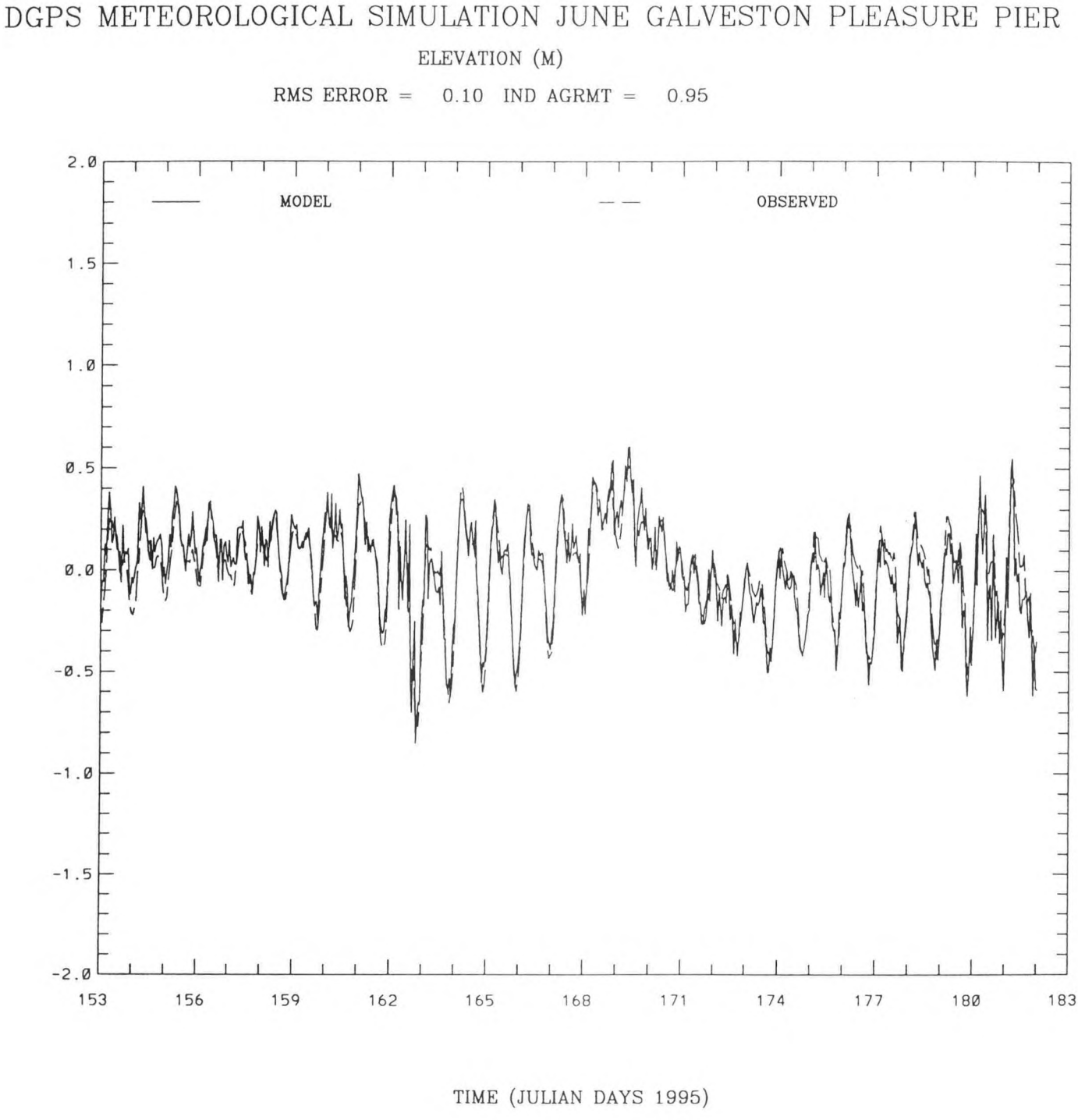

Figure 4.24. June 1995 meteorological simulation: model vs observed demeaned water level at Galveston Pleasure Pier

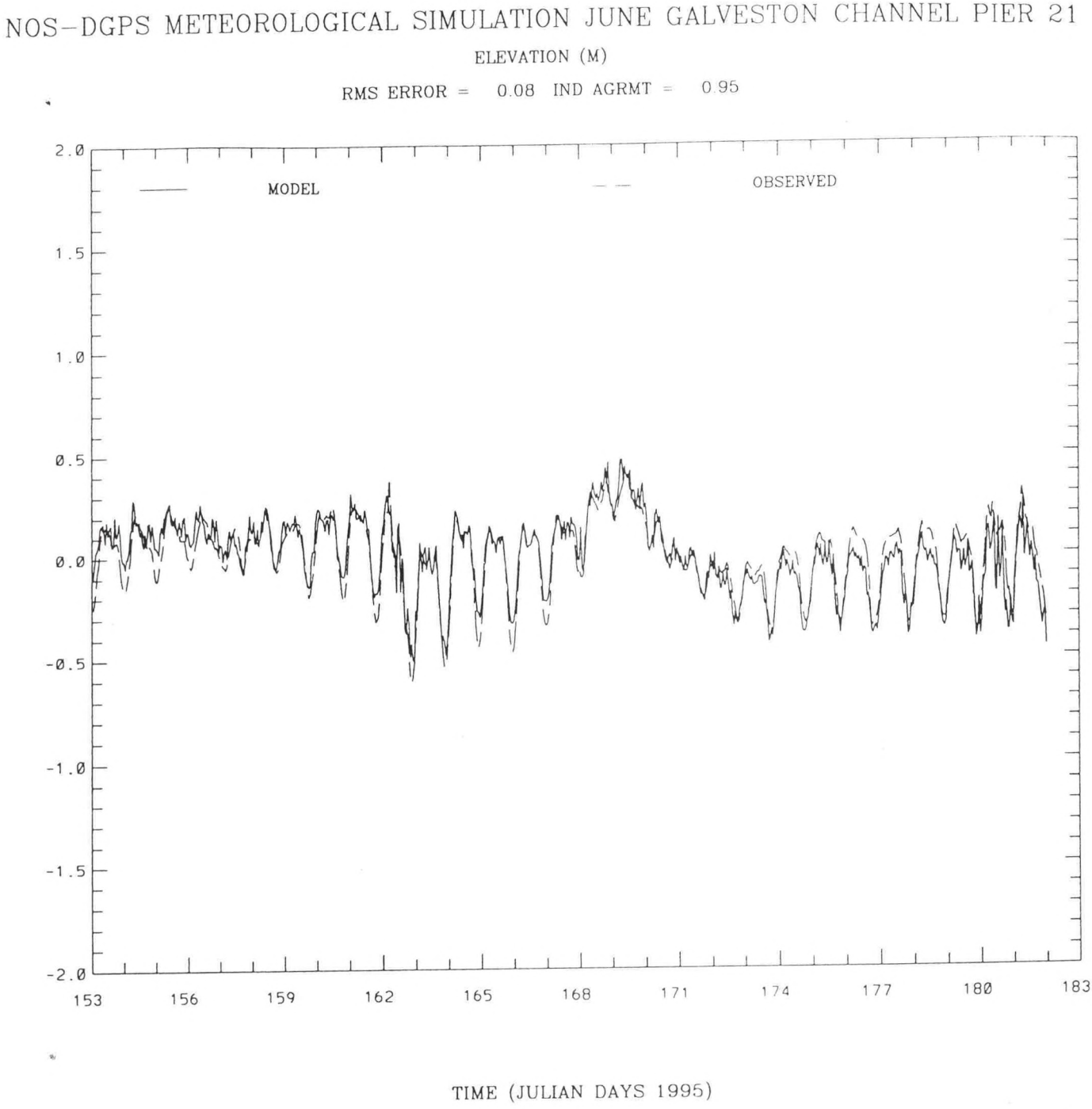

Figure 4.25. June 1995 meteorological simulation: model vs observed demeaned water level at Galveston Pier 21

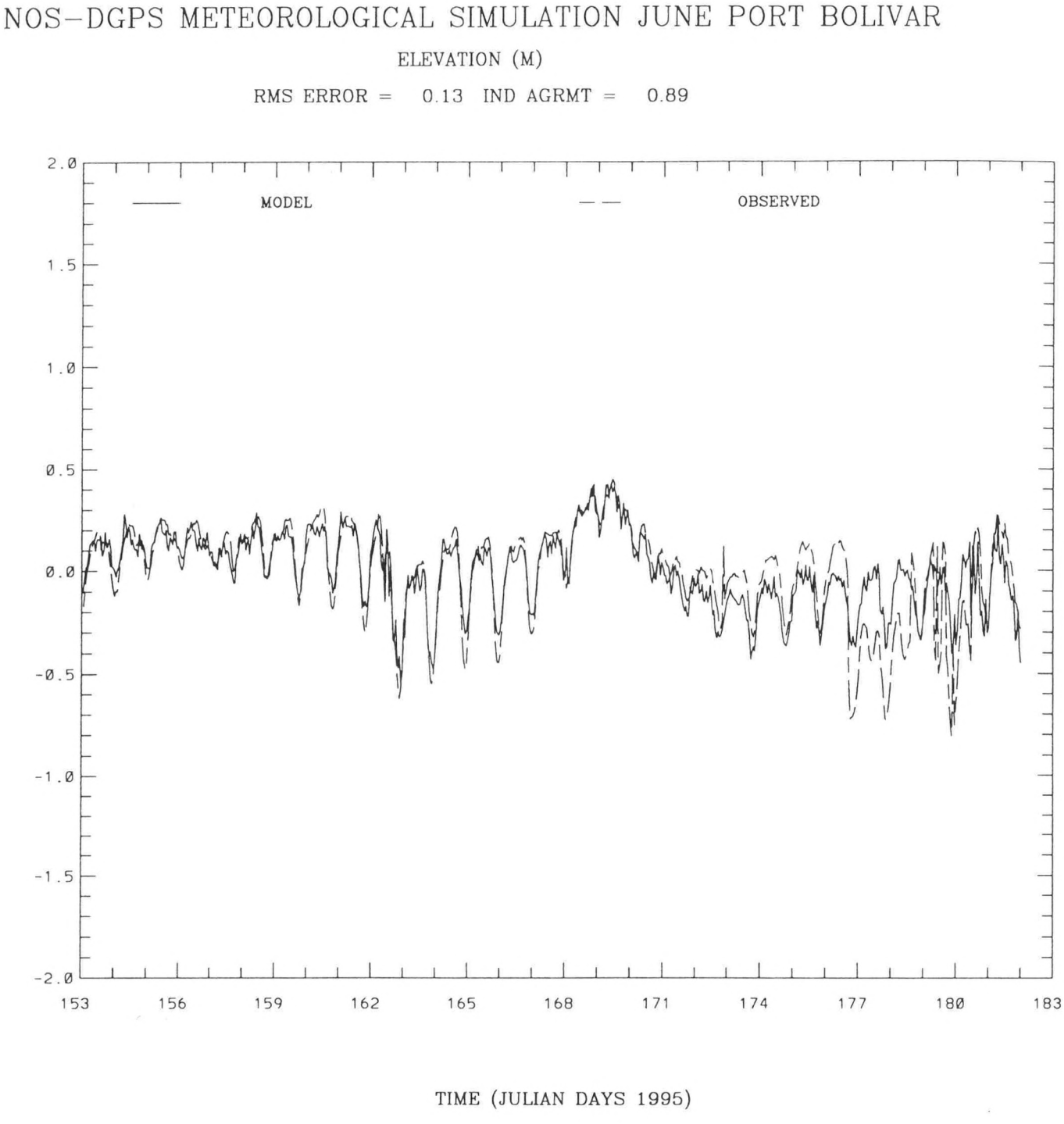

Figure 4.26. June 1995 meteorological simulation: model vs observed demeaned water level at Port Bolivar

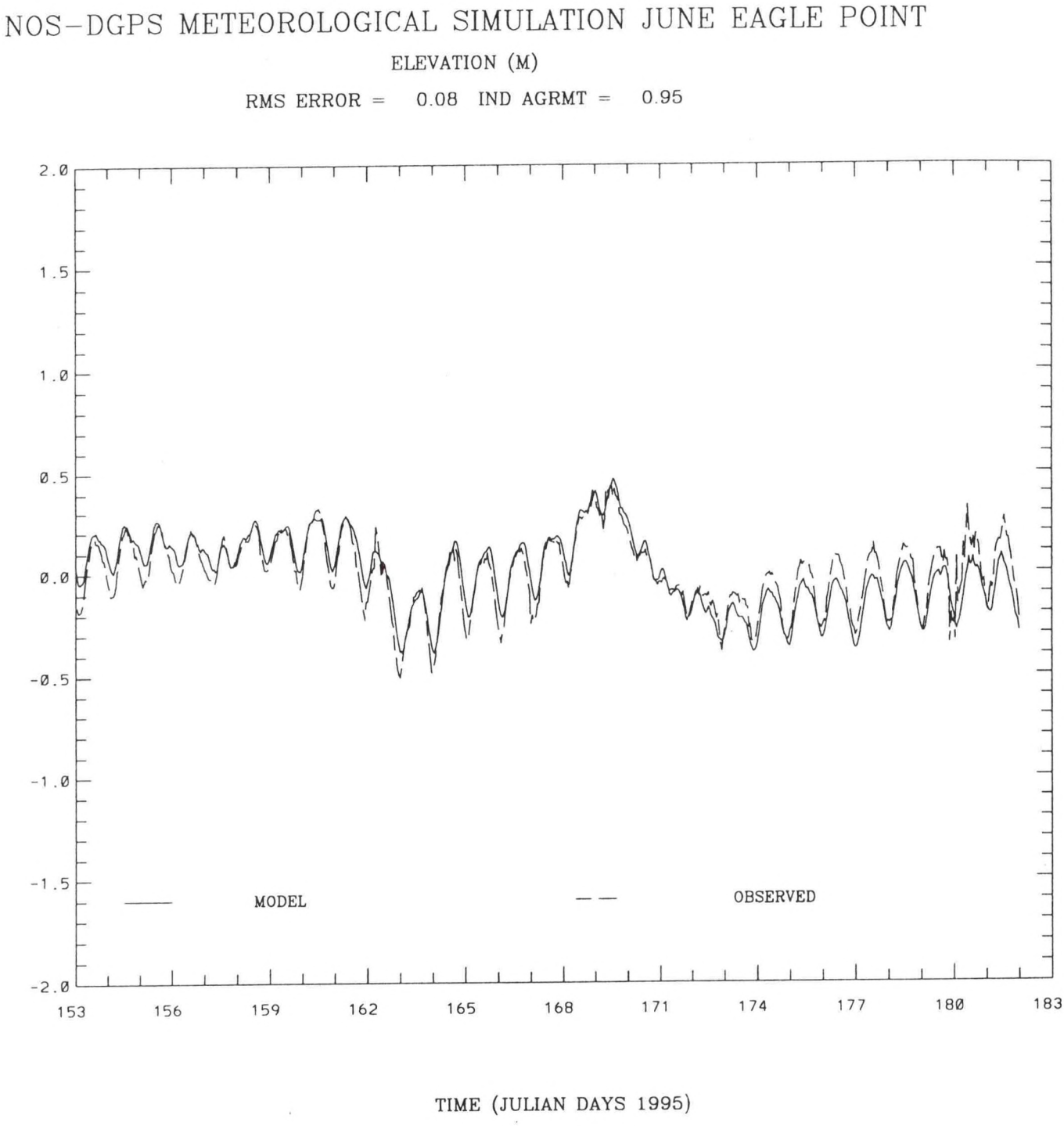

Figure 4.27. June 1995 meteorological simulation: model vs observed demeaned water level at Eagle Point

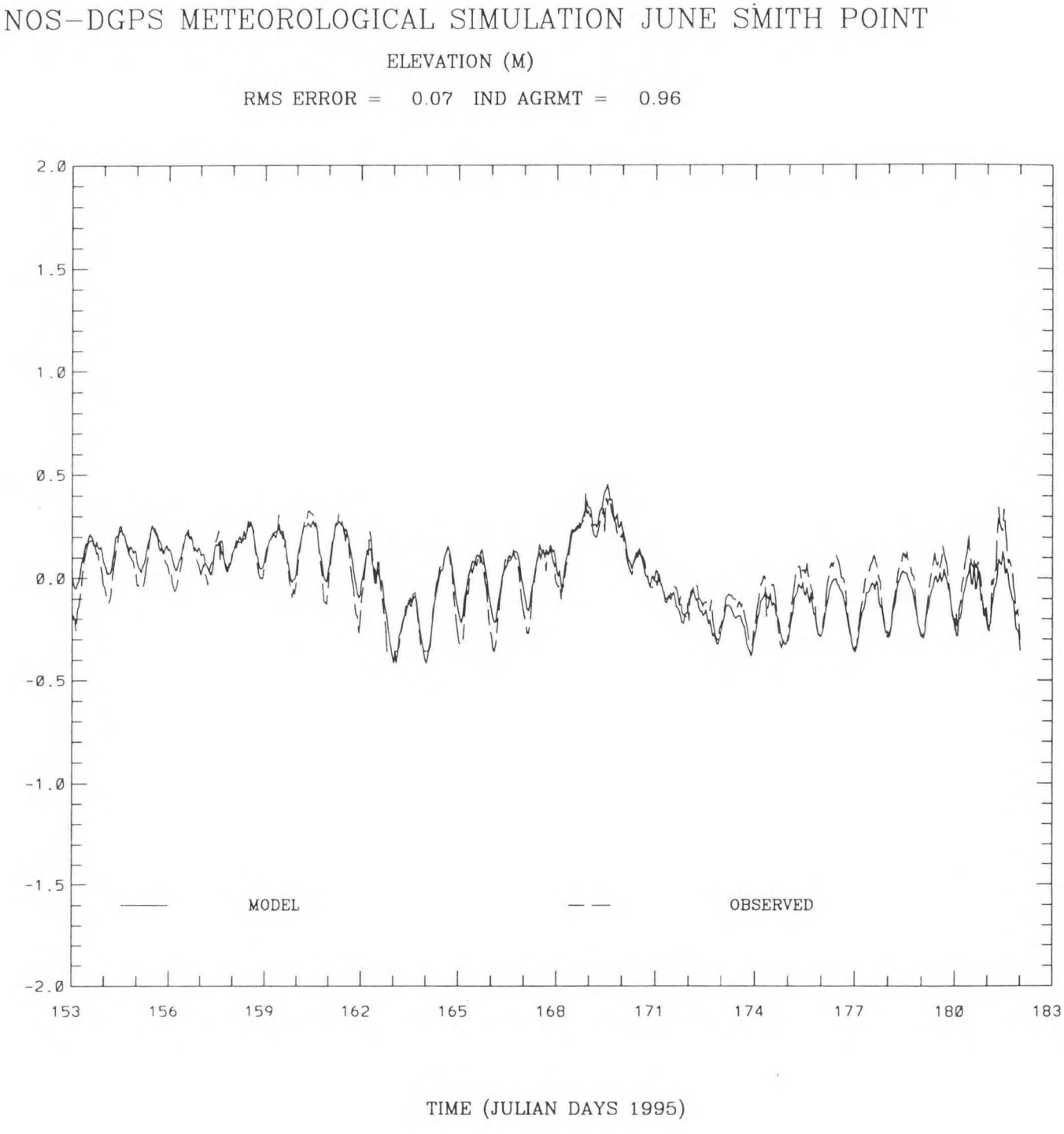

Figure 4.28. June 1995 meteorological simulation: model vs observed demeaned water level at Smith Point

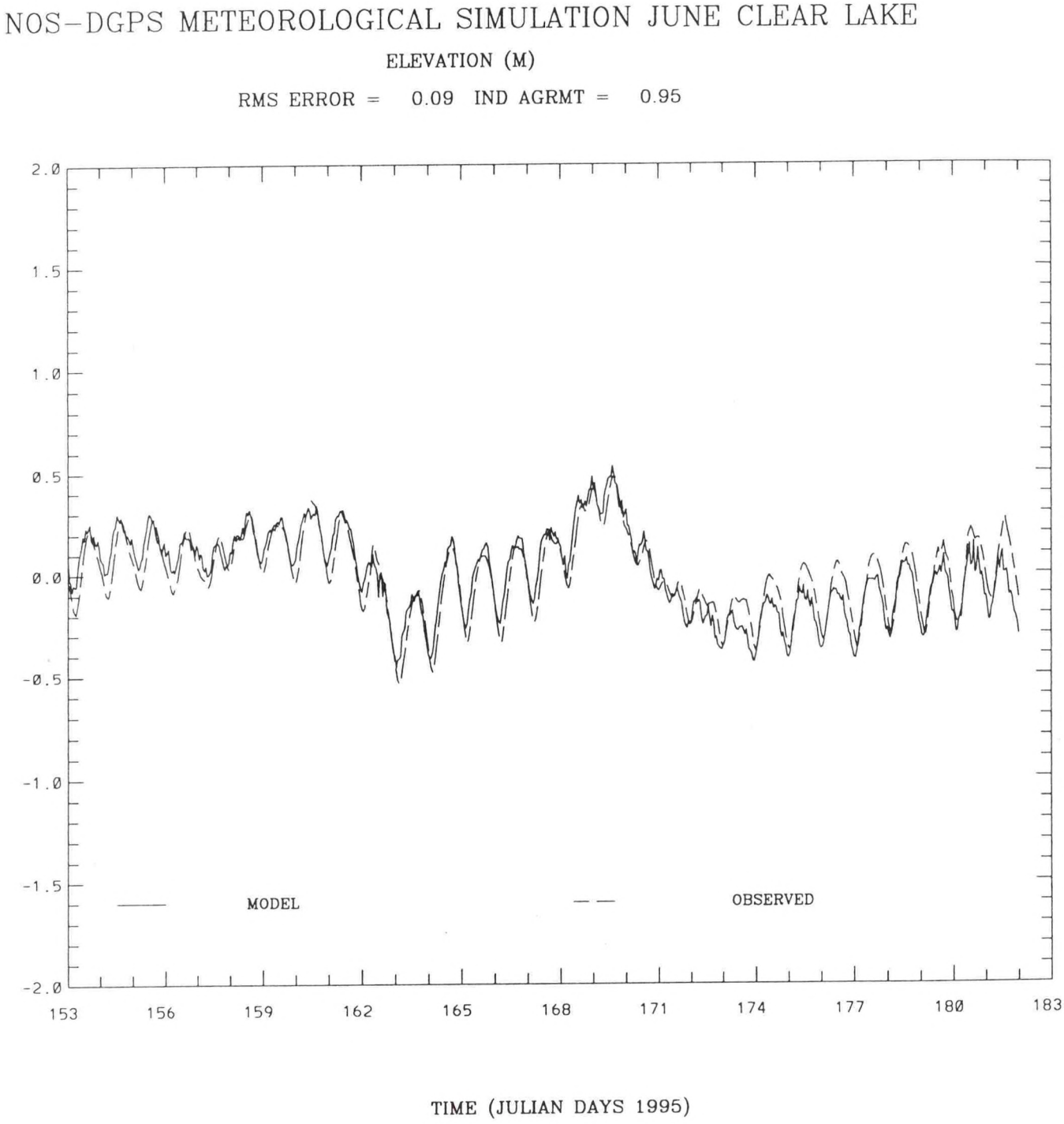

Figure 4.29. June 1995 meteorological simulation: model vs observed demeaned water level at Clear Lake

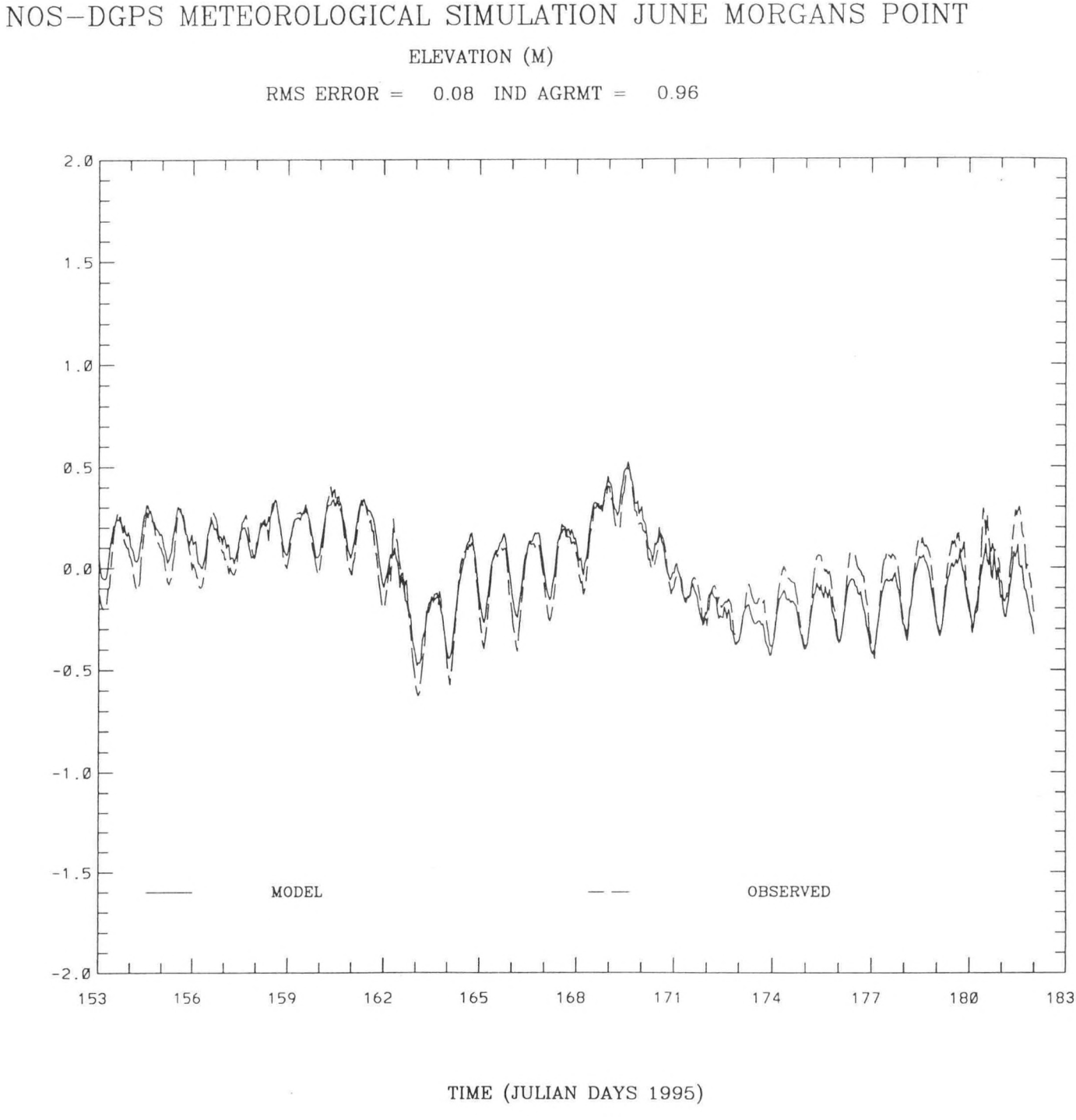

Figure 4.30. June 1995 meteorological simulation: model vs observed demeaned water level at Morgans Point

Figure 4.31. TWDB Conductivity/Temperature Datasonde locations

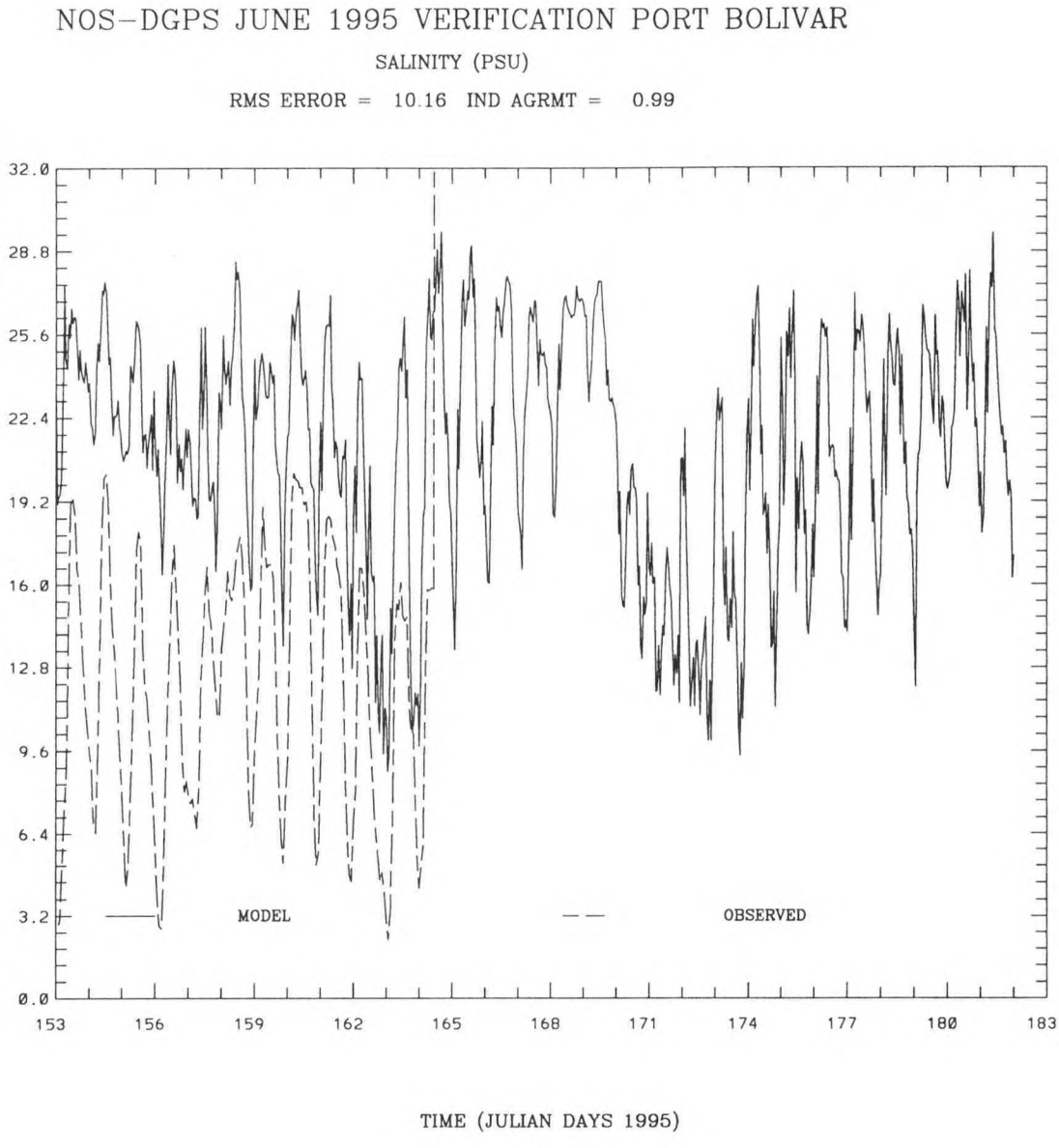

Figure 4.32. June 1995 meteorological simulation: model vs TWDB salinity Port Bolivar

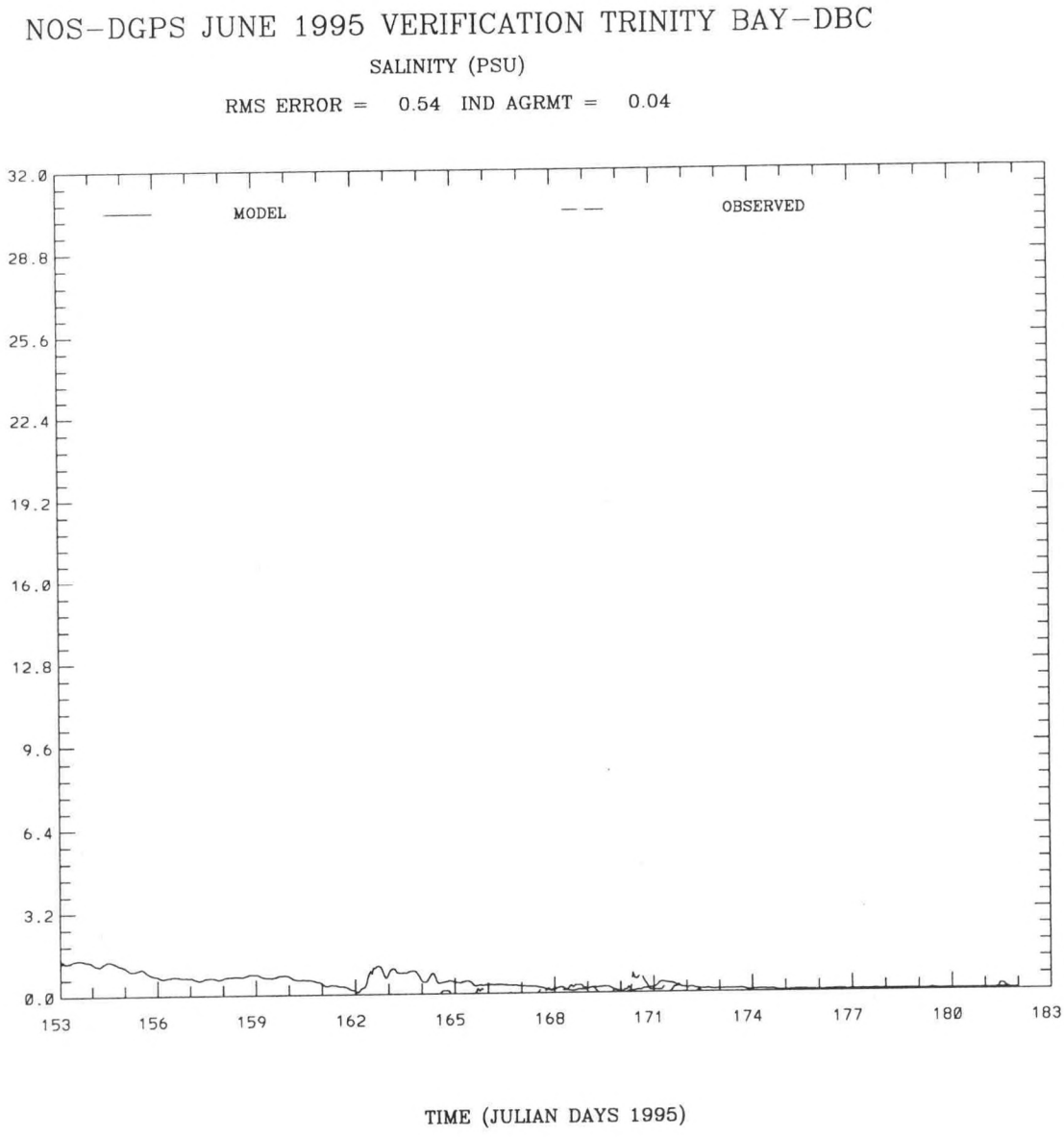

Figure 4.33. June 1995 meteorological simulation: model vs TWDB salinity Trinity Bay - DBC

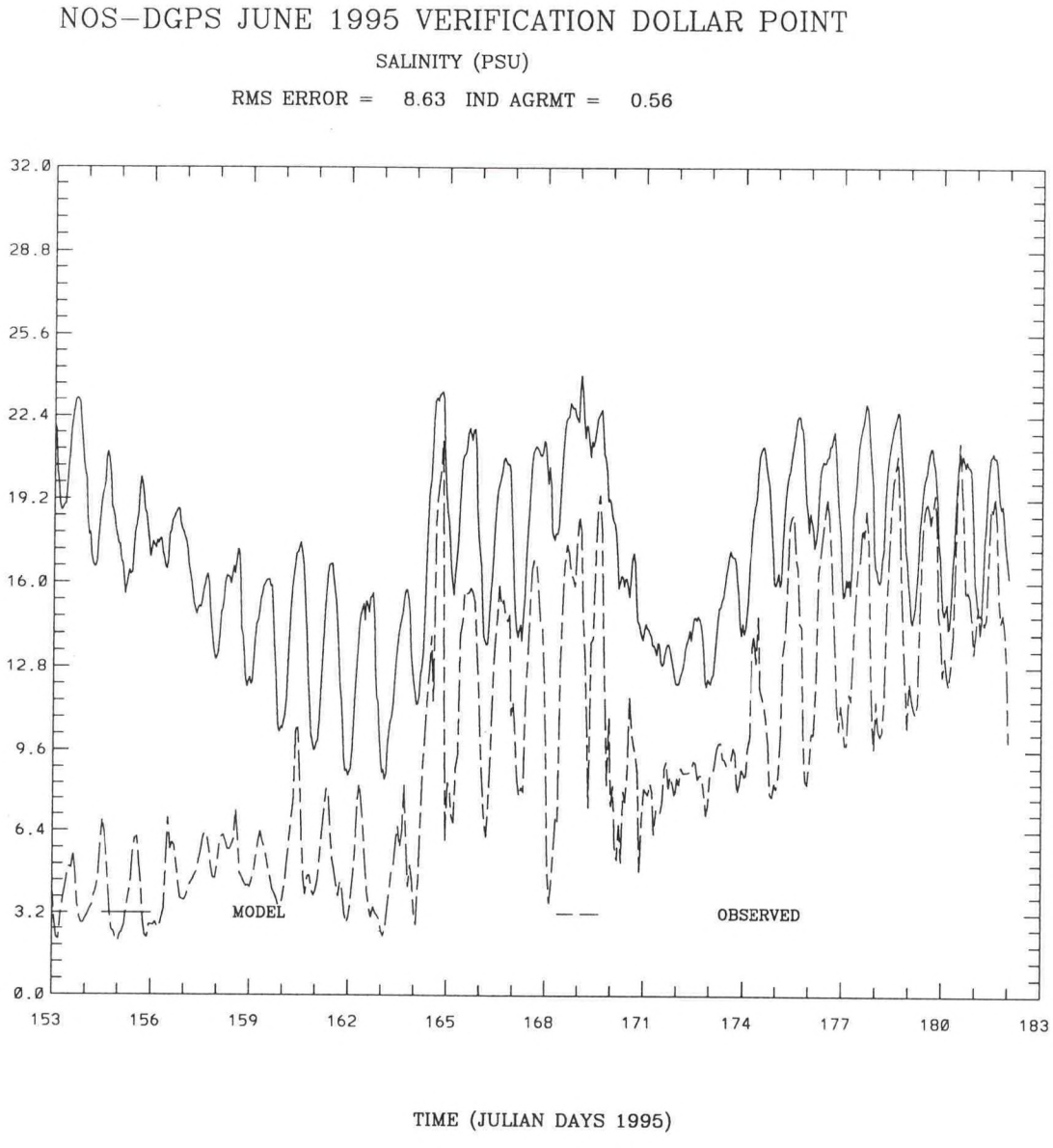

Figure 4.34. June 1995 meteorological simulation: model vs TWDB salinity Dollar Point

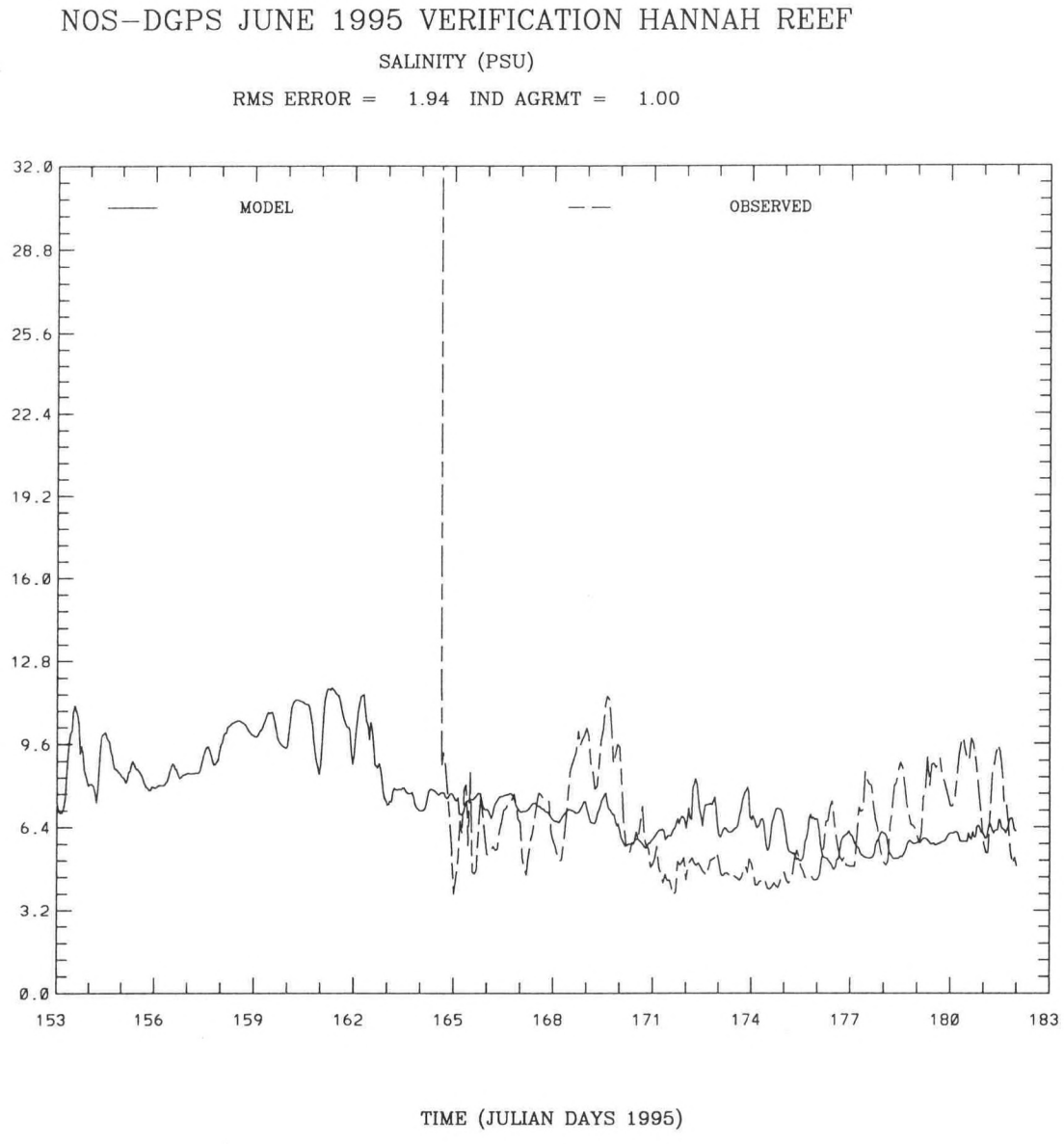

Figure 4.35. June 1995 meteorological simulation: model vs TWDB salinity Hannah Reef

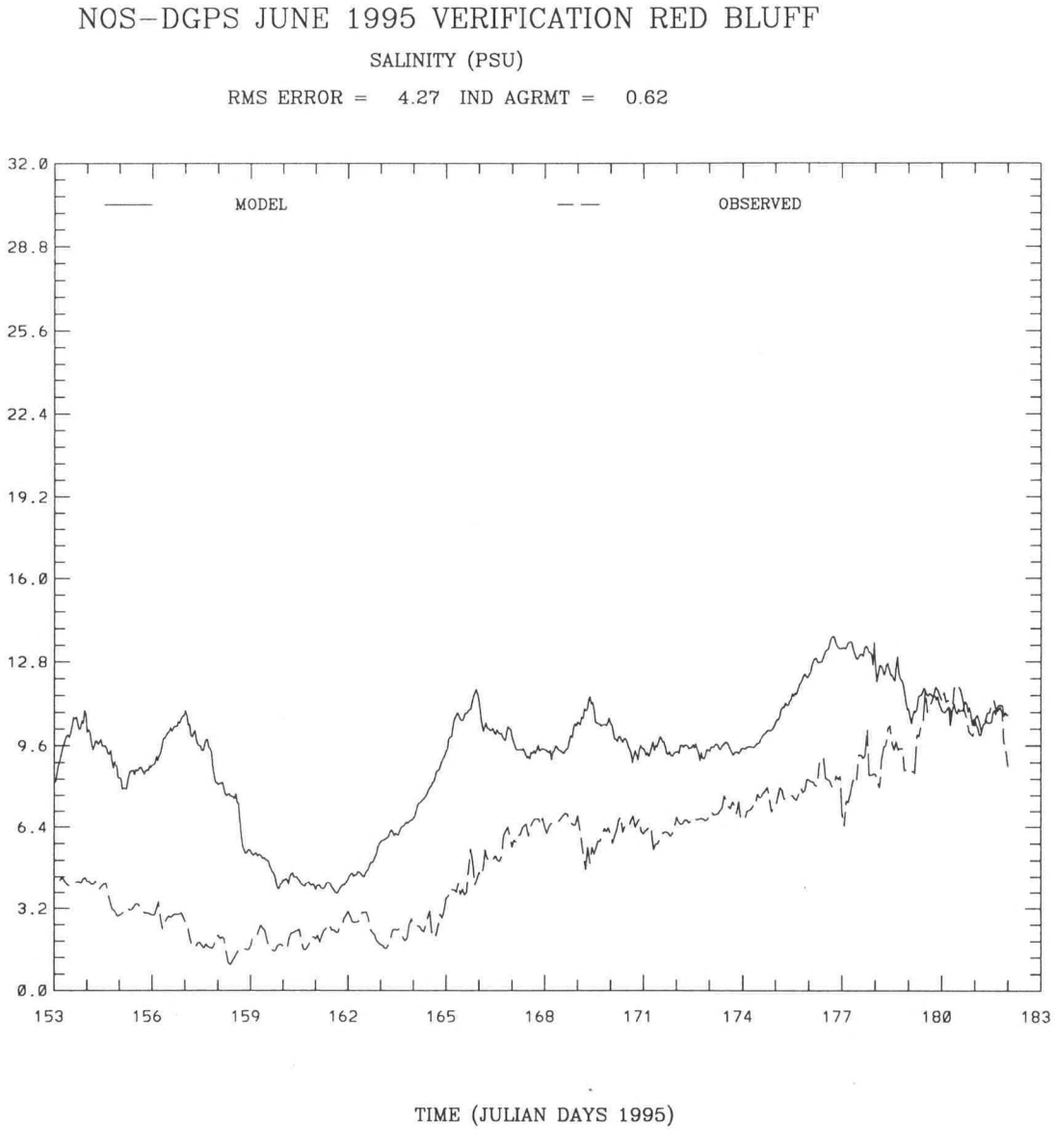

Figure 4.36. June 1995 meteorological simulation: model vs TWDB salinity Red Bluff

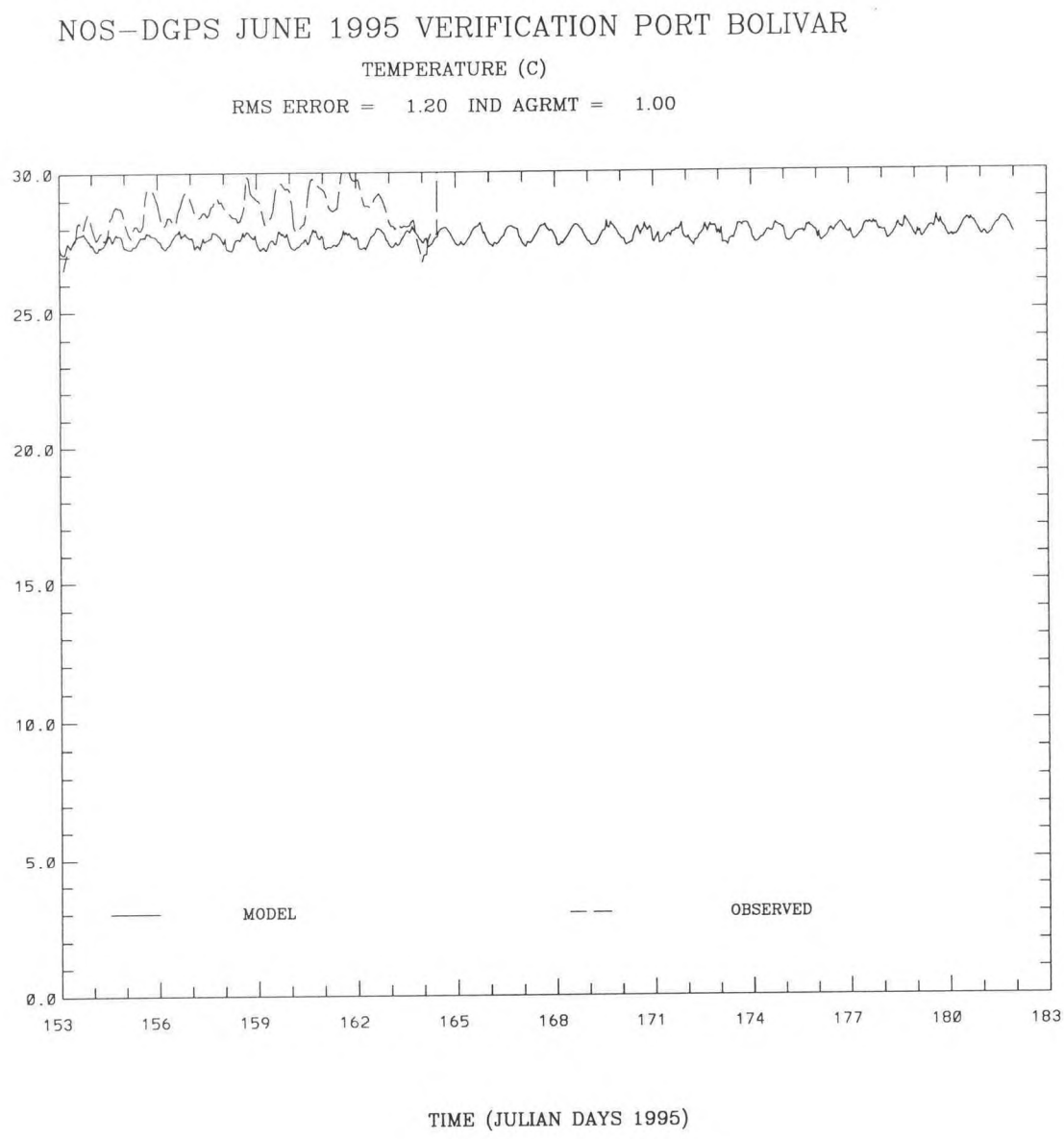

Figure 4.37. June 1995 meteorological simulation: model vs TWDB temperature Port Bolivar

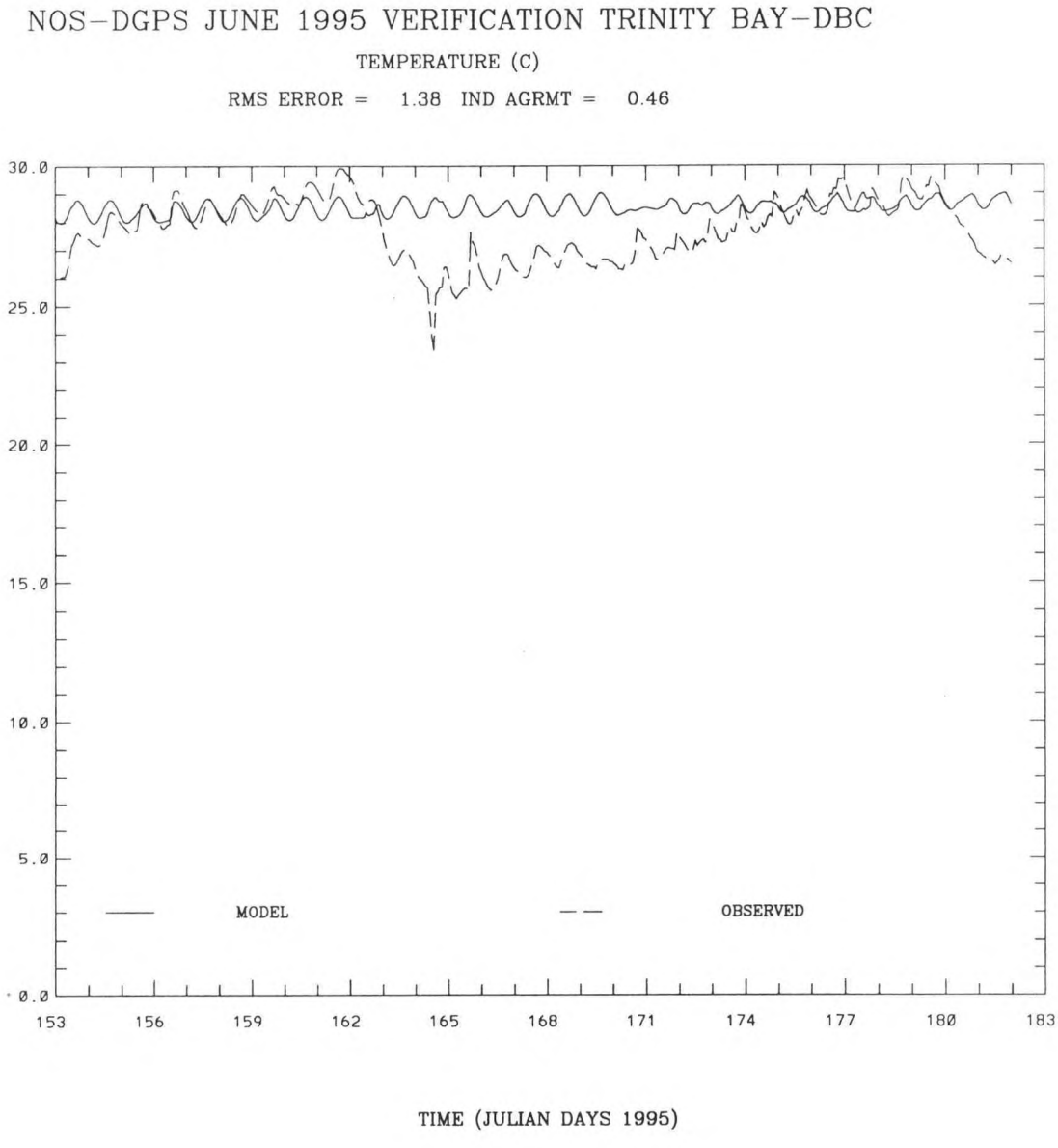

Figure 4.38. June 1995 meteorological simulation: model vs TWDB temperature Trinity Bay - DBC

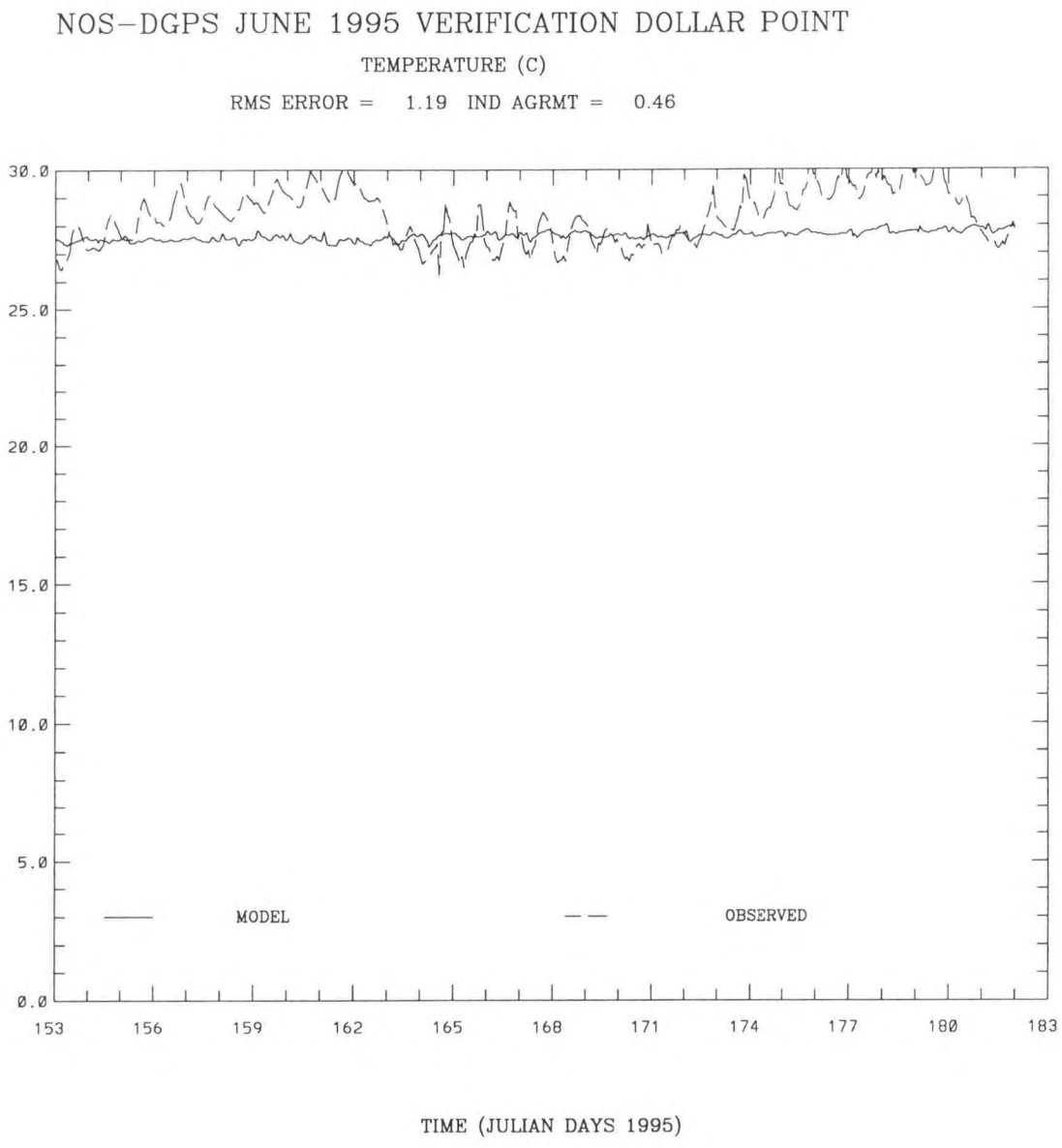

Figure 4.39. June 1995 meteorological simulation: model vs TWDB temperature Dollar Point

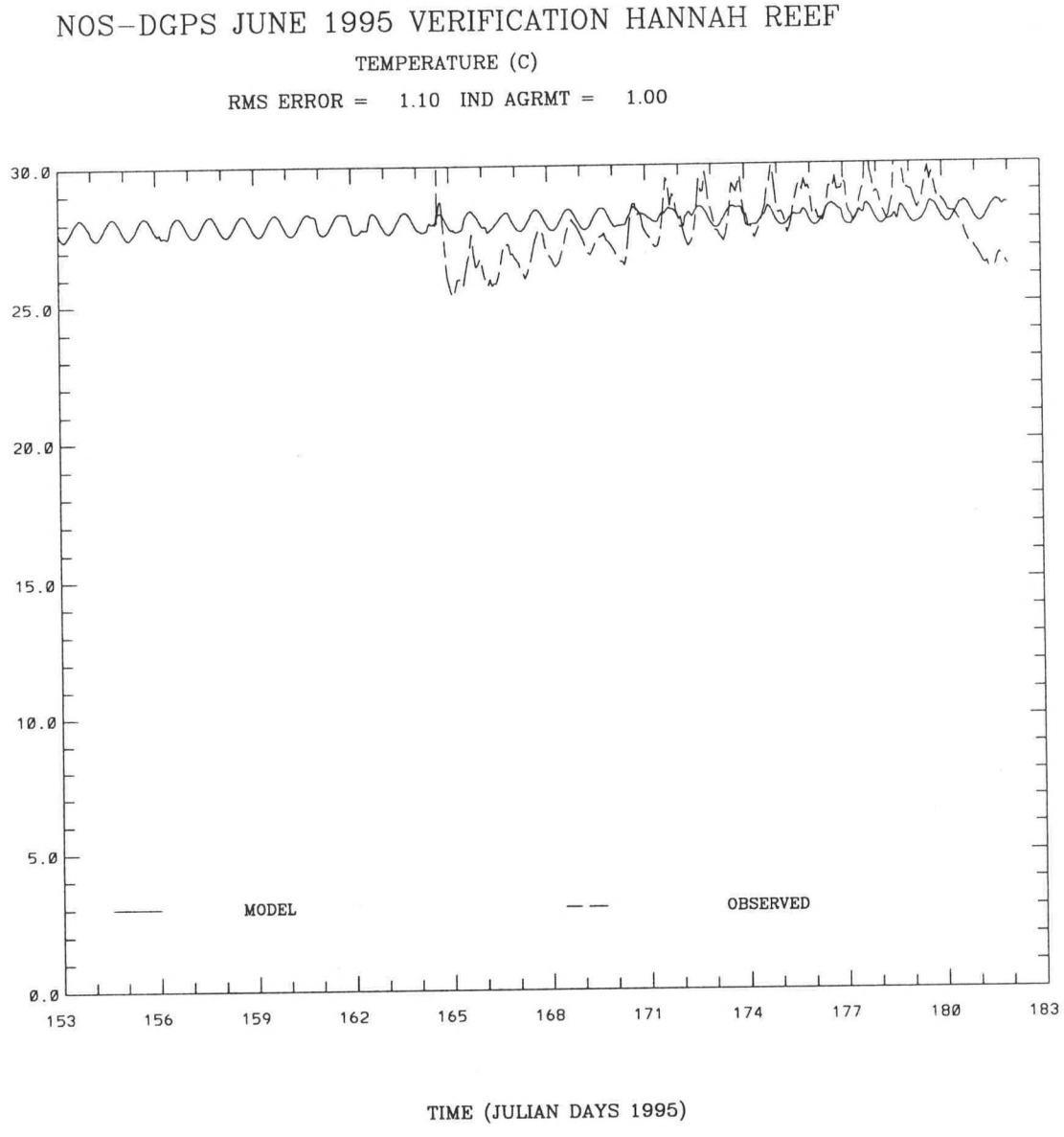

Figure 4.40. June 1995 meteorological simulation: model vs TWDB temperature Hannah Reef

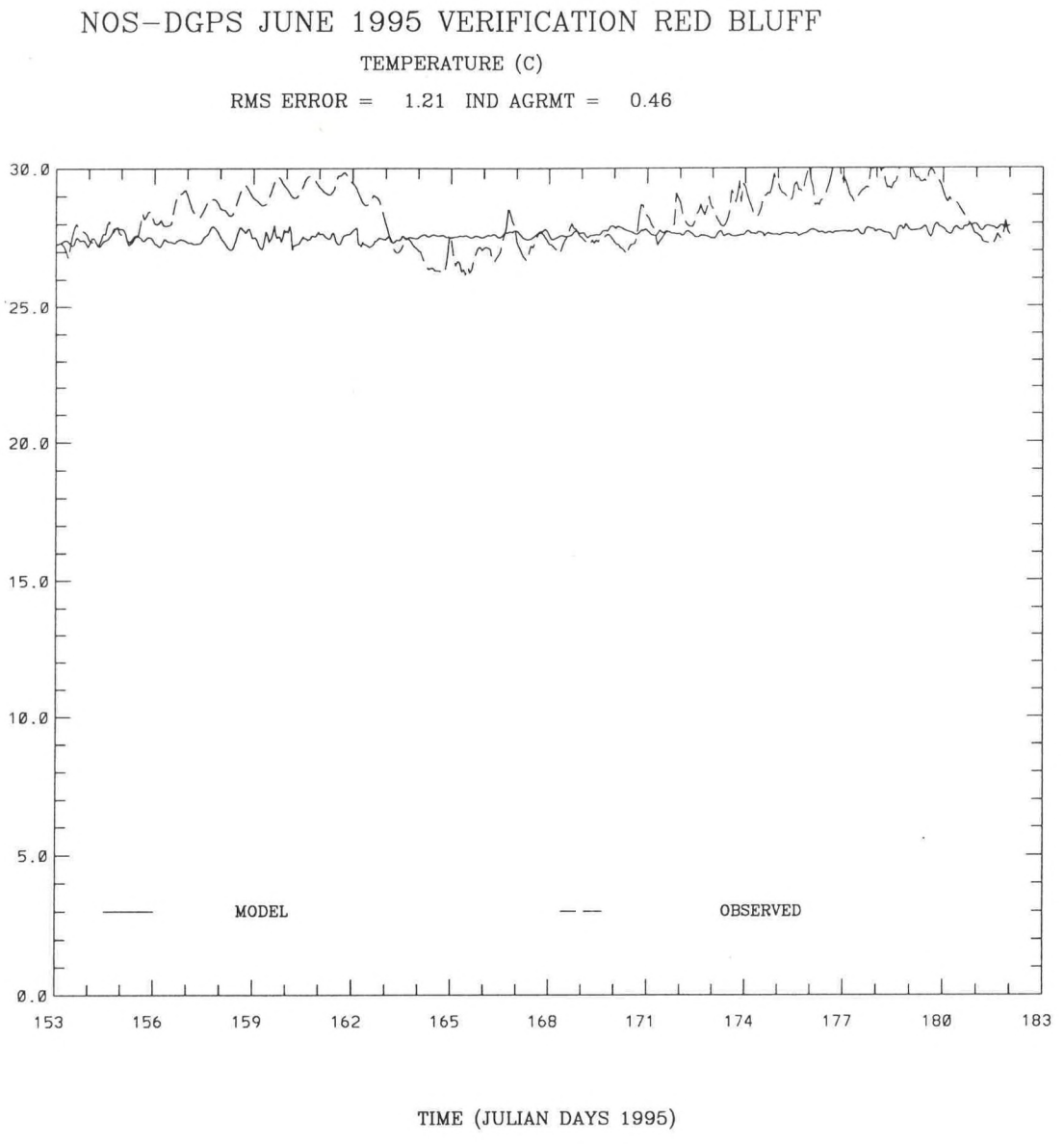

Figure 4.41. June 1995 meteorological simulation: model vs TWDB temperature Red Bluff

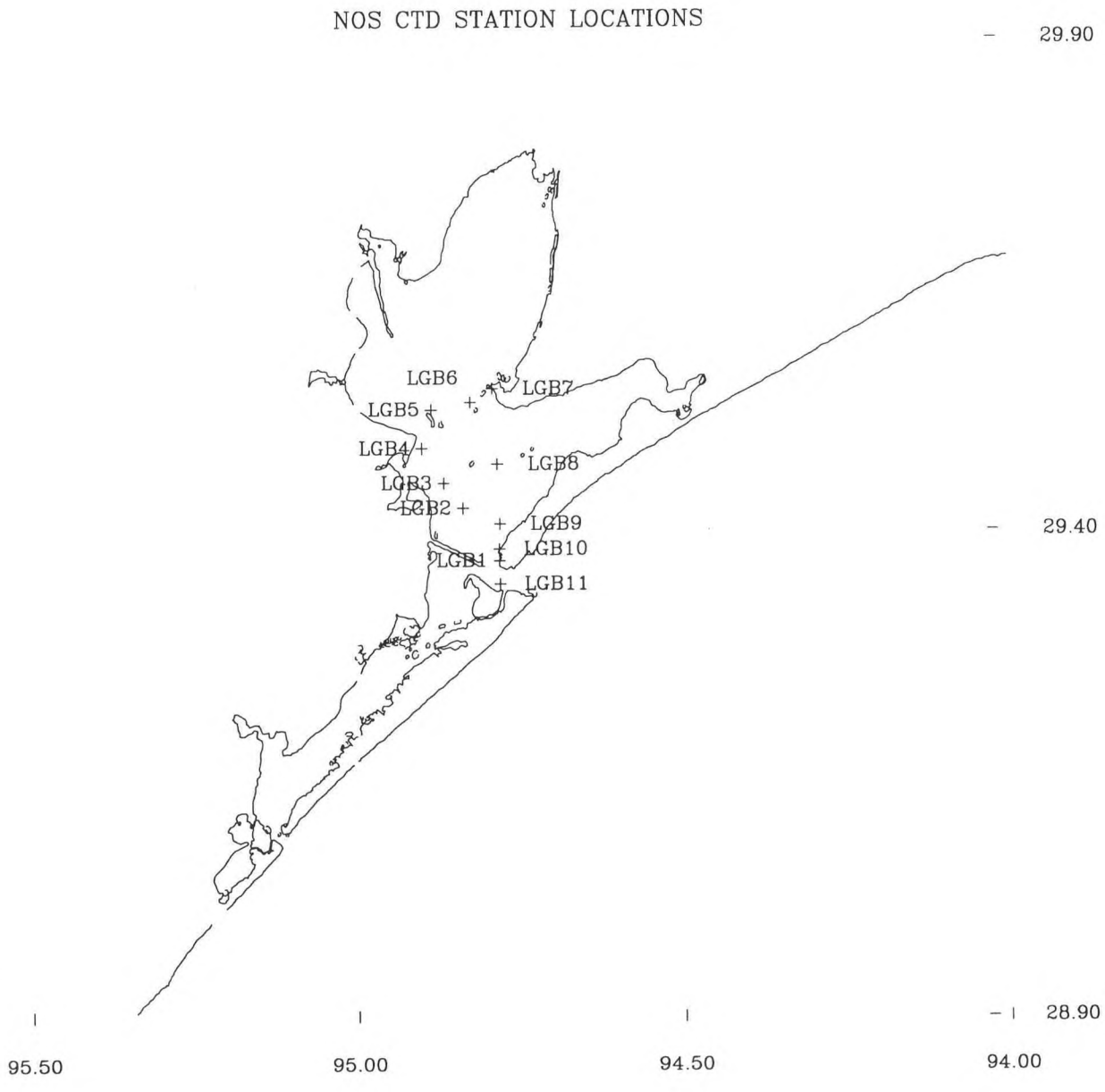

Figure 4.42. DGPS Hydrosurvey CTD cast locations

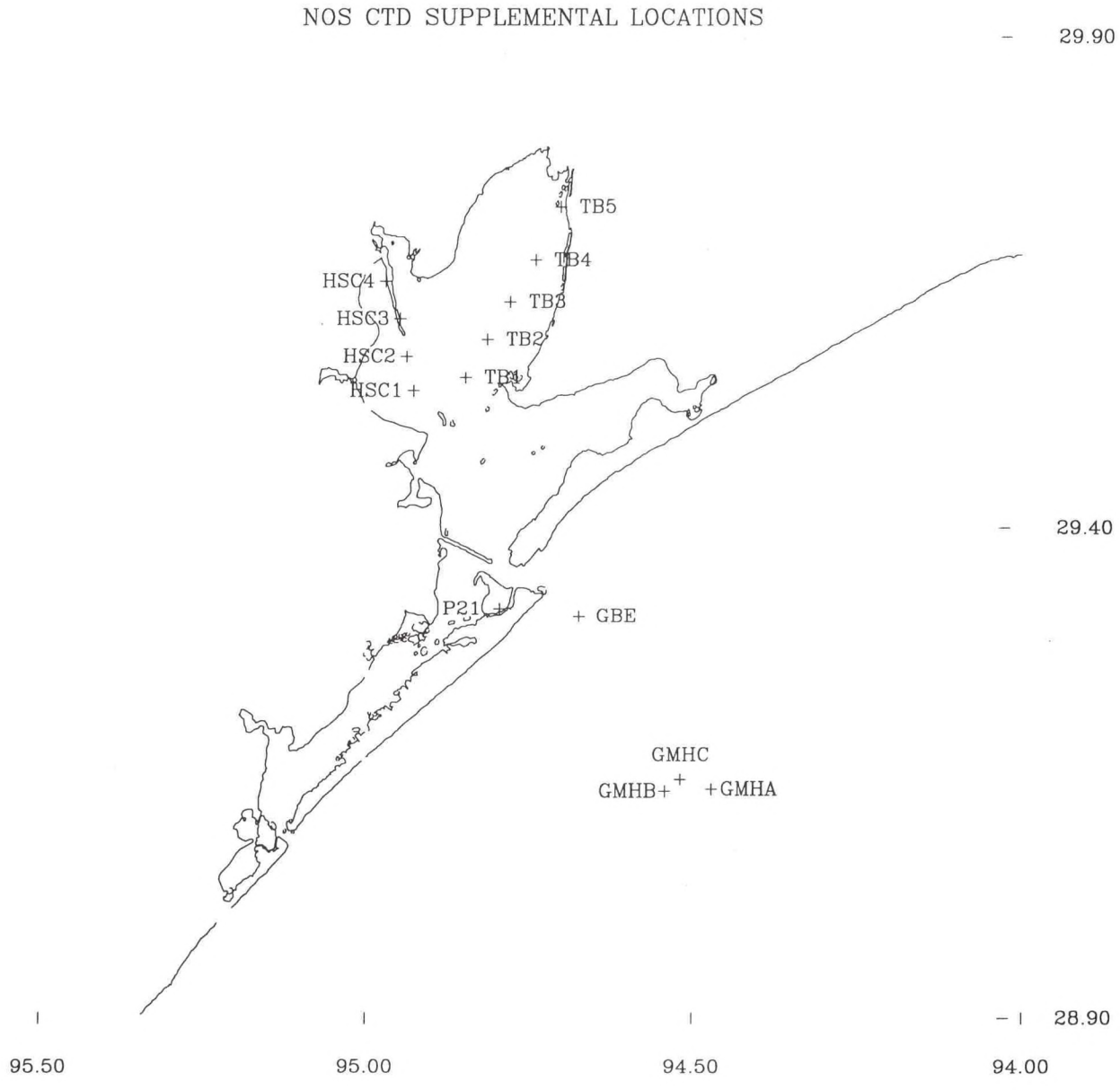

Figure 4.43. DGPS Hydrosurvey CTD supplemental cast locations

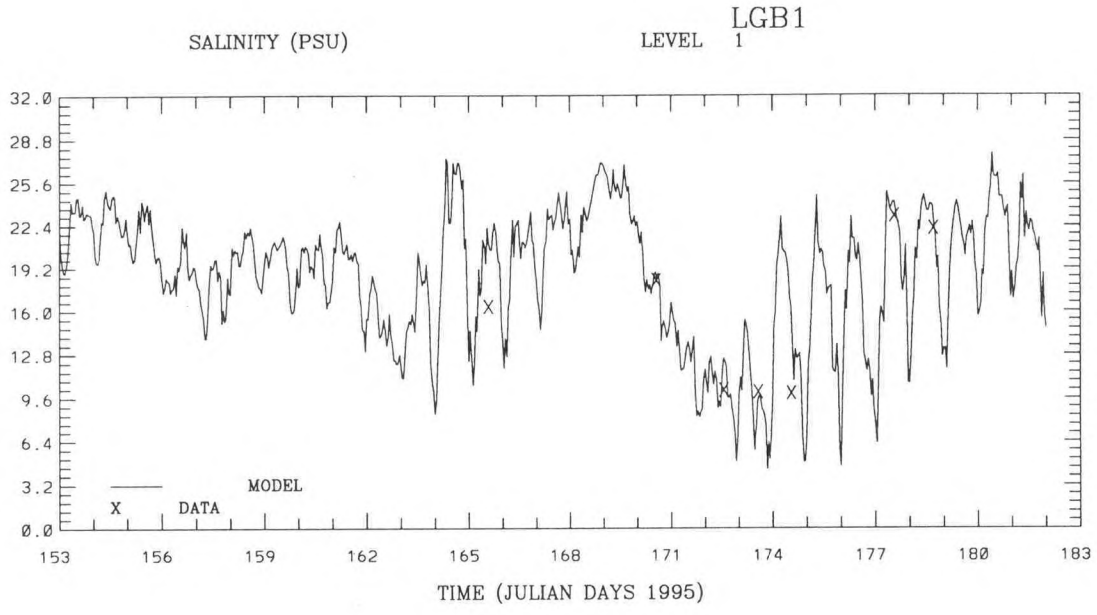

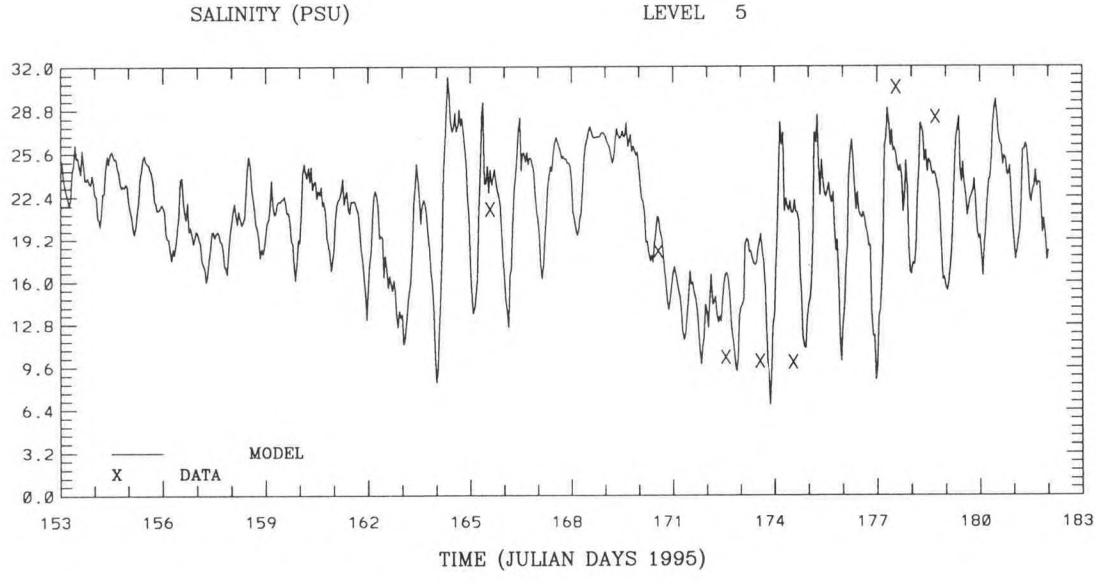

Figure 4.44. Simulated near surface and near bottom salinity vs DGPS Hydrosurvey CTD Port Bolivar

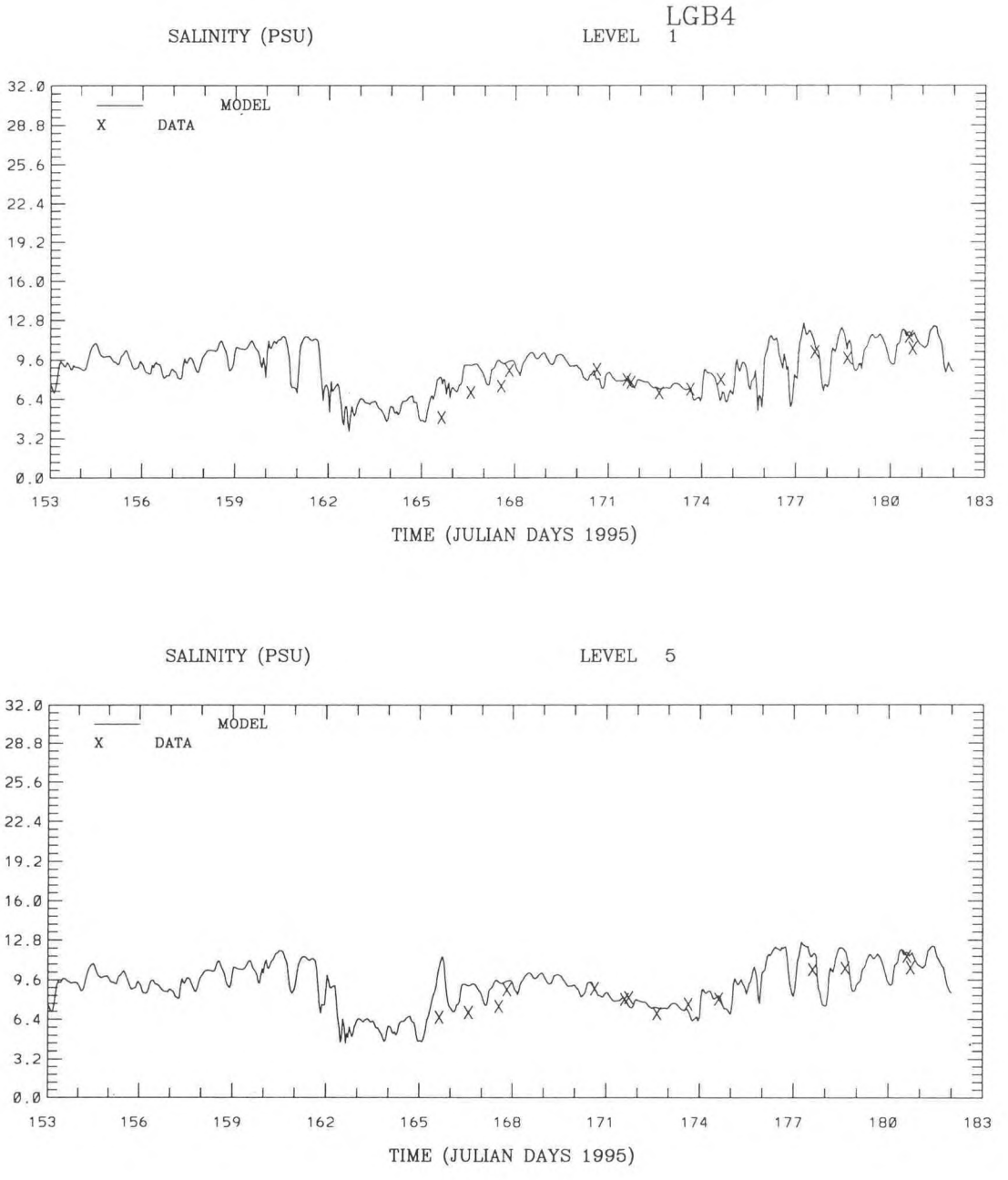

Figure 4.45. Simulated near surface and near bottom salinity vs DGPS Hydrosurvey CTD Eagle Point

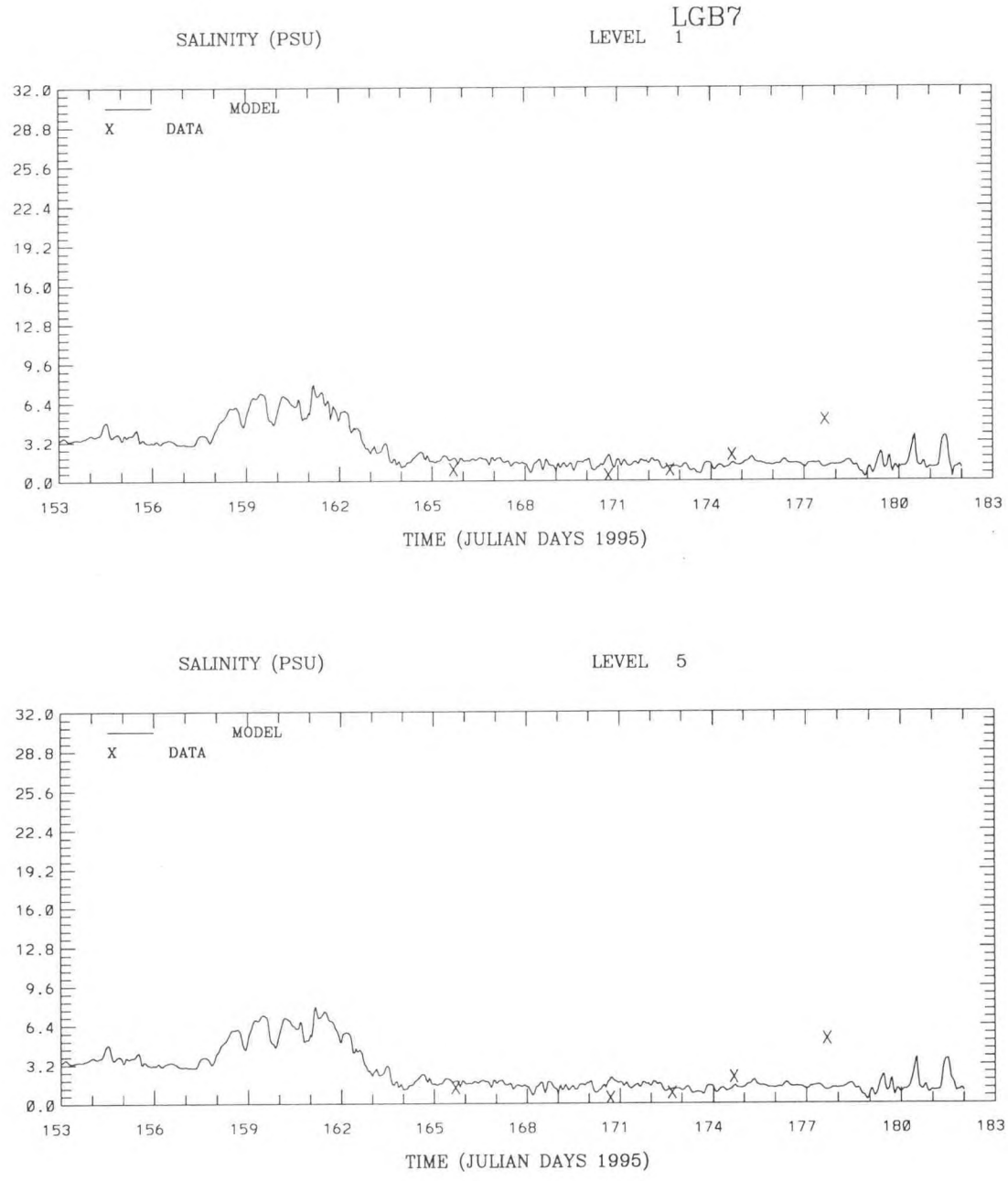

Figure 4.46. Simulated near surface and near bottom salinity vs DGPS Hydrosurvey CTD Smith Point

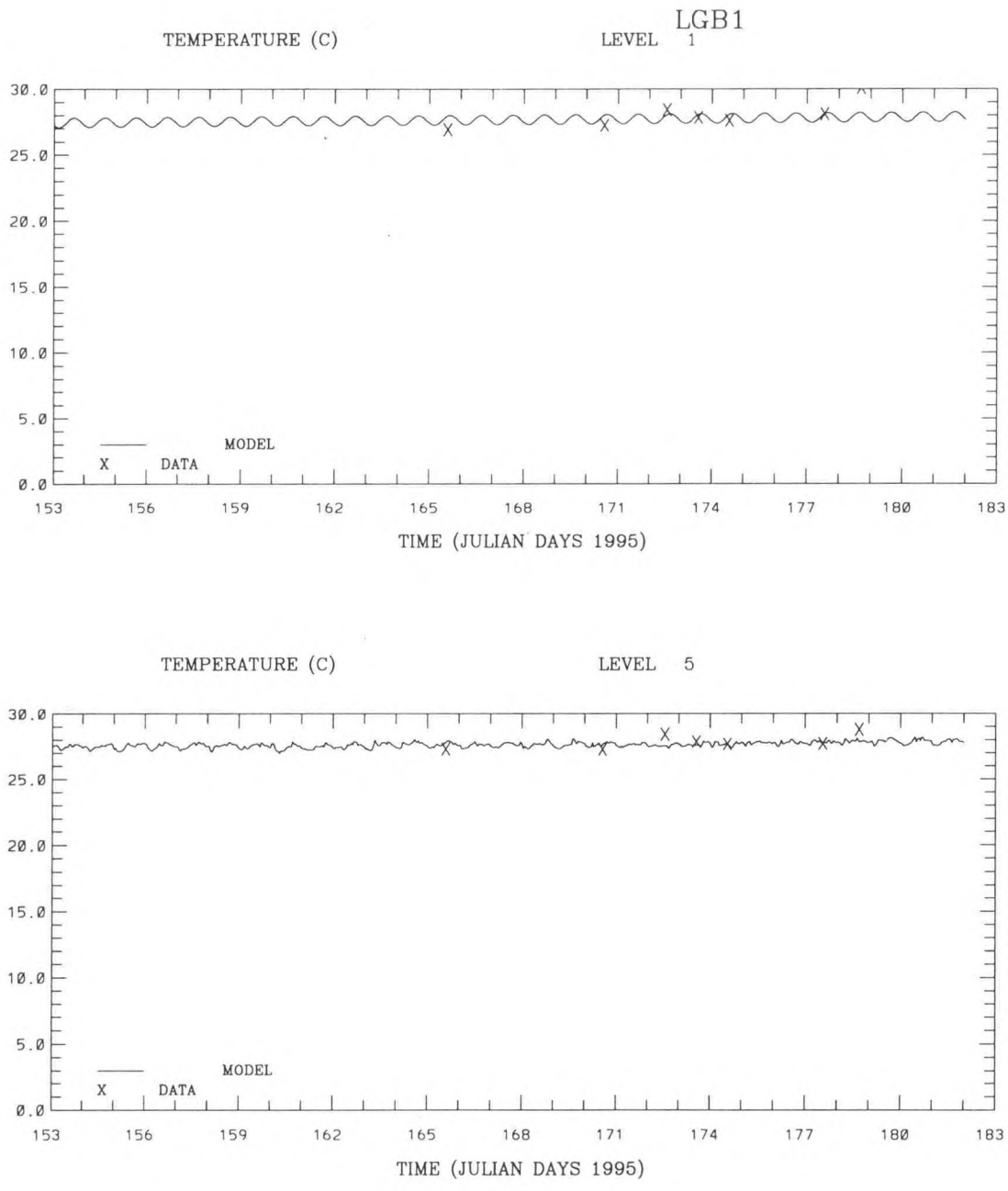

Figure 4.47. Simulated near surface and near bottom temperature vs DGPS Hydrosurvey CTD Port Bolivar

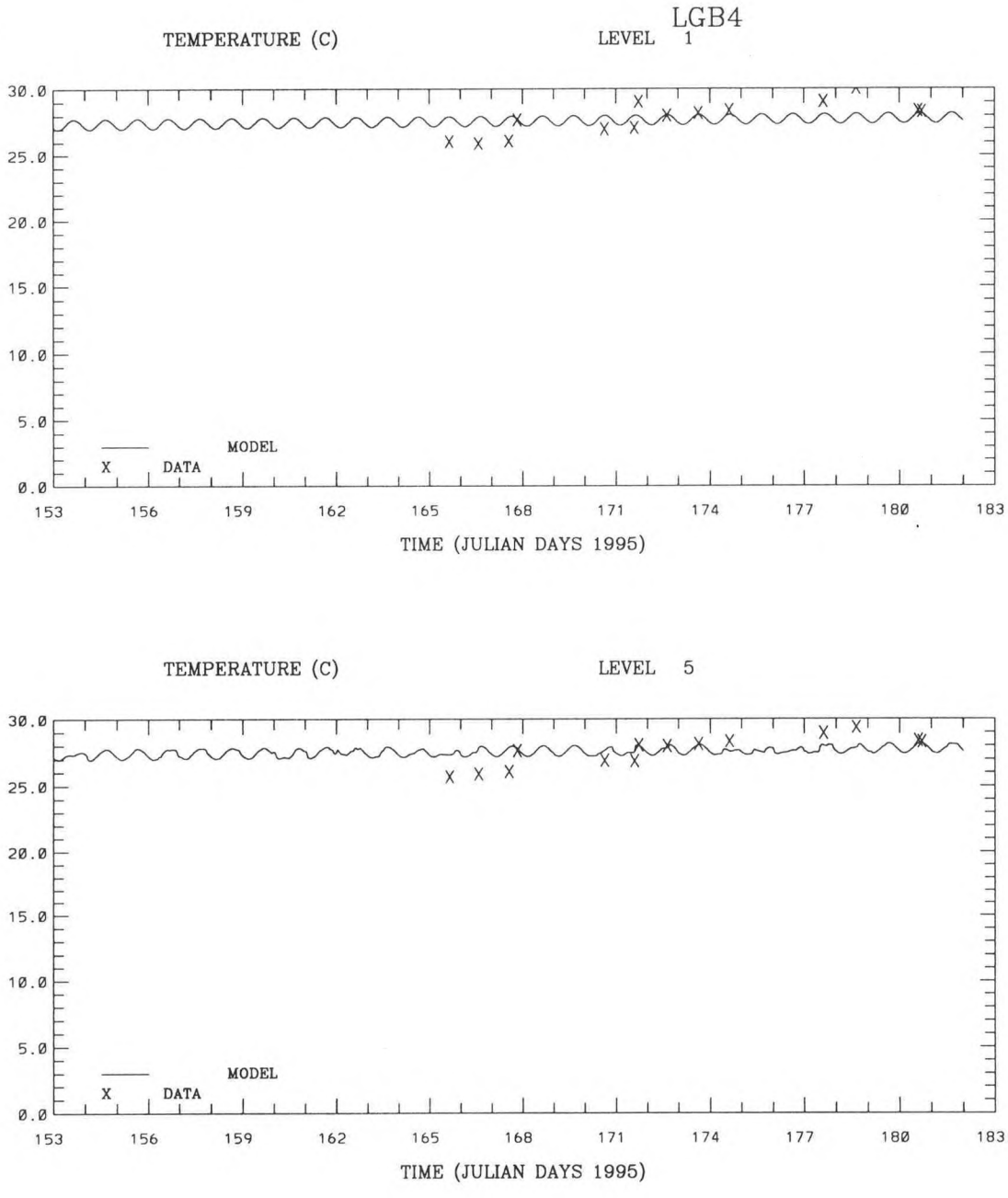

Figure 4.48. Simulated near surface and near bottom temperature vs DGPS Hydrosurvey CTD Eagle Point

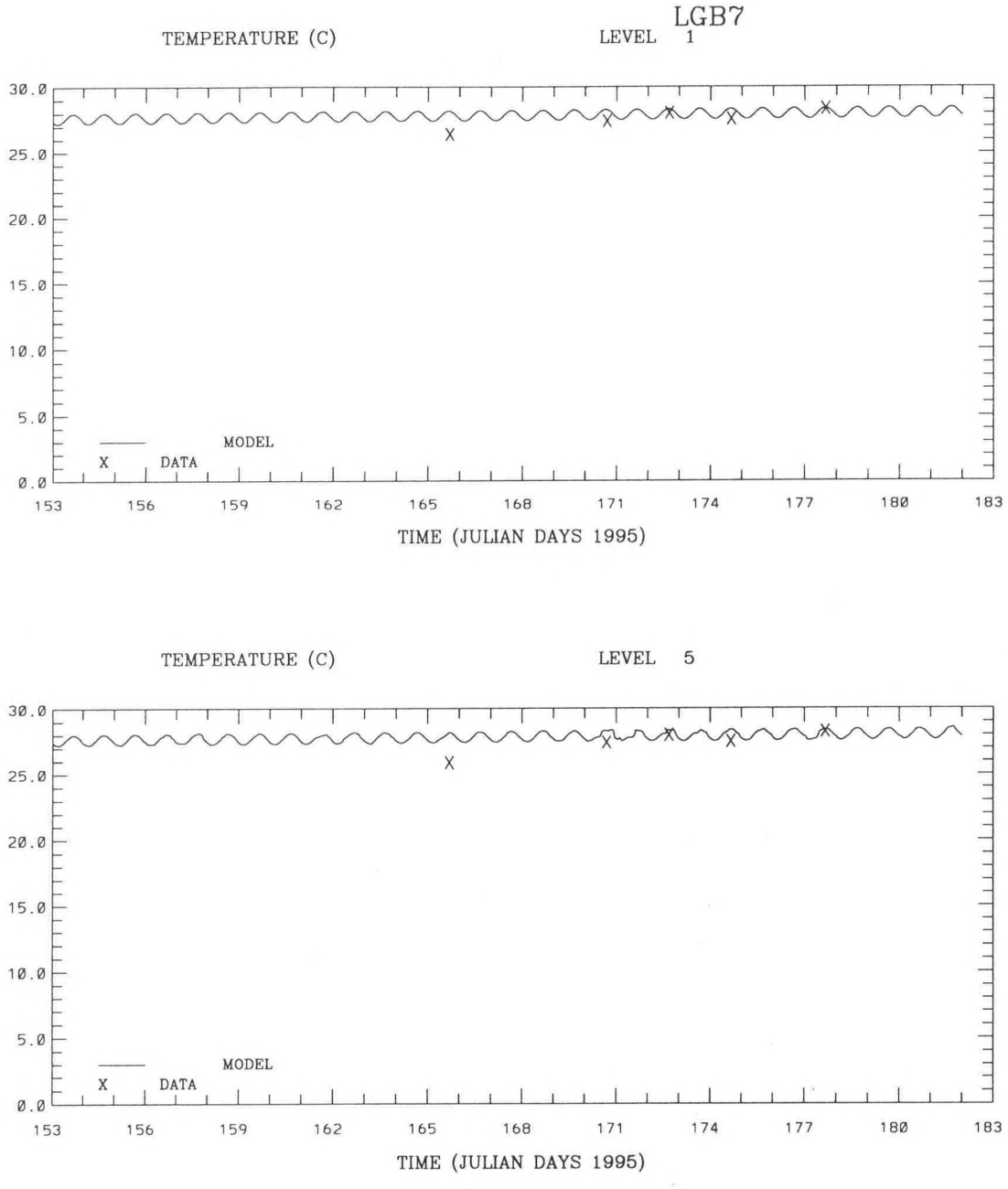

Figure 4.49. Simulated near surface and near bottom temperature vs DGPS Hydrosurvey CTD Smith Point

5. DETERMINATION OF TIDAL EPOCH MEAN LOWER LOW WATER

To motivate the determination of tidal epoch mean lower low water via a numerial modeling approach, it is first necessary to review the determination of tidal epoch datums based on observed water levels at shore-based stations. Modifications to this approach are then introduced in order to allow for a numerical model determination, followed by the presentation of the numerical model derived tidal epoch mean lower low water fields for the previously presented astronomic tide calibration and meteorologically forced simulation. Differences between the numerical model derived fields are presented and preliminary conclusions drawn.

5.1 OBSERVATIONAL APPROACH

The tidal epoch MLLW is determined based on six-minute water levels recorded over a nineteen year period, during which the astronomical motions proceed over a full period. Daily MLLW are estimated from the six-minute series using standard NOS procedures (Schureman, 1958) and averaged over the nineteen year period to determine the tidal epoch mean lower low water. Similarly, the mean higher high water, and mean higher low water and mean lower high waters are computed. The mean tide level (MTL) is defined as the average of the above four levels. The mean higher and lower ranges are determined by subtracting the mean lower low and mean higher low waters from the mean higher high and mean lower high waters, respectively. Thus a direct determination of MTL is only available at the two primary stations, Galveston Pier 21 and Galveston Pleasure Pier on the Gulf, where the complete nineteen year period is available. At secondary stations with shorter records (at least one month in duration), the above tidal datums are computed in the same manner as at the primary stations. To adjust these shorter period values to a full epoch the following procedure is used. The difference between the tidal epoch MTL and the shorter period MTL at the primary station is computed as well as the ratio of tidal epoch higher range to that over the shorter period. It is assumed that the MTL offset at the primary station may be applied to the secondary station assigned as well as the range ratio. Thus one adds to the MTL at the secondary station the primary offset and multiplies the higher range by the range ratio. The epoch MLLW equals the tidal epoch MTL minus one half the above adjusted higher range.

5.2. NUMERICAL MODEL APPROACH

Under this approach, simulated water level time series replace short term observations at secondary stations. However, in order to develop the tidal epoch MLLW surface, it is still necessary to know tidal epoch datums as derived from observations over a network of water level stations, which encompass the hydrosurvey area. In this study, the Eagle Point, Smith Point, and Port Bolivar stations were located at the vertices of the triangular survey area and provided sufficient tidal datum control. Based on a comparison of simulated water levels at the water level stations and a knowledge of the tidal datums at these stations relative to the DGPS hydrosurvey reference frame, it is possible to determine the model datum in ellipsoid space in each grid cell corresponding to the water level station locations. Via the inverse distance interpolation procedure discussed below, the model datum is computed at all other grid cells. This allows the development of a model simulation period (30-day period) mean sea level and

mean lower low water surface. These surfaces are then adjusted to tidal epoch surfaces at the water level station grid cells and via the inverse distance interpolation over the entire grid.

As a prerequiste, it is necessary to establish tidal epoch MTL in the DGPS hydrosurvey ellipsoid reference frame at the water level stations providing hydrosurvey control shown in Figure 5.1. This was accomplished by the NOS/GSL during this project via static DGPS surveys at one benckmark for each tide gauge as given in Table 5.1. In column one of Table 5.1 the appropriate benchmark, which was established via the static DGPS survey is indicated. In column two, the height of this benchmark above tidal epoch (1960 - 1978) mean tide level is given. In column three, the 1960 - 1978 tidal epoch mean range is given. In columns four, five, and six, the height of the benchmark relative to the DGPS ellipsoid, the geoid, and NGVD (1929) is given, respectively. In Table 5.2, the tidal epoch mean tide level relative to each of these three vertical datums is given. The ellipsoid does not constitute an equipotential surface while the second two datums should be close approximations to these surfaces. As a result, tidal epoch mean tide level should stand higher at Morgans Point and Round Point relative to Galveston Pier 21. For the geoid reference frame, the differences are 8.8 cm and 10.7 cm, respectively. There is also a 5.1 cm drop in the mean tide level between Galveston Pier 21 and Pleasure Pier on the Gulf. For NGVD (1929), both Galveston Pier 21 and Pleasure Pier values appear to be anomalous. If we assume Galveston Pier 21 is 12 mm below High Island and Pier 21 is 5.1 cm above Pleasure Pier, then we obtain revised values of 0.219 m at Pier 21 and 0.270 m at Pleasure Pier. Using these values, we would obtain a 18.8 cm increase at Morgans Point and a 17.6 cm increase at Round Point relative to Pier 21 within the NGVD (1929) reference

Table 5.1. Epoch tidal datum analysis

Station	Mtl (m)	Range (m)	Ellp (m)	Geoid (m)	Ngvd29 (m)
GALVESTON PL. PIER - 43 1	7.412	0.649	-21.125	-26.847	7.400
GALVESTON PIER 21 - LUB 1	1.424	0.430	-27.101	-26.886	1.677
EAGLE POINT - 1031A	1.464	0.336	-27.311	-27.191	1.544
CLEAR LAKE - 90026A	0.945	0.366	-27.960	-27.367	1.000
MORGANS POINT - 10 1975	4.170	0.390	-24.883	-27.502	4.201
ROUND POINT - 0559F	0.857	0.427	-28.157	-27.482	0.900
ROLLOVER PASS - 0971F	0.577	0.427	-28.148	-27.123	0.794
PORT BOLIVAR - 1328F	2.278	0.427	-26.346	-26.969	2.400
HIGH ISLAND - 0923F	2.894	0.732	-25.858	-27.125	3.101
SMITH POINT - NO 5 1973	0.876	0.366	-27.969	-27.235	0.977

Table 5.2. Tidal epoch mean tide level analysis

Station	Mtl-Ellp (m)	Mtl-Geoid (m)	Mtl-Ngvd29 (m)
GALVESTON PL. PIER - 43 1	-28.537	-1.690	-0.012
GALVESTON PIER 21 - LUB 1	-28.525	-1.639	0.253
EAGLE POINT - 1031A	-28.775	-1.584	0.080
CLEAR LAKE - 90026A	-28.905	-1.538	0.055
MORGANS POINT - 10 1975	-29.053	-1.551	0.031
ROUND POINT - 0559F	-29.014	-1.532	0.043
ROLLOVER PASS - 0971F	-28.725	-1.602	0.217
PORT BOLIVAR - 1328F	-28.624	-1.655	0.122
HIGH ISLAND - 0923F	-28.752	-1.627	0.207
SMITH POINT - NO 5 1973	-28.845	-1.610	0.101

frame. By subtracting column two from column three in Table 5.2, the ellipsoid relative to the geoid may be determined to be -26.886 m, -27.502 m, and -27.482 m at Galveston Pier 21, Morgans Point, and Round Point, respectively. Thus, there appears to be a downward tilt in the ellipsoid of order 0.5 m relative to the geoid, as one proceeds from Galveston to Morgans Point or from Galveston to Round Point.

5.3. NUMERICAL MODEL EVALUATION EXPERIMENTS

The astronomical tide calibration and the meteorological simulation were considered as two separate evaluation experiments, from which the tidal epoch MLLW fields were determined. To accomplish this, in the hydrodynamic code, the K_1 tidal constituent (the major constituent inside and immediately outside Galveston Bay) cycle was used as a reference cycle over which to determine the mean water level fields and the higher high water and lower low water. Over the two simulations, 29 K_1 cycles were used. The first complete K_1 cycle was not used and allowed for spin-up. The 29 K_1 cycle mean water level, mean higher high water, and mean lower low water fields were written to a transfer file for subsequent use in the datum determination program. This program accessed the shore station datums, previously presented in Tables 5.1 and 5.2, as well as the 29 day predicted means for the astronomic tide experiment and the 29 day observed means for the meteorological tide experiment at these shore stations. In each case, the simulated means at these shore stations were set equal to either the predicted (May 1995) or observed (June 1995) means. The adjustment to tidal epoch mean tide level at the shore based stations was accomplished by computing the model datum at these shore stations then subtracting the appropriate predicted or observed mean and adding the simulation mean. This adjustment procedure assured that at the shore based stations the tidal epoch mean tide levels were recovered.

The following inverse distance interpolation was used to determine the tidal epoch mean tide level field, $T_{i,j}$ at the center of each (i,j) cell with latitude, $alat_{i,j}$, and longitude, $alon_{i,j}$, over the computational grid. For each n and quantity T_n to be interpolated, where $n = 1,nint$ and $nint=10$, of the ten shore stations in Tables 5.1 and 5.2 and shown in Figure 5.1, let (ipt_n, jpt_n) denote their corresponding nearest grid cell center. The following equations are next used in turn below.

$$dy_n = alat_{i,j} - alat_{ipt_n,jpt_n} \tag{5.1}$$

$$dx_n = \frac{\left(alon_{i,j} - alon_{ipt_n,jpt_n}\right)}{\cos\left(\overline{alat_n}\right)} \quad , \quad \overline{alat_n} = .5\left(alat_{i,j} + alat_{ipt_n,jpt_n}\right) \tag{5.2}$$

$$d_n = \left(dx_n^2 + dy_n^2 \right)^{-0.5} \tag{5.3}$$

$$d_T = \sum_{n=1}^{nint} d_n \quad , \quad \omega_n = \frac{d_n}{d_T} \tag{5.4}$$

$$T_{i,j} = \sum_{n=1}^{nint} \omega_n T_n \tag{5.5}$$

At the shore stations, the ratio of the tidal epoch higher high water to lower low water range to the simulated value of this range was determined. The above inverse distance interpolation procedure was used to interpolate the ratio field over the grid. The adjusted tidal epoch mean lower low water field was computed as the epoch adjusted mean tide level minus one half the product of the simulated range times the range ratio.

The Astronomical Tide Case

For the May 1995 astronomical tide simulation, the shore-station simulated means (Mean S) and harmonically reconstructed predicted means (Mean P-O) are given in Table 5.3. The epoch mean tide level adjustment process insures that tidal epoch mean tide level (AE mtl) is recovered at the shore stations by adding the difference between the simulated and predicted mean to the model datum. These constitute the datum offset given in the last column in Table 5.3 and are order 8 cm. The simulated and predicted ranges are given in Table 5.4. The range adjustment factors are determined by dividing the tidal epoch range by the simulated range. For the astronomical tide case, the range ratios are greater than unity at all stations except at Rollover Pass. The simulated tidal range which ranges from 0.23 to 0.78 m is shown in Figure 5.2. In Figure 5.3, the difference between the simulated range and the tidal epoch range as determined from inverse distance interpolation is shown. In the hydrosurvey area, the difference is -11.0 cm. The tidal epoch mean lower low water field with respect to the GPS reference ellipsoid is shown in Figure 5.4. The tidal epoch mean lower low water fields with respect to the geoid and NGVD (1929) are given in Figures 5.5 and 5.6, respectively. Since the majority of the shore stations are within Galveston Bay, the fields are not as accurate on the shelf as within the Bay proper. The range of the fields are 49, 31, and 38 cm with respect to the GPS reference ellipsoid, geoid, and NGVD (1929) datums, respectively. Due to the nature of the interpolation, there appears to be some "bull's eyes" in the fields in the vicinity of the shore stations. Note in Figures 5.2 - 5.6, in region A consisting of boundary cells (54,2) - (60,2), the contour lines are concentrated due to the revised spatial interpolation of the tide signals 1 and 2 discussed in section 3.5.

Table 5.3. Astronomical tide simulation epoch mean tide level adjustment analysis

Station	Model Datum (m)	Mean S (m)	Mean P-O (m)	AE mtl (m)	Off. (m)
GALVESTON PL. PIER - 43 1	-28.627	0.120	0.030	-28.536	-0.090
GALVESTON PIER 21 - LUB 1	-28.635	0.140	0.030	-28.525	-0.110
EAGLE POINT - 1031A	-28.875	0.150	0.050	-28.775	-0.100
CLEAR LAKE - 90026A	-28.995	0.150	0.060	-28.905	-0.090
MORGANS POINT - 10 1975	-29.133	0.150	0.070	-29.053	-0.080
ROUND POINT - 0559F	-29.104	0.160	0.070	-29.014	-0.090
ROLLOVER PASS - 0971F	-28.785	0.150	0.090	-28.725	-0.060
PORT BOLIVAR - 1328F	-28.544	0.130	0.210	-28.624	0.080
HIGH ISLAND - 0923F	-28.792	0.140	0.100	-28.753	-0.040
SMITH POINT - NO 5 1973	-28.935	0.140	0.050	-28.845	-0.090

Table 5.4. Astronomical tide simulation epoch tidal range adjustment analysis

Station	Epoch Range (m)	Sim. Range (m)	Range Adj. Fact. (-)
GALVESTON PL. PIER - 43 1	0.649	0.553	1.173
GALVESTON PIER 21 - LUB 1	0.430	0.335	1.285
EAGLE POINT - 1031A	0.336	0.279	1.204
CLEAR LAKE - 90026A	0.366	0.337	1.086
MORGANS POINT - 10 1975	0.390	0.344	1.133
ROUND POINT - 0559F	0.427	0.354	1.207
ROLLOVER PASS - 0971F	0.427	0.582	0.733
PORT BOLIVAR - 1328F	0.427	0.322	1.324
HIGH ISLAND - 0923F	0.732	0.603	1.215
SMITH POINT - NO 5 1973	0.366	0.325	1.127

The Meteorological Simulation Case

For the June 1995 meteorological simulation, the shore-station simulated means (Mean S) and observed means (Mean P-O) are given in Table 5.5. The epoch mean tide level adjustment process insures that tidal epoch mean tide level (AE mtl) is recovered at the shore stations by adding the difference between the simulated and observed mean to the model datum. These constitute the datum offsets shown in the last column of Table 5.5 and are order 10 cm. The simulated and predicted ranges are given in Table 5.6. The range adjustment factors are determined by dividing the tidal epoch range by the simulated range. For the meteorological tide case, the range ratios are greater than unity inside the Bay and less than unity at the Gulf stations. The simulated tidal range which ranges from 0.26 to 1.04 m is shown in Figure 5.7. In Figure 5.8, the difference between the simulated range and the tidal epoch range as determined from the above inverse distance interpolation is shown. In the hydrosurvey area, the difference is -15.0 cm. The tidal epoch mean lower low water field with respect to the GPS reference ellipsoid is shown in Figure 5.9. The tidal epoch mean lower low water fields with respect to the geoid and NGVD (1929) are given in Figures 5.10 and 5.11, respectively. Since the majority of the shore stations are within Galveston Bay, the fields are not as accurate on the shelf as within the Bay proper. The range of the fields are 49, 40, and 42 cm with respect to the GPS reference ellipsoid, geoid, and NGVD (1929) datums, respectively. Due to the nature of the interpolation, there appears to be some "bull's eyes" in the fields in the vicinity of the shore stations.

5.4. NUMERICAL MODEL DIFFERENCE FIELDS

To further study the results of the two experiments, the difference between the meteorological and astronomical tide simulation derived tidal epoch mean tide level and mean lower low water fields were generated. The differences in the mean tide level fields were order 10^{-2} mm, since the epoch mean tide levels are completely recovered at the shore stations in the adjustment

Table 5.5. Meteorological simulation epoch mean tide level adjustment analysis

Station	Model Datum (m)	Mean S (m)	Mean P-O (m)	AE mtl (m)	Off. (m)
GALVESTON PL. PIER - 43 1	-28.617	0.280	0.200	-28.536	-0.080
GALVESTON PIER 21 - LUB 1	-28.625	0.290	0.190	-28.525	-0.100
EAGLE POINT - 1031A	-28.895	0.340	0.220	-28.775	-0.120
CLEAR LAKE - 90026A	-29.065	0.360	0.200	-28.905	-0.160
MORGANS POINT - 10 1975	-29.183	0.360	0.230	-29.053	-0.130
ROUND POINT - 0559F	-29.144	0.360	0.230	-29.014	-0.130
ROLLOVER PASS - 0971F	-28.805	0.280	0.200	-28.725	-0.080
PORT BOLIVAR - 1328F	-28.744	0.290	0.170	-28.624	-0.120
HIGH ISLAND - 0923F	-28.833	0.280	0.200	-28.753	-0.080
SMITH POINT - NO 5 1973	-28.955	0.330	0.220	-28.845	-0.110

Table 5.6. Meteorological simulation tidal epoch range adjustment analysis

Station	Epoch Range (m)	Sim. Range (m)	Range Adj. Fact. (-)
GALVESTON PL. PIER - 43 1	0.649	0.833	0.779
GALVESTON PIER 21 - LUB 1	0.430	0.469	0.917
EAGLE POINT - 1031A	0.336	0.306	1.099
CLEAR LAKE - 90026A	0.366	0.356	1.028
MORGANS POINT - 10 1975	0.390	0.344	1.134
ROUND POINT - 0559F	0.427	0.346	1.235
ROLLOVER PASS - 0971F	0.427	0.767	0.557
PORT BOLIVAR - 1328F	0.427	0.427	1.001
HIGH ISLAND - 0923F	0.732	0.759	0.964
SMITH POINT - NO 5 1973	0.366	0.314	1.166

process. The differences in the tidal epoch mean lower low water fields were order 2.0 cm within the hydrosurvey area as shown in Figure 5.12, which constitutes approximately 10 percent of the total hydrosurvey error budget of 18.2 cm. Note along the Gulf coast, due to the distance between tide stations and the influence of wind effects in the meteorological simulation, the differences in the tidal epoch MLLW estimates are order 5 - 10 cm. Note the differences in region A along the southern boundary are due to the different local boundary condition specification as discussed in sections 3.5 and 4.1.

As a result, it appears feasible to use a purely astronomic tide simulation of order 29 days to determine the tidal epoch mean lower low water field for use with DGPS hydrosurveying, if there is adequate shore tide station control.

5.5. ADDITIONAL ISSUES

In addition, the issue of accuracy of the tidal epoch mean lower low water needs further investigation. Of concern is the accuracy of the tidal epoch datum determination at secondary

stations based on short (order one month) time periods. Marmer (1951) states as general guidance that the estimated tidal epoch mean sea level and mean tide levels from one month, one year, three years, and nine years of data are within 30 mm, 15 mm, 9 mm, and 6 mm, of the true tidal epoch values. This might be further evaluated by studying the Galveston Pleasure Pier and Galveston Pier 21 water level time series. Since all other stations have only been in operation for order one to two years, it is seen based on Marmer (1951) that the tidal epoch estimates are probably order 1.5 cm in accuracy at the shore stations. Since the epoch mean lower low water estimates differ by order 2.0 cm, the total accuracy of the epoch mean lower low water surface might be estimated to order 3.5 cm.

The Trinity River Channel platform gauge (877-1021), shown in Figure 3.8, 29 day water level series in Table 3.3 was used to estimate an adjusted tidal epoch MLLW value of -28.9968 m with respect to the DGPS ellipsoid. Based on Marmer (1951) this level is within 3 cm of the true value. Using the above inverse distance interpolation of tidal epoch MTL and higher ranges at the shore stations, one computes a MLLW of -29.9925 m with respect to the DGPS ellipsoid. Based on the astronomical tide calibration and meteorological simulations, MLLW is estimated as -28.9548 m and -28.9378 m with respect to the DGPS ellipsoid, respectively. These three estimates differ from the Trinity River Channel adjusted value by 4.3 mm, 42 mm, and 59 mm, respectively. It is recommended that additional water level measurements in the center of the triangular survey area over at least a one month period using DGPS on a buoy and at a nearby stable platform be taken and datums computed for further comparisons.

The inverse distance interpolation used here represents only one approach towards the interpolation of arbitrarily spaced data values onto a structured grid. It would be useful to consider the Barnes (1973) interpolation as well as finite element interpolation schemes.

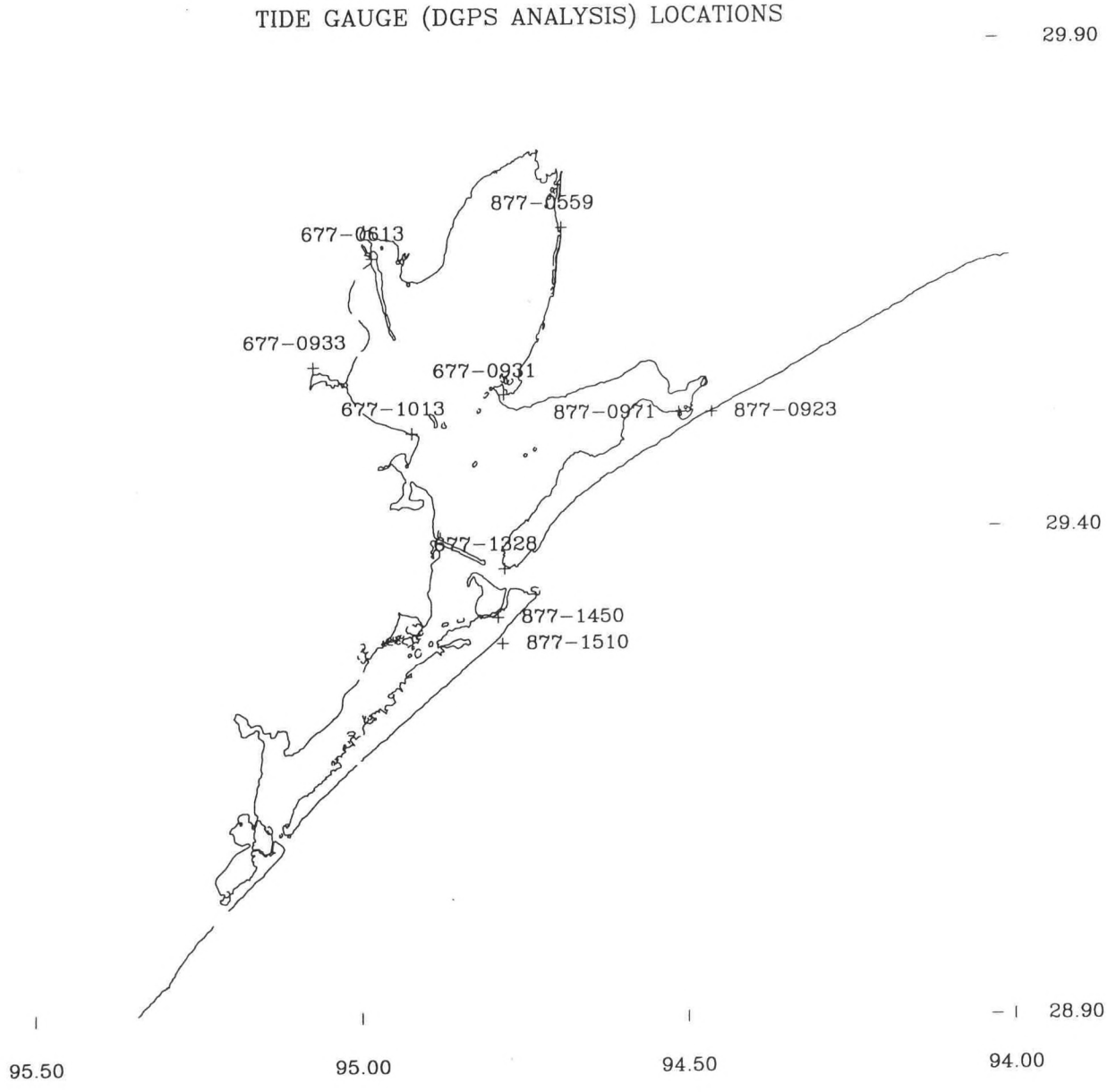

Figure 5.1. Static DGPS tidal station benchmark survey locations

Figure 5.2. May 1995 Astronomical tide simulation range field (m)

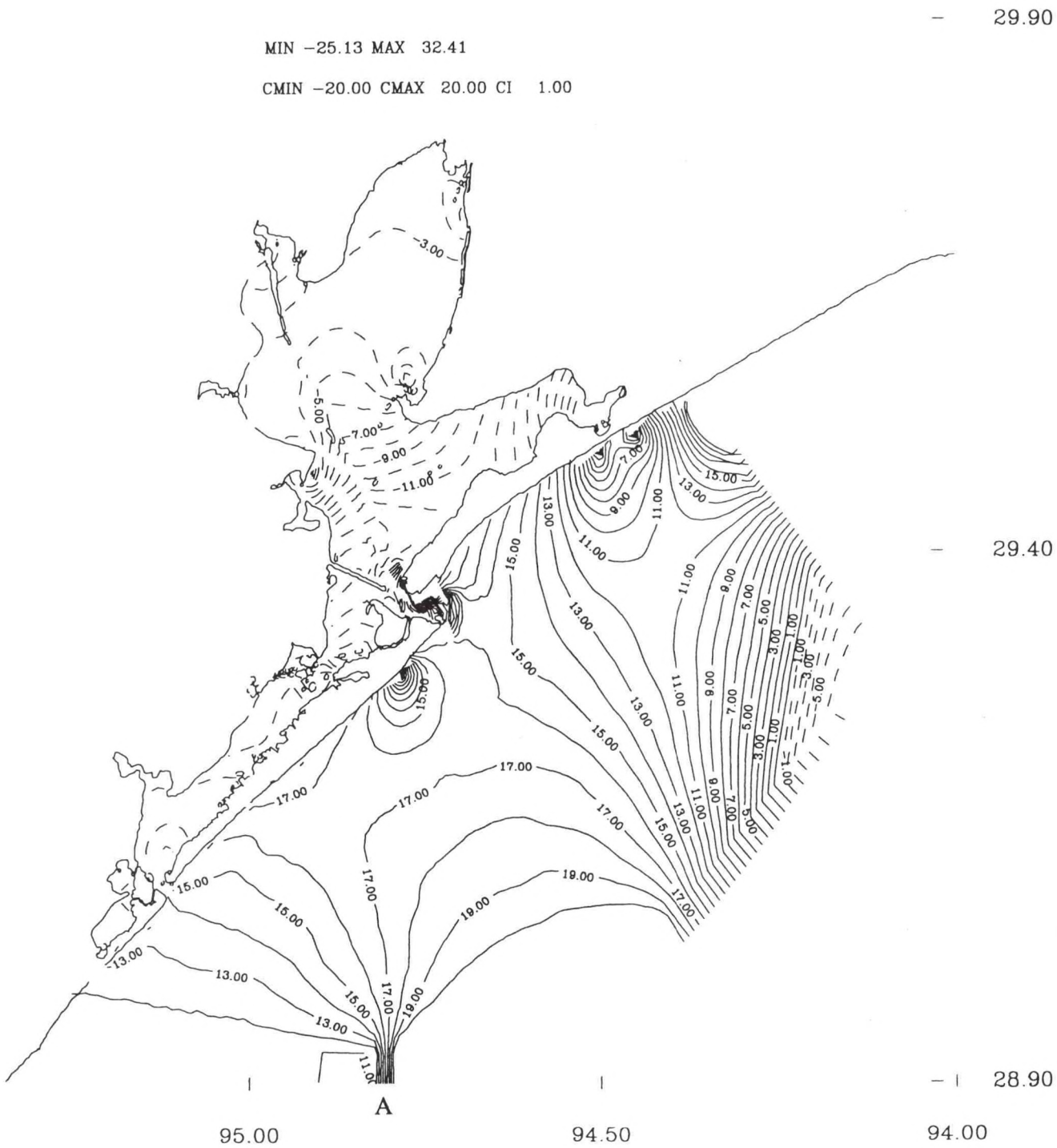

Figure 5.3. May 1995 Astronomical tide simulation minus tidal epoch (1/r) range field (cm)

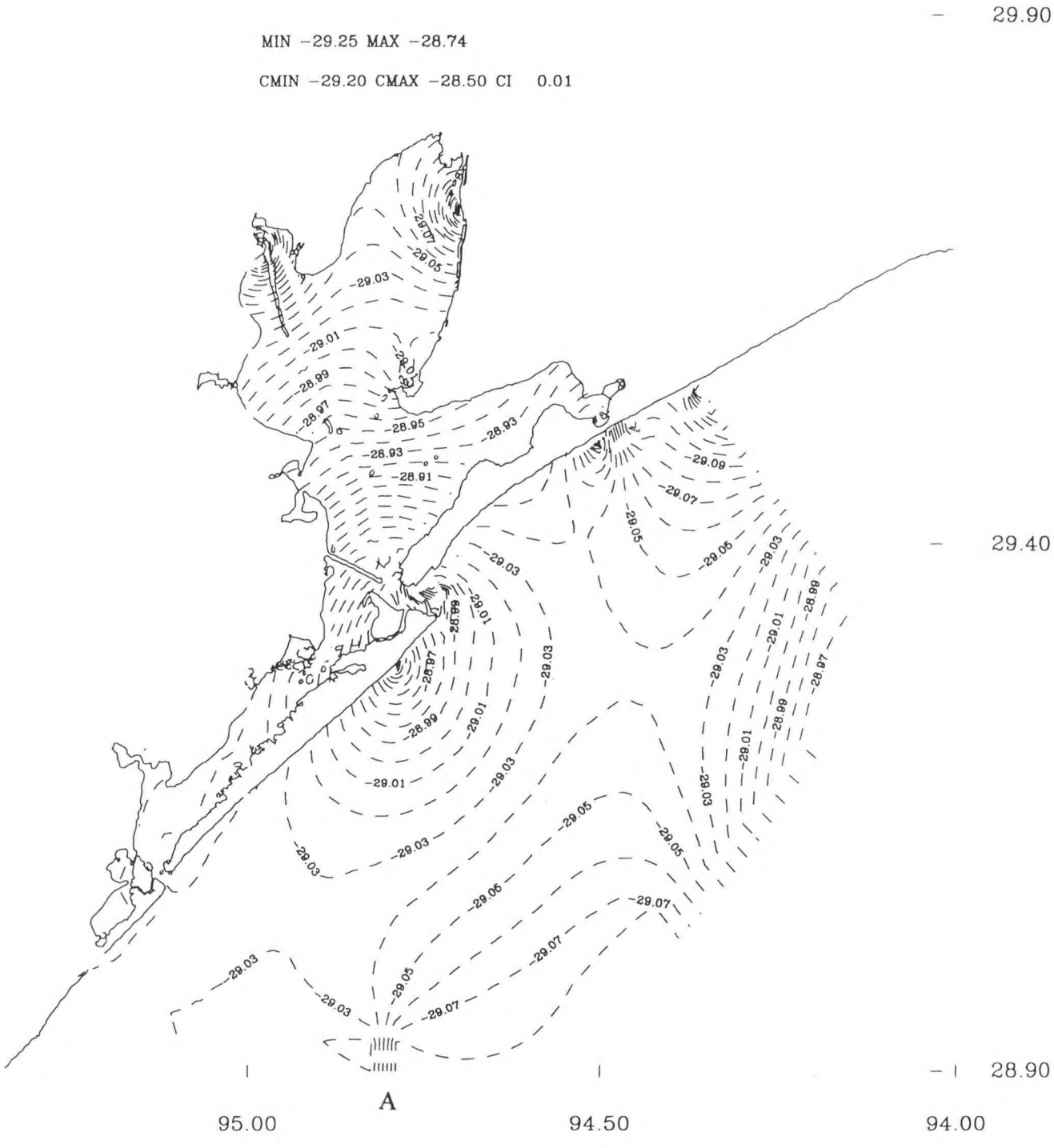

Figure 5.4. May 1995 Astronomical tide simulation tidal epoch MLLW wrt Ellipsoid (m)

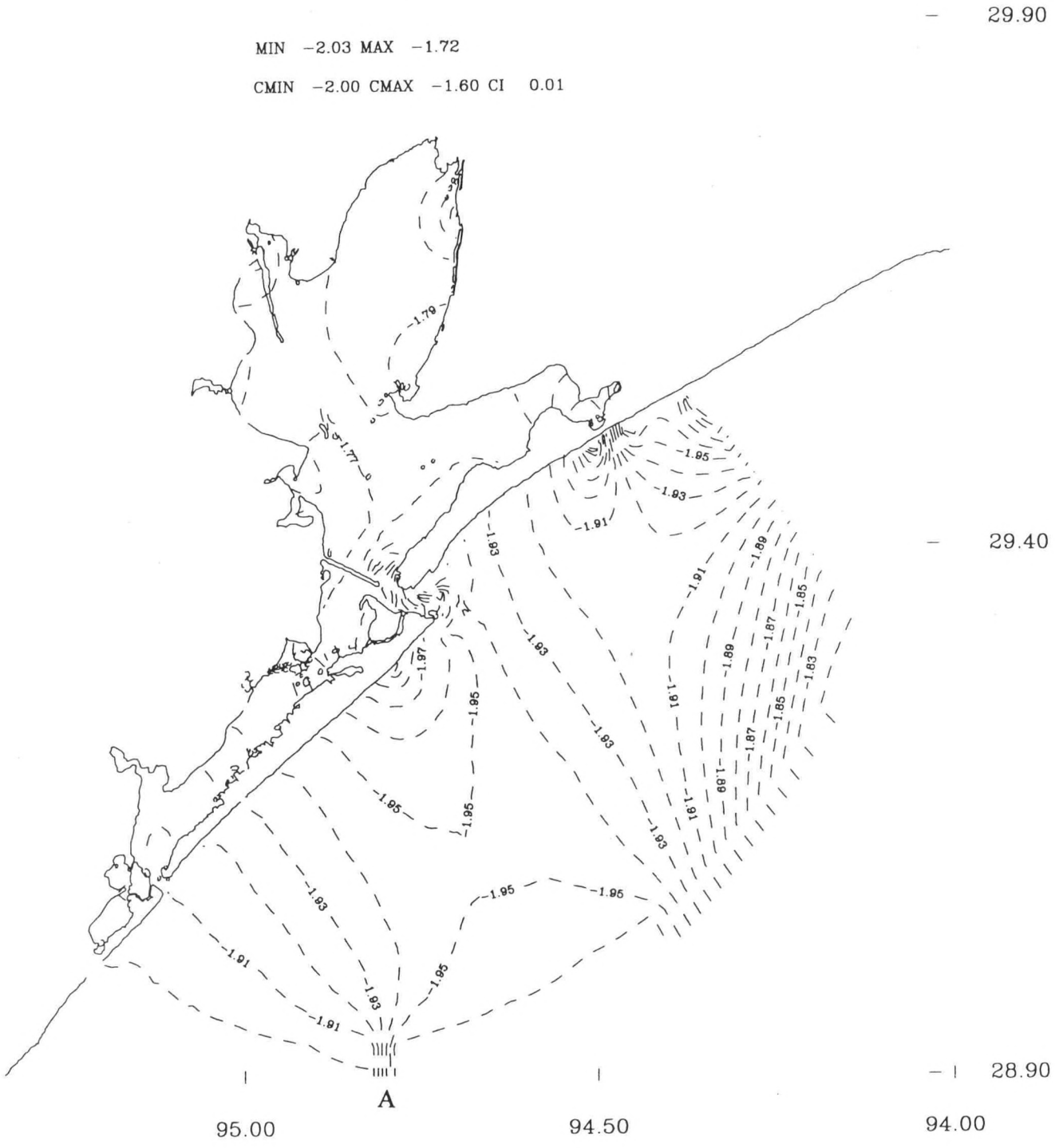

Figure 5.5. May 1995 Astronomical tide simulation tidal epoch MLLW wrt Geoid (m)

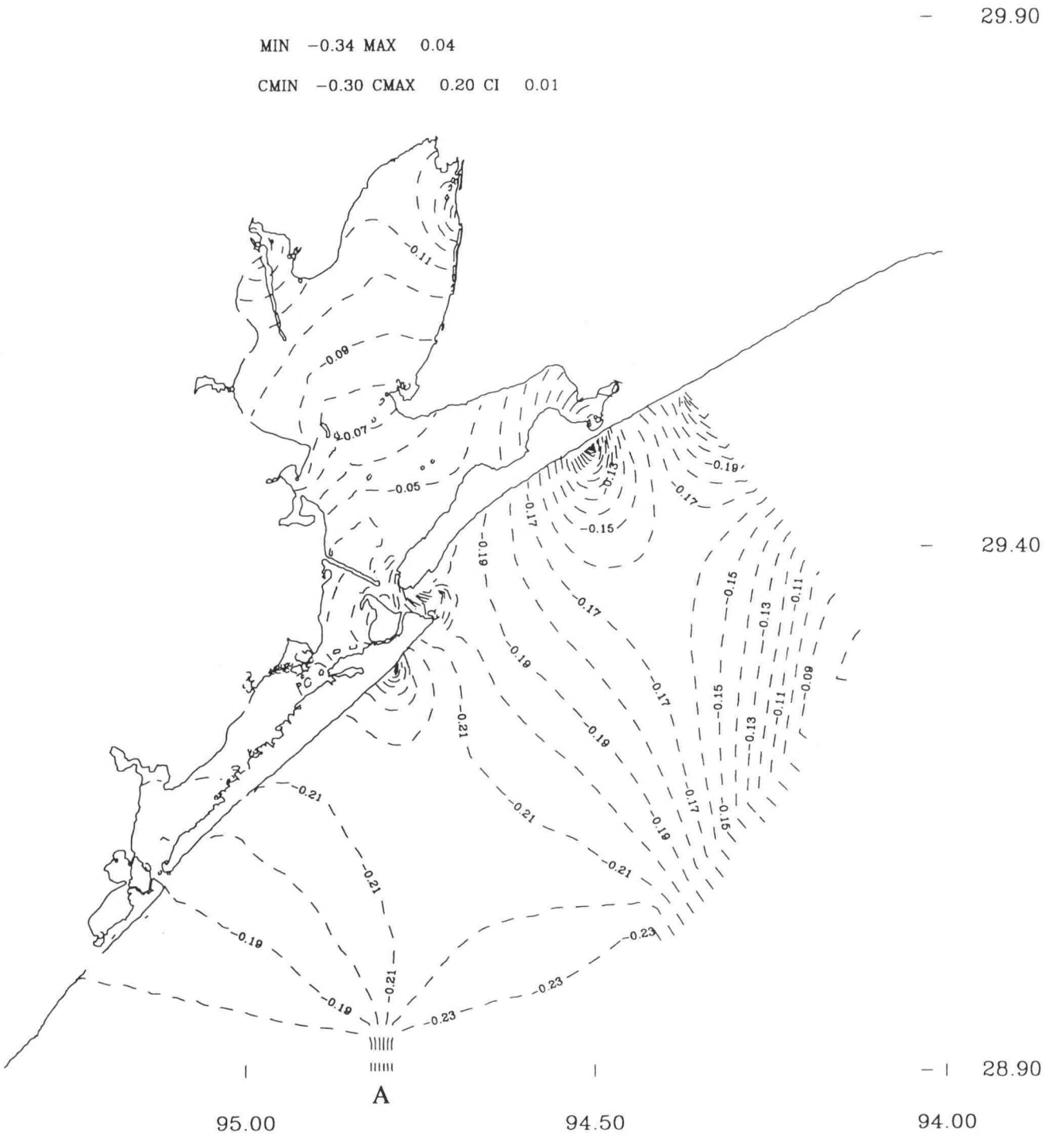

Figure 5.6. May 1995 Astronomical tide simulation tidal epoch MLLW wrt NGVD (1929) (m)

Figure 5.7. June 1995 Meteorological simulation range field (m)

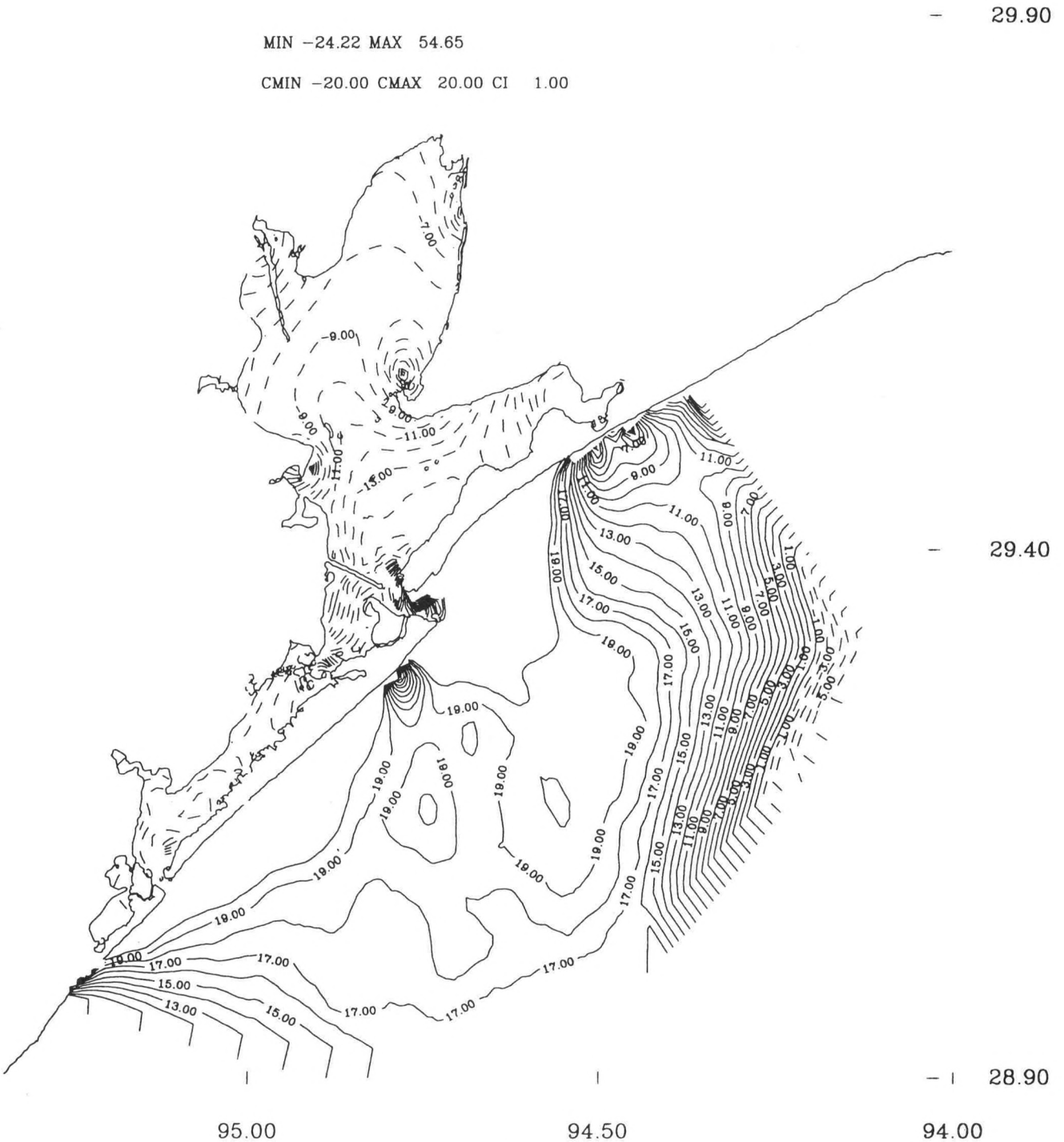

Figure 5.8. June 1995 Meteorological simulation minus tidal epoch (1/r) range field (cm)

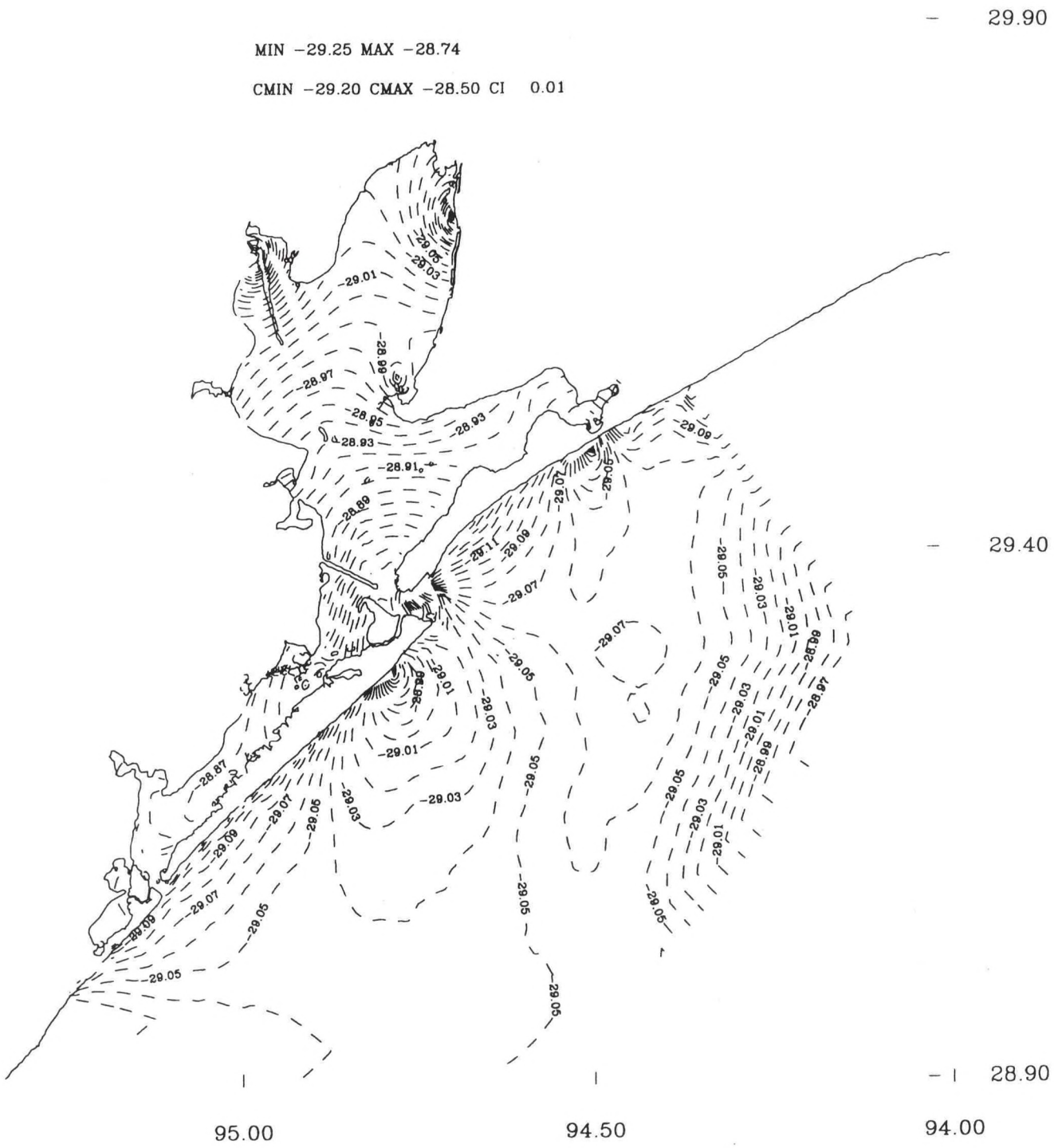

Figure 5.9. June 1995 Meteorological simulation tidal epoch MLLW wrt Ellipsoid (m)

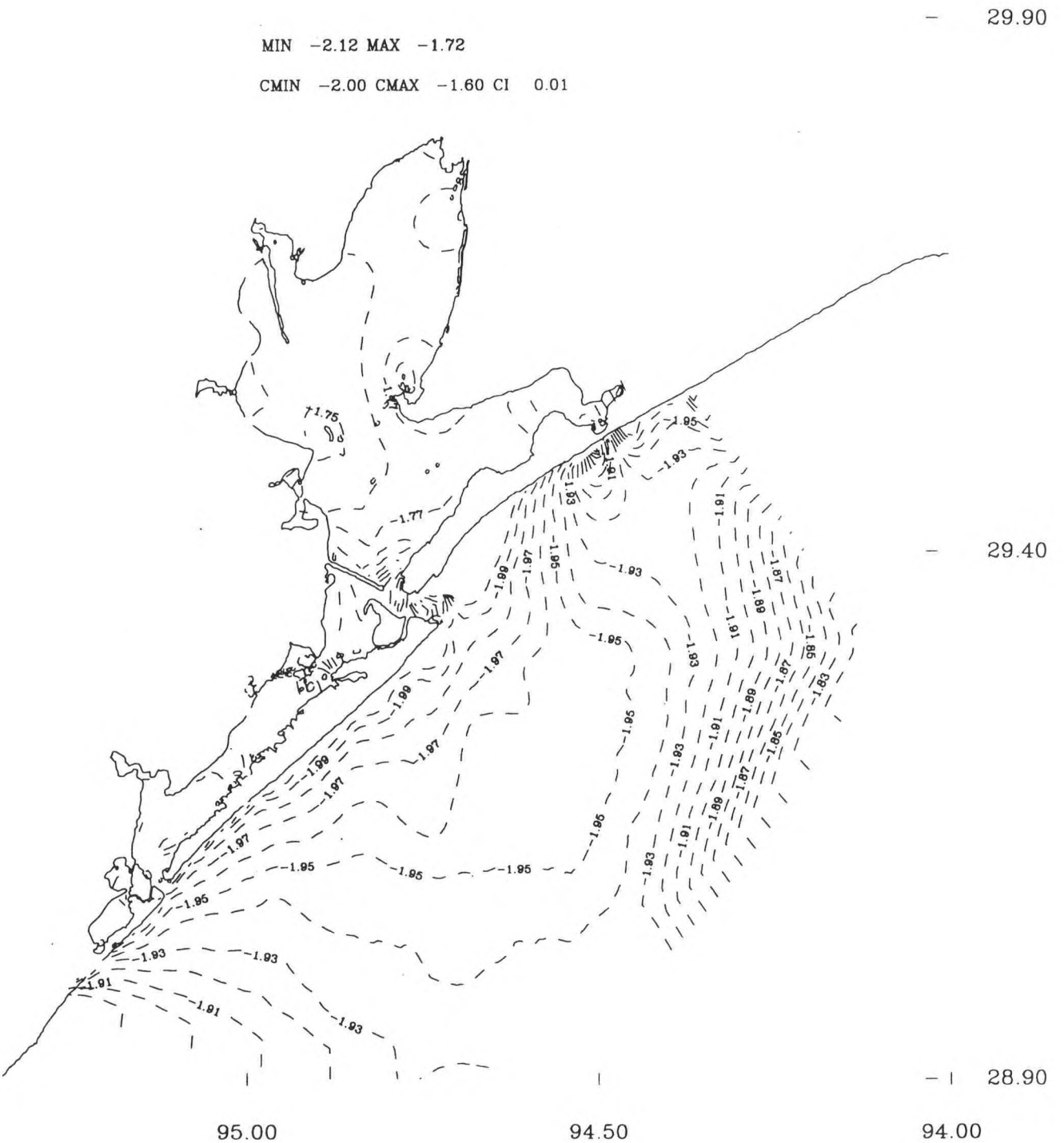

Figure 5.10. June 1995 Meteorological simulation tidal epoch MLLW wrt Geoid (m)

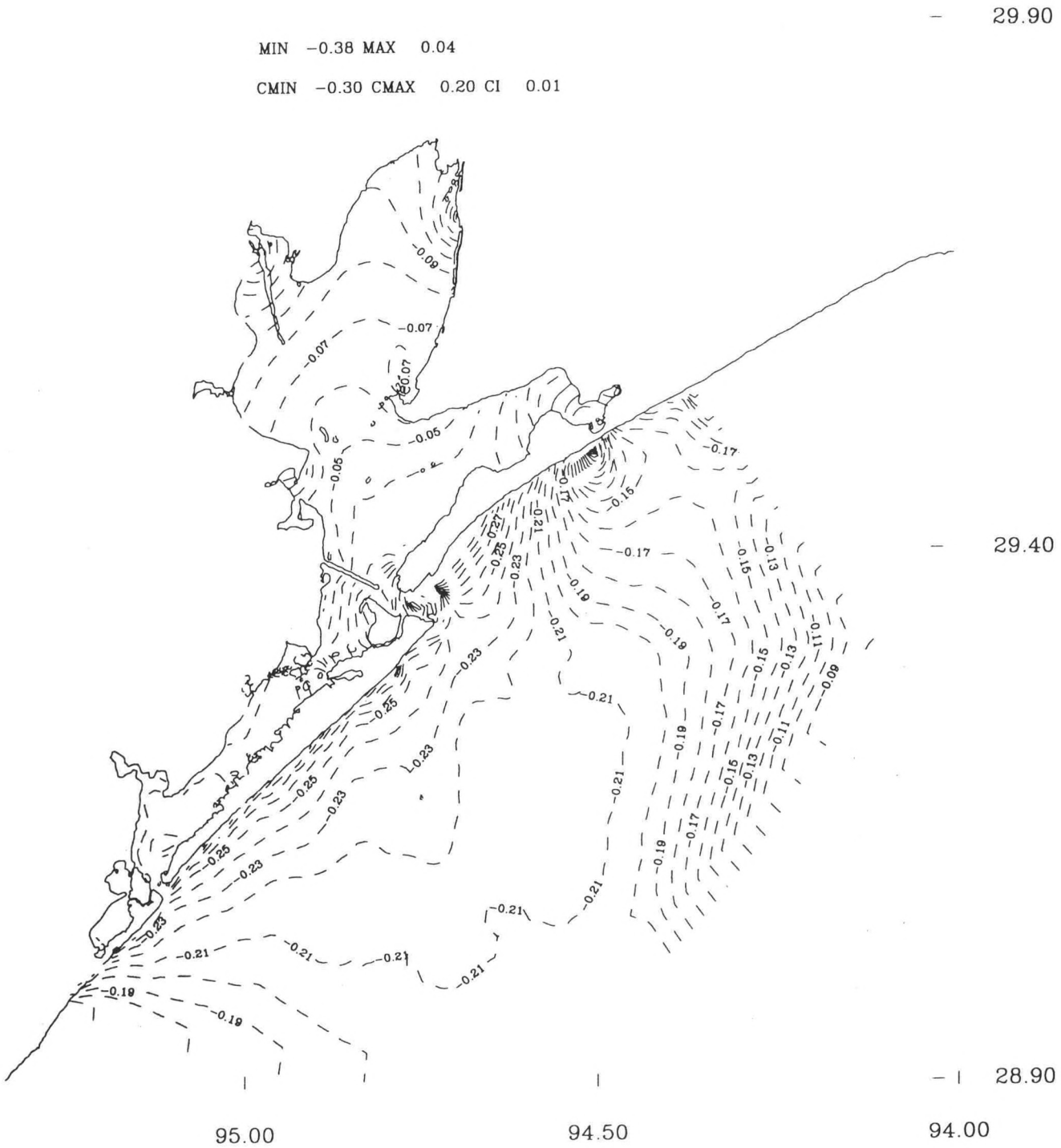

Figure 5.11. June 1995 Meteorological simulation tidal epoch MLLW wrt NGVD (1929) (m)

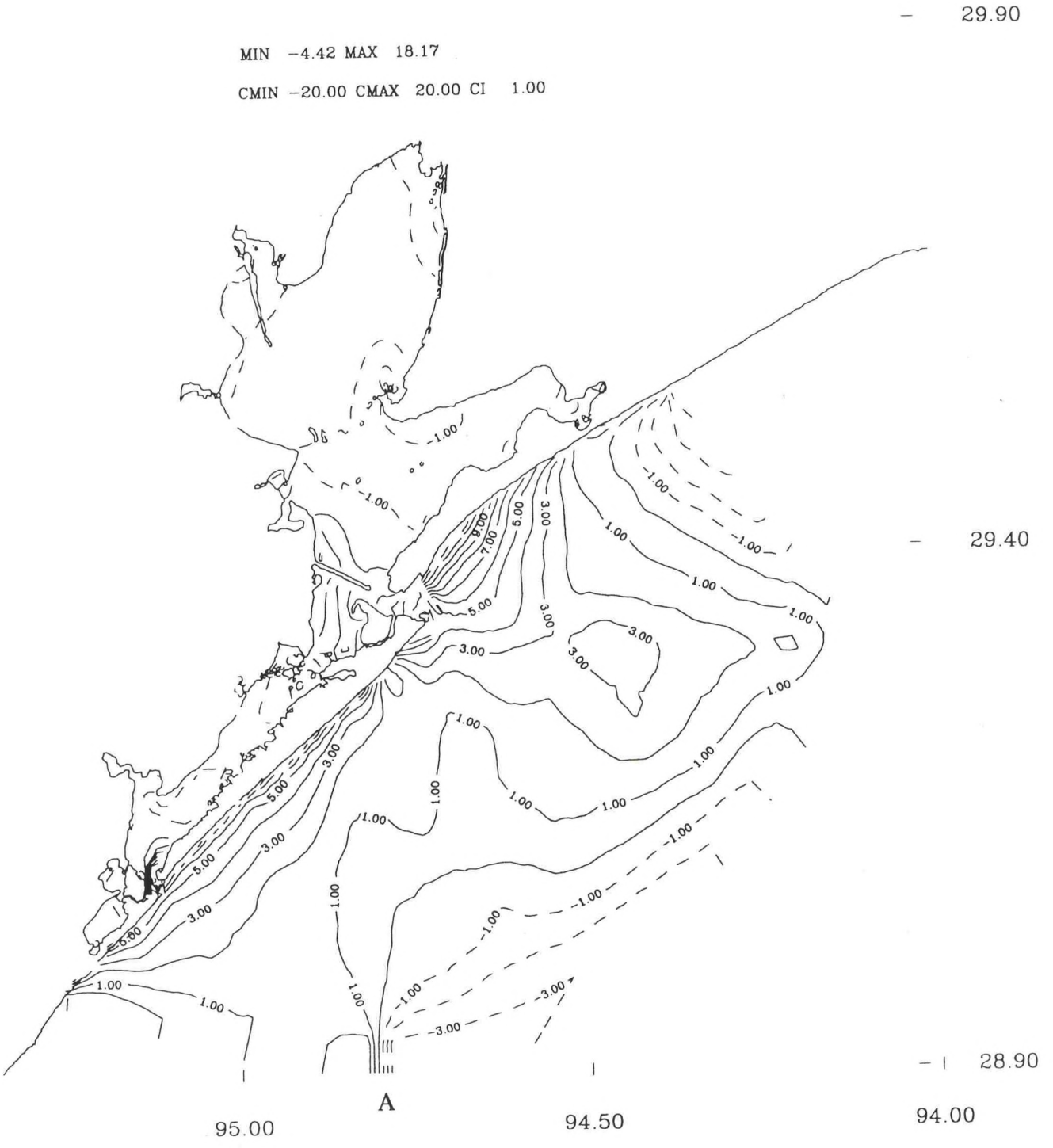

Figure 5.12. Difference between May 1995 Astronomical tide simulation and June 1995 meteorological simulation derived tidal epoch MLLW fields (cm)

6. SUMMARY AND CONCLUSIONS

The NOS three-dimensional model developed and applied to Galveston Bay has been calibrated to astronomical tide water level fluctuations over the one month period May 1995. Salinity and temperature initial and boundary conditions were derived from climatology. In addition, sea surface temperature was specified in lieu of heat flux and was also based on climatology. Climatological inflows were used for the Trinity River, San Jacinto River, and Buffalo Bayou. While it is possible to employ a longer simulation period to account for model spin-up of the density fields, the one day spin-up period used in this study appeared adequate due to the nearly dynamically consistent initial density fields. The model demonstrated considerable skill in reproducing the predicted tide levels throughout the Galveston Bay System (Galveston Bay, Trinity Bay, West Bay, and East Bay).

The model was further used to replicate the conditions encountered during the performance of the DGPS hydrosurvey during June 1995. Meteorological conditions were considered as completely as possible. Seven stations were used to develop surface wind and pressure fields every three hours over the thirty day period. Due to a lack of prototype data, salinity and temperature initial and boundary conditions as well as sea surface temperature were specified based on climatology. However, daily average USGS observed flow rates were specified for three inflows. Despite the climatological forcings for salinity and temperature and the use of a one day spin-up, the model reproduced the salinity fields to order 2-3 psu and the temperature fields to within 1-2 °C. The model reproduced the large horizontal and vertical density gradients derived from the CTD measurements taken during the hydrosurvey. Despite the use of the water level residual obtained at Galveston Pleasure Pier to specify the subtidal water level signal along the entire open boundary, the model reproduced the considerable water level fluctuations measured throughout Galveston Bay.

Simulated June 1995 water surface elevations with respect to the DGPS ellipsoid were provided as well at tidal epoch MLLW at 470 launch hydrosurvey track locations to NCD for direct comparison with OLLD tidal zoning derived NCD water surface elevations and for direct determination of water depths with respect to chart datum. These comparisons as well as an evaluation of traditional versus DGPS hydrosurvey resource and data processing requirements are to be performed and reported on by NCD.

The major findings of the modeling component of the NOS Partnership Project are as follows:

- In the determination of the tidal epoch MLLW distribution based on astronomical tide simulations and harmonic analysis of water level gauge data, it is recommended to use Sa and Ssa constituents derived over the same period of order the tidal epoch.

- To mitigate the "bull's eyes" in the spatial interpolation of the tidal epoch MLLW fields, it is recommended to further investigate the Barnes (1973) scheme.

- Reconstructed water levels at 14 tide gauges within the Bay were reproduced by the model to within 5 cm rms over the 30 day astronomical tide simulation during May 1995.

- Measured water levels at 7 tide gauges were reproduced to within 10 cm rms over the 30 day complete meteorologically forced simulation during June 1995. Model comparsions with DGPS levels at 470 launch hydrosurvey track locations were within 15 cm rms. Model data discrepancies were insensitive to launch speed and distance to the nearest tide gauge.

- Tidal epoch MLLW distributions derived from the two 30-day simulations differed by order 2 cm within the hydrosurvey area. This suggests that it may be feasible to determine the MLLW distribution prior to the conduct of the hydrosurvey based on astronomical tide simulation. This result could be further confirmed by considering additional meteorological periods of at least one month duration.

REFERENCES

Barnes, S. L., 1973: Mesoscale objective map analysis using weighted time-series observations, **NOAA Technical Memorandum ERL NSSL-62**, National Severe Storms Laboratory, Norman,OK.

Bennett, A. F., 1990: Inverse Methods for assessing ship-of-opportunity networks and estimating circulation and winds from tropical expendable baththermograph data, **Journal of Geophysical Research**, C9, 16,111-16,148.

Berger, R., W. Martin, R. McAdory, and J. Schmidt, 1994a: Houston-Galveston navigation channels, Texas: Three dimenisonal hydrodynamics model verification, **Hydraulics Laboratory** Draft Report 3, , U.S. Army Engineer Waterways Experiment Station, Vicksburg, MS.

___,1994b: Galveston Bay 3D model study, channel deepening, circulation, and salinity results. **Proceedings, 3rd International Conference on Estuarine and Coastal Modeling**, Oak Brook, IL, September 8-10, 1993, 1 - 13.

Bethem, T. D., and H. R. Frey, 1991: Operational physical oceanographic real-time data dissemination. **Proceedings, IEEE Oceans 91**, 865 - 867.

Blumberg, A. F., and H. J. Herring, 1987: Circulation modeling using orthogonal curvilinear coordinates. in **Three-Dimensional Models of Marine and Estuarine Dynamics** (J. C. J. Nihoul and B. M. Jamart, eds), Elsevier Oceanography Series, 45, 55 - 88.

Blumberg, A. F., and G. L. Mellor, 1987: A description of a three-dimensional coastal ocean circulation model. **Three-Dimensional Coastal Ocean Models**, (ed. Heaps), American Geophysical Union, Washington, DC., 1 - 16.

Bobb, W. H., R. A. Boland, and A. J. Banchetti, 1973: Houston Ship Channel Galveston Bay, Texas; Report 1; Hydraulic and salinity verification, Technical Report H-73-12, USAE Waterways Experiment Station, Vicksburg, MS.

Bryan, K. and M. D. Cox, 1968. A nonlinear model of an ocean driven by wind and differential heating: Parts I and II, **Journal of Atmospheric Science**, 25:945-978.

Butler, H. L., 1980: Evolution of a numerical model for simulating long-period wave behavior in ocean-estuarine systems, in **Estuaries and wetland processes with emphassis on modeling**, P. Hamilton and K.B. Macdonald (eds), Plenum Press, NY, 147-182.

Chuang, W-S and W. J. Wiseman, 1983: Coastal sea level response to frontal passages on the Louisiana-Texas shelf, **Journal of Geophysical Research**, C4, 2615-2620.

Cochrane, J. D. and F. J. Kelly, 1986. Low-frequency circulation on the Texas-Louisiana continental shelf, **Journal of Geophysical Research**, C9, 10645-10659.

Defant, A., 1958: **Ebb and Flow: the Tides of the Earth, Air, and Water.** University of Michigan Press, Ann Arbor, MI, 121 pp.

Dennis, R. E., and E. E. Long, 1971: A user's guide to a computer program for harmonic analysis of data at tidal frequencies. **NOAA Technical Report** NOS 41. NOAA, National Ocean Service, Office of Oceanography and Marine Assessment, Rockville, MD, 31 pp.

Dietrich, D. E. and C. A. Lin, 1994: Numerical studies of eddy shedding in the Gulf of Mexico, **Journal of Geophysical Research**, C4, 7599-7615.

Dinnel, S. J. and W. J. Wiseman, 1986. Fresh water on the Louisiana and Texas shelf, **Continental Shelf Research**, 6(6), 765-784.

Foreman, M. G., 1995: Formulas supplied with the Bennett-OSU Global Tide Model solution.

Haney, R. L., 1991: On the pressure gradient force over steep topography in sigma coordinate ocean models, **Journal of Physical Oceanography**, 21: 610-619.

Hellerman, S. and M. Rosenstein, 1983: Normal monthly wind stress over the world ocean with error estimates, **Journal of Physical Oceanography**, 13: 1093-1104.

Hess, K. W., 1994: Tampa Bay Oceanography Project: Development and Application of the Numerical Circulation Model. NOAA, National Ocean Service, Office of Ocean and Earth Sciences, **NOAA Technical Report** NOS OES 005, Silver Spring, MD.

___ and K. T. Bosley, 1992: Techniques for validation of a model for Tampa Bay, **Proceedings Second International Conference on Estuarine and Coastal Modeling**, Tampa, FL, November 11-13, 1991, 83-94.

Hsu, S. A., 1988: **Coastal Meteorology**, Academic Press, Inc., New York, NY.

Ives, D. C. and R. M. Zacharias, 1987: Conformal mapping and orthogonal grid generation, Paper No. 87-2057, **AIAA/SAE/ASME/ASEE 23rd Joint Propulsion Conference**, San Diego, CA.

Jelesnianski, C. P., J. Chen, W. A. Shaffer, and A. J. Gilad, 1984: SLOSH - a hurricane storm surge forecasting model. **Preprints, Oceans 84**, Washington, DC, Marine Technology Society and IEEE/Oceanic Engineering Society, 314 - 317.

Lane, W. G., 1994: Regional monitoring program for the Galveston Bay plan, **Galveston Bay National Estuary Program, GBNEP-45**, Houston, TX.

Large, W. G., and S. Pond, 1981: Open ocean momentum flux measurements in moderate to strong winds. **Journal of Physical Oceanography** 11, 324 - 336.

Leendertse, J. J. 1967: Aspects of a computational model for long-period water-wave propagation. RAND Technical Memorandum RM-5294-PR, The RAND Corp, Santa Monica, CA.

Levitus, S., 1982: Climatological atlas of the world ocean, **NOAA Professional Paper 13**, U.S. Department of Commerce, Rockville, MD.

Liscum, F. and J. W. East, 1995: Floods in southeast Texas, October 1994, in **Proceedings of Texas Water '95**, Texas Section of the American Society of Civil Engineers, August 16-17, 1995, San Antonio, TX, 367-372.

Marmer, H. A., 1951. **Tidal Datum Planes**. U.S. Department of Commerce, Coast and Geodetic Survey, Special Publication No. 135 [revised 1951 edition, reprinted 1977], Rockville, MD.

Mellor, G. L., 1993: User's guide for a three-dimensional, primitive equation, numerical ocean model. Atmospheric and Oceanic Sciences Program, Princeton University, Princeton, NJ, (unpublished manuscript).

___, and A. F. Blumberg, 1985: Modeling vertical and horizontal diffusivities with the sigma coordinate system. **Monthly Weather Review**, 113, 1379 - 1383.

NOS, 1995. **Houston/Galveston Physical Oceanographic Real-Time System (PORTS): FY 95 Implementation Plan**, NOAA, National Ocean Service, Rockville, MD.

Oey, L.-Y., 1995. Eddy and wind-forced circulation, **Journal of Geophysical Research**,100, C5, 8621-8638.

Orlando, S. P., L. P. Rozas, G. H. Ward, and C. J. Klein, 1993. **Salinity characterization of Gulf of Mexico estuaries**, NOAA, Office of Ocean Resources Conservation and Assessment, Silver Spring, MD.

Orlanski, I., 1976: A simple boundary condition for unbounded hyperbolic flows. **Journal of Computational Physics**, 21, 251 - 269.

Parker, B. B., and R. C. Patchen, 1987: The circulation and water level forecast atlas: a new product in development at NOS. **Proceedings, Oceans 87**, Halifax, NS, September 28 - October 1, 1987. 857 - 862.

Pullen, E. J., W. L. Trent, G. B. Adams, 1971. A hydrographic survey of the Galveston Bay system, Texas, 1963-1966, **NOAA Technical Report** NMFS SSRF-639, Seattle, WA.

Reid, R. O., and B. R. Bodine, 1968: Numerical model for storm surges in Galveston Bay. **Journal of the Waterways and Harbors Division**, ASCE, 94, No. WW1, Proceedings Paper 5805, 33 - 57.

___ and R. E. Whitaker, 1981: Numerical model for astronomical tides in the Gulf of Mexico, Volume I: theory and application, Texas A&M University, College of Geosciences, College Station, TX.

Schmalz, R. A., 1985: Numerical Model Investigation of Mississippi Sound and Adjacent Areas, **Miscellaneous Paper CERC-85-2**, US Army Engineer Waterways Experiment Station, Vicksburg, MS.

___, 1994: Long Island Sound Oceanography Project, Summary Report, Volume 1: Application and Documentation of the Long Island Sound Three-Dimensional Circulation Model. NOAA, National Ocean Service, Office of Ocean and Earth Sciences, Silver Spring, MD.

___, M. F. Devine, and P. H. Richardson, 1994: Long Island Sound Oceanography Project, Summary Report, Volume 2: Residual Circulation and Thermohaline Structure. NOAA, National Ocean Service, Office of Ocean and Earth Sciences, Silver Spring, MD.

Schureman, P., 1958: **Manual of Harmonic Analysis and Prediction of Tides**. U.S. Department of Commerce, Coast and Geodetic Survey, Special Publication No. 98 [revised 1940 edition, reprinted 1988], Rockville, MD.

Schwiderski, E. W., 1980: On charting global ocean tides. **Reviews of Geophysics and Space Physics** 18 (1), 243 - 268.

Shaffer, W. A., C. P. Jelesnianski, and J. Chen, 1986: Hurricane storm surge forecasting. **Preprints, Oceans 86**, Washington, DC, Marine Technology Society and IEEE/Oceanic Engineering Society, 1379 - 1385.

Shankar, N. J. and F. D. Masch, 1970: Influence of tidal inlets on salinity and related phenomena in estuaries, **Technical Report HYD 16-7001, CRWR 49**, University of Texas, Austin, TX.

Sheng, Y. P., H.-K. Lee, and K. H. Wang, 1990: On numerical strategies of estuarine and coastal modeling, **Proceedings First International Conference on Estuarine and Coastal Modeling**, Newport, RI, November 15-17, 1989, 291-301.

Shipley, F. S. and R. W. Kiesling (eds.), 1991: Proceedings: Galveston Bay Characterization Workshop, **Galveston Bay National Estuary Program** GBNEP-6, Houston, TX.

___, 1994: The State of the Bay: A Characterization of the Galveston Bay Ecosystem, **Galveston Bay National Estuary Program** GBNEP-44, Houston, TX.

Solis, R. S., 1994. Calibration of a circulation and salinity transport model for Galveston Bay, **Texas Water Development Board** Draft Report, Texas Water Development Board, Austin, TX.

Sparr, T. M., C. R. Sprague, R. W. Hann, 1973. A study of the flushing times of the Houston Ship Channel and Galveston Bay, **Estuarine systems Projects Technical Report** No. 12, Texas A&M University, College Station, TX.

Sturges, W. and S. Welch, 1991, Numerical modeling studies of the Gulf of Mexico and the Caribbean Sea using the Bryan-Cox model, **OCS Study Report** MMS 91-0061, U.S. department of the Interior, Minerals Management Service, Gulf of Mexico OCS Regional Office, New Orleans, LA.

Temple, R. F., D. L. Harrington, J. A. Martin, 1977. Monthly temperature and salinity measurements of continental shelf waters of the northwestern Gulf of Mexico, 1963-1965., **NOAA Technical Report** NMFS SSRF-707, Rockville, MD.

Wang, K-H, 1994. Characterization of circulation and salinity change in Galveston Bay, **Journal of Engineering Mechanics**, Vol. 120, No. 3, 557-579.

Ward, G. H., 1980: Hydrography and circulation of Gulf estuaries, in **Estuaries and wetland processes with emphassis on modeling**, P. Hamilton and K.B. Macdonald (eds), Plenum Press, NY, 183-215.

___ and N. E. Armstrong: 1992, Ambient water and sediment quality of Galveston Bay: present status and historical trends, **Galveston Bay National Estuary Program** GBNEP-22, Houston, TX.

___, 1993. Galveston Bay hydrography and transport model validation, Center for Research in Water Resources, The University of Texas, Austin, TX.

Westerink, J. J., R. A. Luettich, and N. Scheffner, 1993: ADCIRC: An advanced three-dimensional circulaiton model for shelves, coasts, and estuaries, Report 3 Development of a tidal constituent database for the western North Atlantic and Gulf of Mexico, **Technical Report DRP-92-6**, US Army Engineer Waterways Experiment Station, Vicksburg, MS.

Whitledge, T. E. and S. M. Ray, 1989: **Galveston Bay: Issues, Resources, Status, and Management**. NOAA Estuary-of-the-Month Seminar Series No. 13, Washington, DC.

Wilken, J. L., 1988: A computer program for generating two-dimensional orthogonal curvilinear coordinate grids, Woods Hole Oceanographic Institution, (unpublished), Woods Hole, MA.

Williams, R. G., H. R. Frey, T. Bethem, 1990. Houston Ship Channel/Galveston Bay current prediction quality assurance miniproject, **NOAA Technical Memorandum** NOS OMA 53, Rockville, MD.

Willmott, C. J., S. G. Ackleson, R. E. Davis, J. J. Feddema, K. M. Klink, D. R. Legates, J. O'Donnell, and C. M. Rowe, 1985: Statistics for the evaluation and comparison of models. **Journal of Geophysical Research**, 90, 8995 - 9005.

Zetler, B. D., 1982: **Computer Applications to Tides in the National Ocean Survey. Supplement to Manual of Harmonic Analysis and Prediction of Tides** (Special Publication No. 98). National Ocean Service, Rockville, MD.

Zilkoski, D. B., J. H. Richards, and G. M. Young, 1992: Results of the general adjustment of the North American Vertical Datum of 1988, **Surveying and Land Information Systems**, Volume 52, (3):133-149.

ACKNOWLEDGEMENTS

The following people made important contributions to the completion of this report. Dr. Bruce B. Parker, Chief of the Coastal and Estuarine Oceanography Branch, conceived of this Partnership Project and provided leadership and critical resources. Dr. Kurt W. Hess supplied a wealth of information on modeling shallow bay systems. Mr. Phillip H. Richardson developed the wind and atmospheric pressure field interpolation program and assisted in the development of the finalized CTD casts. Mr. Godwin Darko, a 1995 NOS Summer Student, reviewed and edited the CTD datasets for use in the development of model initialization and point comparison with model results.

APPENDIX A. METEOROLOGICAL SIMULATION: DGPS WATER LEVEL COMPARISON PLOT SET

WATER SURFACE ELEVATION WRT GPS ELLIPSOID (M)

JD 164.49 – JD 164.94

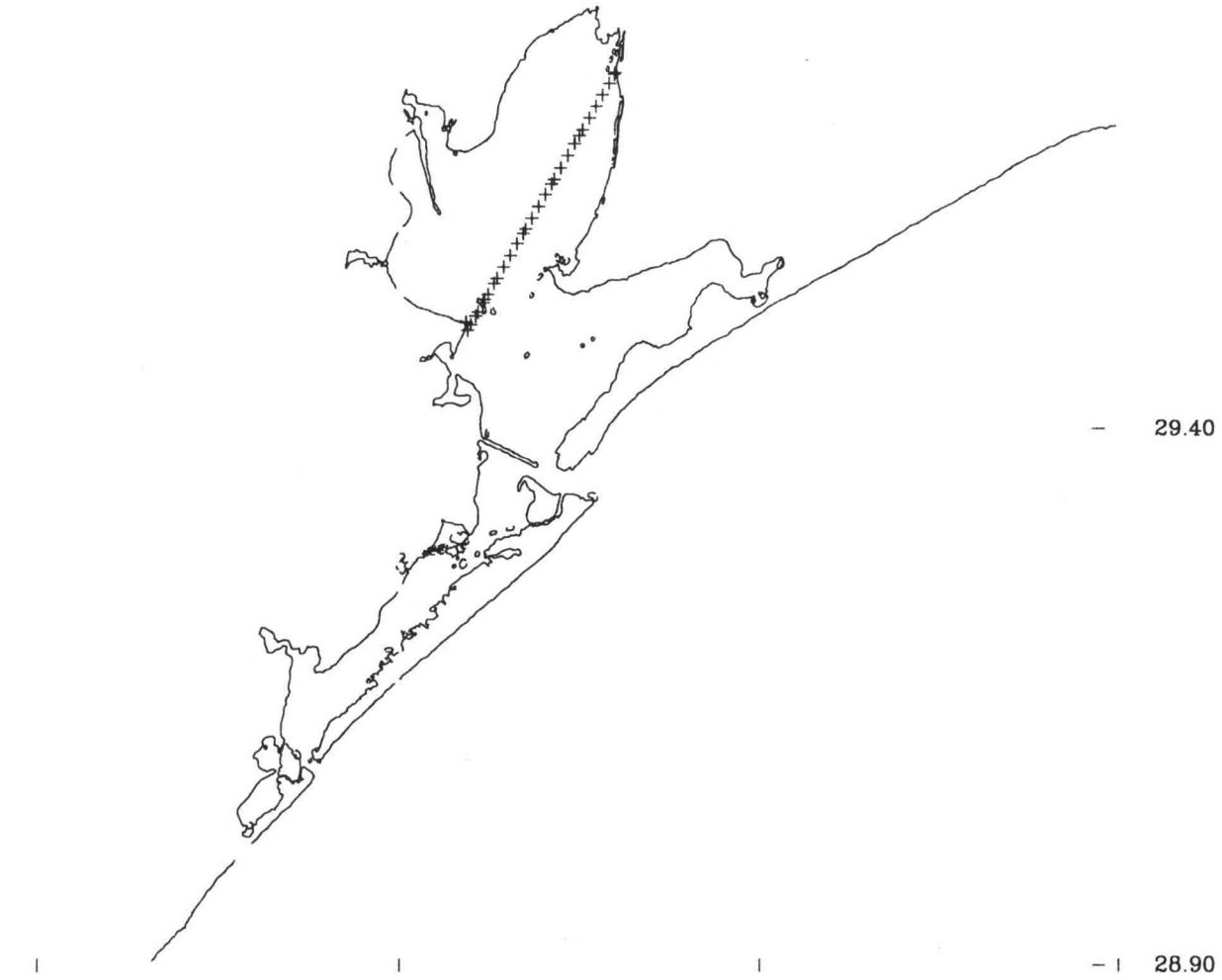

WATER SURFACE ELEVATION WRT GPS ELLIPSOID (M)

WATER SURFACE ELEVATION (M)

RMS 0.19 IN. AGT 0.68

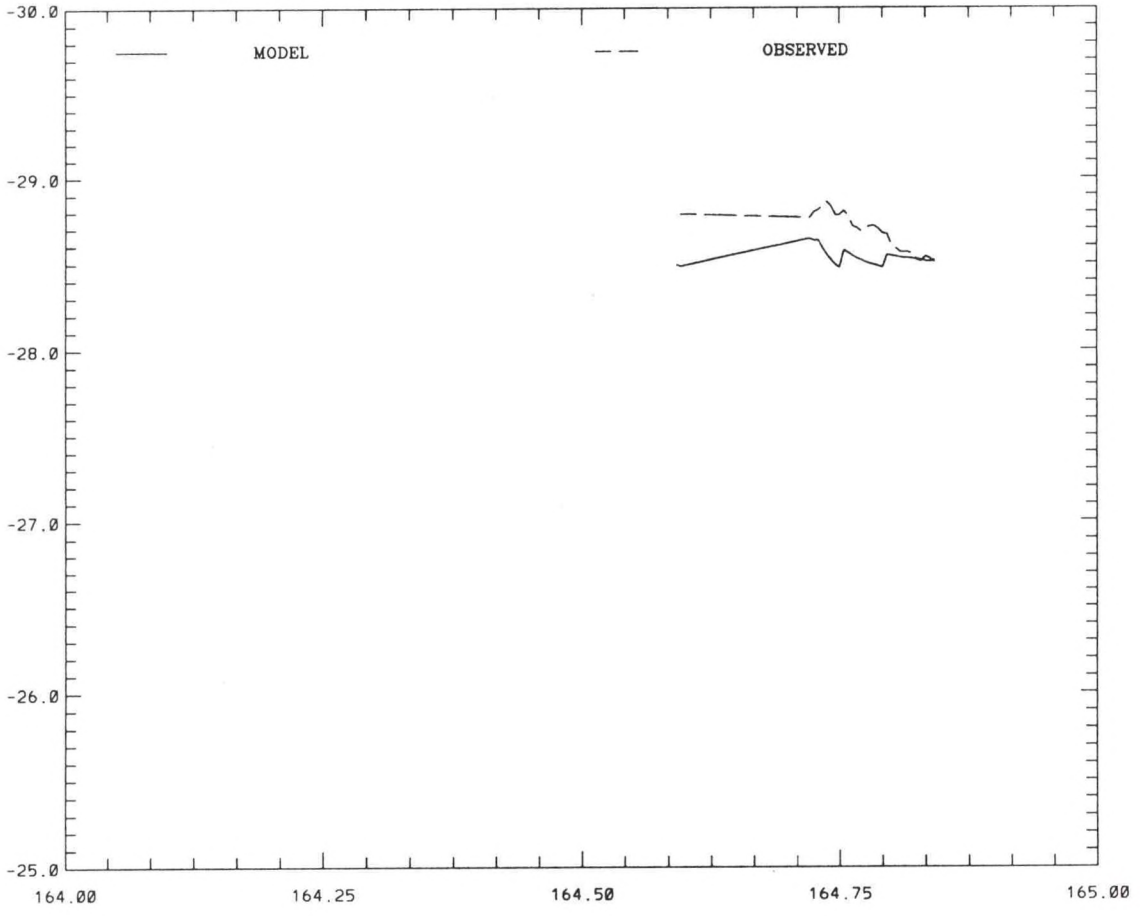

TIME (JULIAN DAYS 1995)

WATER SURFACE ELEVATION WRT GPS ELLIPSOID (M)

JD 165.45 - JD 165.87

WATER SURFACE ELEVATION WRT GPS ELLIPSOID (M)

WATER SURFACE ELEVATION (M)

RMS 0.18 IN. AGT 0.68

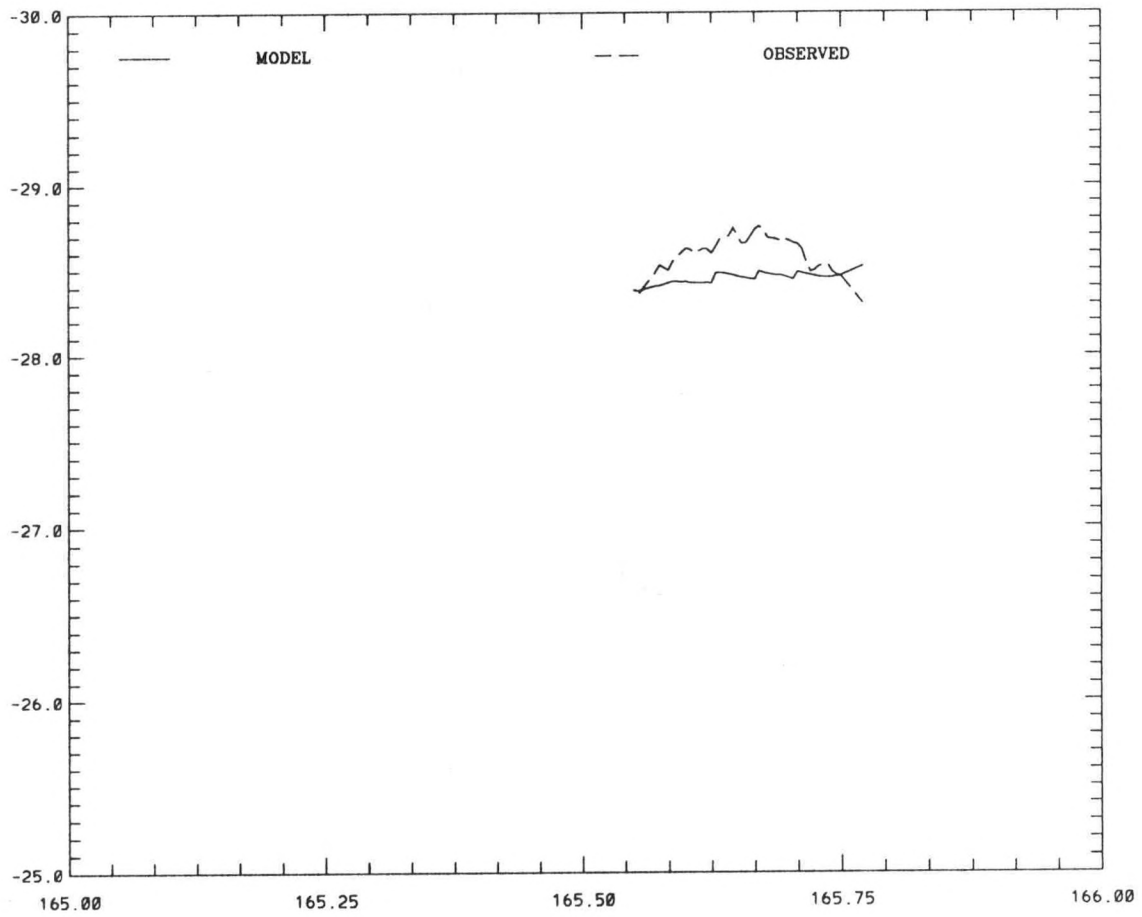

TIME (JULIAN DAYS 1995)

WATER SURFACE ELEVATION WRT GPS ELLIPSOID (M)

JD 166.51 – JD 166.72

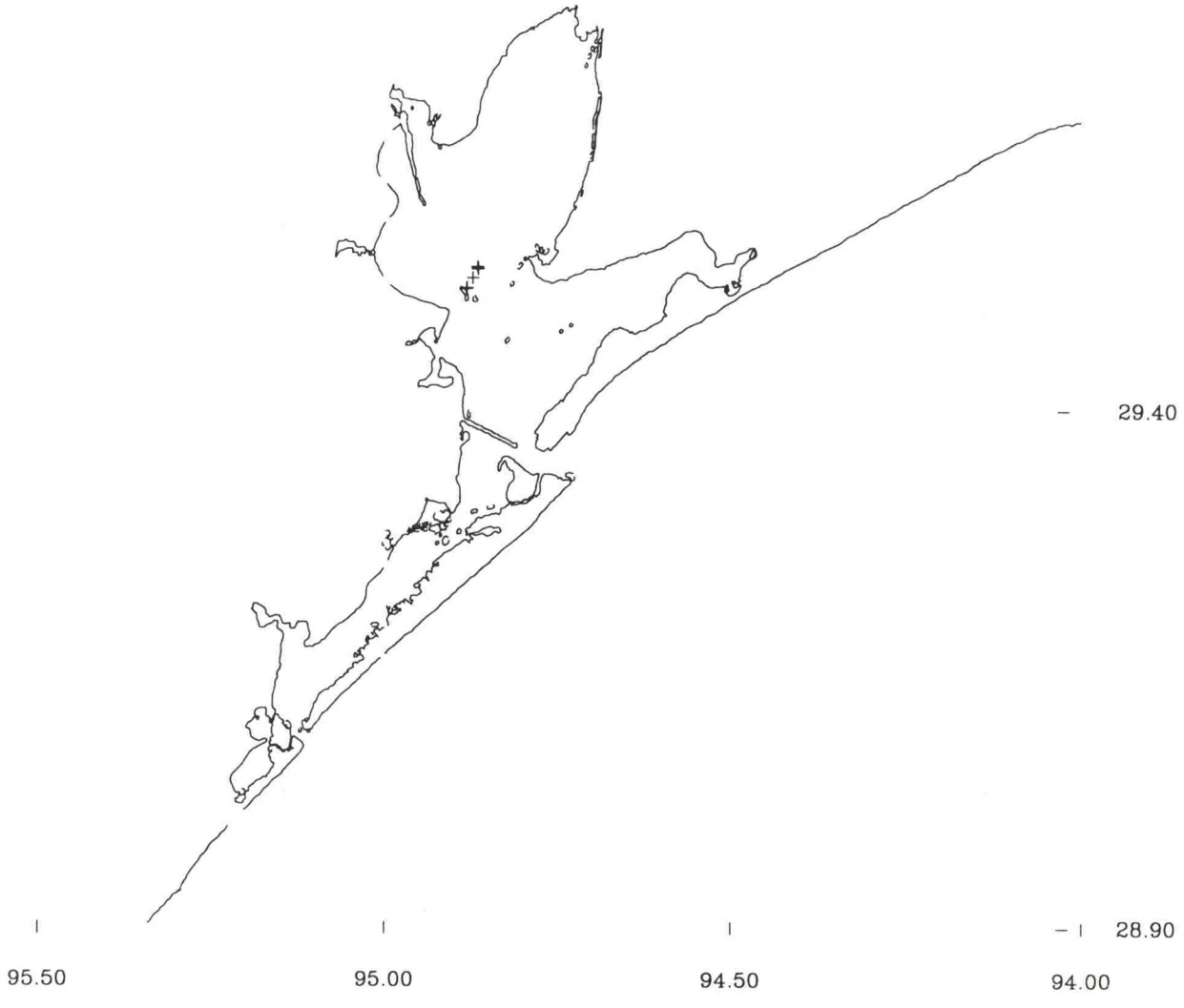

WATER SURFACE ELEVATION WRT GPS ELLIPSOID (M)

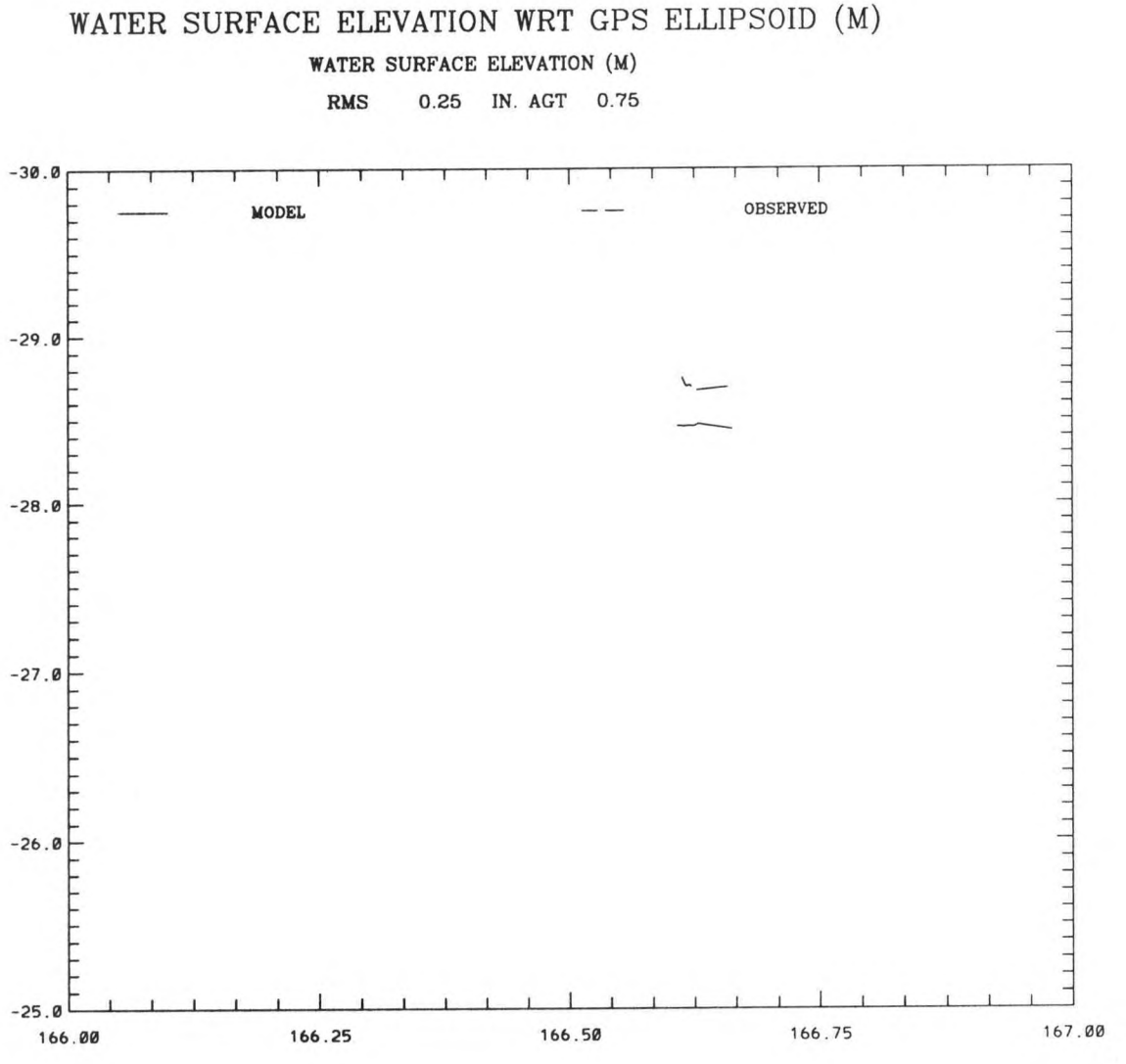

WATER SURFACE ELEVATION WRT GPS ELLIPSOID (M)

JD 167.47 – JD 167.92

WATER SURFACE ELEVATION WRT GPS ELLIPSOID (M)

WATER SURFACE ELEVATION (M)

RMS 0.20 IN. AGT 0.64

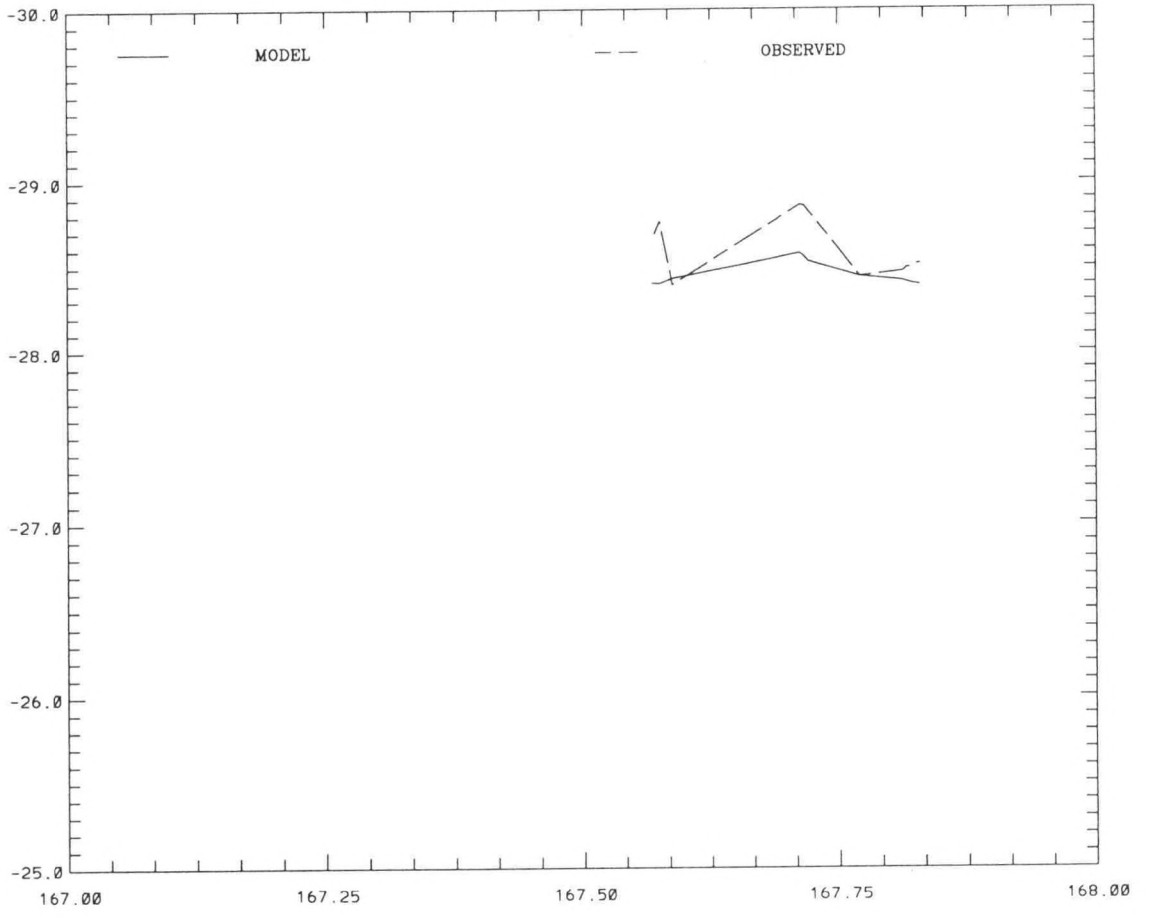

TIME (JULIAN DAYS 1995)

WATER SURFACE ELEVATION WRT GPS ELLIPSOID (M)

JD 170.48 – JD 170.88

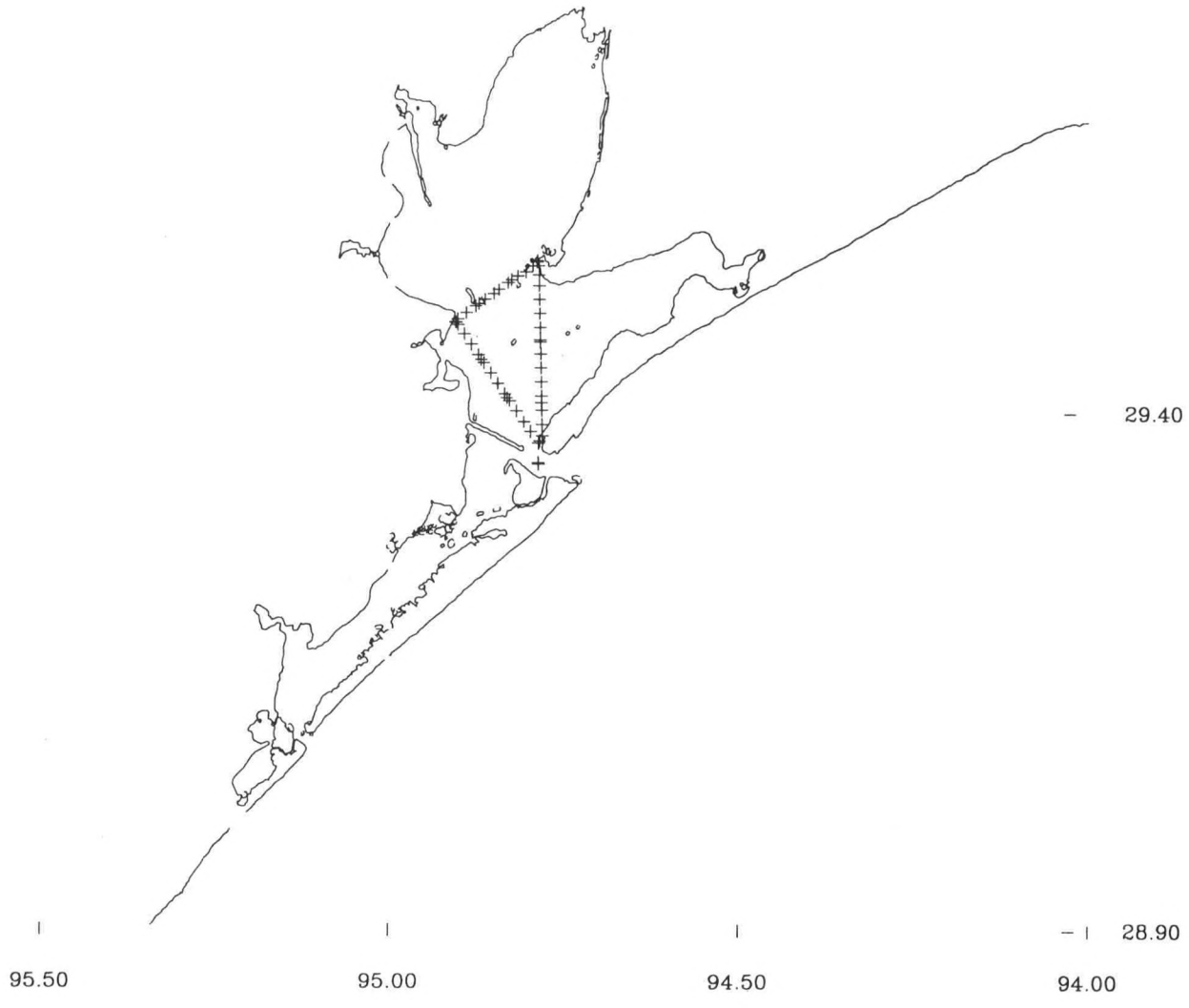

WATER SURFACE ELEVATION WRT GPS ELLIPSOID (M)

WATER SURFACE ELEVATION (M)

RMS 0.11 IN. AGT 0.61

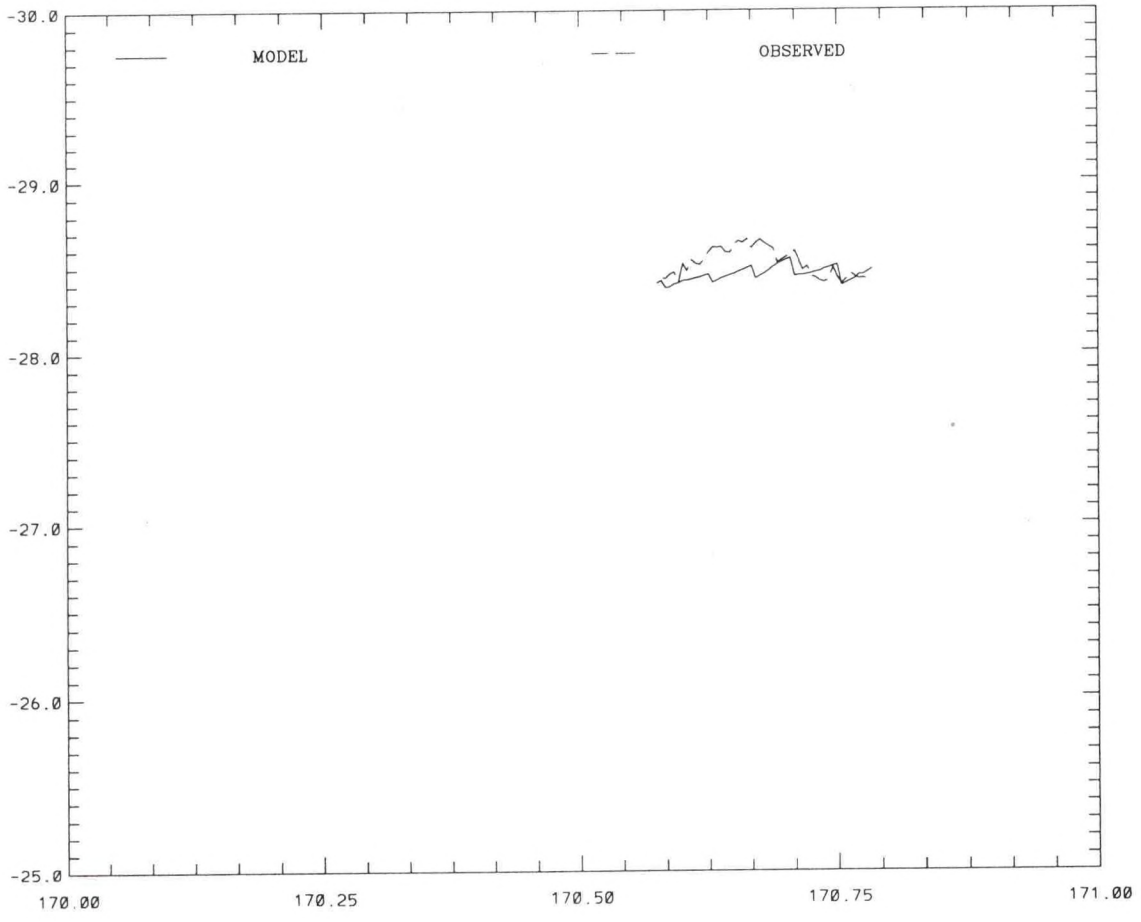

TIME (JULIAN DAYS 1995)

WATER SURFACE ELEVATION WRT GPS ELLIPSOID (M)

JD 171.49 – JD 171.80

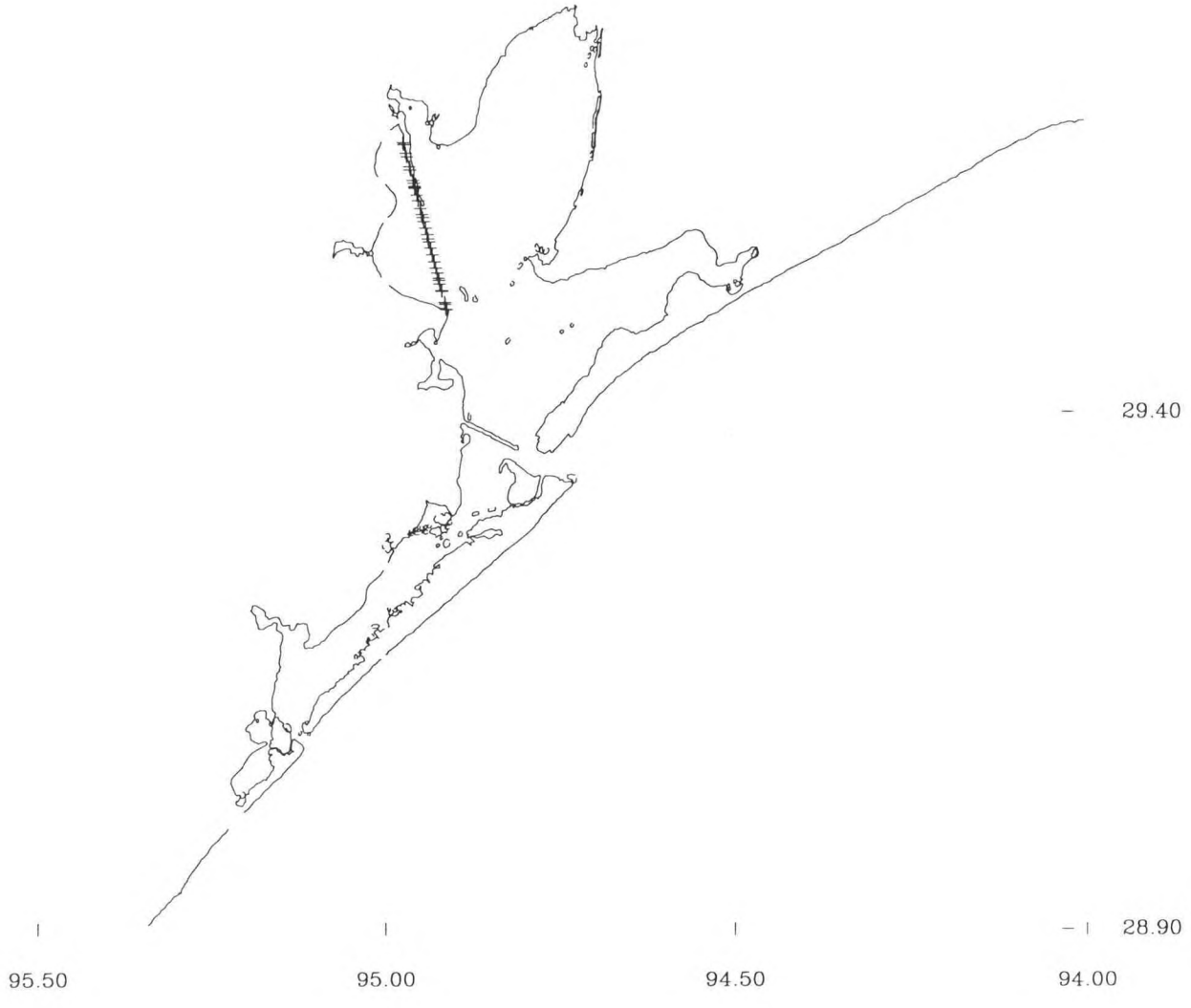

WATER SURFACE ELEVATION WRT GPS ELLIPSOID (M)

WATER SURFACE ELEVATION (M)

RMS 0.21 IN. AGT 0.73

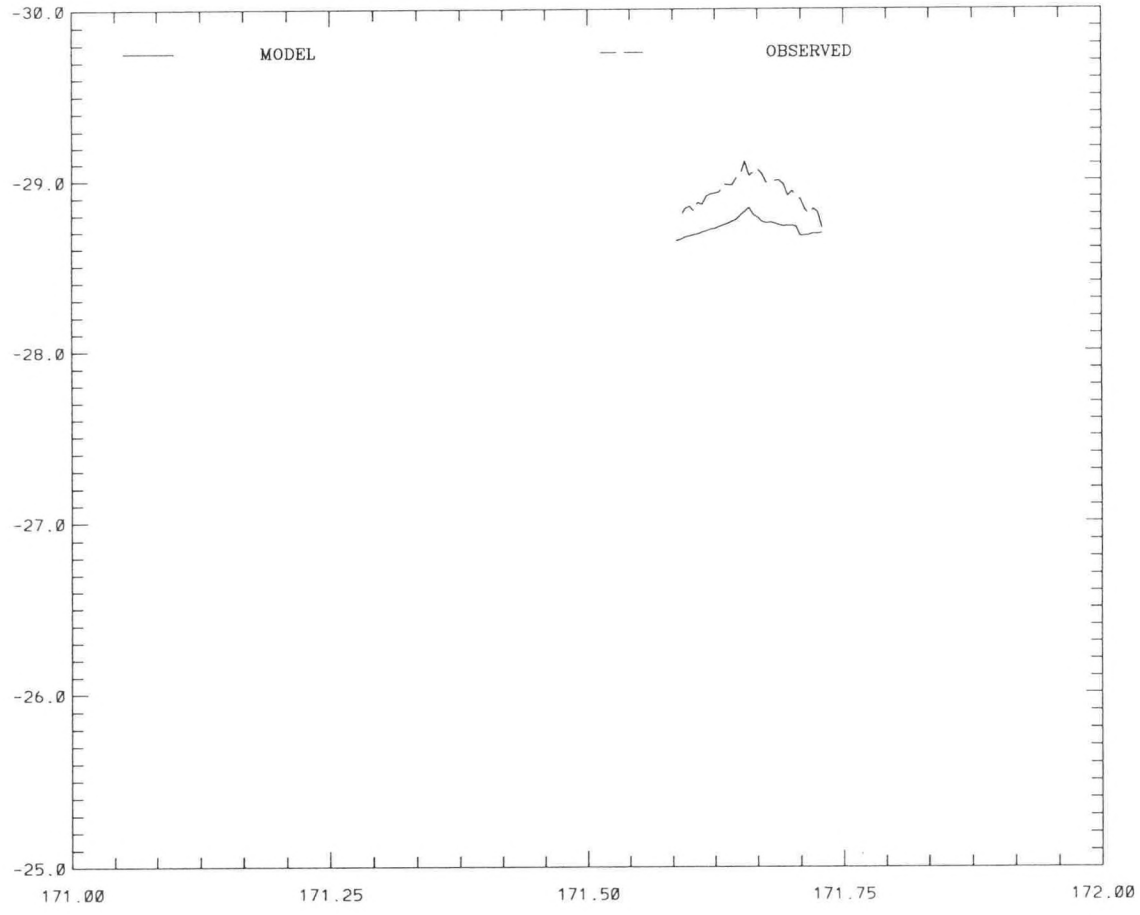

TIME (JULIAN DAYS 1995)

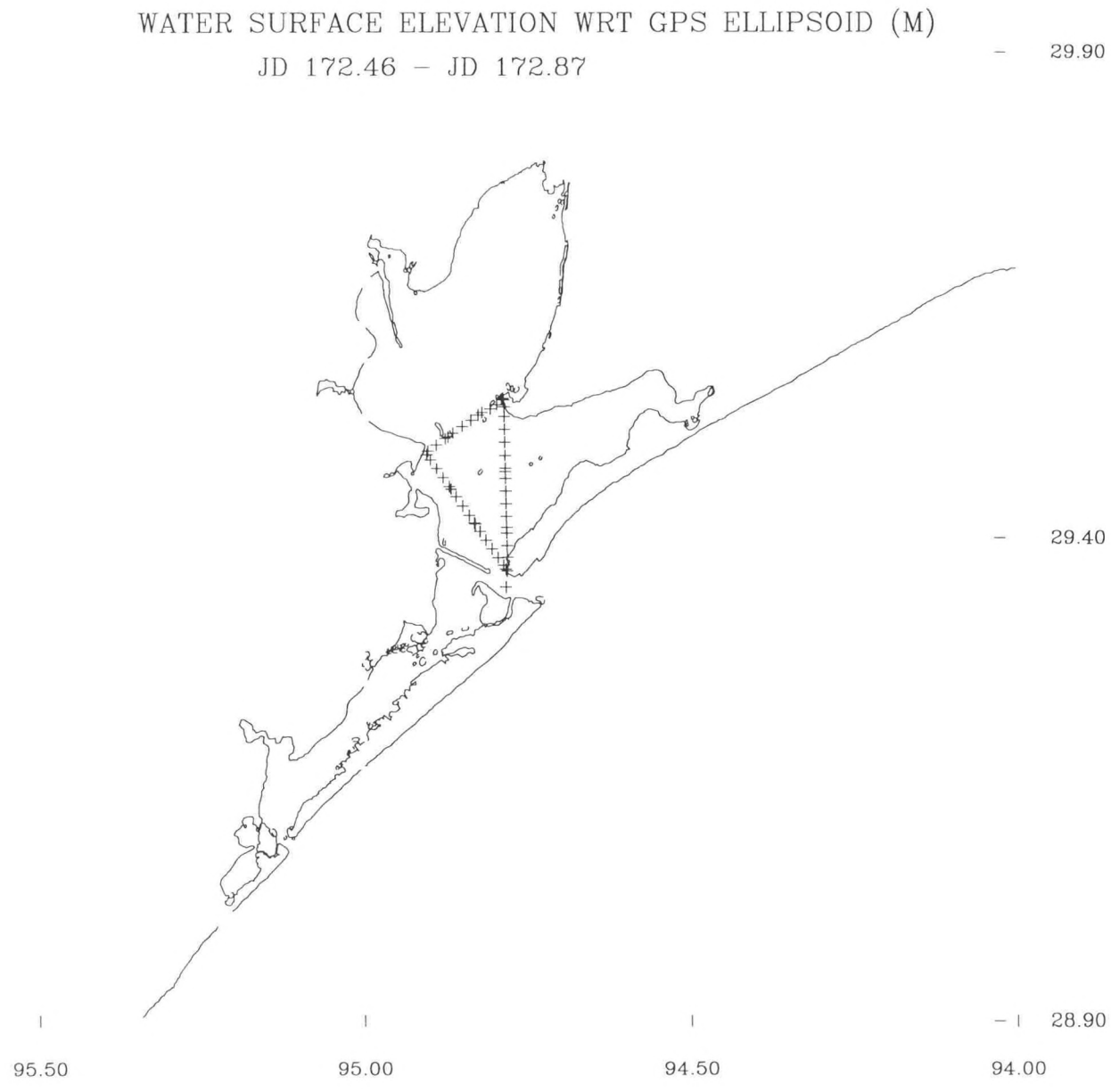
WATER SURFACE ELEVATION WRT GPS ELLIPSOID (M)
JD 172.46 - JD 172.87
29.90
29.40
28.90
95.50
95.00
94.50
94.00

WATER SURFACE ELEVATION WRT GPS ELLIPSOID (M)

WATER SURFACE ELEVATION (M)

RMS 0.07 IN. AGT 0.63

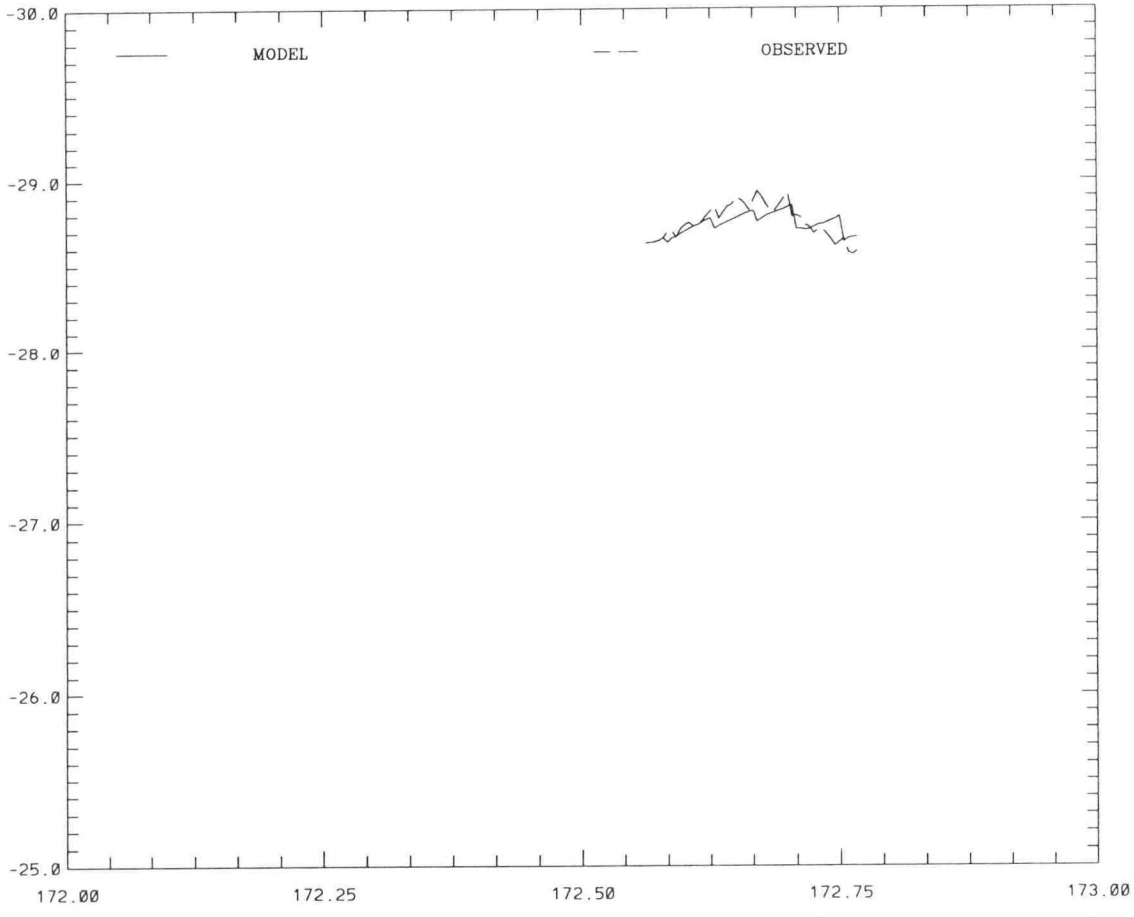

TIME (JULIAN DAYS 1995)

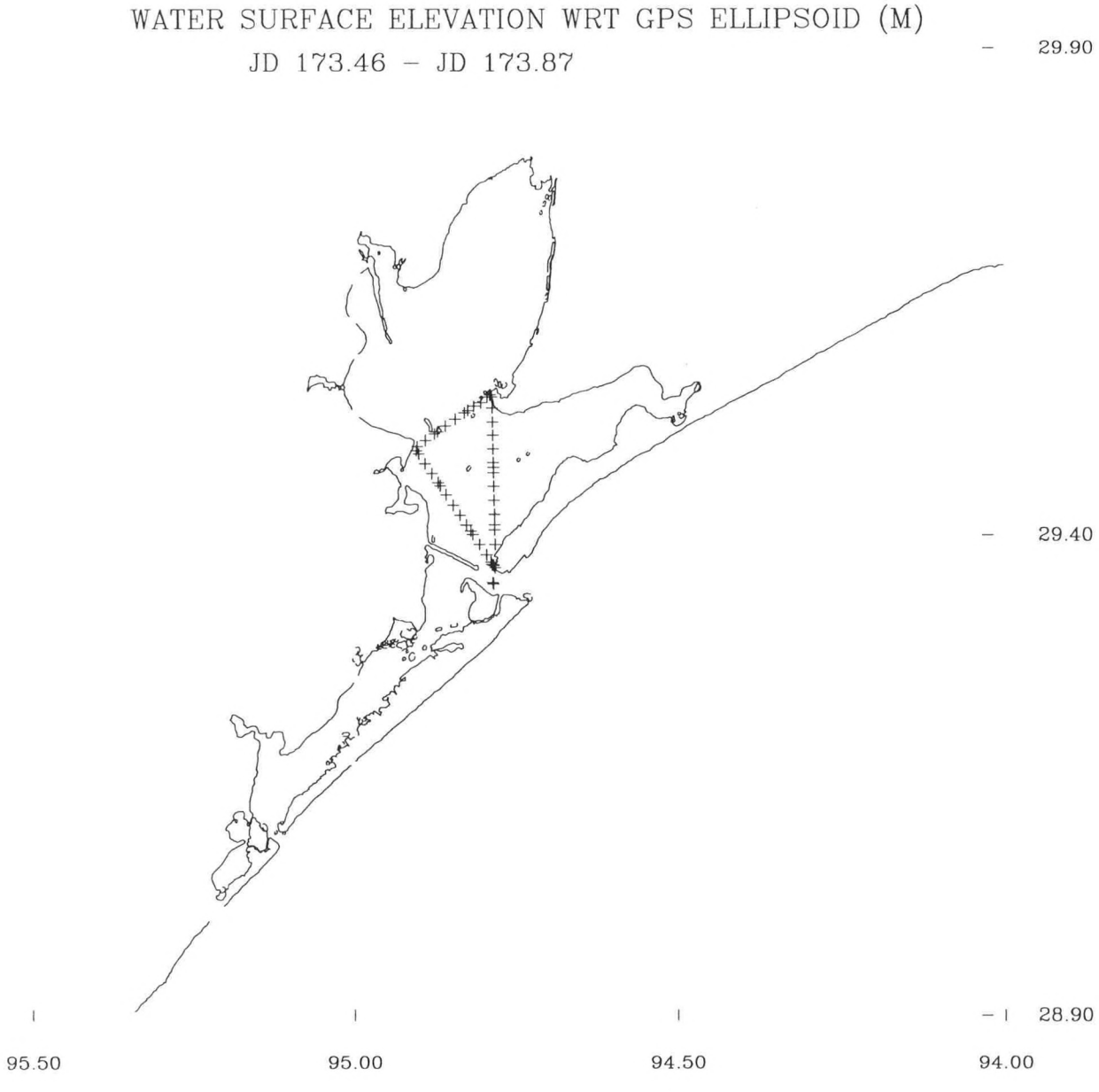
WATER SURFACE ELEVATION WRT GPS ELLIPSOID (M)
JD 173.46 - JD 173.87
29.90
29.40
28.90
95.50
95.00
94.50
94.00

WATER SURFACE ELEVATION WRT GPS ELLIPSOID (M)

WATER SURFACE ELEVATION (M)

RMS 0.09 IN. AGT 0.66

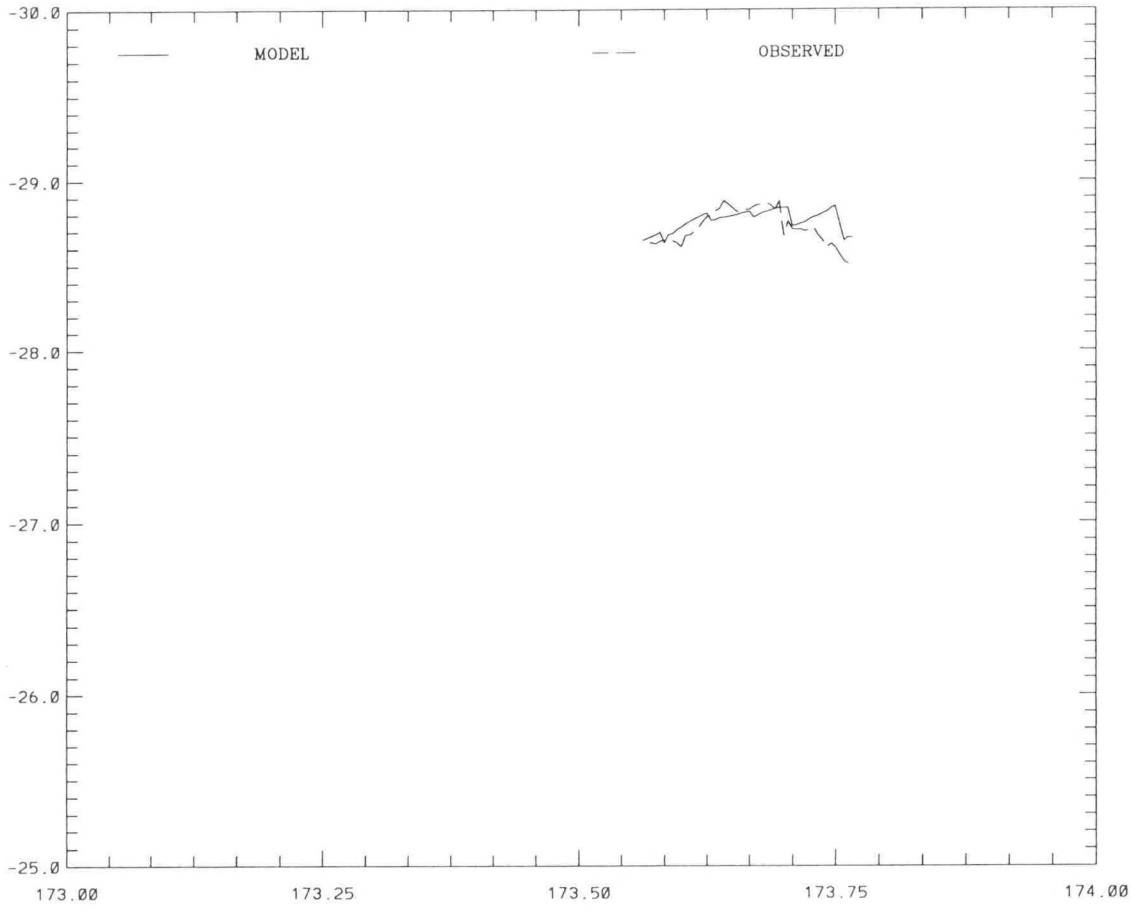

TIME (JULIAN DAYS 1995)

WATER SURFACE ELEVATION WRT GPS ELLIPSOID (M)

JD 174.45 – JD 174.85

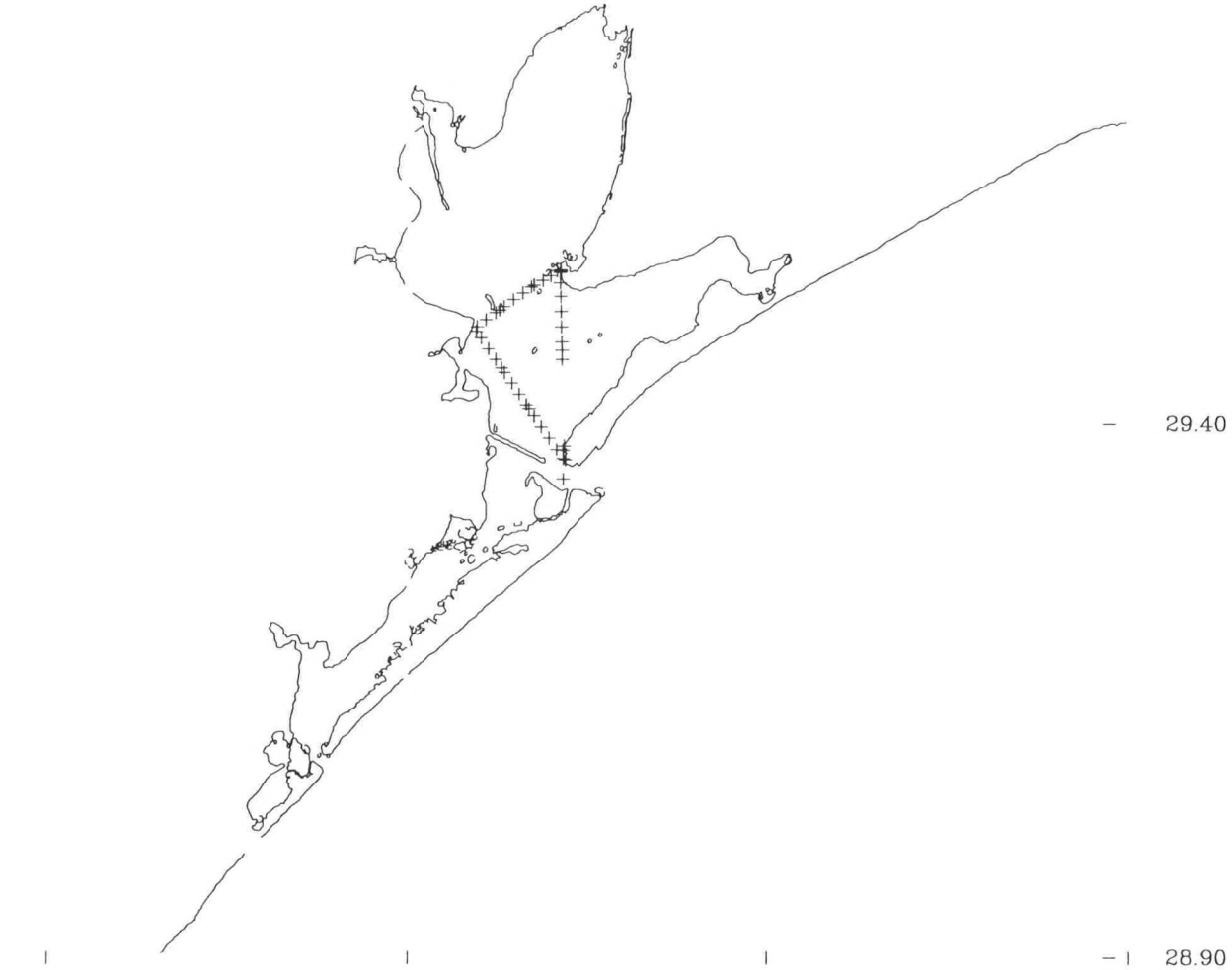

WATER SURFACE ELEVATION WRT GPS ELLIPSOID (M)

WATER SURFACE ELEVATION (M)

RMS 0.09 IN. AGT 0.63

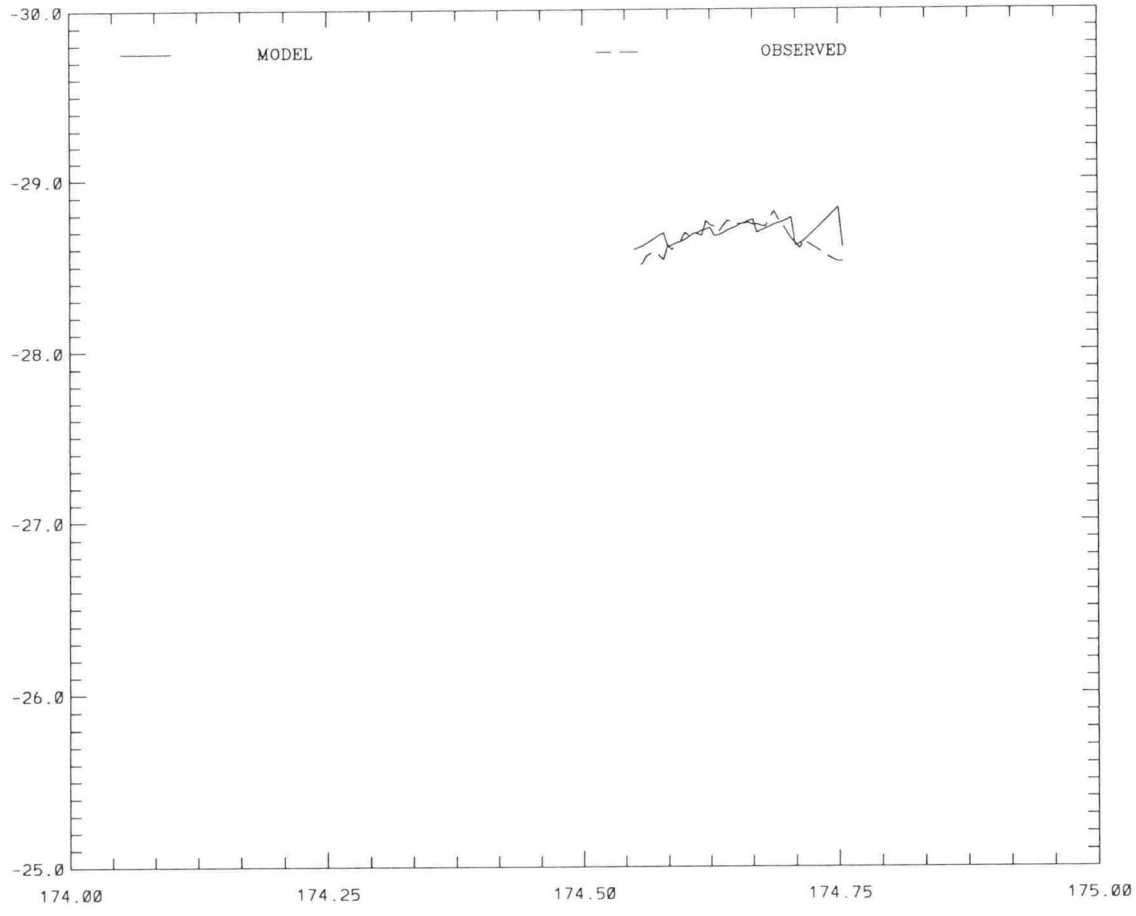

TIME (JULIAN DAYS 1995)

WATER SURFACE ELEVATION WRT GPS ELLIPSOID (M)

JD 177.45 – JD 177.83

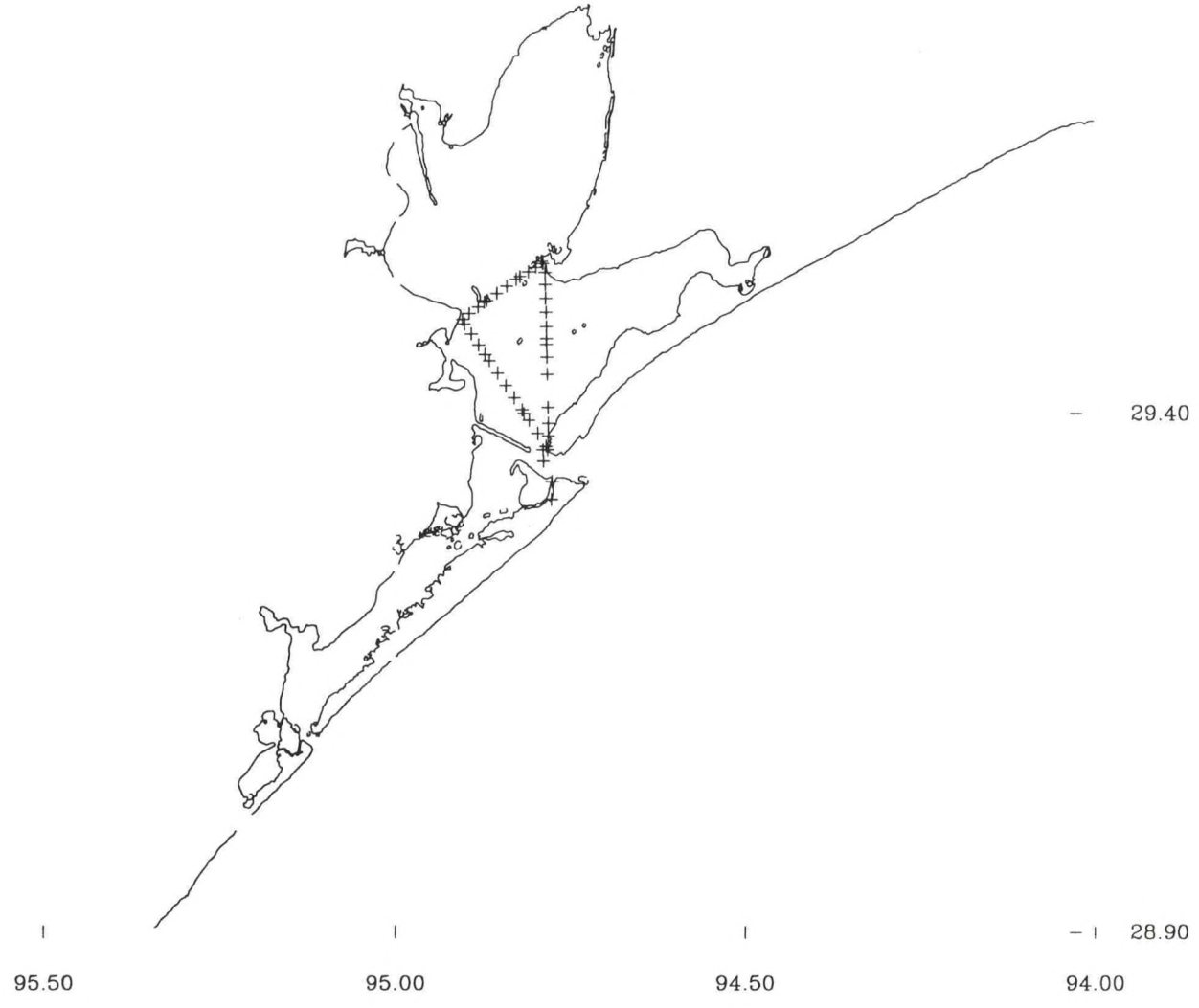

WATER SURFACE ELEVATION WRT GPS ELLIPSOID (M)

WATER SURFACE ELEVATION (M)

RMS 0.09 IN. AGT 0.63

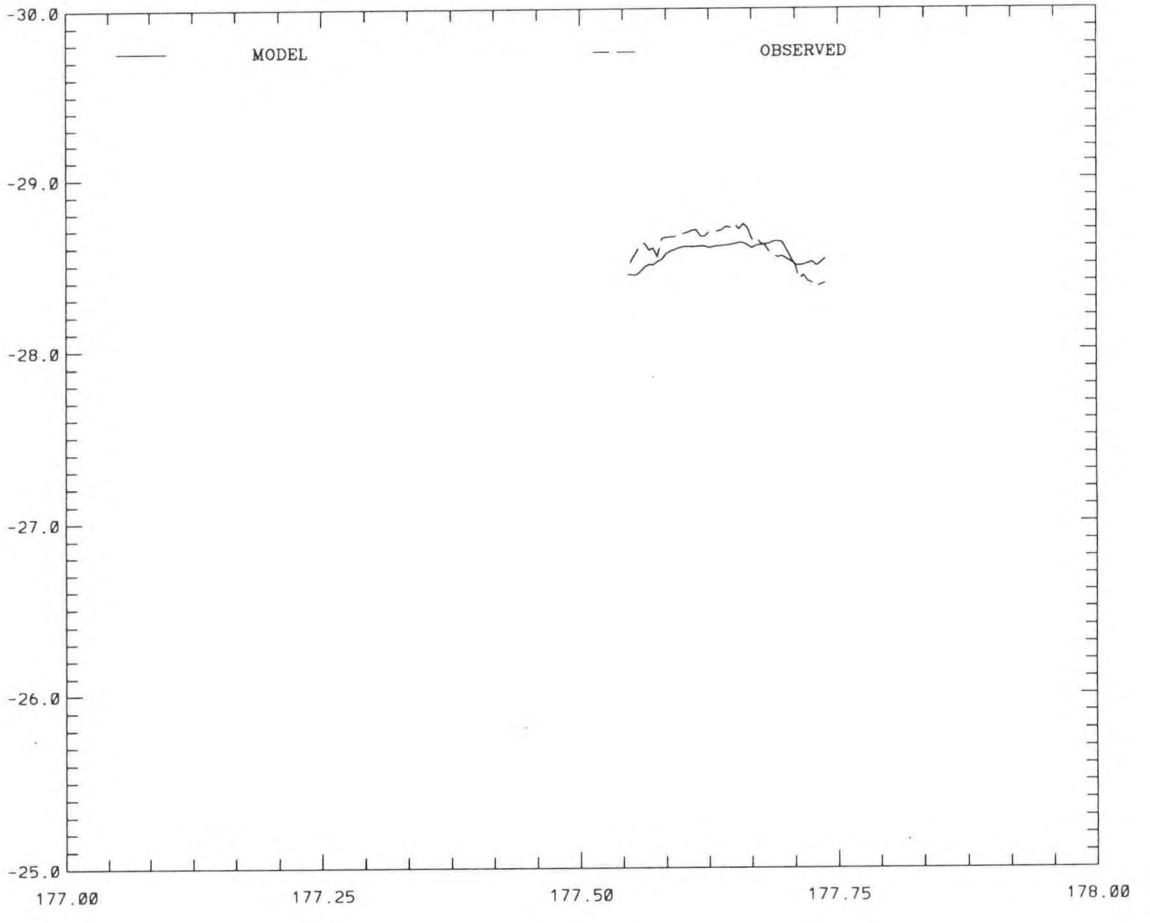

TIME (JULIAN DAYS 1995)

WATER SURFACE ELEVATION WRT GPS ELLIPSOID (M)

JD 178.40 - JD 178.83

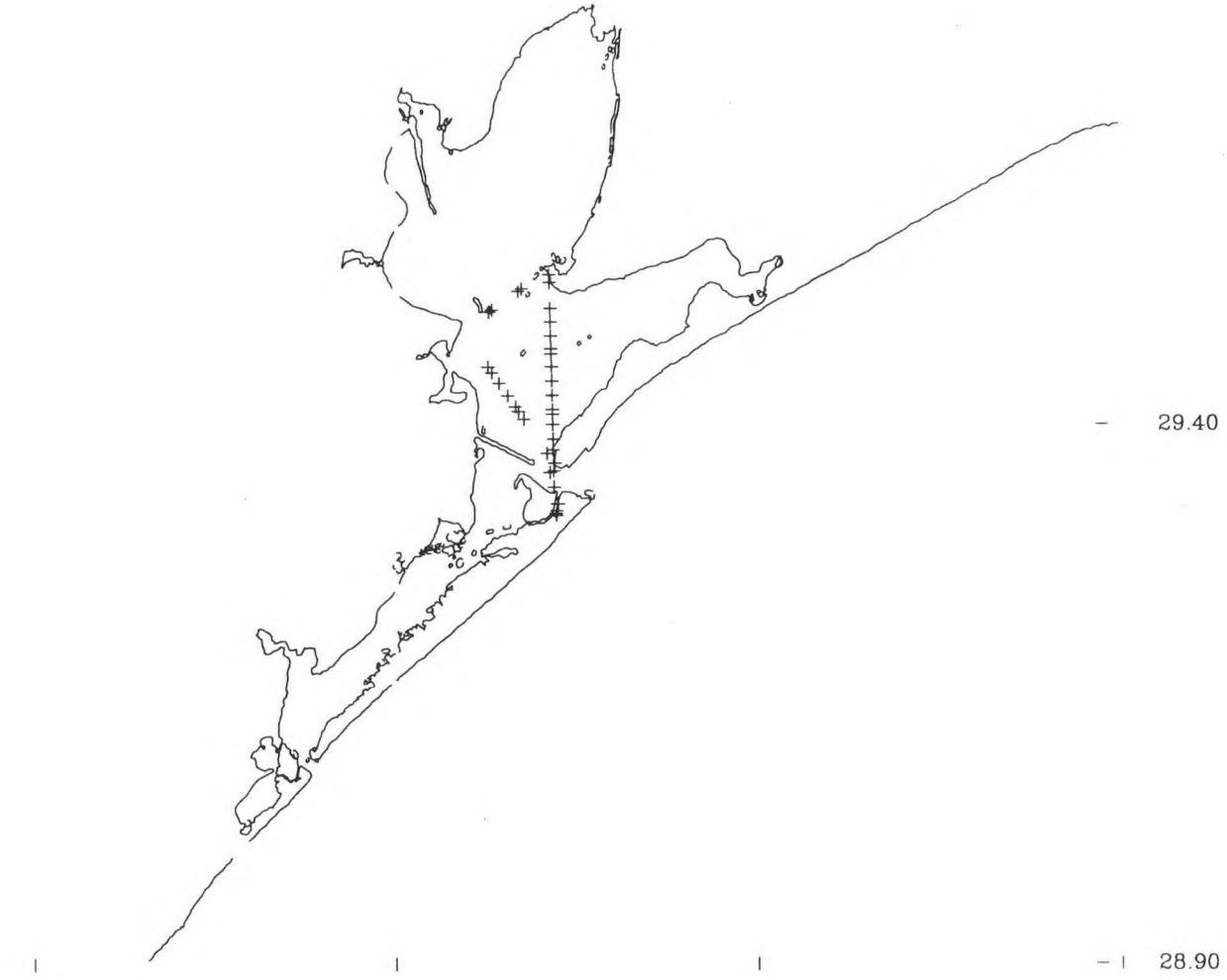

WATER SURFACE ELEVATION WRT GPS ELLIPSOID (M)

WATER SURFACE ELEVATION (M)

RMS 0.12 IN. AGT 0.40

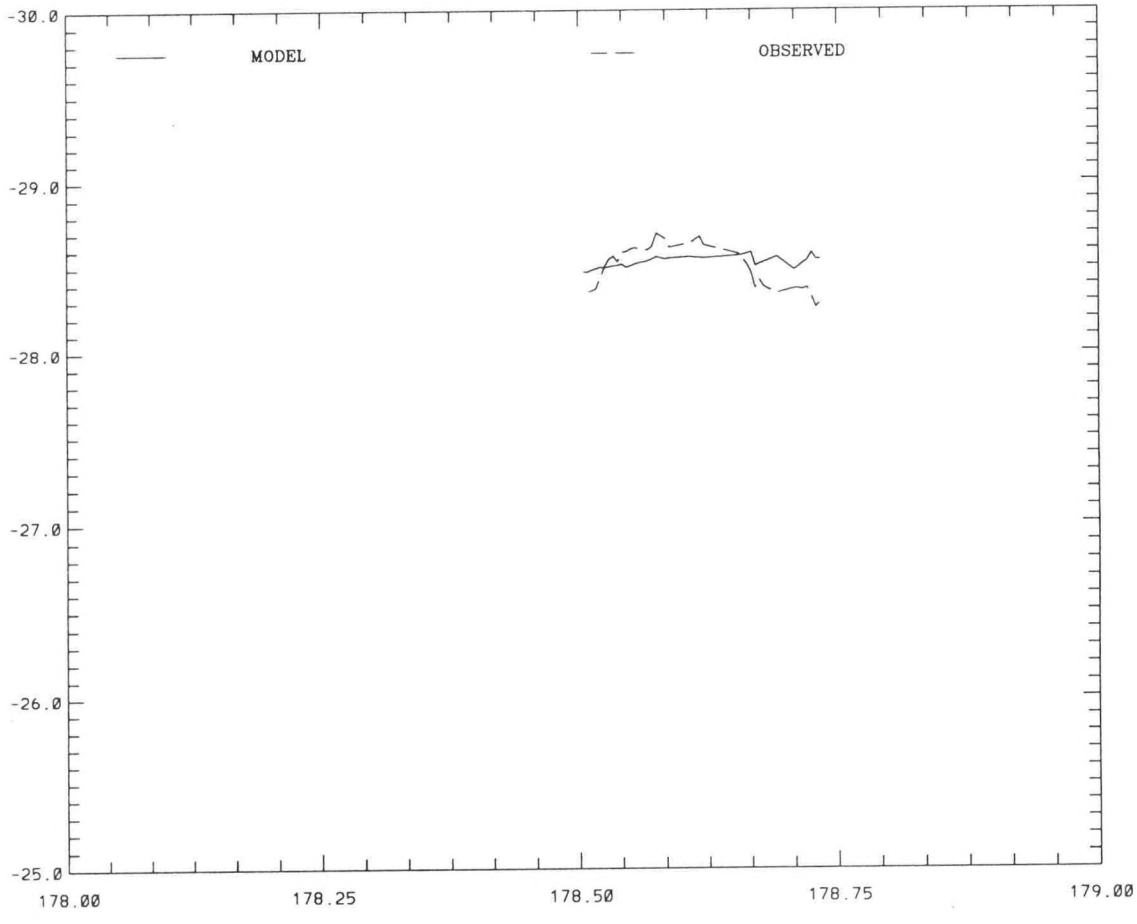

TIME (JULIAN DAYS 1995)

WATER SURFACE ELEVATION WRT GPS ELLIPSOID (M)

JD 179.44 – JD 179.69

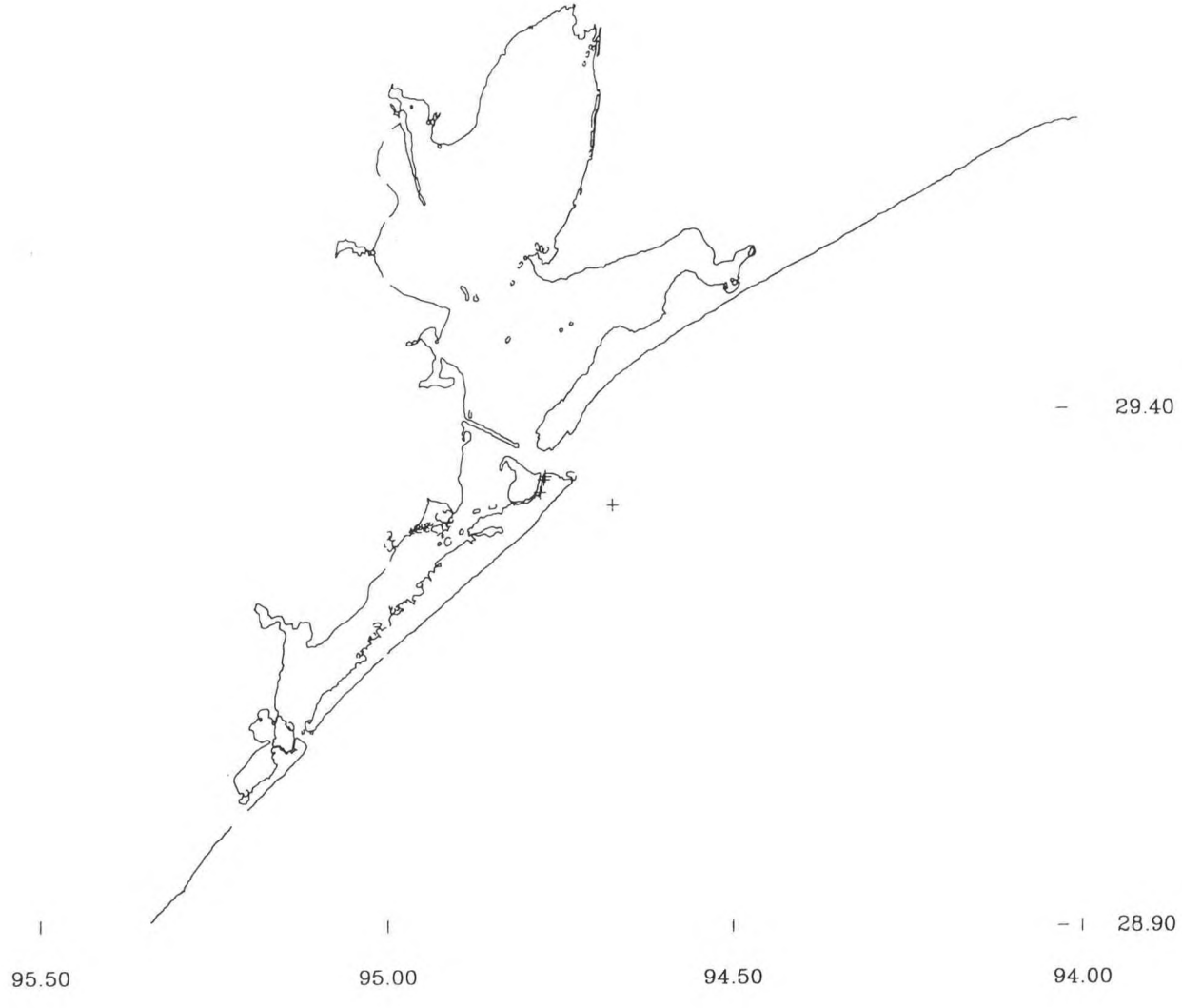

WATER SURFACE ELEVATION WRT GPS ELLIPSOID (M)

WATER SURFACE ELEVATION (M)

RMS 0.27 IN. AGT 0.75

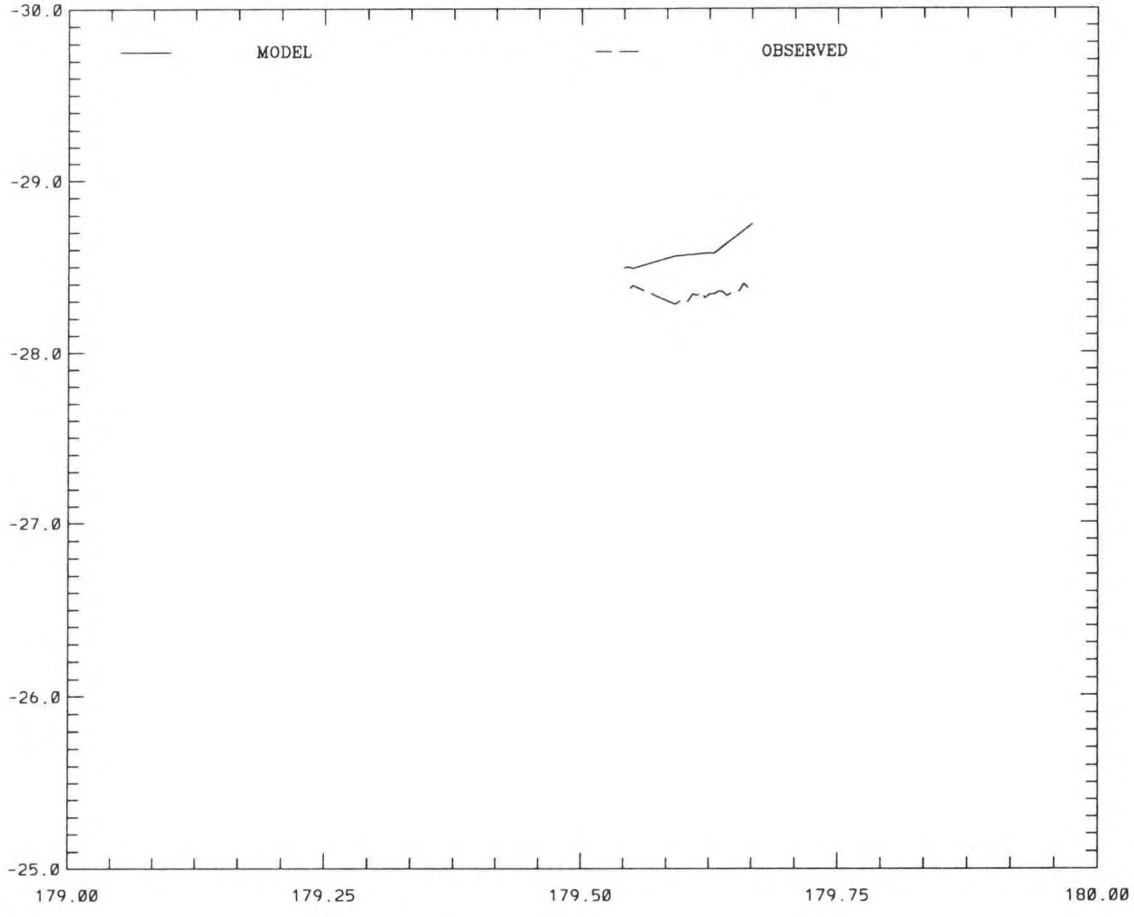

TIME (JULIAN DAYS 1995)

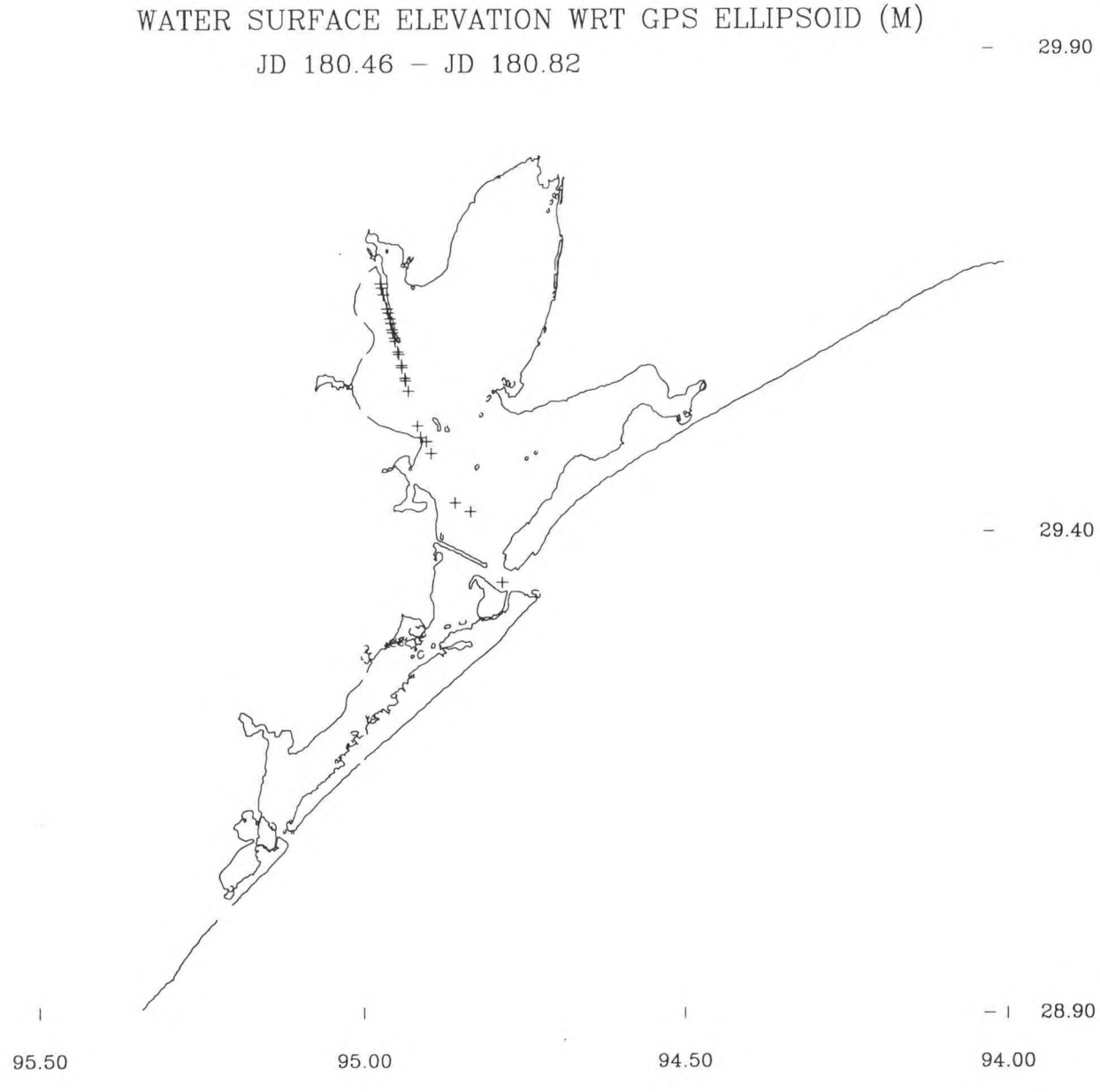
WATER SURFACE ELEVATION WRT GPS ELLIPSOID (M)
JD 180.46 – JD 180.82
29.90
29.40
28.90
95.50
95.00
94.50
94.00

WATER SURFACE ELEVATION WRT GPS ELLIPSOID (M)

WATER SURFACE ELEVATION (M)

RMS 0.14 IN. AGT 0.43

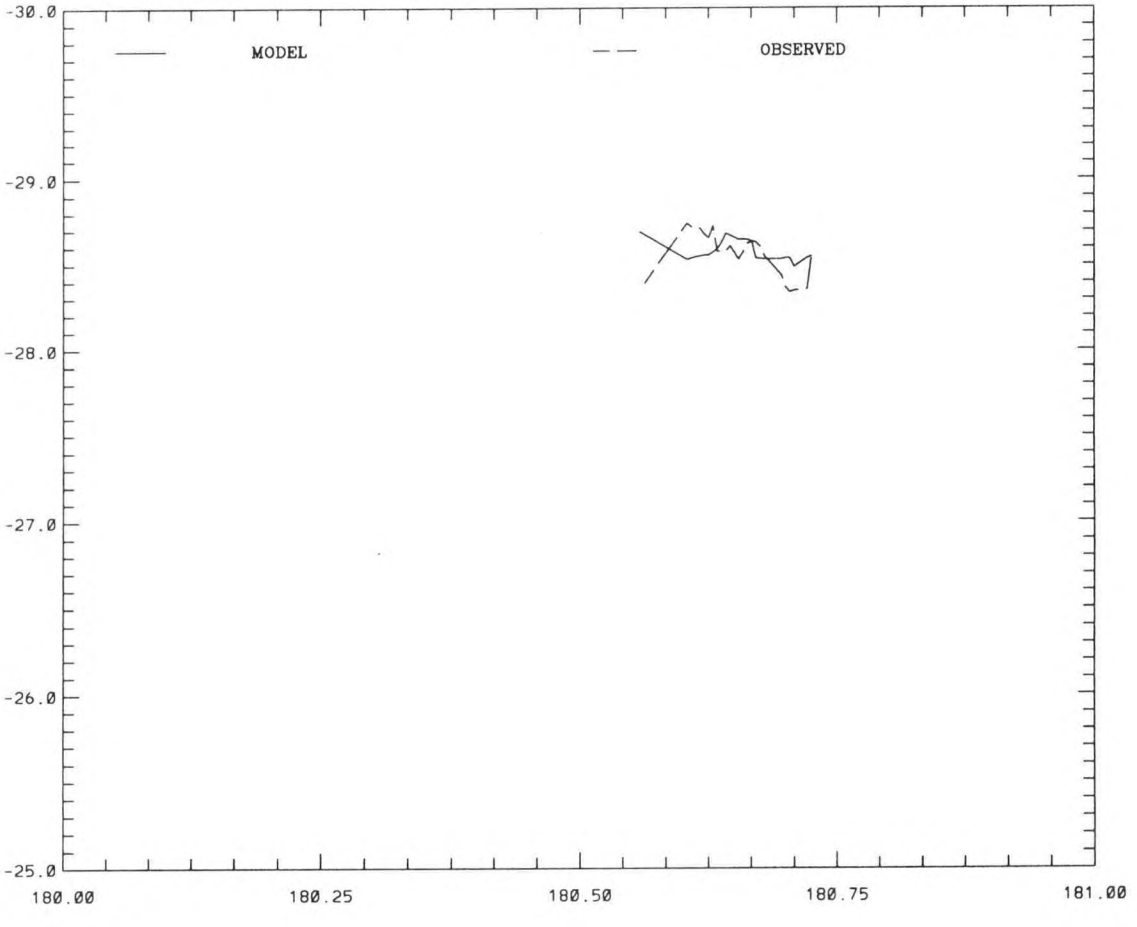

TIME (JULIAN DAYS 1995)

WATER SURFACE ELEVATION WRT GPS ELLIPSOID (M)

JD 181.48 – JD 181.73

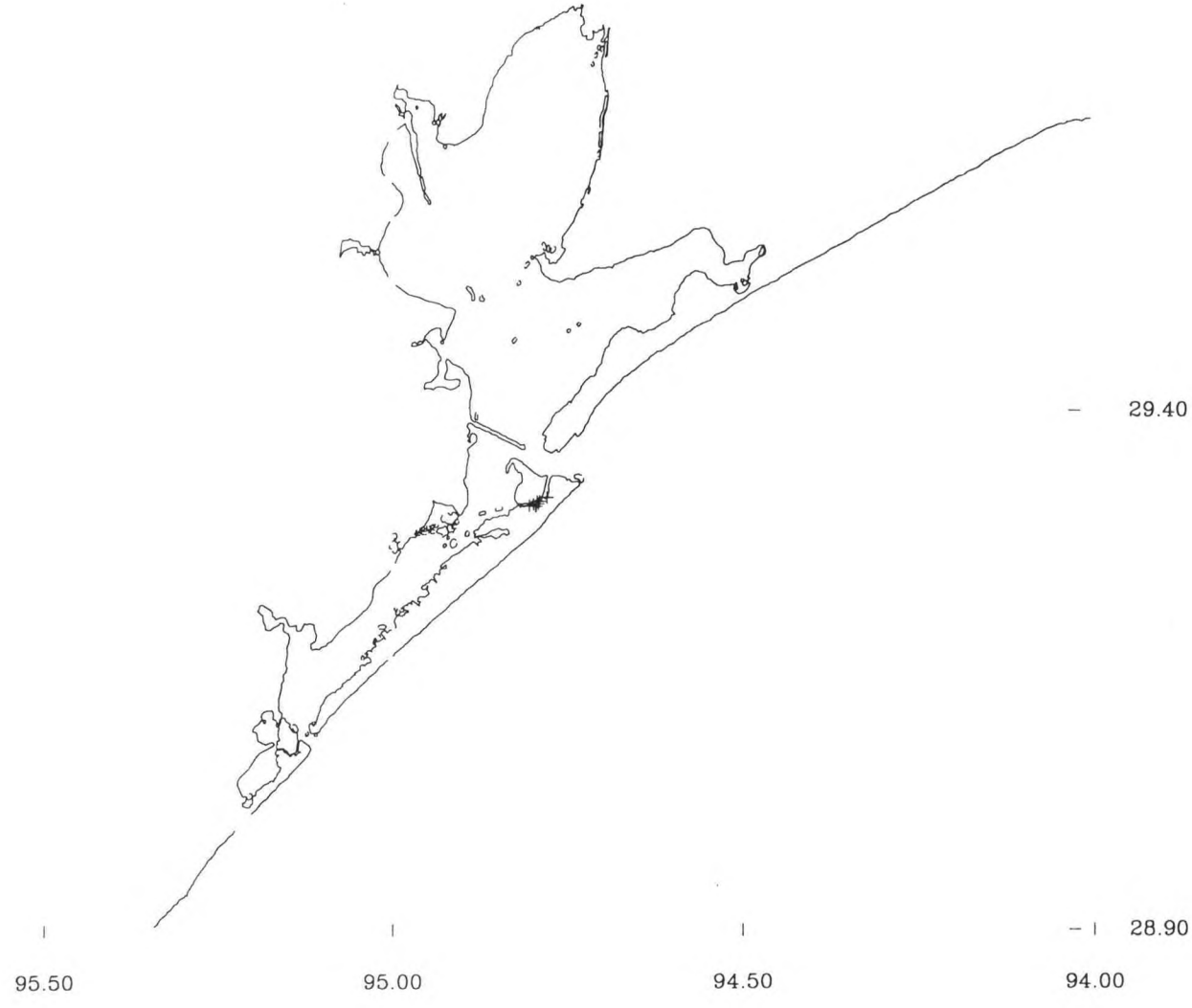

WATER SURFACE ELEVATION WRT GPS ELLIPSOID (M)

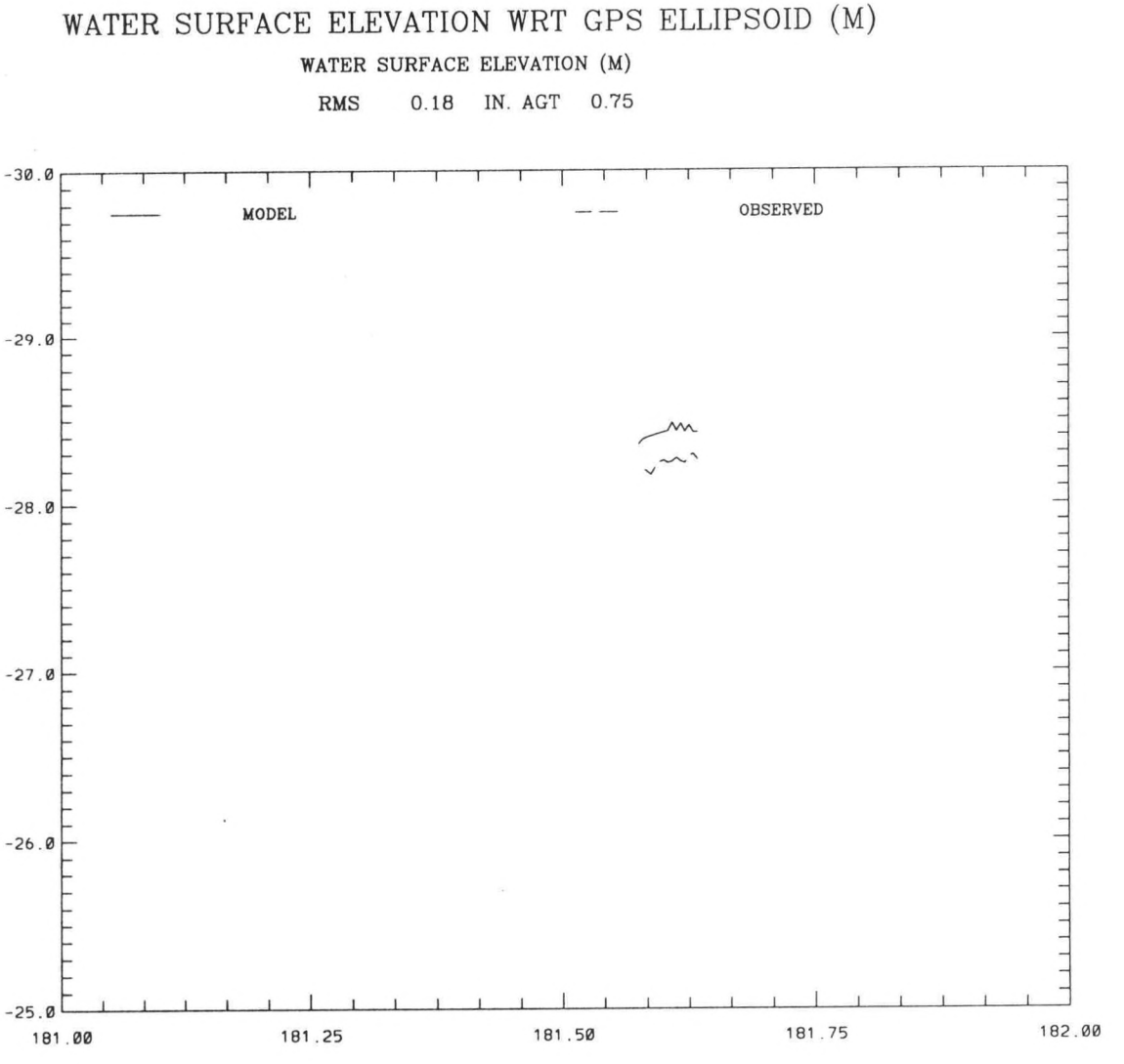

APPENDIX B. METEOROLOGICAL SIMULATION: DGPS WATER LEVEL COMPARISON SUMMARY

TIDE STATION DISTANCE STATISTICS:

DISTANCE RANGE 0.0 - 2.0 (KM)

NO.	SPEED RANGE (M/S)	MEAN DGPS (M)	MEAN SIM. (M)	SDV. DGPS (M)	SDV. SIM. (M)	RMS (M)	REL. ERR. (-)
24	0.0 - 1.0	-28.47	-28.38	0.08	0.16	0.15	0.38
10	1.0 - 2.0	-28.54	-28.56	0.14	0.17	0.12	0.25
14	2.0 - 3.0	-28.53	-28.55	0.12	0.17	0.16	0.37
14	3.0 - 4.0	-28.63	-28.61	0.14	0.20	0.15	0.33
17	4.0 - 5.0	-28.55	-28.53	0.11	0.16	0.12	0.33
10	5.0 - 99.0	-28.51	-28.42	0.09	0.11	0.15	0.34

TIDE STATION DISTANCE STATISTICS:

DISTANCE RANGE 2.0 - 4.0 (KM)

NO.	SPEED RANGE (M/S)	MEAN DGPS (M)	MEAN SIM. (M)	SDV. DGPS (M)	SDV. SIM. (M)	RMS (M)	REL. ERR. (-)
19	0.0 - 1.0	-28.68	-28.71	0.13	0.14	0.11	0.25
11	1.0 - 2.0	-28.66	-28.69	0.13	0.18	0.12	0.25
17	2.0 - 3.0	-28.62	-28.72	0.16	0.17	0.16	0.23
17	3.0 - 4.0	-28.62	-28.68	0.11	0.14	0.12	0.28
35	4.0 - 5.0	-28.57	-28.61	0.14	0.16	0.14	0.27
6	5.0 - 99.0	-28.52	-28.39	0.09	0.11	0.20	0.33

TIDE STATION DISTANCE STATISTICS:

DISTANCE RANGE 4.0 - 6.0 (KM)

NO.	SPEED RANGE (M/S)	MEAN DGPS (M)	MEAN SIM. (M)	SDV. DGPS (M)	SDV. SIM. (M)	RMS (M)	REL. ERR. (-)
3	0.0 - 1.0	-28.43	-28.51	0.03	0.19	0.16	0.54
16	1.0 - 2.0	-28.59	-28.63	0.14	0.11	0.11	0.22
14	2.0 - 3.0	-28.62	-28.68	0.13	0.12	0.09	0.19
31	3.0 - 4.0	-28.60	-28.68	0.13	0.11	0.13	0.23
39	4.0 - 5.0	-28.61	-28.69	0.14	0.15	0.15	0.27

TIDE STATION DISTANCE STATISTICS:

DISTANCE RANGE 6.0 - 8.0 (KM)

NO.	SPEED RANGE (M/S)	MEAN DGPS (M)	MEAN SIM. (M)	SDV. DGPS (M)	SDV. SIM. (M)	RMS (M)	REL. ERR. (-)
3	0.0 - 1.0	-28.63	-28.79	0.20	0.33	0.19	0.36
6	1.0 - 2.0	-28.53	-28.67	0.11	0.08	0.20	0.30
9	2.0 - 3.0	-28.66	-28.71	0.11	0.11	0.09	0.22
21	3.0 - 4.0	-28.56	-28.64	0.12	0.15	0.14	0.27
44	4.0 - 5.0	-28.60	-28.67	0.12	0.13	0.13	0.27

TIDE STATION DISTANCE STATISTICS:

DISTANCE RANGE 8.0 - 10.0 (KM)

NO.	SPEED RANGE (M/S)	MEAN DGPS (M)	MEAN SIM. (M)	SDV. DGPS (M)	SDV. SIM. (M)	RMS (M)	REL. ERR. (-)
3	0.0 - 1.0	-28.46	-28.68	0.02	0.01	0.22	0.25
2	1.0 - 2.0	-28.60	-28.81	0.19	0.15	0.21	0.22
7	3.0 - 4.0	-28.55	-28.62	0.11	0.15	0.09	0.21
33	4.0 - 5.0	-28.61	-28.67	0.12	0.14	0.13	0.28

TIDE STATION DISTANCE STATISTICS:

DISTANCE RANGE 10.0 - 99.0 (KM)

NO.	SPEED RANGE (M/S)	MEAN DGPS (M)	MEAN SIM. (M)	SDV. DGPS (M)	SDV. SIM. (M)	RMS (M)	REL. ERR. (-)
19	0.0 - 1.0	-28.62	-28.34	0.06	0.03	0.28	0.25
5	1.0 - 2.0	-28.69	-28.69	0.06	0.14	0.10	0.52
4	2.0 - 3.0	-28.48	-28.48	0.03	0.09	0.06	0.57
4	3.0 - 4.0	-28.64	-28.70	0.09	0.16	0.12	0.42
13	4.0 - 5.0	-28.66	-28.76	0.09	0.14	0.15	0.35

GLOBAL STATISTICS: 470 TOTAL POINTS

MEAN DGPS (M)	MEAN SIM. (M)	SDV. DGPS (M)	SDV. SIM. (M)	RMS (M)	REL. ERR. (-)
-28.59	-28.62	0.13	0.18	0.15	0.32